論文 / 著書情報
Article / Book Information

題目(和文)	垂直方向並列給電多層平行平板スロットアレーアンテナの研究
Title(English)	Study of Perpendicular-Corporate Feed in Multi-Layer Parallel-Plate Slot Array Antennas
著者(和文)	入江寿憲
Author(English)	Hisanori Irie
出典(和文)	学位:博士(工学), 学位授与機関:東京工業大学, 報告番号:甲第11130号, 授与年月日:2019年3月26日, 学位の種別:課程博士, 審査員:廣川 二郎,阪口 啓,西方 敦博,青柳 貴洋,西山 伸彦
Citation(English)	Degree:Doctor (Engineering), Conferring organization: Tokyo Institute of Technology, Report number:甲第11130号, Conferred date:2019/3/26, Degree Type:Course doctor, Examiner:,,,,
学位種別(和文)	博士論文
Type(English)	Doctoral Thesis

Doctoral Dissertation

Study of Perpendicular-Corporate Feed in Multi-Layer Parallel-Plate Slot Array Antennas

February, 2019

Under the supervision of

Professor Jiro Hirokawa

Presented by

Hisanori Irie

Department of Electrical and Electronic Engineering

Tokyo Institute of Technology

Contents

Chapter 1
Introduction

1.1 Millimeter-Wave Wireless Communications

Recently, applications of wireless communications have been steadily increasing due to the spread of mobile devices operated by 4th generation mobile and wireless communication technologies (2010-2020, 4G). The communication speed of 4G-mobile devices is almost 1 Gbps, nearly 50,000 times in thirty years (1980-2010,1G-4G). The 4G is operated in microwave bands from a technical reason. However, the capacity of microwaves has almost been at full operation because of a wide range of applications. Also, further increase in the use of wireless communications will be expected in the future. Therefore, 5th generation mobile and communication technologies (5G) has been discussed lately as a solution of future wireless communications. Some projects of the 5G have already been advanced to be in services around 2020-. The features of the 5G are ultra-high speed, ultra-low latency and hyper connectivity, and contribute to a wide variety of services such as agriculture retail, financial, automotive, media, entertainment, health care, public safety, manufacturing and energy. Fig. 1.1 describes the transition of mobile and wireless communication technologies [1.1] - [1.3].

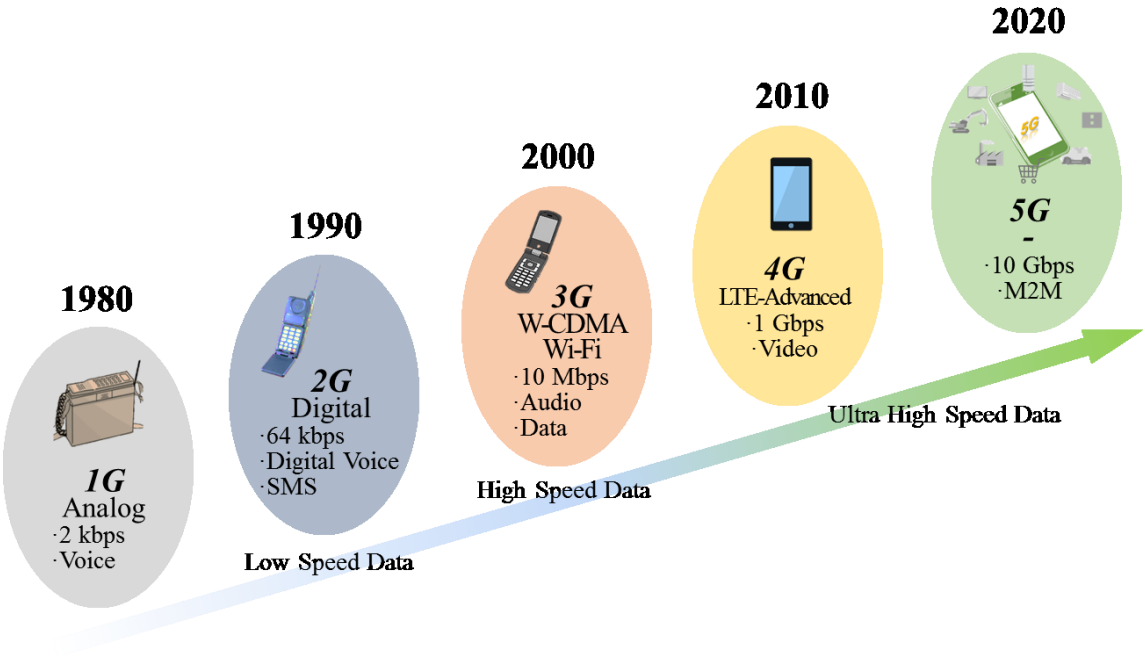

Fig. 1.1 Transition of mobile and wireless communication technologies.

To realize the ultra-high speed communication with the 5G, the utilization of millimeter-wave bands is indispensable because of its plentiful frequency resource. However, millimeter-wave propagation suffers from atmospheric attenuation caused by oxygen and vapor [1.11], [1.12], resulting in short communication range. Consequently, trade-off relation exists between communication speed and range, and some applications are subject to restrictions in use. Fig. 1.2 shows the characteristic of mobile and wireless communication technologies in generations [1.10]. To achieve sustainable services in millimeter-wave bands, antennas in millimeter-wave bands have been widely studied [1.4] - [1.9]. Most of them focus on the high gain and efficiency characteristic of antennas to enable stable operation of millimeter-wave systems even in attenuating environment. Some studies also discuss the low-profile feature of planer antennas in millimeter-wave use. Basically millimeter-wave antennas have advantages over low-profile features due to their operational wavelength enabling small sizes of systems. Therefore, planer millimeter-wave antennas can contribute to many services in terms of the easy installation and good appearance of systems.

<table>
<tr><td>Generation</td><td>3G</td><td>4G</td><td>5G†</td></tr>
<tr><td>Comm. Speed</td><td>☹2 Mbps</td><td>1 Gbps</td><td>☺10 Gbps</td></tr>
<tr><td>Comm. Range</td><td>☺Longer</td><td>Long</td><td>☹ Short</td></tr>
<tr><td rowspan="3">Frequency Band</td><td colspan="2">Microwave</td><td>Millimeter Wave</td></tr>
<tr><td>0.7 - 2.1 GHz</td><td>3.4 - 3.6 GHz etc.</td><td>27.5 - 29.5 GHz‡
37.0 - 40.0 GHz
40.5 - 43.5 GHz etc.</td></tr>
<tr><td colspan="2"><u>Lower Frequency Band</u>
➢ Small Atmospheric Attenuation
? ☺Long Comm. Range
➢ Limited Frequency Resources
? ☹Low Comm. Speed</td><td><u>Higher Frequency Band</u>
➢ Large Atmospheric Att.
? ☹Short Comm. Range
➢ Plentiful Freq. Resources
? ☺High Comm. Speed</td></tr>
</table>

†: [1.10] Ministry of Internal Affairs and Communications, "The Draft Guideline of the Establishment of Specific Base Stations to Introduce 5G Mobile Communication Systems," Nov. 2018, Website: http://www.soumu.go.jp/main_content/000582765.pdf
‡: Microwave

Fig. 1.2 Characteristic of mobile and wireless communication technologies in generations.

1.2 High Gain Antennas

To realize 5G services, the high gain and efficiency characteristic of antennas are indispensable as the requirement of systems. Fig. 1.3 shows the comparison of high gain antennas. As a typical high-gain antenna in microwave bands, Parabolic antennas are used for ground communications and space communications [1.13]. Antennas have strong

directivity by the action of a mirror reflector. However, they are unsuitable for millimeter-wave use because they are supported by large supporters mechanically and composed of large feeding systems geometrically. As a typical planner array antenna in microwave bands, microstrip array antennas are used for radar systems of airplanes due to the feature of their low profile [1.14]. Antennas consist of radiating elements printed on a dielectric substrate and a grounded conductor plate at the bottom of the substrate. This structure has a good connection with microwave circuits because they can be integrated on the dielectric substrate, resulting in low profile. However, dielectric substrates include a higher dielectric loss when being in millimeter-wave-band operations. As a typical low-loss and planner antennas in microwave and millimeter-wave bands, waveguide slot arrays are used for fixed-wireless-access systems and automobile radar systems because of their low-profile and low-loss structure based on the composition of waveguides with no dielectric. These features lead to high gain and efficiency, and easy installation of systems. Waveguide slot arrays can be classified into the series feed and the corporate feed. A single-layer slot array antenna with phase-reversal series-feed consists of two parts: a slotted plate and a feeding groove plate, and they are no electrical contact because of an air gap between the two [1.15]. This structure contributes to mass production. However, as the feeding waveguide is placed at the edge of the antenna due to the series feed, in particular large-sized arrays cannot offer wide bandwidth because of the long line effect. This effect is based on the phase difference among radiating slots, which are excited by traveling waves. To solve this problem, a center-feed single-layer slotted waveguide array was proposed [1.16]. The feeding waveguide of the antenna is placed in the center of arrays and this structure can reduce the long line effect. Also, a partially-corporate feed using E-plane coupler in a single-layer slotted waveguide array was proposed [1.17]. This antenna is divided into four subarrays with a partially corporate-feed waveguide to reduce the long line effect. These antennas with the center feed or the partially corporate feed are a single layer structure considering mass production. Consequently, both structures offer higher sidelobes resulting in lower antenna efficiency because radiating slots cannot be placed on the feeding waveguide physically. To solve this problem, a double-layer full-corporate-feed hollow-waveguide slot array antenna was proposed [1.18]. This antenna consists of a feeding circuit part on the bottom and a radiating part on the top, and the double-layer structure contributes to the characteristic of wide bandwidth and higher antenna efficiency due to the flexible placement of radiating slots. Also, the antenna is fabricated by the diffusion bonding of laminated thin copper plates, and so leads to mass production. Therefore, we focus on the study of parallel-plate slot array antennas in millimeter-wave bands in this thesis.

Types	Parabolic	Microstrip Array	Waveguide Slot Array			
Structure		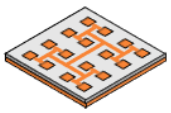	Series Feed			Corporate Feed
			Edge Feed	Center Feed	Partially-Corporate Feed	
			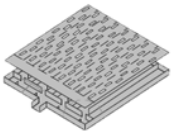	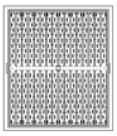	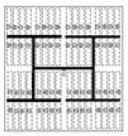	
Planation	☹	☺	☺	☺	☺	☺
Higher Frequency	☹	☹	☺	☺	☺	☺
Wider Bandwidth	☺	☺	☹	Wider Bandwidth		☺
Reference	[1.13] J. Hiang and Y. Rahmat-Samii, "Fan Beam Generated by a Linear-Array Fed Parabolic Reflector," IEEE Trans. Antennas Propag., vol.38, no. 7, pp.1046-1053, July 1990.	[1.14] D.M. Pozar, S.D. Targonski, and H.D. Syrigos, "Design of Millimeter Wave Microstrip Reflectarrays," IEEE Trans. Antennas Propag., vol.45, no. 2, pp.287-296, Feb. 1997.	[1.15] Y. Kimura, and etc., "A low-cost and very compact wireless terminal integrated on the back of a waveguide planar array for 26GHz band Fixed Wireless Access (FWA) systems," IEEE Trans. Antennas Propag., vol.53, no. 8, pp.2456-2463, Aug.2005.	[1.16] S. Park, Y. Tsunemitsu, J. Hirokawa and M. Ando,Center Feed Single Layer Slotted Waveguide Array, " IEEE Trans. Antennas Propag., vol.54, no.5, pp.1474-1480, May 2006.	[1.17] S. Fujii, and etc., "Partially Corporate Feed using E-plane Coupler in a Single-Layer Slotted Waveguide Array," IEICE Technical Report, vol. 107, no.431, AP2007-150, pp.163-168, Jan. 2008.	[1.18] Y. Miura, J. Hirokawa, M. Ando, Y. Shibuya, and G. Yoshida, "Double-layer full-corporate-feed hollow-waveguide slot array antenna in the 60-GHz band," IEEE Trans. Antennas Propag., vol.59, no.8, pp.2844-2851, Aug. 2011.

Fig. 1.3 Comparison of high gain antennas.

1.3 Array Antennas with Corporate Feed

Fig. 1.4 shows the comparison of array antennas with the corporate feed in past studies as a reference. a receiving planar array antenna for direct broadcasting satellites was proposed [1.19]. The antenna is a short waveguide aperture mounted in the ground plane, loaded with the dielectric and the polarizers, and excited through its side wall by another feeding rectangular waveguide. The gain of the antenna loaded with a dielectric is so high that the grating lobes can be reduced sufficiently even if the element spacing in the array is wider than the wavelength in free space. Therefore, the number of the array elements is reduced, and the parallel feeding by the low-loss waveguide network can be feasible to be an excellent planar array antenna. In a 12 GHz band, the planar antenna with 64-element radiators has the maximum gain of 31.9 dBi with the aperture efficiency of 94.7 %, the 1 dB-down bandwidth of the gain of about 800 MHz, 6.7% for center frequency 11.85 GHz, and the frequency bandwidth of the axial ratio less than 1 dB of 850 MHz, 7.2 %. A low-profile high-gain antenna array of box horns for the frequency band 57.2–58.2 GHz is presented [1.20]. The antenna consists of 256 radiating elements divided into two subgroups of 128 elements fed by a rectangular waveguide feed network. The radiating elements are fed in parallel and the waveguides are connected with T-junctions. The matching of the T-junctions is improved with a matching pin and a splitter. The element spacing is larger than one wavelength, which causes grating lobes, because of the waveguide feed network. The grating lobes and sidelobes in the H-plane have been suppressed by the use of a combination of subarrays, a special characteristic of the box horn and an array amplitude tapering. The measured sidelobe levels in the H-plane are

below –30 dB at angles larger than 8 deg. from boresight. A gain higher than 35.7 dBi and a return loss higher than 14.4 dB have been measured for the antenna over the band 57.2–58.2 GHz. A 24×24 two-layer slotted-waveguide array antenna is presented [1.21]. The subarray concept is introduced to provide a broad reflection and gain bandwidth. A waveguide-feeding network feeds at equal amplitudes and phases to the subarrays composed of two layers, and so is more compact and simpler than conventional feeding networks. The subarray consists of a feeding waveguide, a coupling slot, a radiating waveguide and a radiating slot. The measured reflection bandwidth is 5.5% of the VSWR less than 2.0. The antenna gain varies within 2.1 dB over 4 GHz, 9.5 %. The maximum gain is 33.8 dBi at 41.5 and 42.5 GHz. To achieve a wide bandwidth characteristic of high gain and high efficiency antennas, a double-layer hollow-waveguide slot array is proposed, where a full-corporate-feed waveguide is arranged in the lower layer [1.18]. This antenna can be built up easily by the diffusion bonding of laminated thin metal etching plates, which has high precision and is possibly a low cost technique. The radiating elements and the feed waveguide are designed to suppress the reflection over a wideband. The predicted bandwidth of the reflection less than -14 dB is 8.3 % for a 16×16-element array antenna. A test antenna is fabricated in the 60 GHz band, and about 80 % antenna efficiency with more than 32 dBi is achieved over 4.8 GHz.

Types	**Dielectric-Loaded Array**	**Box-Horn Array**	**Double-layer Slot Array**	**W.G. Slot Array (Diffusion bonding)**
Overall	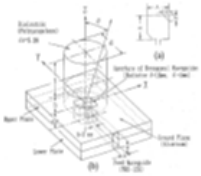	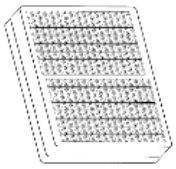	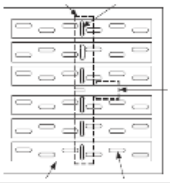	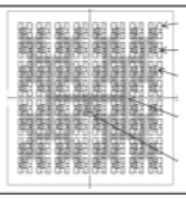
Feeding Circuit	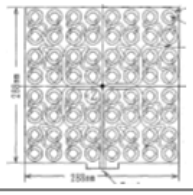	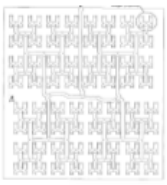	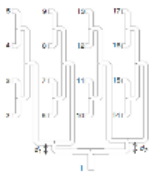	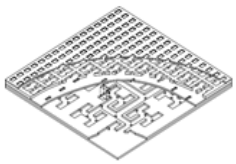
Frequency	12 GHz	58 GHz	40 GHz	60 GHz
Gain	31.9 dBi	35.8 dBi	33.8 dBi	32.6 dBi
Antenna Efficiency	94.7 %	33.0 %	51.0 %	83.6 %
1dB-down Gain B.W.	6.7 %	-	9.5 %	13.1 %
Side lobe Level	-13.3 dB	-12.0 dB	-12.0 dB	-14.4 dB
Reference	[1.19] T. Tsugawa, Y. Sugio, and Y. Yamada, "Circularly Polarized Dielectric-Loaded Planner Antenna Excited by the Parallel Feeding Waveguide Network," IEEE Trans. Broadcasting, vol. 43, no. 2, pp. 205-212, June 1997.	[1.20] T. Sehm, A. Lehto, and A. V. Räisänen, "A High-Gain 58-GHz Box-Horn Array Antenna with Suppressed Grating Lobes," IEEE Trans. Antennas Propag., vol.47, no. 7, pp.1125-1130, July 1999.	[1.21] S.-S. Oh, J.-W. Lee, M.-S. Song and Y.-S. Kim, "Two-layer slotted-waveguide antenna array with broad reflection/gain bandwidth at millimetre-wave frequencies," IEE Proc.-Microw. Antennas Propag., vol.51, no. 5, pp. 393-398, Oct. 2004.	[1.18] Y. Miura, J. Hirokawa, M. Ando, Y. Shibuya, and G. Yoshida, "Double-layer full-corporate-feed hollow-waveguide slot array antenna in the 60-GHz band," IEEE Trans. Antennas Propag., vol.59, no.8, pp.2844-2851, Aug. 2011.

Fig. 1.4 Comparison of array antennas with a corporate feed in past studies.

1.4 Parallel-Plate Slot Arrays with Corporate Feed in Millimeter-Wave bands

As we elucidate the better characteristic of waveguide slot arrays with the corporate feed in section 1.2 and 1.3, we focus on the study of parallel-plate slot array antennas in millimeter-wave bands. As a typical parallel-plate slot arrays with the corporate feed in millimeter-wave bands, the double-layer full-corporate-feed hollow-waveguide slot array antenna in 60 GHz bands was proposed [1.18]. This antenna is fabricated by the diffusion bonding of laminated thin copper plates. These plates are categorized in several layers: a radiating-slot layer, a cavity layer, a coupling-aperture layer and a planar corporate-feed circuit layer. The circuit layer is a cascade of H-planes and T-junctions, and the shape results in the feeding of all of the coupling apertures at equal amplitudes and phases. The coupling apertures excite 2×2-element radiating slots through a cavity that can hold electromagnetic fields without leakage to peripheral cavities due to its x-shaped walls. This structure provides high gains and efficiencies by using hollow waveguides and a wide bandwidth by using the corporate feed. This structure is also extended to circularly- and 45^{o} linearly-polarized aperture array antennas [1.22], [1.23]. These antennas have additional-slot layers to generate the desired polarization.

Recently, corporate-feed waveguide slot array antennas based on [1.18] have been further advanced by various technologies. Fig. 1.5 shows the comparison of parallel-plate slot arrays. The direct metal laser sintering 3-D printing technique was used to fabricate an 8×8 waveguide array with an integrated corporate-fed network [1.24]. The design frequency is lower: 15 GHz because of its fabrication constraint. The measured results showed greater than 80 % antenna efficiency and the bandwidth of 12.6 % (14.2 - 16.1 GHz) for VSWR < 2.0. Cavity-backed patch antenna arrays with a full corporate substrate integrated waveguide feed networks were reported [1.25]. The antenna composed of 16×16 radiating elements is fabricated by using the standard printed circuit board (PCB) technology. The measured results provided gain up to 30.1 dBi with a 3-dB gain bandwidth of 16.1 % and the bandwidth of 15.3 % for VSWR < 2.0. Antenna efficiency is lower: less than 50 % because of its material losses. We also advanced [1.18] by introducing an additional layer to enhance the VSWR bandwidth. The antenna offers the bandwidth of 21.9 % for VSWR < 2.0 and greater than 70 % antenna efficiency in 80 GHz band [1.26]. Above-mentioned antennas are fabricated with metal contact of layers, resulting in small losses. To remove the metal contact in the feeding circuit, a 76 GHz multi-layer phased array antenna using waffle-iron ridge waveguides was proposed [1.27], [1.28]. The structure has waffle-iron conductor rods, which are a quarter wavelength in

height and allows the top surface of rods to form EMB (Equivalent Magnetic Boundary). The EMB enables the electromagnetic to propagate between two parallel plates without the metal contact. The structure has the advantage of avoiding losses due to imperfect metal contacts. In addition, a corrugated slot antenna array with ridge gap waveguide was studied [1.29], [1.30]. There is no requirement for metal contact in the feeding circuit layer or in the radiating-slot and cavity layers because of the incorporation of the EMB into the multi-layer parallel plates. The measured results demonstrated larger than 32.5 dBi over the 60 GHz band with more than 70 % antenna efficiency and the bandwidth of 15.3% for VSWR < 2.0 [1.31].

Expansion

Tech.	3D Print	Printed Circuit Board	Diffusion Bonding	Gap Waveguide	Perpendicular Corporate Feed
Ref.	[1.24] IEEE MTT-S International MW Symp., Conf. Publications, May 2015	[1.25] IEEE Trans. on AP, Journals & Magazines Vol. 63, Mar 2015	[1.18] IEEE Trans. on AP, Journals & Magazines, Vol. 59 Aug "2011" (2016†)	[1.30] IEEE Trans. on AP, Journals & Magazines, Vol. 64, July 2016	This Work
Org.	National Univ. of Singapore, SGP	City Univ. of Hong Kong, CHN	Tokyo Institute of Tech., JPN	Chalmers Univ. of Tech., SWE	Tokyo Institute of Tech., JPN
Config.		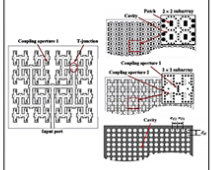	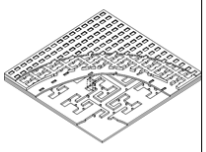	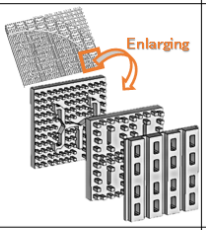	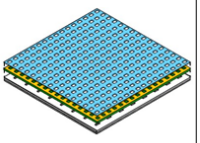
Frequency Band	15GHz	60GHz	60GHz (80GHz)	60GHz	60GHz
Feeding Part	Contact	Contact	Contact	No Contact (w/ Pins)	Contact
Radiating Part	Contact	Contact	Contact	No Contact (w/ Pins)	No Contact (w/ Parallel Plates)
Num. of Element	64	256	256 (256)	256	256
Bandwidth	12.6% (VSWR < 2.0)	15.3% (VSWR < 2.0)	8.3% (VSWR < "1.5") (21.9% (VSWR < 2.0))	16% (VSWR < 2.0)	–
Antenna Efficiency	> 80%	< 50%	> 70% (> 70%)	> 70%	–

†: [1.26] X. Xu, M. Zhang, J. Hirokawa, and M. Ando, "E-band plate-laminated waveguide filters and their integration into a corporate-feed slot array antenna with diffusion bonding technology," IEEE Trans. Micro. Theory Tech., vol. 64, no. 11, pp. 3592 - 3603, Nov. 2016.

Fig. 1.5 Comparison of parallel-plate slot arrays.

1.5 Objectives

In this thesis, we propose a perpendicular-corporate feed in multi-layer parallel-plate slot array antennas. A proposed structure is to remove the x-shaped cavity walls completely in the radiating part of the conventional planar corporate-feed waveguide slot array antenna [1.18]. Coupling apertures on the bottom excite radiating slots. Note that the spacing of the radiating slots is half as spacing as the coupling apertures in a two-dimensional array. This means the corporate feed is achieved in the perpendicular direction so that the number ratio of the radiating slots over the coupling apertures can be 4:1 in a two-dimensional array. Dielectric with adequate permittivity is placed in the region between the coupling-aperture layer and the radiating-slot layer so that the equivalent spacing of the coupling apertures and the radiating slots can be two and one wavelength in this dielectric-filled region, respectively. This results in exciting standing waves strongly there for a large number of slots [1.32], [1.33].

The objectives of this thesis is to reveal the above-mentioned operation of the perpendicular-corporate feed as a feasibility study. Also, we elucidate the enhancement of the VSWR bandwidth by introducing other layers on the top of the radiating-slot layer in the perpendicular corporate feed. In addition, we demonstrate this multi-layered structure contributes to achieving the multi functionalities such as circular polarization, 45 deg. polarization and dual polarization by changing only the configuration of slots in layers, depending on operations.

In this thesis, we set a frequency range from 57.0 GHz to 66.0 GHz as a target, and so the center frequency is at 61.5 GHz except for the chapter 5 (62.625 GHz). The target bandwidth of the VSWR less than 1.5 is over 15.0 % as a guide.

1.6 Outlines of Remaining Chapters

The flow chart of this thesis is shown in Fig. 1.6.

Chapter 2 presents the design process and characterization of a perpendicular-corporate feed in a three-layer linearly-polarized parallel-plate slot array antenna. In the design process, we discuss the effect of dielectric, which porous polytetrafluoroethylene (porous PTFE) is used. Also, we describe the wideband design of the VSWR by introducing a parasitic-slot layer on the top of the radiating-slot layer, with an air gap in the region between the two.

Chapter 3 presents the design process and characterization of a perpendicular-corporate feed in a four-layer parallel-plate circularly-polarized slot array antenna. In the design process, we discuss the configuration of slots to generate the circular polarization. Considering the fabrication constraint, instead of using porous PTFE we describe how to form a new dielectric layer by the combination of PTFE ($\varepsilon_r = 2.17$) and air, achieving the desired permittivity ($\varepsilon_r = 1.28$) equivalently. Also, we elucidate how to improve the bandwidth of the VSWR and the axial ratio by introducing an additional-slot layer on top of a parasitic-slot layer, with an air gap in the region between the two.

Chapter 4 presents the design process and characterization of a perpendicular-corporate feed in a four-layer parallel-plate linearly-polarized slot array antenna. First, we discuss the design process of a wideband structure with an additional-slot layer in a linearly-polarized antenna. Secondly, the configuration of pair slot is introduced in the additional slot layer to suppress grating lobes of the above-mentioned antenna as a reference. Lastly, we explain how to create 45-deg. polarization based on linearly-polarized slot array antenna by inclining only additional slots at a 45-deg. angle with respect to the principal axis.

Chapter 5 presents the design process and characterization of a perpendicular-corporate feed in a three-layer parallel-plate dual-polarized slot array antenna. We discuss the design process of creating dual polarization by focusing on the configuration of slots. In this process, the layered structure of the feeding circuit is also included. To enhance the bandwidth of the VSWR, we describe the effect of introducing a parasitic-slot layer mounted on a new dielectric layer, with an air gap in the region between the dielectric layer and the radiating-slot layer.

In Chapter 6, this thesis is summarized and future studies are proposed.

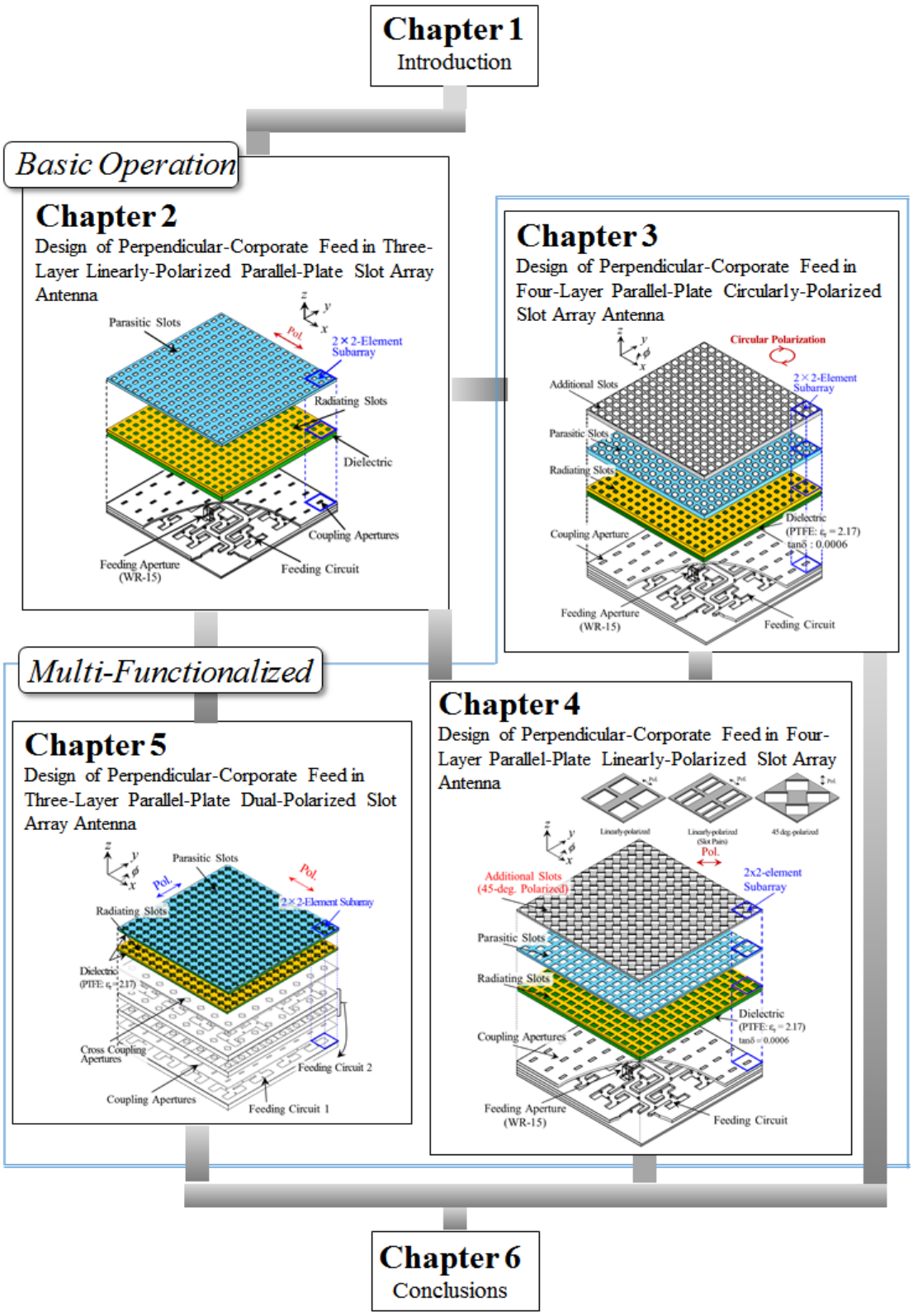

Fig. 1.6 Flow chart of thesis.

References

[1.1] Yoshihisa Yamagishi, NTT Docomo (2017), Telescope Magazine, Retrieved Aug. 24, 2018, from Tokyo Telecom Website:
http://www.tel.co.jp/museum/magazine/015/interview01/02.htm
[1.2] Jeffrey G. Andrews, Stefano Buzzi, Wan Choi; Stephen V. Hanly, Angel Lozano, Anthony C. K. Soong, Jianzhong Charlie Zhang, "What Will 5G Be?," IEEE Journal on Selected Areas in Communication, vol. 32, no. 6, pp.1065-1082, June 2014.
[1.3] Mamta Agiwal, Abhishek Roy, Navrati Saxena, "Next Generation 5G Wireless Networks: A Comprehensive Survey," IEEE communications Surveys & Tutorials, vol. 18, no. 3, pp. 1617 – 1655, Third Quarter 2016.
[1.4] W. Menzel, D. Pilz, and R. Leberer, "A 77-GHz FM/CW radar front-end with a low-profile low-loss printed antenna," IEEE Trans. Microw. Theory Tech., vol. 47, no. 12, pp. 2237-2241, Dec. 1999.
[1.5] W. Menzel, and A. Moebius, "Antenna concepts for millimeter-wave automotive radar sensors," Proc. IEEE, vol. 100, no. 7, pp. 2372-2379, July 2012.
[1.6] B. Biglarbegian, M. Fakharzadeh, D. Busuioc, Mohammad-Reza Nezhad-Ahmadi, and S. Safavi-Naeini, "Optimized microstrip antenna arrays for emerging millimeter-wave wireless applications," IEEE Trans. Antennas Propag., vol.59, no.5, pp. 1742-1747, May. 2011.
[1.7] T. S. Rappaport, J. N. Murdock, and F. Gutierrez, "State of the art in 60-GHz integrated circuits and systems for wireless communications," Proc. IEEE, vol. 99, no. 8, pp. 1390 - 1436, Aug. 2011.
[1.8] S. Rangan, T. S. Rappaport, and E. Erkip, "Millimeter-wave cellular wireless networks: potentials and challenges," Proc. IEEE, vol. 102, no. 3, pp. 366 - 385, Mar. 2014.
[1.9] A. Ghosh, T. A. Thomas, M. C. Cudak, R. Ratasuk, P. Moorut, F. W. Vook, T. S. Rappaport, G. R. MacCartney, S. Sun, and S. Nie, "Millimeter-wave enhanced local area systems: a high-data-rate approach for future wireless networks," IEEE J. Sel. Areas Comm., vol.32, no.6, pp. 1152 - 1163, June 2014.
[1.10] Ministry of Internal Affairs and Communications, "The Draft Guideline of the Establishment of Specific Base Stations to Introduce 5G Mobile Communication Systems," Nov. 2018, Website: http://www.soumu.go.jp/main_content/000582765.pdf
[1.11] R. Fellers, "Millimeter waves and their applications," Electrical Engineering, vol.

75, no. 10, pp. 914-917, Oct. 1956.
[1.12] C. Tolbert, and A. Straiton, “Experimental measurement of the absorption of millimeter radio waves over extended ranges,” IEEE Trans. Antennas Propag., vol. 5, no. 2, pp. 239-241, Apr. 1957.
[1.13] J. Huang, and Y. Rahmat-Samii, “Fan Beam Generated by a Linear-Array Fed Parabolic Reflector,” IEEE Trans. Antennas Propag., vol.38, no. 7, pp.1046-1053, July 1990.
[1.14] D.M. Pozar, S.D. Targonski, and H.D. Syrigos, “Design of Millimeter Wave Microstrip Reflectarrays,” IEEE Trans. Antennas Propag., vol.45, no. 2, pp.287-296, Feb. 1997.
[1.15] Y. Kimura, Y. Miura, T. Shirosaki, T. Taniguchi, Y.Kazama, J. Hirokawa and M. Ando, “A low-cost and very compact wireless terminal integrated on the back of a waveguide planar array for 26GHz band Fixed Wireless Access (FWA) systems,” IEEE Trans. Antennas Propag., vol.53, no. 8, pp.2456-2463, Aug.2005.
[1.16] S. Park, Y. Tsunemitsu, J. Hirokawa and M. Ando,Center Feed Single Layer Slotted Waveguide Array, ” IEEE Trans. Antennas Propag., vol.54, no.5, pp.1474-1480, May 2006.
[1.17] S. Fujii, Y. Tsunemitsu, G. Yoshida, N. Goto, J. Hirokawa, and M. Ando, “Partially Corporate Feed using E-plane Coupler in a Single-Layer Slotted Waveguide Array,” IEICE Technical Report, vol. 107, no.431, AP2007-150, pp.163-168, Jan. 2008.
[1.18] Y. Miura, J. Hirokawa, M. Ando, Y. Shibuya, and G. Yoshida, “Double-layer full-corporate-feed hollow-waveguide slot array antenna in the 60-GHz band,” IEEE Trans. Antennas Propag., vol.59, no.8, pp.2844-2851, Aug. 2011.
[1.19] T. Tsugawa, Y. Sugio, and Y. Yamada, “Circularly Polarized Dielectric-Loaded Planner Antenna Excited by the Parallel Feeding Waveguide Network,” IEEE Trans. Broadcasting, vol. 43, no. 2, pp. 205-212, June 1997.
[1.20] T. Sehm, A. Lehto, and A. V. R¨ais¨anen, “A High-Gain 58-GHz Box-Horn Array Antenna with Suppressed Grating Lobes,” IEEE Trans. Antennas Propag., vol.47, no. 7, pp.1125-1130, July 1999.
[1.21] S.-S. Oh, J.-W. Lee, M.-S. Song and Y.-S. Kim, “Two-layer slotted-waveguide antenna array with broad reflection/gain bandwidth at millimetre-wave frequencies,” IEE Proc.-Microw. Antennas Propag., vol.51, no. 5, pp. 393-398, Oct. 2004.
[1.22] T. Yamamoto, M. Zhang, J. Hirokawa, T. Hirano, and M. Ando, “Wideband design of a circularly-polarized plate-laminated waveguide slot array antenna,” Intl. Symp. Antenna Propagat., WE1B-02, Dec. 2014.
[1.23] T. Tomura, J. Hirokawa, T. Hirano, and M. Ando, “A 45-degree linearly polarized

hollow–waveguide 16 ×16-slot array antenna covering 71–86 GHz band," IEEE Trans. Antennas Propag., vol. 62, no. 10, pp. 5061-5067, Oct. 2014.
[1.24] G.-L. Huang, S.-G. Zhou, T.-H. Chio, and T.-S. Yeo, "3-D metal-direct-printed wideband and high-efficiency waveguide-fed antenna array," 2015 IEEE MTT-S Intl. Microw. Symp., DOI: 10.1109/MWSYM.2015.7166882, May 2015
[1.25] Y. J. Li, and K. M. Luk, "60-GHz substrate integrated waveguide fed cavity-backed aperture-coupled microstrip patch antenna arrays," IEEE Trans. Antennas Propag., vol. 63, no. 3, pp. 1075-1085, Mar. 2015.
[1.26] X. Xu, M. Zhang, J. Hirokawa, and M. Ando, "E-band plate-laminated waveguide filters and their integration into a corporate-feed slot array antenna with diffusion bonding technology," IEEE Trans. Micro. Theory Tech., vol. 64, no. 11, pp. 3592 - 3603, Nov. 2016.
[1.27] H. Kirino, and K. Ogawa, "A 76 GHz phased array antenna using a waffle-iron ridge waveguide," Proc. Euro. Conf. Antenna Propag., C32P2-2, Apr. 2010.
[1.28] H. Kirino, and K. Ogawa, "A 76 GHz multi-layered phased array antenna using a non-metal contact metamaterial waveguide," IEEE Trans. Antennas Propag., vol. 60, no. 2, pp. 840 - 853, Feb. 2012.
[1.29] P.-S. Kildal, E. Alfonso, A. Valero-Nogueira, and E. Rajo-Iglesias, "Local metamaterial-based waveguides in gaps between parallel metal plates," IEEE Antennas Propag. Lett., vol. 8, no. 4, pp. 84-87, Apr. 2009.
[1.30] P. -S. Kildal, A. U. Zaman, E. Rajo-Iglesias, E. Alfonso, and A. Valero-Nogueira "Design and experimental verification of ridge gap waveguide in bed of nails for parallel-plate mode suppression," IET Microw., Antenna Propag., vol. 5, no. 3, pp. 262-270, Feb. 2011.
[1.31] D. Zarifi; A. Farahbakhsh, A. Uz Zaman, and P.-S. Kildal "Design and fabrication of a high-gain 60-GHz corrugated slot antenna array with ridge gap waveguide distribution layer," IEEE Trans. Antennas Propag., vol. 64, no. 7, pp. 2905 – 2913, July 2016.
[1.32] K. Tsukamoto, and H. Arai, "Characteristic of linearly polarized aperture array antenna," IEICE Trans. Commun., vol. J78-B-II, no. 3, pp. 160-166, Mar. 1995.
[1.33] K. Tsukamoto, and H. Arai, "Input characteristic of tri-plate aperture array antenna," IEICE Trans. Commun., vol. J79-B-II, no. 1, pp. 26-32, Jan. 1996.

Chapter 2

Design of Perpendicular-Corporate Feed in Three-Layer Linearly-Polarized Parallel-Plate Slot Array Antenna

2.1 Introductory Remarks

This chapter presents a perpendicular-corporate feed in a three-layered parallel-plate radiating slot array. This antenna enables the complete removal of the x-shaped cavity walls in the radiating part of conventional planar corporate-feed waveguide slot array antennas [2.1]. The coupling apertures at the bottom excite the radiating slots placed with the half spacing of coupling apertures. This enables the corporate feed in the perpendicular direction so that the number ratio of the radiating slots over the coupling apertures can be 4:1 in a two-dimensional array. A dielectric layer is placed in the region between the coupling-aperture layer and the radiating-slot layer allowing the equivalent spacing of the coupling apertures and the radiating slots to be two and one wavelength respectively in this dielectric-filled region. These wavelengths are capable of exciting standing waves strongly for a large number of slots [2.2], [2.3], and this structure contributes to avoiding metal contact without using any rods in only the radiating part. Also, to enhance the VSWR bandwidth, the antenna has a parasitic-slot layer over the radiating-slot layer with an air gap between the two.

This chapter is organized as follows. Section 2.2 describes the antenna configuration. In section 2.3, we present the design procedure of the perpendicular-corporate feed by using a 2×2-element subarray as a feasibility study. An 8×8-element subarray is analyzed to describe the effect of the dielectric. The effect of parasitic slots for wideband design is also confirmed by the analysis of both the 2×2-element subarray and 8×8-element subarray. Then, the simulated results of a 16×16-element array fed by a planar corporate-feed circuit are discussed. In section 2.4, we compare the measured results of the fabricated antenna with the simulated ones. In section 2.5, we conclude this chapter. The above-mentioned design flow is described in Fig .2.1 and applied for chapter

3, 4 and 5. We analyze models by using the Finite Element Method (FEM) and measure prototypes by using a network analyzer, a spectrum analyzer in this thesis. Note that we have not had measurement of antennas described in the chapter 4 and 5 yet.

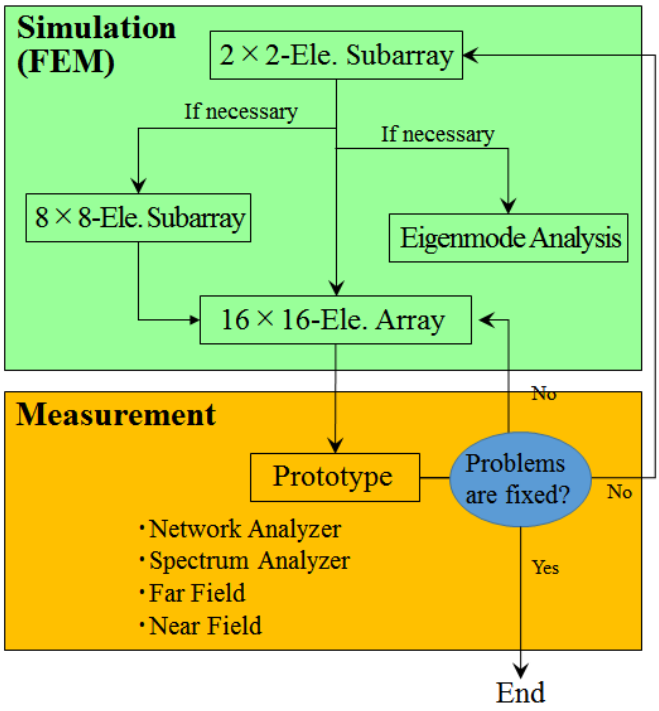

Fig. 2.1 Design flow.

2.2 Antenna Configuration

Fig. 2.2 shows the configuration of a perpendicular-corporate feed in a three-layered parallel-plate slot array antenna. The antenna consists of a parasitic-slot layer, a radiating-slot layer with dielectric and a coupling-aperture layer with a planar feeding circuit. In Fig. 2.2, the layers are described with a distance to show the internal structure. However, in the actual antenna, they are stacked much more closely together. The antenna is fed by the feeding aperture, which is the same size as the standard waveguide WR-15, from its backside. The feeding circuit is a planar-corporate feed composed of H-planes and T-junctions. The coupling-aperture layer is placed between the feeding circuit and the dielectric. The radiating-slot layer is mounted on the dielectric directly. The parasitic-slot layer is placed on the top of the radiating-slot layer with an air gap. this air gap between the radiating-slot and the parasitic-slot layers is hollow. For radiating slots and parasitic ones, the slot spacing is constant: $0.86\lambda_0$ (4.20 mm) in the x and y directions. λ_0 is the wavelength at the design frequency of 61.5 GHz. The polarization is along the x-axis.

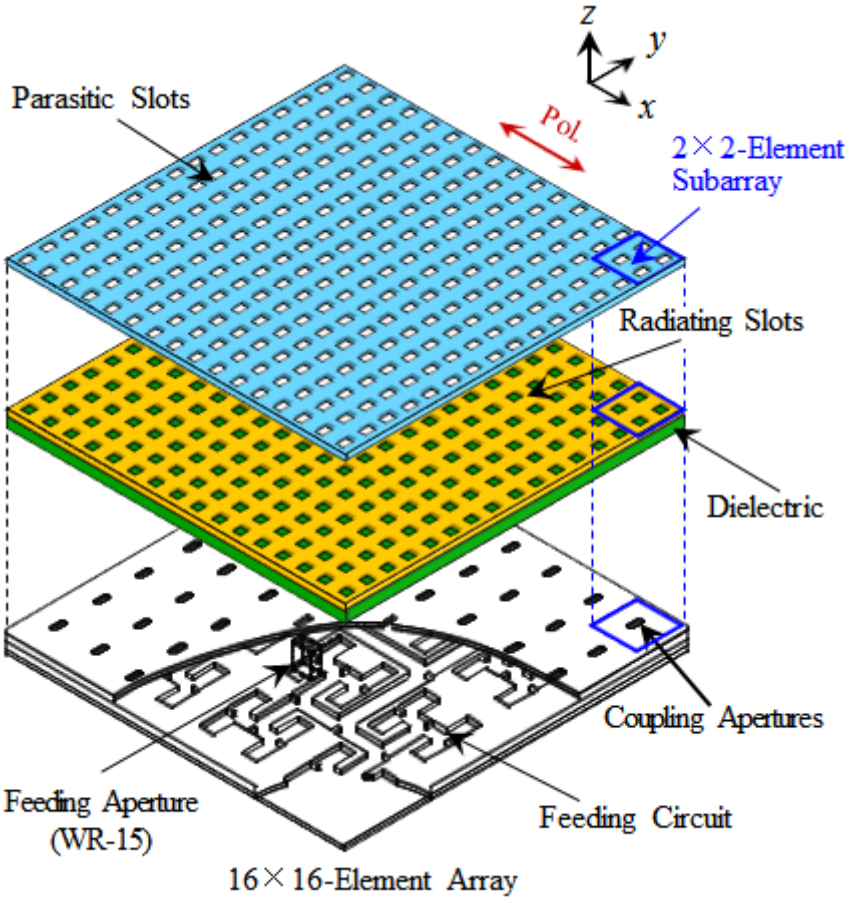

Fig. 2.2 Perpendicular-corporate feed in a three-layered parallel-plate slot array antenna.

2.3 Design

2.3.1 Effect of Dielectric

Fig. 2.3 shows the structural difference between the proposed and the conventional models in the 2×2-element subarray. In the external regions, two sets of periodic boundaries and a radiation boundary are introduced as well as in Fig.2.4, even though they are not shown in Fig. 2.3. The two sets of periodic boundaries are used to include the mutual coupling in the infinite two-dimensional array. The conventional model holds electromagnetic field in the x-shaped cavity by the side walls of PEC (perfect electrical conductor). On the other hand, the proposed model removes the side walls and fills dielectric with adequate permittivity in the region between the coupling-aperture layer and the radiating-slot layer so that the effective electrical size can be increased from 1.72 free-space wavelength to two wavelengths (about 1.72 $\lambda_0 \times \sqrt{\varepsilon_r}$). They lead to exciting standing waves in the region. The pink parallelograms are ports for the simulations.

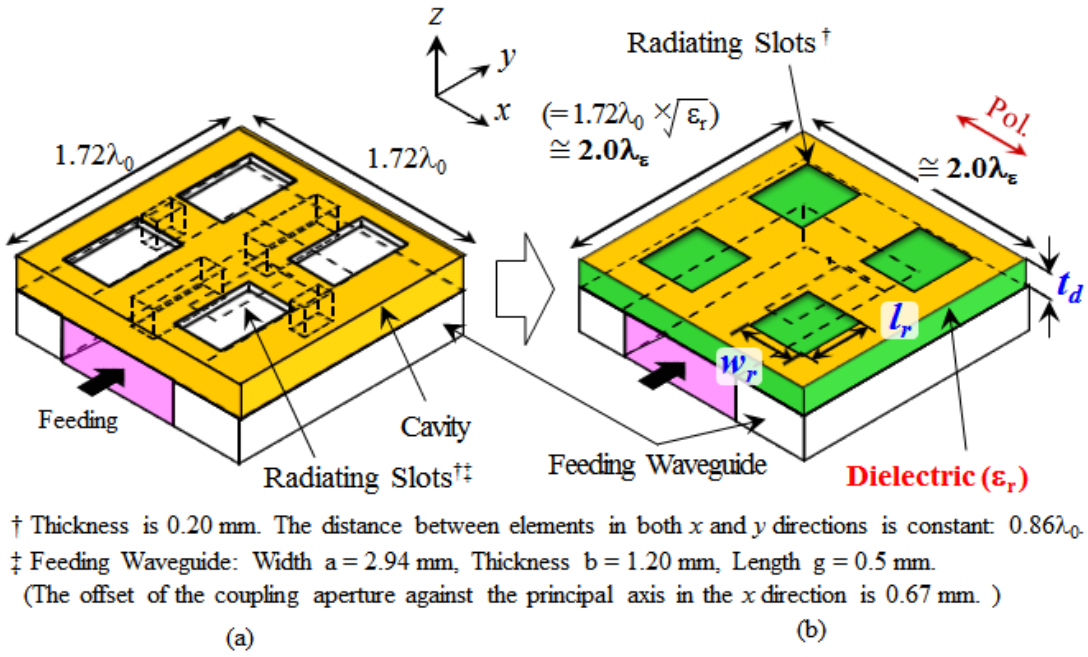

Fig. 2.3 Difference between the conventional (a) and the proposed (b) models.

Fig. 2.4 is particulars of the model for the analysis of the 8×8-element subarray including the symmetry of the 16×16-element array. The radiating-slot layer with dielectric, and PEC, PMC (perfect magnetic conductor) and radiation boundaries at the front are described with a distance from the coupling-aperture layer to show the internal structure of the feed. Each of the coupling apertures is fed by a longitudinal coupling aperture on the broad wall of a waveguide as shown in Fig. 2.3 (b). Around the periphery of the 8×8-element subarray, PEC boundaries parallel to the *yz*-plane and PMC boundaries parallel to the *xz*-plane are introduced for the *x*-polarized operation. The parallel plates are truncated by PEC and PMC by considering the polarization. For the external region, radiation boundaries are introduced for analyzing by ANSYS HFSS Ver. 16.

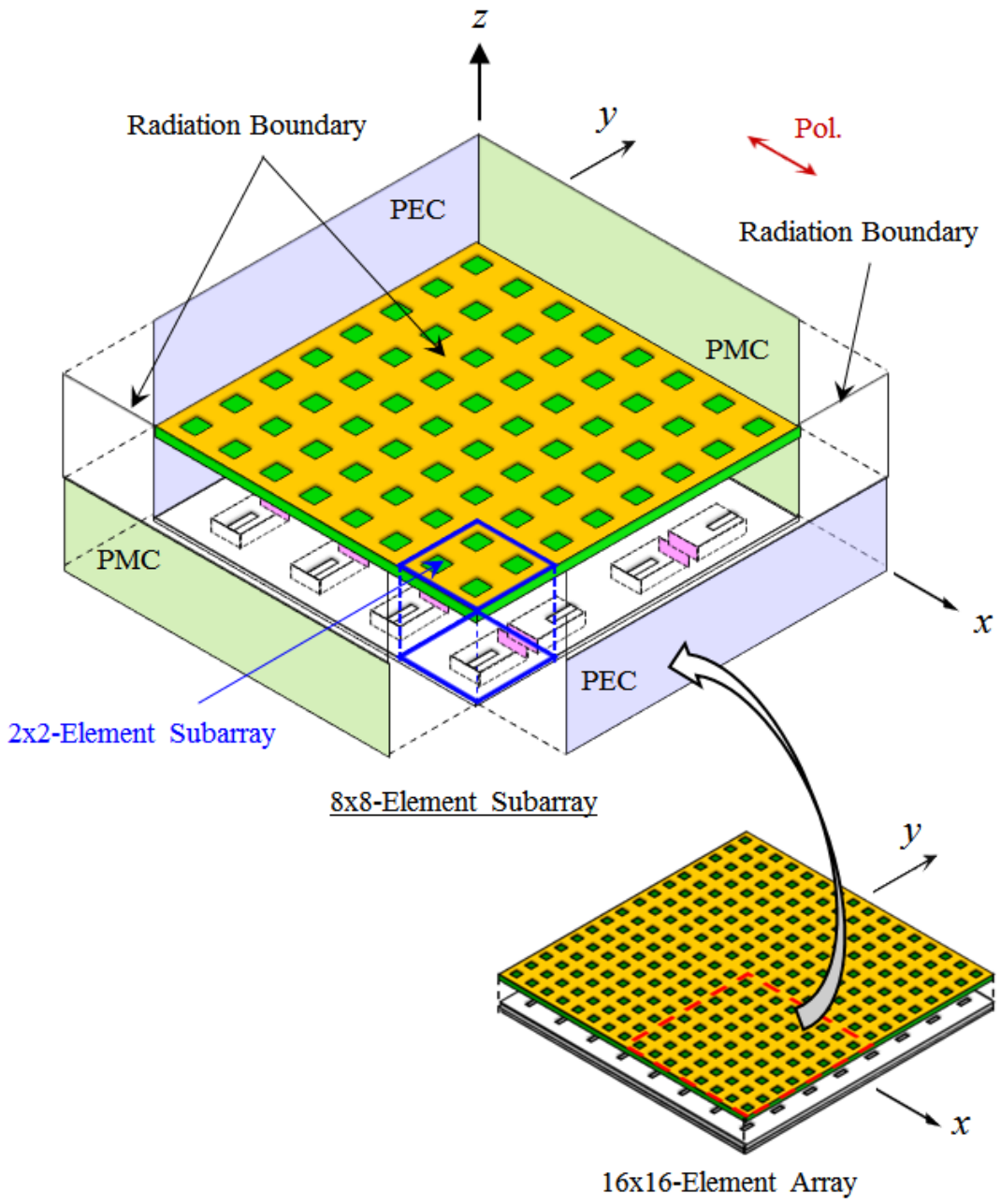

Fig. 2.4 Model for the analysis of the 8×8-element subarray.

We analyze both the 2×2-element and the 8×8-element subarrays. The size of the feeding waveguide is fixed: width a = 2.94 mm, height b = 1.20 mm and length g = 0.5 mm, and it has short end. The offset of the coupling aperture against the principal axis in the x direction is also fixed: 0.67 mm. The parameters are the size l_r and w_r of the radiating slots, the thickness t_d of the dielectric and its relative permittivity ε_r as shown in Fig. 2.3 (b). These parameters are determined so that the desired operation can be achieved where the frequency characteristic of the reflection of the 16 coupling apertures should be identical in the 8×8-element subarray and should agree with that of the 2×2-element subarray. Furthermore, the other parameters relating to the coupling aperture are determined to minimize the reflection at the design frequency. Once the desired operation is achieved, all the radiating slots are considered as excited uniformly because of their periodic arrangement.

Fig. 2.5 shows the frequency characteristic of reflections from 16 coupling apertures in the 8×8 radiating slot subarray by 16 gray lines for ε_r = 1.00 and ε_r = 1.28. All the reflections include the action of phase and amplitude caused by all the 16 coupling apertures. A red dashed line shows the reflection from the coupling aperture in the 2×2 radiating slot subarray as reference. For ε_r = 1.28 the above-mentioned desired operation is achieved while for ε_r = 1.00 it is not. When the dielectric constant is changed, the effective wavelength in the dielectric region is changed. As a result, for ε_r = 1.28, the effect from a radiating slot to adjacent slots and that from the adjacent slots to the radiating slot are balanced, so that all the radiating slots in the 8×8-element subarray are expected to have uniform excitation. However, for ε_r = 1.00, these two effects are unbalanced, so that the radiating slots in the 8×8-element subarray are excited differently. The effect of the dielectric is confirmed. However, the bandwidth for the VSWR less than -14 dB is very narrow, about 0.5 %.

To support the frequency characteristic of the reflections as shown in Fig. 2.5 (b), we also show the E-field distribution (f = 61.5 GHz) on the cross section (xz-plane) of the 8×8-element subarray in Fig. 2.6 as a physical interpretation. In addition, Fig 2.7 describes a certain image of incident waves, reflected waves and synthetic waves in the 2×2-element subarray with dielectric or air for the better understanding. When ε_r is 1.28, standing waves are generated in the xz plane, resulting in uniform excitation in Fig. 2.6 (b) because the electrical wavelength is enhanced and almost becomes 2.00 λ_ε (about 1.72 $\lambda_0 \times \sqrt{\varepsilon_r}$) as referred in Fig. 2.7 (b). In other words, as introduced dielectric (ε_r = 1.28) shortens the electrical wavelength, the effective size in 2×2-element subarrays can be extended to 2.00 λ_ε equivalently there. In consequence, ε_r with 1.28 can create

standing waves in the 8×8-element subarray and strong E-field is arisen under both the edges of radiating slots, having uniform excitation there. On the other hand, when ε_r is 1.00, there is not strong E-field in the *xz* plane in Fig 2.6 (a). Especially, the edge of the 8×8-element subarray does not have E-field at all. Waves of E-field are canceled out together due to the phase difference between incident waves and reflected waves depending on the physical wavelength of 1.72 λ_0, and so strong E-field is not generated under both the edges of radiating slots as referred in Fig. 2.7(a).

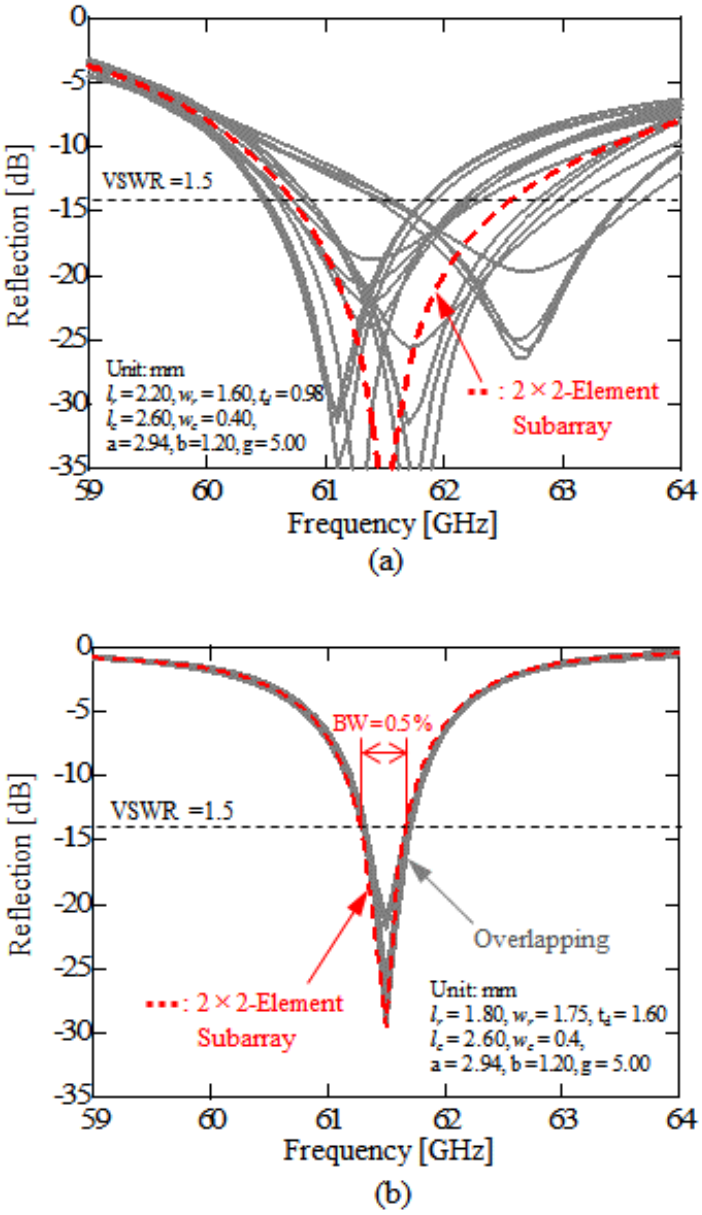

Fig. 2.5 Frequency characteristic of reflections. (a) ε_r = 1.00. (b) ε_r = 1.28.

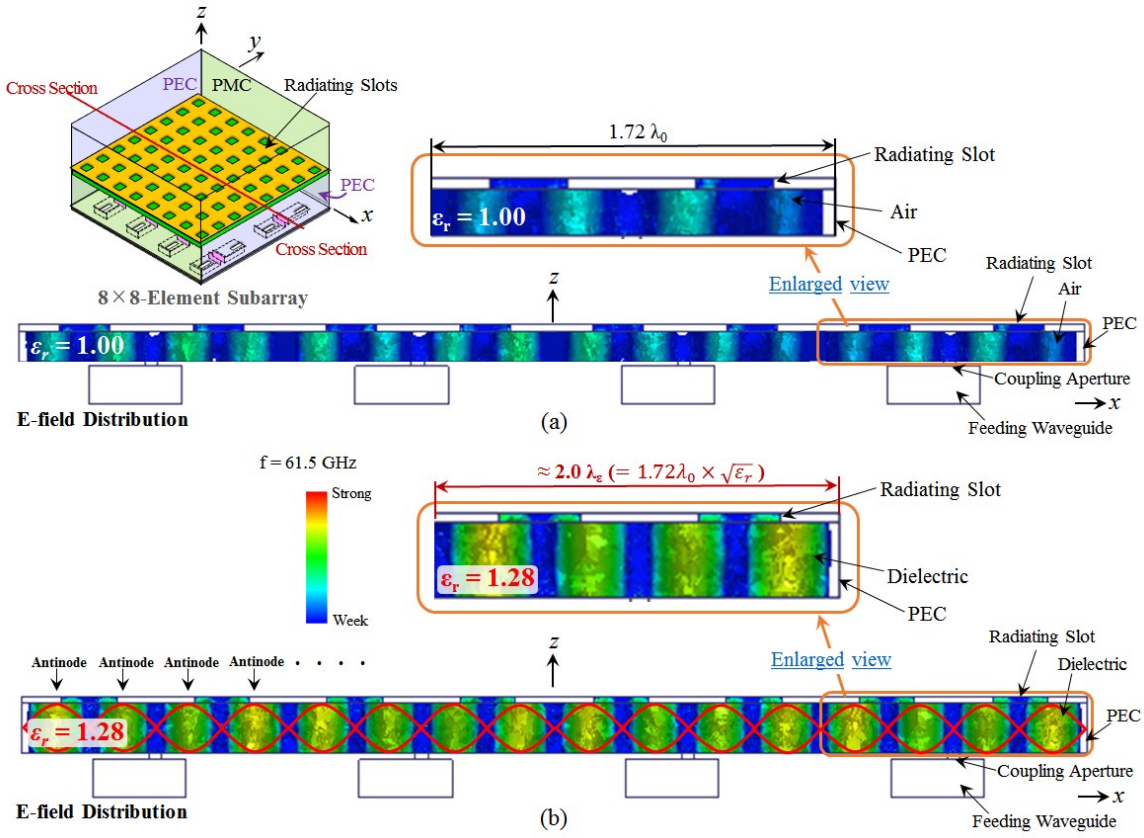

Fig. 2.6 E-field distribution on the cross section of the 8×8-element subarray. (a) $\varepsilon_r = 1.00$. (b) $\varepsilon_r = 1.28$.

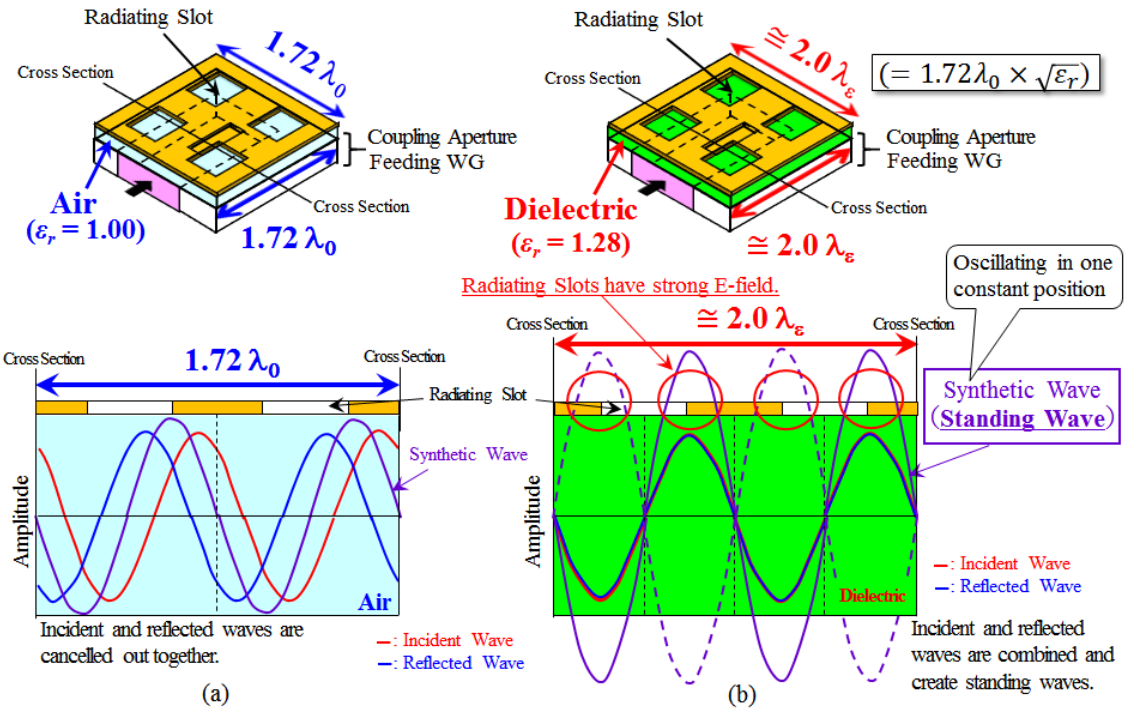

Fig. 2.7 Image of incident waves, reflected waves and synthetic waves in the 2×2-element subarray. (a) $\varepsilon_r = 1.00$. (b) $\varepsilon_r = 1.28$.

2.3.2 Effect of Parasitic Slots

To improve the bandwidth for $\varepsilon_r = 1.28$, we place the parasitic-slot layer over the radiating-slot layer with an air gap in between two. Fig. 2.8 shows a 2×2-element subarray with parasitic slots. The parameters are the size of the parasitic slots: l_p and w_p, and the spacing between the parasitic-slot and the radiating-slot layers: h_{pr}. We also include l_r, w_r, l_c, w_c and t_d into the parameters in the analysis. The size of the feeding waveguide is fixed: width a = 2.94mm, thickness b = 1.00mm and length g =5.59 mm, and it has short end. The offset of the coupling aperture against principal axis in the x direction is also fixed: 0.58 mm. Fig. 2.9 shows the analysis model of the 8×8-element subarray with the parasitic-slot layer. The design process is the same as that of the previous subsection.

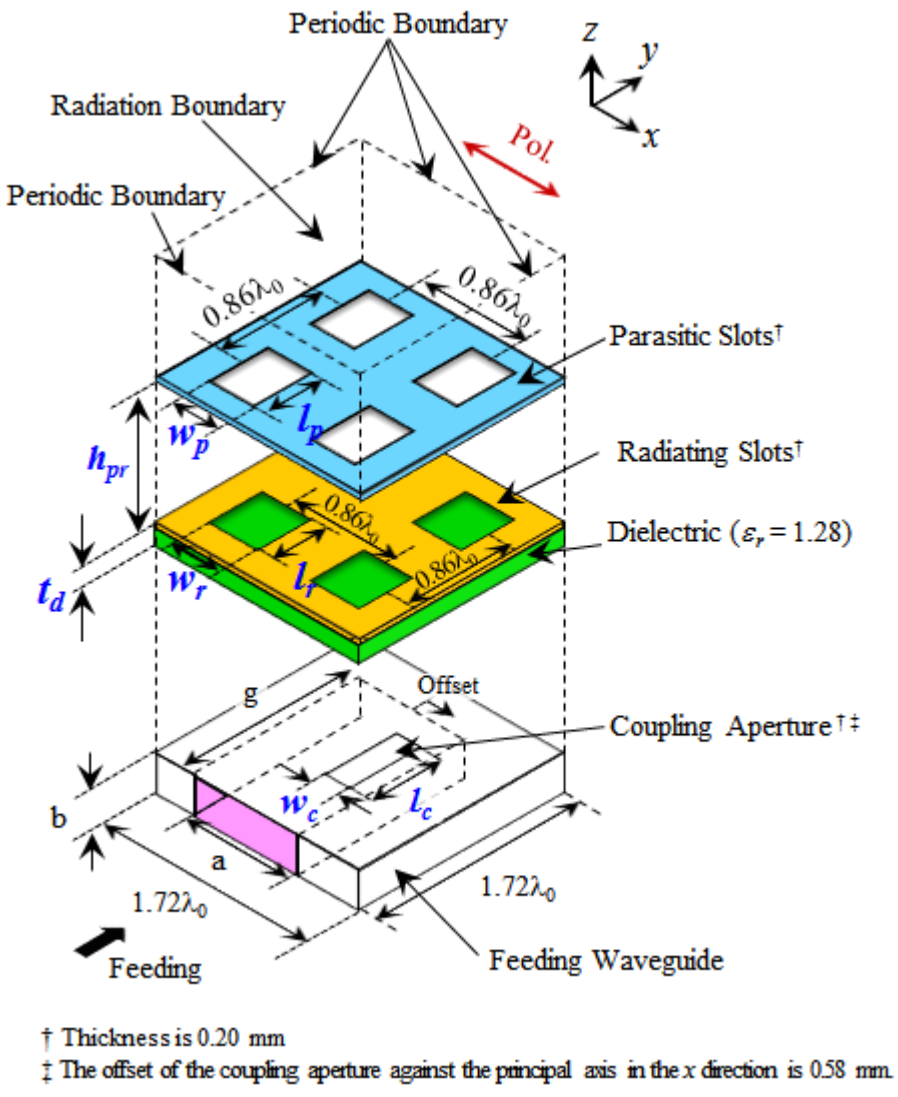

† Thickness is 0.20 mm
‡ The offset of the coupling aperture against the principal axis in the x direction is 0.58 mm.

Fig. 2.8 2×2-element subarray with parasitic slots.

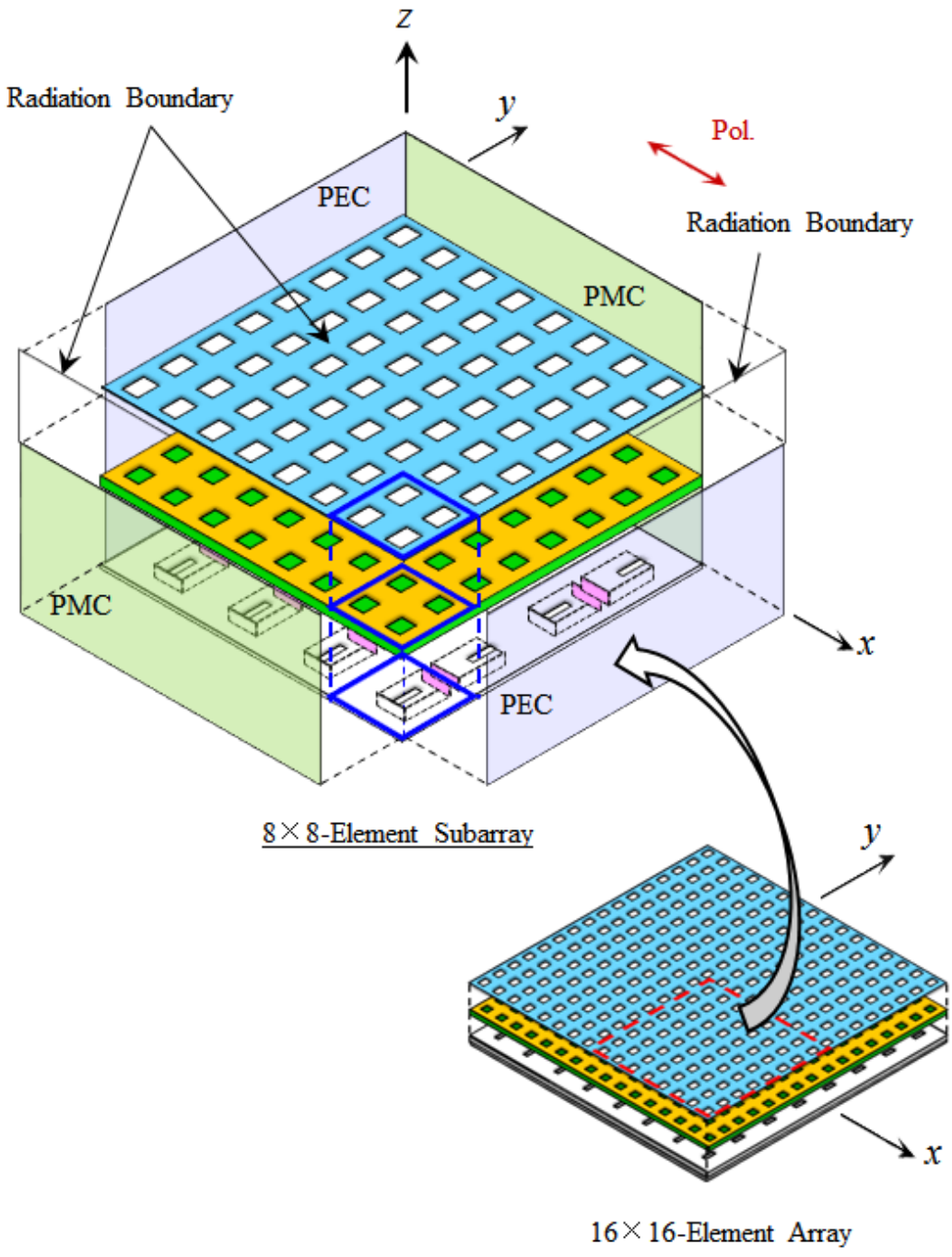

Fig. 2.9 Analysis model of the 8×8-element subarray with the parasitic-slot layer.

Fig. 2.10 shows the frequency characteristic of the reflection. The reflection of the 2×2-element subarray is less than -14 dB over 7.7 % bandwidth ranging from 59.1 GHz to 63.9 GHz. The bandwidth is improved from 0.5 % to 7.7 % by placing the parasitic-slot layer. The deviation of the frequency characteristic of the reflection among the 16 coupling apertures in the 8×8-element subarray cannot be suppressed completely; however, it is small.

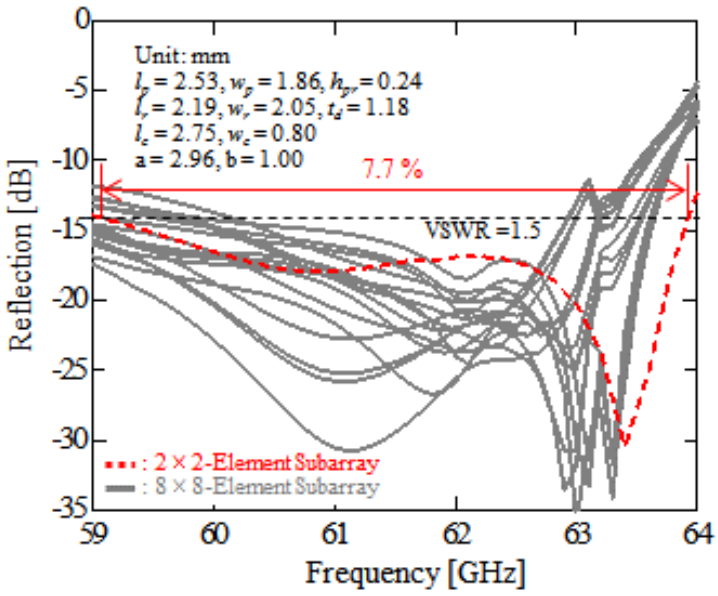

Fig. 2.10 Frequency characteristic of reflections.

2.3.3 Full Structure Analysis

Fig. 2.11 shows the full structure of a perpendicular-corporate feed in a three-layered parallel-plate slot array antenna. In Fig. 2.11, the plates are described with a distance to show the internal structure. However, in the actual antenna, they are stacked. In the simulation, the conductivity 5.8×10^7 S/m of copper and the loss tangent 0.002 of the dielectric are assumed. The periphery of the three-layered parallel plates is terminated by copper, considering the fabrication to keep the flatness. Note that this copper termination does not mean to form a large cavity for the antenna operation. The operation as the large cavity could degrade the antenna characteristic. All the metal plates are connected by fixing screws in the fabrication.

Fig. 2.12 shows the periphery of structure. The edge as PMC of the parallel plates only in the y direction is extended by 1.2 mm ($\approx 0.25\lambda_0$) and terminated by a conductor.

The dimension of the antenna in the *xy* plane is 81.0 mm × 79.0 mm. Although we slightly modify only h_{pr} (0.24 → 0.20 mm) and td (1.18 → 1.20 mm) to consider the fabrication limitation on the thickness of the copper plate and the dielectric, the parameters of the antenna are the same as the 8×8-element array with the parasitic-slot layer.

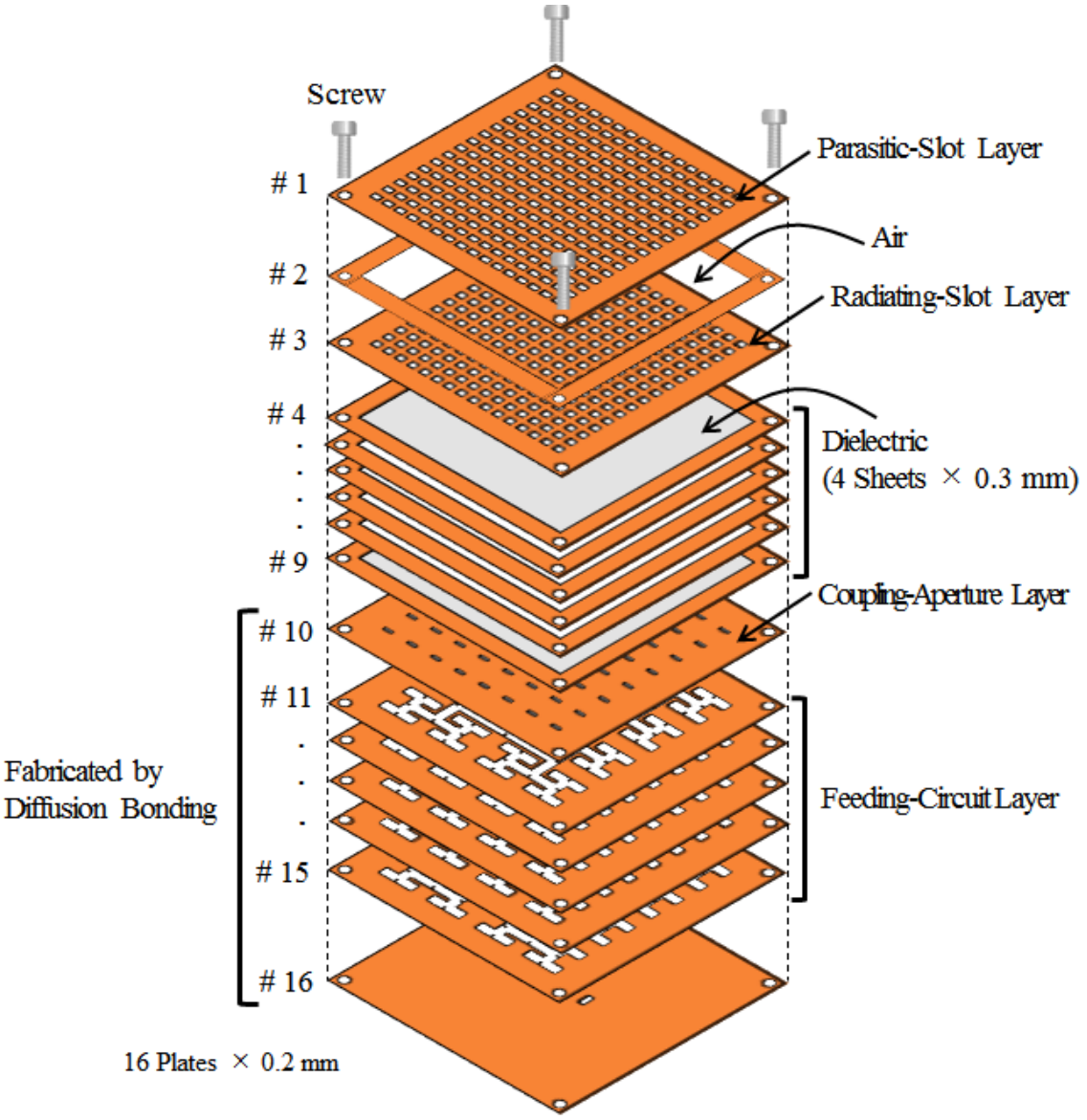

Fig. 2.11 Full structure of the perpendicular-corporate feed in the three-layered parallel-plate slot array antenna.

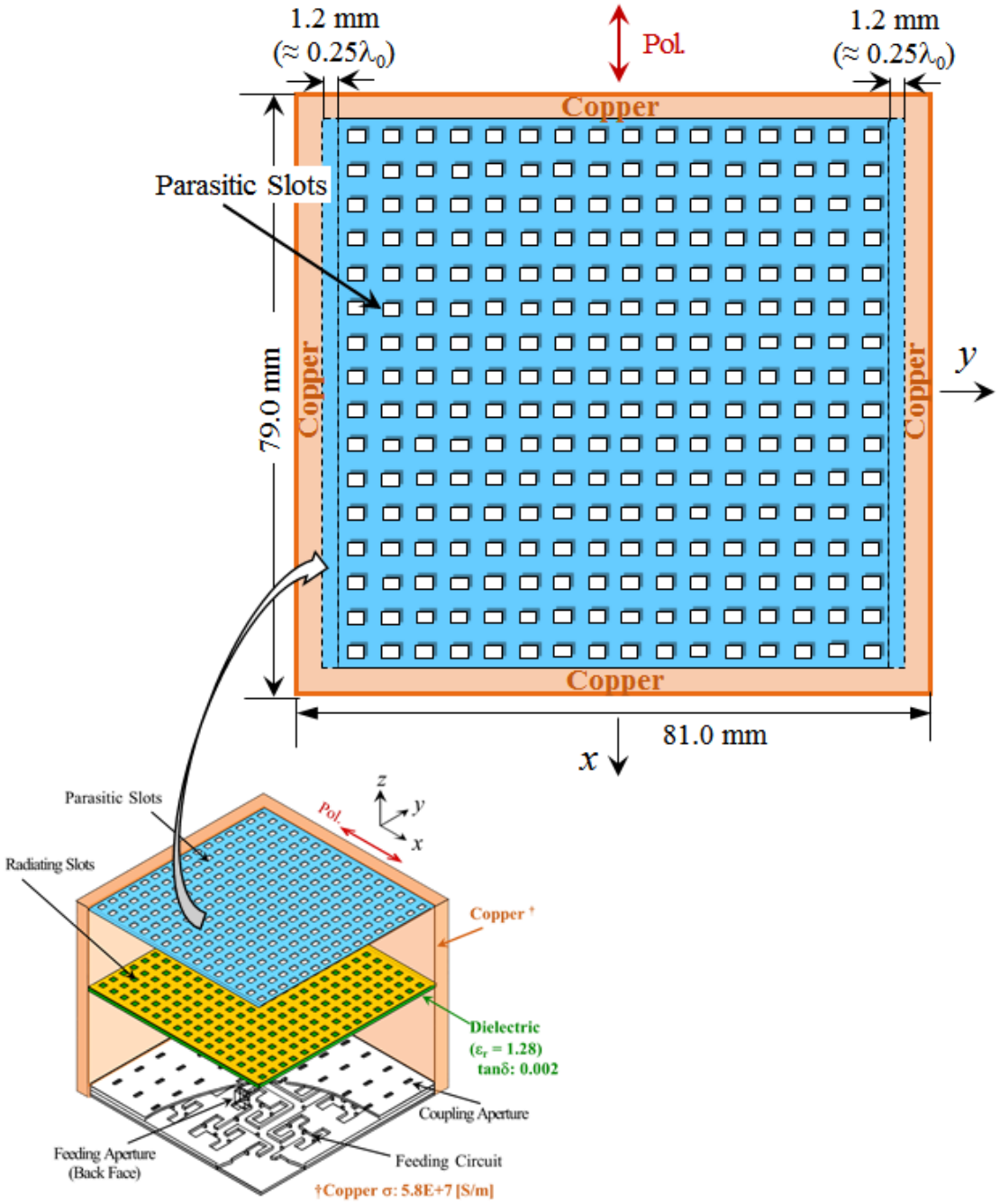

Fig. 2.12 Periphery of the structure.

Fig. 2.13 shows the frequency characteristic of the reflection. The reflection of the antenna is less than -14 dB over 7.3 % bandwidth ranging from 59.1 GHz to 63.6 GHz. The bandwidth is the almost same as that of the 2×2-element subarray. The reflection of the antenna has a ripple caused by the reflection of the planar corporate-feed circuit. The final design parameters are listed in Table I.

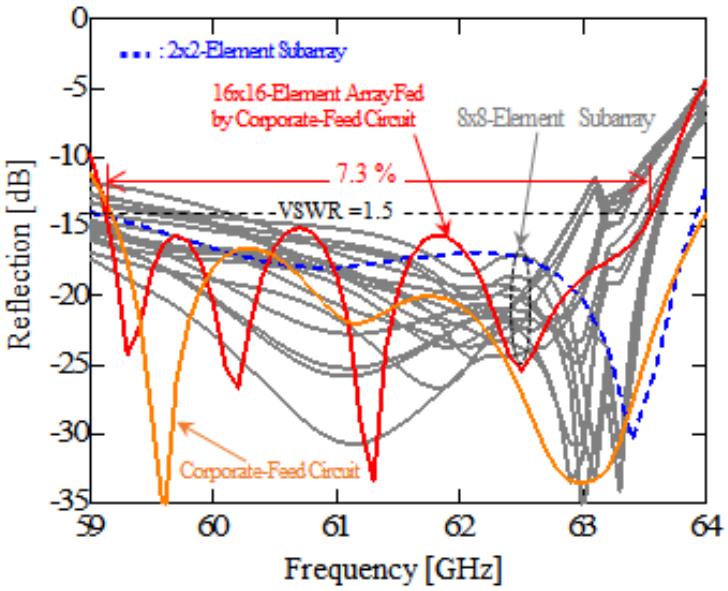

Fig. 2.13 Frequency characteristic of the reflection.

TABLE I

Design parameters of the perpendicular-corporate feed in the three-layered parallel-plate slot array antenna.

Fixed Parameters		
Relative permitivity of the Dielectric	ε_r	1.28
Dielectric loss tangent	tanδ	0.002
Width of the Feeding Waveguide	a	2.96 mm
Thickness of the Feeding Waveguide	b	1.00 mm
Length of the Feeding Waveguide	g	5.59 mm
Offset of C.A. Against Principal Axis	-	0.58 mm
Thickness of the Bottom of the Feeding WG	-	0.20 mm
Thickness of the Coupling Aperture	-	0.20 mm
Thickness of Radiating Slot	-	0.20 mm
Thickness of the Parasitic Slot	-	0.20 mm
Variable Parameters		
Length of the Coupling Aperture	l_c	2.75 mm
Width of the Coupling Aperture	w_c	0.80 mm
Length of Radiating Slot	l_r	2.19 mm
Width of Radiating Slot	w_r	2.05 mm
Thickness of the Dielectric	t_d	1.20 mm
Length of the Parasitic Slot	l_p	2.53 mm
Width of the Parasitic Slot	w_p	1.86 mm
Spacing Between the Par. Slot and Rad. One	h_{pr}	0.20 mm

2.4 Experimental Results

2.4.1 Fabricated Antenna

Fig. 2.14 shows the photos of the fabricated antenna. The total number of plates is 16. The feeding-circuit layer with the coupling-aperture layer composed of 7 plates is fabricated by the diffusion bonding of laminated thin copper plates. We screw the rest of plates with the feeding-circuit layer including the coupling-aperture layer after putting the dielectric between the coupling-aperture layer and the radiating-slot layer. The material of the dielectric is porous PTFE (Polytetrafluoroethylene). Its relative permittivity is 1.25 in the measurements, slightly smaller than that in the simulations. The region between the radiating-slot and parasitic-slot layers is mechanically supported by a copper frame (plate #2) as shown in Fig. 2.11. The dimension of each plate is 79.0 mm × 81.0 mm. The total thickness of the fabricated antenna is 3.2 mm; 1.2 mm for the feeding-circuit layer, 0.2 mm for the coupling-aperture layer, 1.2 mm for the dielectric, 0.2 mm for the radiating-slot layer, 0.2 mm for the spacing between the radiating-slot and the parasitic-slot layers, and 0.2 mm for the parasitic-slot layer. We attach a choke flange and its thickness is 6.0 mm, to the antenna by screws to connect a standard WR-15 waveguide for the measurement. The thickness of 6.0 mm is not required for the antenna operation, but for inserting the choke flange pins.

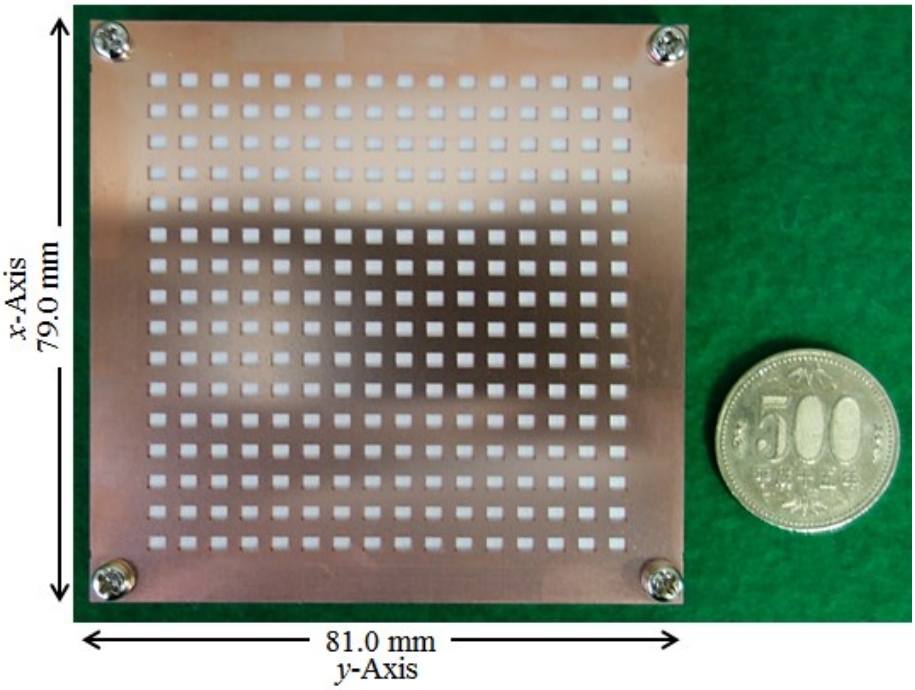

(a) Top view

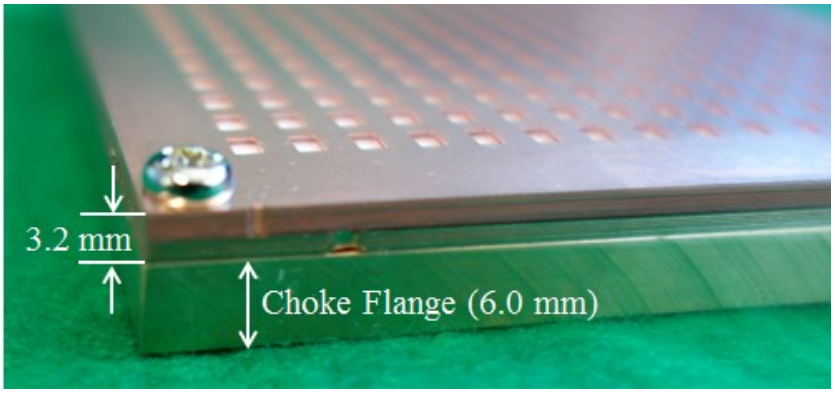

(b) Side view

Fig. 2.14 Photos of the fabricated antenna. (a) Top view. (b) Side view.

2.4.2 Reflection

Fig. 2.15 shows the measured and the simulated reflection characteristic. Each result includes the reflection characteristic of a choke flange. There is a large reflection in measurement. To identify the reason, Fig. 2.16 shows the time-gating analysis by a vector network analyzer (VNA). The frequency range used in the VNA is from 56 GHz – 94 GHz. The time-domain response has two large reflections as shown in Fig. 2.16 (a). We estimate one comes around the feeding aperture and the other comes around the radiating part. The frequency-domain response from each of them is added in Fig. 2.16 (b). The reflection around the radiating part is comparable with the overall reflection from 58 GHz to 65 GHz. However, the reflection around the feeding aperture is small around this frequency band. We conclude the main reason of the large reflection comes around the radiating part. In order to support this reason, we simulate reflection by changing the relative permittivity of the dielectric as shown in Fig. 2.17. Lower permittivity can simulate the large reflection in measurement. The region between the radiating-slot layer and coupling-aperture layer is filled by stacking four thin dielectric sheets. Small air gaps among the dielectric sheets could be created, decreasing the relative permittivity equivalently. Other reasons such as the size errors in the radiating slots and parasitic slots would be possible. As an example, Fig. 2.18 shows the reflection for changing length of the radiating slots. The reflection is not degraded significantly for ± 20 μm change.

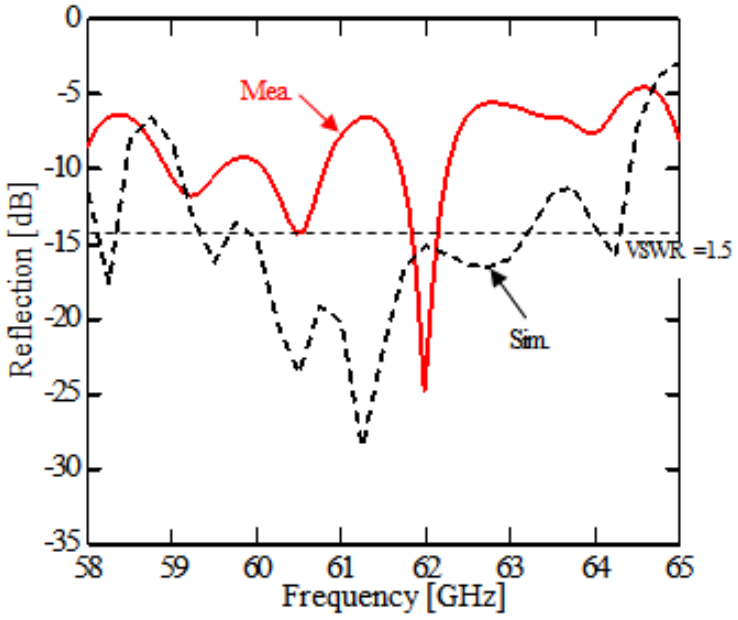

Fig. 2.15 Measured and simulated reflection characteristic.

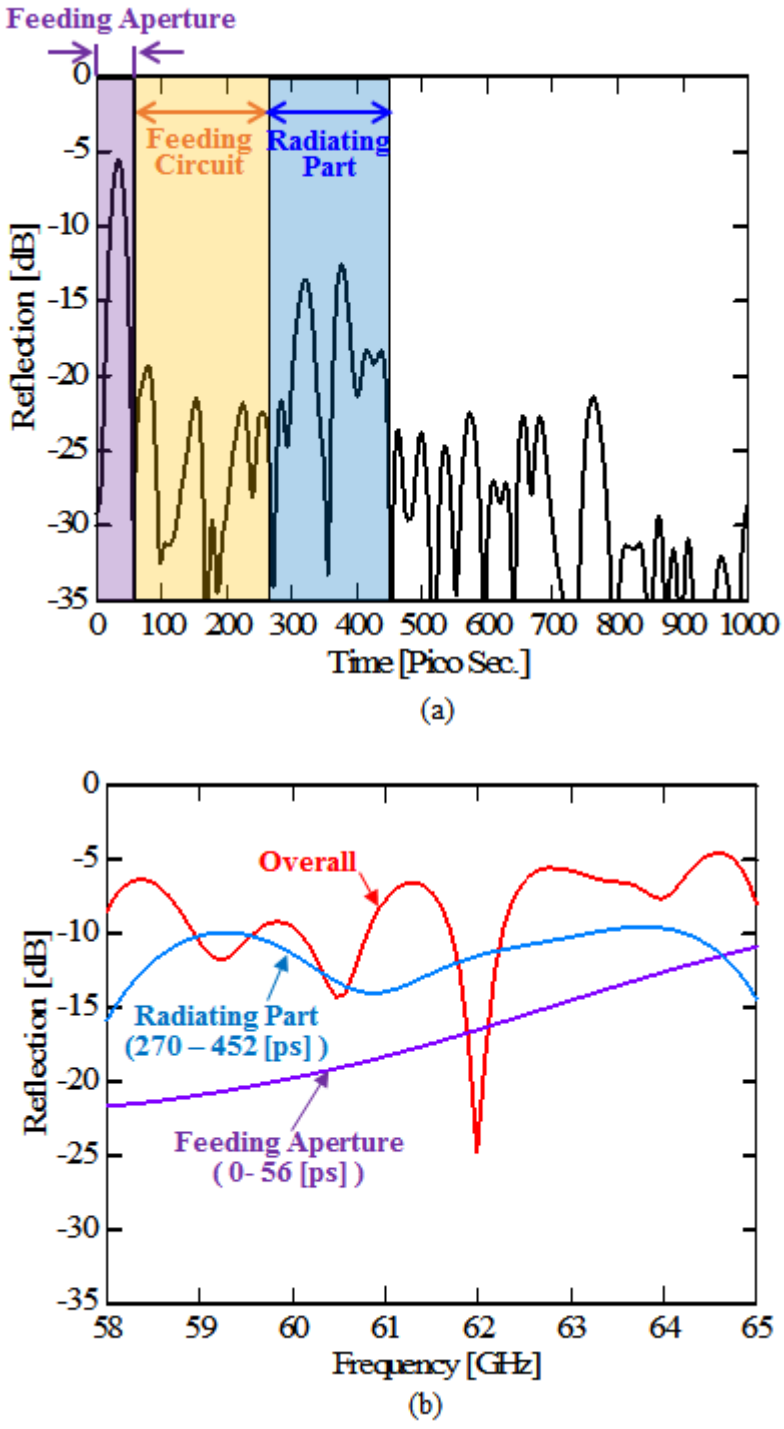

Fig. 2.16 Time-gating Analysis. (a) Time domain. (b) Frequency domain.

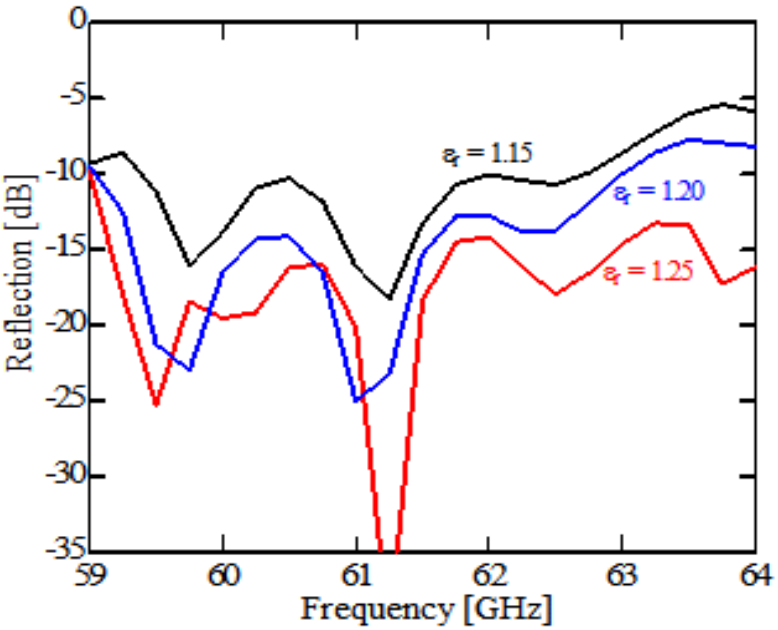

Fig. 2.17 Simulated reflection characteristic for various relative permittivity of dielectric.

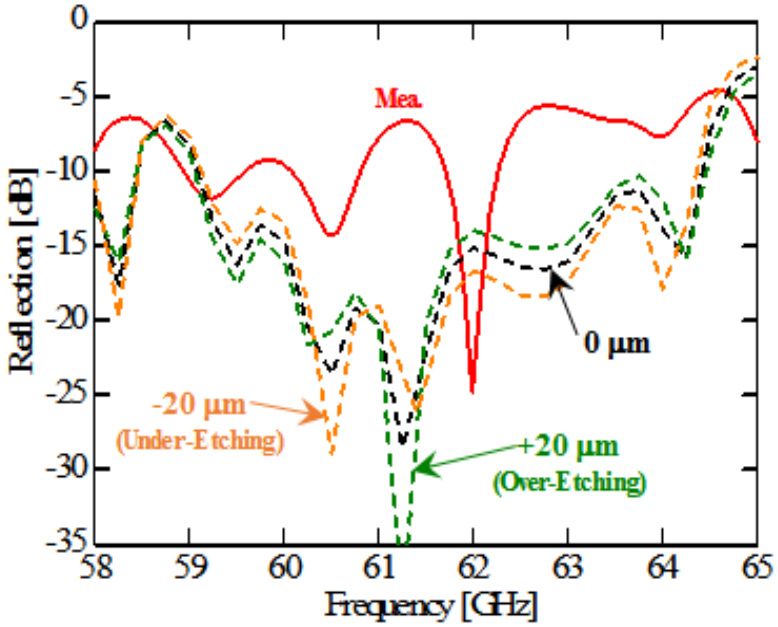

Fig. 2.18 Reflection for changing length of the radiating slots.

2.4.3 Near-field Distribution

Fig. 2.19 demonstrates the measured and the simulated amplitude, and measured phase distributions of the near-field at the design frequency of 61.5 GHz. As for the amplitude, we observe a symmetric distribution with respect to both the *x*-axis and *y*-axis. The variation in the measured amplitude is in good agreement with that of the simulated result. The measured amplitude variation over the aperture area is about 5 dB. The phase variation over the aperture area is about 60 degrees. Nevertheless, the proposed structure has a sufficient uniformity based on the configuration of radiation patterns (Fig. 2.20) and the efficiency of the directivity (Fig. 2.22).

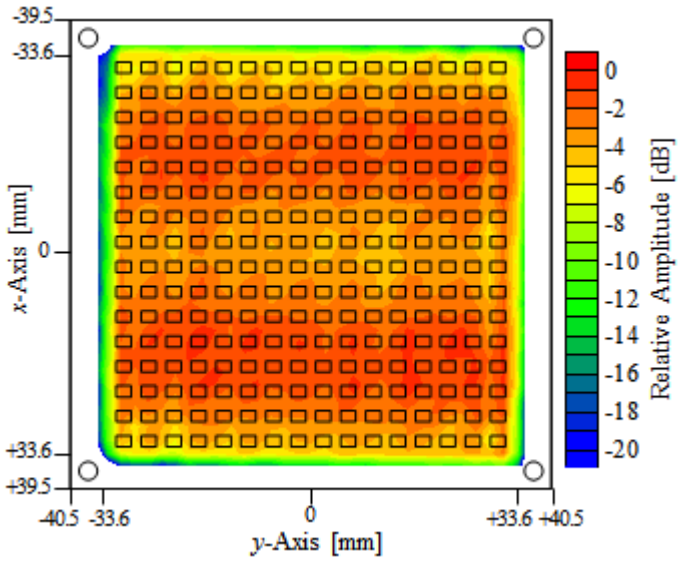

(a) Measured amplitude

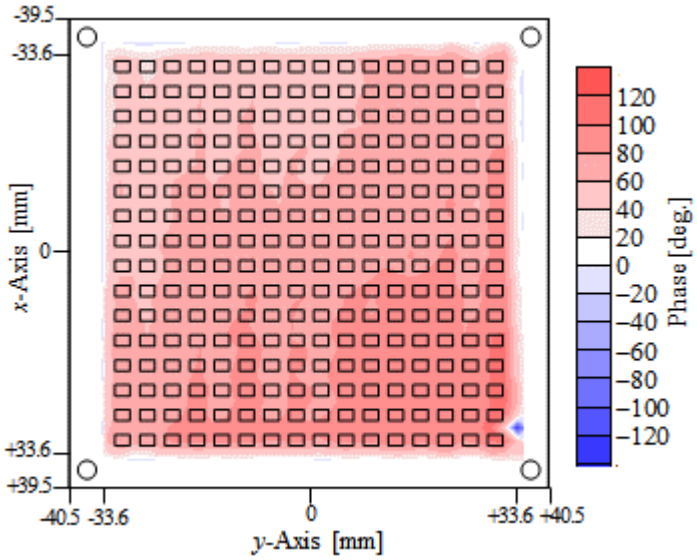

(b) Measured phase

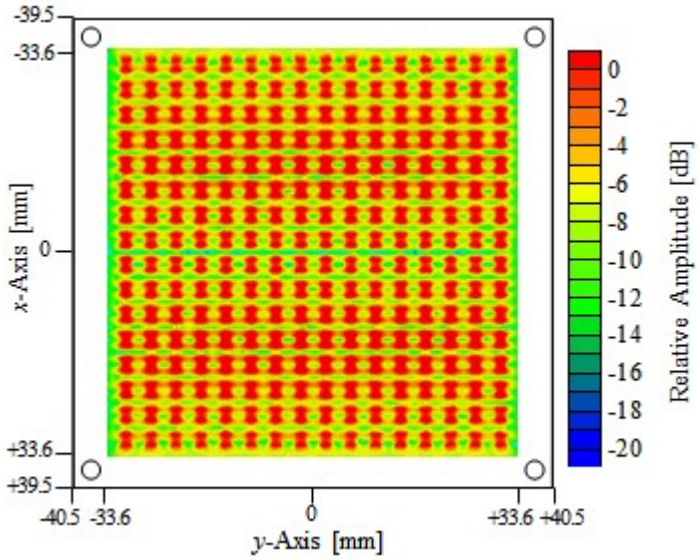

(c) Simulated amplitude

Fig. 2.19 Near-field distribution at 61.5 GHz.

2.4.4 Radiation patterns

Fig. 2.20 shows the measured and the simulated radiation patterns at 61.5 GHz in the E-plane (*xz*), H-plane (*yz*) and 45 deg.-plane. In the E-plane and H-plane, the measured patterns are in good agreement with the simulated ones. In the 45 deg.-plane, the measured pattern is almost the same as the simulated one except for ± 50-60 deg. region. The reasons of the discrepancy around ± 50-60 deg. region are not clear enough at this moment, but errors of under-etching in the size of slots would be main cause considering supplemental simulations by the analysis of a 2×2-element subarray as shown in Fig. 2.21. Parameters are the relative permittivity of dielectric and the size of slots. These results present errors of under-etching have lower grating lobes, but the discrepancy is still in the results. Another reason would be the leakage of electromagnetic field from very slight gaps of copper plates due to screw looseness. This leakage could mitigate the difference of the phase and amplitude in the 45-deg. plane, resulting in lower grating lobes. The sidelobe level is small (-30 dB in simulation and -40 dB in measurement), which could not cause problems. These patterns present uniform-excitation patterns including an element pattern. The measured first-sidelobe levels are as follows: -12.3dB at -6.5 deg., -13.2dB at +3.5 deg. in the E-plane, -12.5 dB at -6.0 deg., -13.6 dB at +6.0 deg. in the H-plane, and -26.1 dB at -9.0 deg., -25.8 dB at +9.0 deg. in the 45 deg.-plane. The structure is symmetrical in the *y*-direction, however, it is not in the *x*-direction because all the coupling slots have an offset in the same + *x*-direction. This

gives slightly unsymmetrical patterns in the *xz*-plane even in the simulation. The measured pattern in each plane is not completely symmetrical because of a manufacturing error in etching and laminating processes; however, the difference is very small.

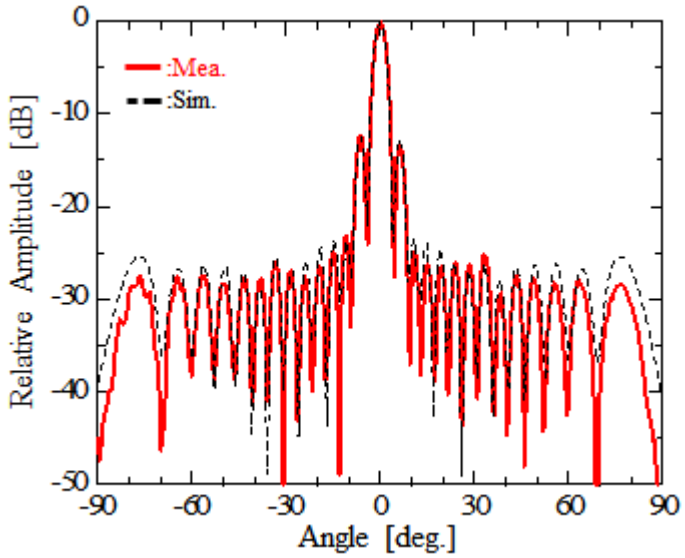

(a)

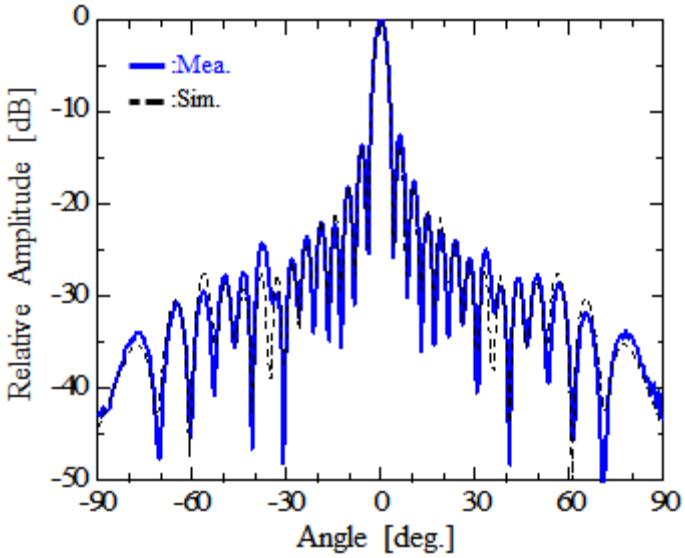

(b)

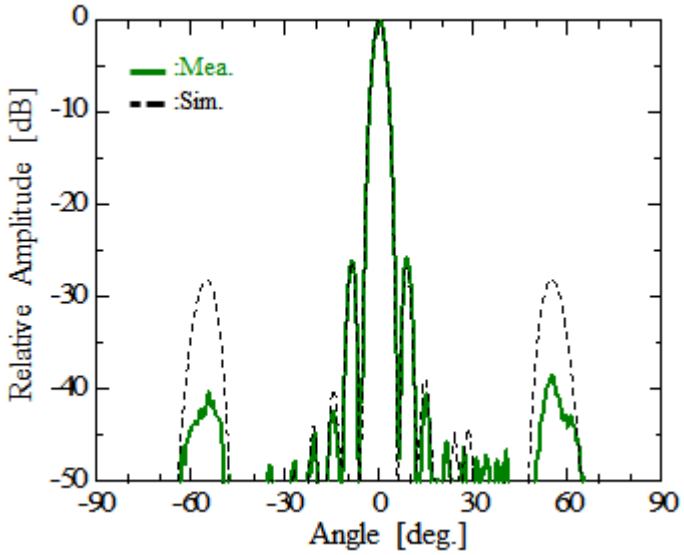

(c)

Fig. 2.20 Radiation patterns at 61.5 GHz. (a) E-plane (*xz*). (b) H-plane (*yz*). (c) 45 deg.- plane.

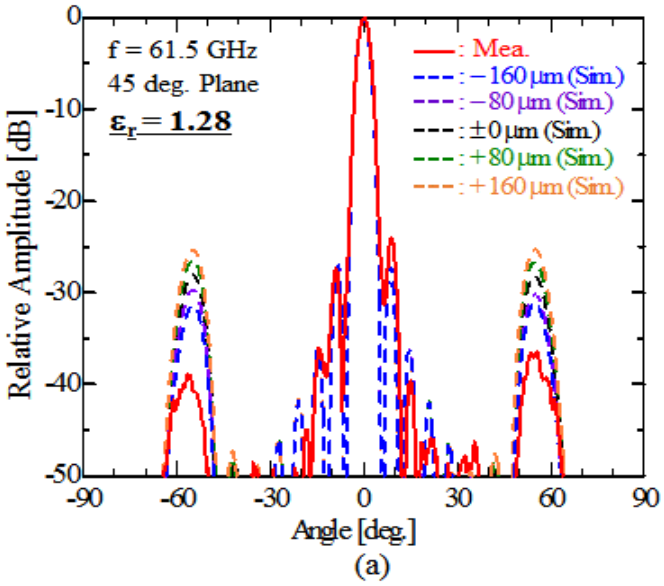

(a)

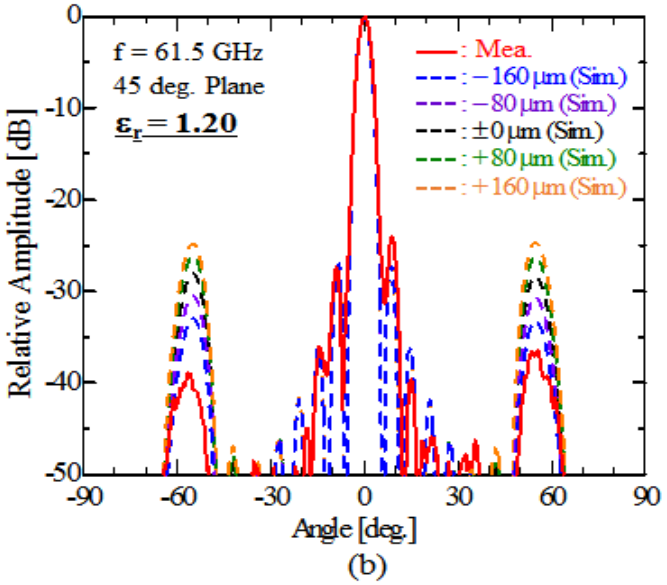

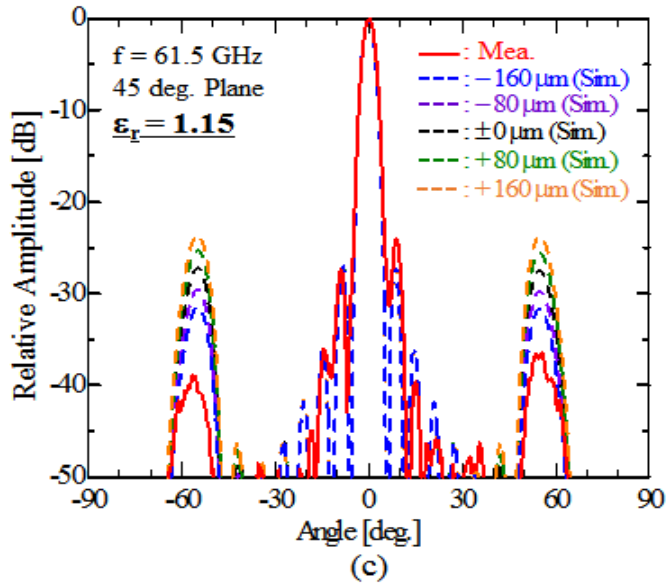

Fig. 2.21 Radiation patterns in the 45-deg. plane at 61.5 GHz by changing the relative permittivity of dielectric and size of slots.

2.4.5 Realized Gain, Gain and Directivity

Fig. 2.22 reveals the measured and the simulated realized gain, gain, and directivity. The realized gain, which includes the reflection loss, and conductor and dielectric losses, is measured by the comparison with a standard gain horn antenna in an anechoic chamber. The directivity is derived from the measured near-field distribution by the Fourier transform. The measured gain is calculated by adding the measured reflection

loss into the measured realized-gain. The measured realized gain is degraded comparing to the simulated one because of the reflection loss. Then, the measured gain is also degraded due to the same reason. However, the measured directivity is in good agreement with the simulated one. The aperture efficiency greater than 90 % is achieved over 5-GHz bandwidth. At the design frequency, the measured directivity is 33.5 dBi with the aperture efficiency of 90.6 % and the realized gain is 31.7 dBi with the antenna efficiency of 61.0 %.

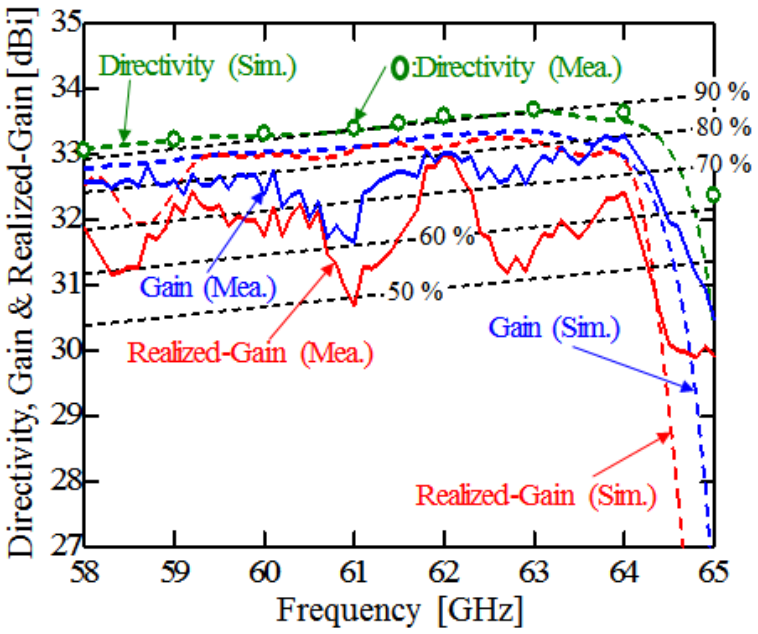

Fig. 2.22 Frequency characteristic of realized-gain, gain, and directivity.

2.5 Concluding remarks

In this chapter, we have proposed the perpendicular-corporate feed for a three-layered parallel-plate slot array antenna. The introduction of dielectric with adequate permittivity in the region between the coupling-aperture layer and the radiating-slot layer can offer uniform excitation because of generating standing waves. The measured amplitude distribution of the near-field demonstrates a symmetric distribution on both the *x*-axis and *y*-axis, which indicates the uniform excitation, in the 16×16-element array antenna. The aperture efficiency greater than 90 % is achieved over 5-GHz bandwidth in the measured directivity. At the design frequency, the measured directivity is 33.5 dBi with the antenna efficiency of 90.6 %.

2.6 Acknowledgement

The authors are thankful to Mr. Naoki Shibata and Mr. Masayoshi Nakamura of Nitto Denko Corp. for providing the dielectric sheets.

References

[2.1] Y. Miura, J. Hirokawa, M. Ando, Y. Shibuya, and G. Yoshida, "Double-layer full-corporate-feed hollow-waveguide slot array antenna in the 60-GHz band," IEEE Trans. Antennas Propag., vol.59, no.8, pp.2844-2851, Aug. 2011.

[2.2] K. Tsukamoto, and H. Arai, "Characteristic of linearly polarized aperture array antenna," IEICE Trans. Commun., vol. J78-B-II, no. 3, pp. 160-166, Mar. 1995.

[2.3] K. Tsukamoto, and H. Arai, "Input characteristic of tri-plate aperture array antenna," IEICE Trans. Commun., vol. J79-B-II, no. 1, pp. 26-32, Jan. 1996.

Chapter 3

Design of Perpendicular-Corporate Feed in Four-Layer Parallel-Plate Circularly-Polarized Slot Array Antenna

3.1 Introductory Remarks

This chapter presents a perpendicular-corporate feed in a four-layer parallel-plate circularly-polarized slot array antenna. This antenna is based on the structure of a perpendicular-corporate feed in a three-layer parallel-plate slot array antenna as shown in Fig. 2.13, but a few structural differences are involved as follows. The configuration of slots in all slot layers except for a coupling-aperture layer uses a hexagonal aperture to generate the circular polarization. A dielectric layer is formed by the combination of polytetrafluoroethylene (PTFE), with ε_r 2.17, and air to achieve desired permittivity. To improve the bandwidth of the VSWR and the axial ratio, the proposed antenna has a new slot layer defined as additional-slot layer on top of a parasitic-slot layer, with an air gap in the region between the two.

This chapter is organized as follows. Section 3.2 describes the antenna configuration. In section 3.3, we discuss the design process of the perpendicular-corporate feed for the circularly-polarized slot array by the analysis of the 2×2-element subarray and how to form the dielectric layer of PTFE and air by the analysis of an 8×8-element subarray. In addition, we introduce an eigenmode analysis to review the improvement of the axial ratio. Finally, the analysis of a 16×16-element array is presented. In section 3.4, we compare the measured results of the fabricated antenna with the simulations. In section 3.5, we conclude this chapter.

3.2 Antenna Configuration

Fig. 3.1 shows a perpendicular-corporate feed in a four-layer parallel-plate circularly-polarized slot array. The antenna consists of the additional-slot layer, the parasitic-slot layer, the radiating-slot layer, the dielectric layer, the coupling-aperture layer, and the feeding-circuit layer. There are air gaps between the slot layers including the coupling-aperture layer, and so there is no metal to metal contact in the radiating part. In Fig. 3.1, the layers are drawn widely apart to show the internal structure. However, in the actual antenna, the layers are stacked much more closely together. The antenna is fed from the back (bottom in the figure) by a feed aperture, which has the size of the standard WR-15 waveguide. The feeding circuit layer is a planar-corporate feed composed of H-planes and T-junctions, and feeds the coupling apertures in equal amplitude and phase. The coupling-aperture layer is placed between the feeding-circuit layer and the dielectric layer, with an air gap in between. The radiating-slot layer is mounted directly on the dielectric layer. The parasitic-slot layer is on top of the radiating-slot layer also with an air gap in between. The additional-slot layer is over the parasitic-slot layer, similarly with an air gap to improve the axial ratio and VSWR bandwidth. The coupling apertures excite 2×2 radiating slots and the electromagnetic field moves to the additional slots through the parasitic slots. The spacing of all the slot types is constant: $0.86\lambda_0$ (4.20 mm) in the *x* and *y* directions. Here, the λ_0 is the wavelength at the design frequency of 61.5 GHz. The configuration of all the slot layers except in the coupling-aperture layer is an aperture with two corners of the square trimmed to degenerate the modes for circular polarization. By adjusting the aperture size in each slot layer, two radiating perpendicular electric fields: E_α and E_β, are generated. Both of E_α and E_β have equal amplitudes and a 90-degree phase difference, and the combination of the two creates the circular polarization. The top slot layer has larger sized slots in this structure.

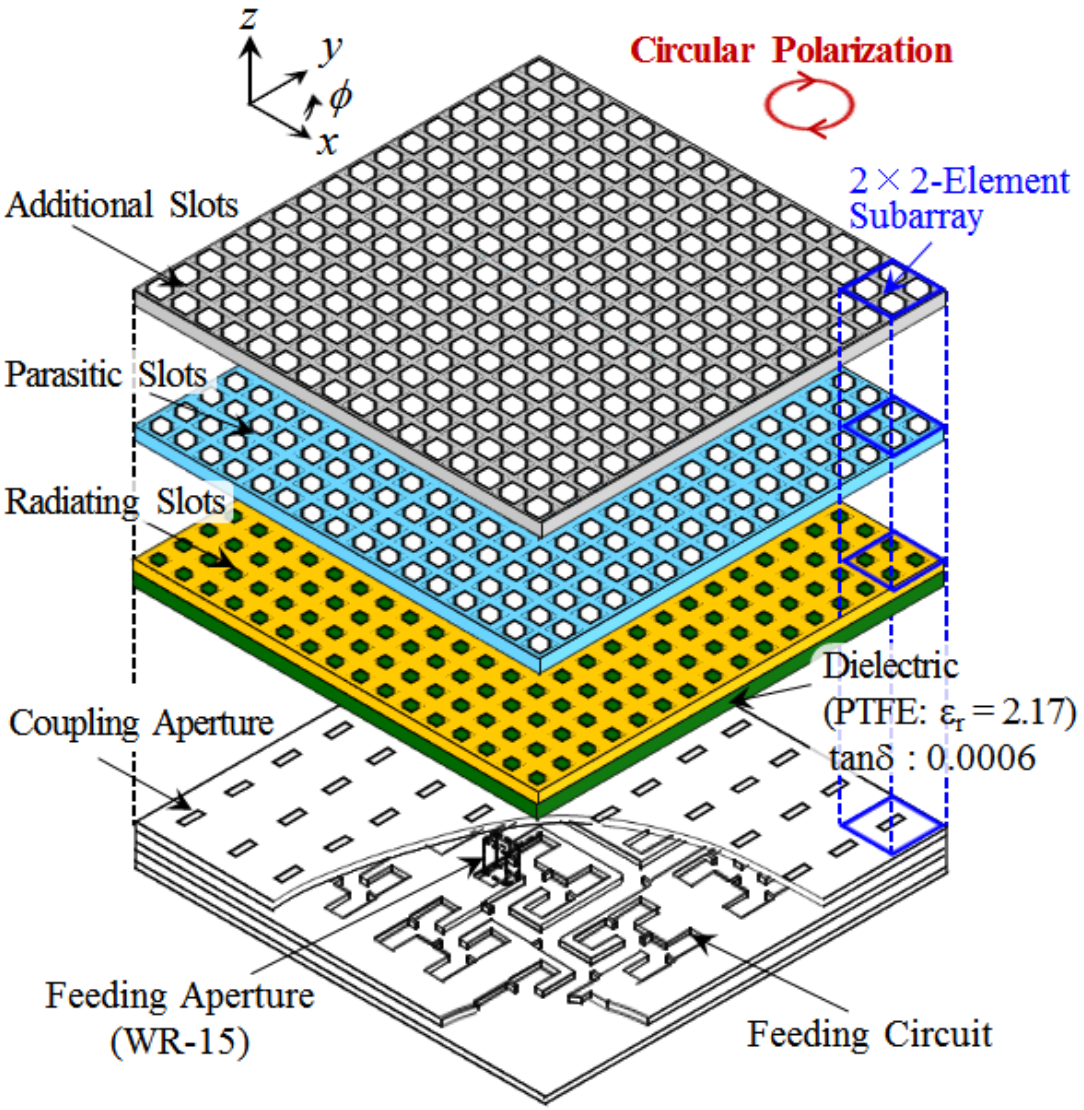

Fig. 3.1 Perpendicular-corporate feed in a four-layer parallel-plate circularly-polarized slot array

3.3 Design

3.3.1 Dielectric layer

In the conventional model shown in chapter 2, the design used a dielectric with a relative permittivity of $\varepsilon_r = 1.28$. This permittivity is based on the effective electrical size increased from 1.72 free-space wavelengths to two wavelengths (about $1.72\lambda_0 \times \sqrt{\varepsilon_r}$), and leads to the excitation of a standing wave in the region between the coupling aperture-

layer and the radiating-slot layer. The dielectric material is a porous PTFE. Given the availability of dielectric materials, the proposed model uses the dielectric layer of a combination of solid PTFE, where ε_r is 2.17, and air. To determine the effective combination, we analyzed both a 2×2-element subarray and an 8×8-element subarray. The analysis of the 8×8-element subarray uses PEC and PMC values for the polarization, equivalent to the analysis of a 16×16-element array because of its symmetric structure.

Fig. 3.2 shows the differences between the conventional and the proposed models in the 2×2-element subarray. The proposed model consists of only the radiating-slot layer, the dielectric layer with the air gap, the coupling-aperture layer and the feeding waveguide. This analysis does not include a parasitic-slot layer to simplify the structural effects. The parameters are as follows: the dimensions of the radiating slots l_r and w_r, the thickness of the dielectric layer t_d, and the size of the air gap h_{rc}. The size of the feeding waveguide is width a = 2.96 mm and thickness b = 1.00 mm. The size of the coupling aperture is length l_c = 2.75. and width w_c = 0.15 mm. The offset of the coupling aperture against the principal axis is 0.50 mm in the x axis. The feeding waveguide has short end and the length is 5.59 mm. In addition, we use rectangular apertures for simplification. In the external regions, two sets of periodic boundaries and a radiation boundary are introduced. The two sets of periodic boundaries are used to include the mutual coupling in the infinite two-dimensional array. Pink parallelograms are the ports in the simulations.

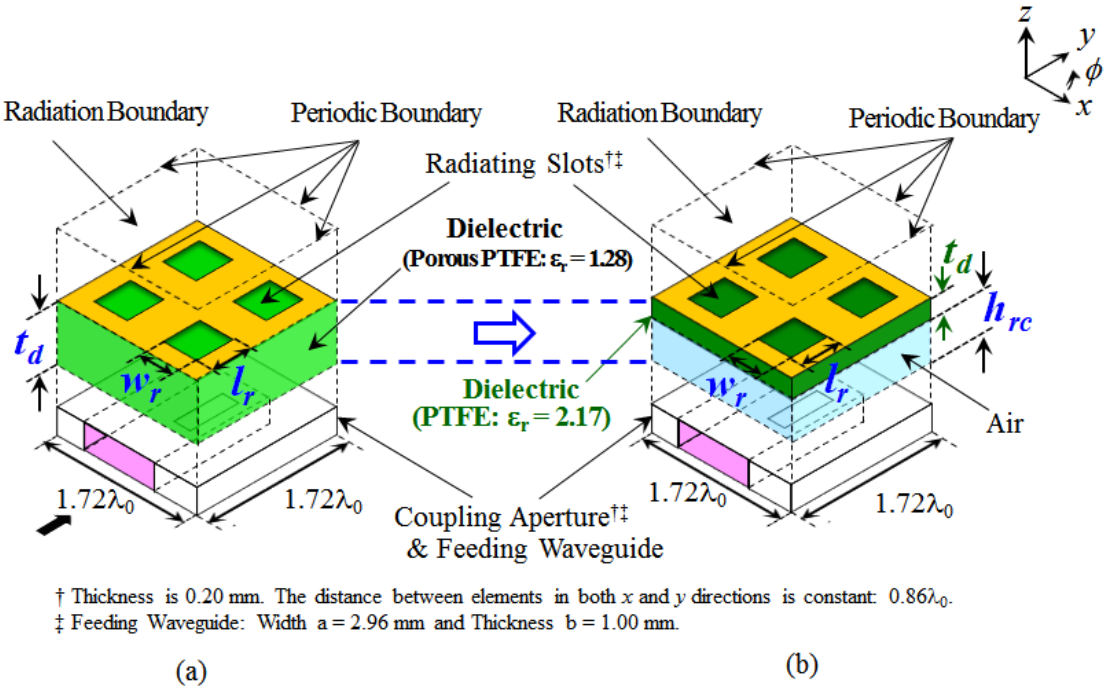

Fig. 3.2 Outlines of the (a) conventional and (b) proposed models.

Fig. 3.3 shows particulars of the model for the analysis of the 8×8-element subarray. The parameters are the same as for the analysis of the 2×2-element subarray, and are determined so that the desired operation can be achieved; the frequency characteristic of the reflection for the 16 ports will be identical to that of the 8×8-element subarray and agree with that of the 2×2-element subarray. Further, other parameters regarding the coupling aperture are determined to minimize the reflection at the design frequency. Once the desired operation is achieved, all the radiating slots are excited uniformly because of the periodic arrangement. Around the periphery of the 8×8-element subarray, perfect electric conductor (PEC) boundaries parallel to the *yz*-plane and perfect magnetic conductor (PMC) boundaries parallel to the *xz*-plane are introduced for the *x*-polarized operation. The parallel plates are truncated by PEC and PMC considering the polarization. For the external region, radiation boundaries are introduced for the analysis by ANSYS HFSS Ver. 16.

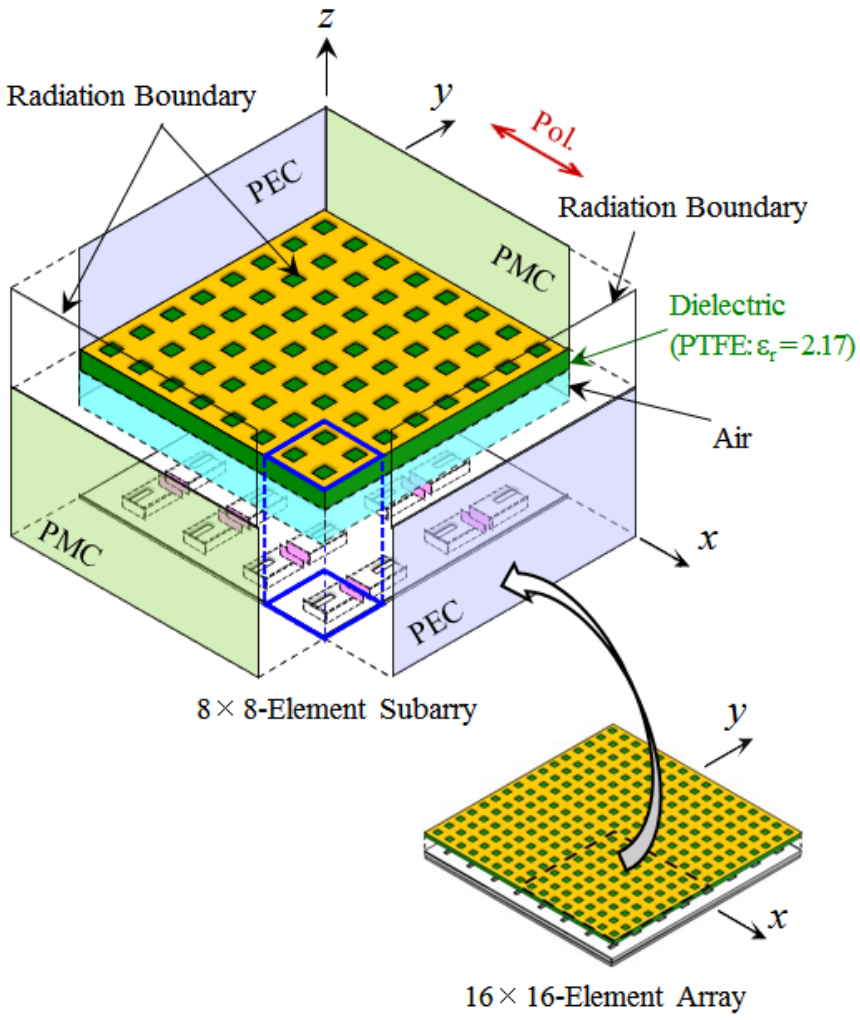

Fig. 3.3 Model for the analysis of the 8×8-element subarray.

Fig. 3.4 shows the frequency characteristic of reflections from the 16 ports in the 8×8-element subarray by 16 gray lines for both the proposed and the conventional models. A red dashed line shows the reflection in the 2×2-element subarray as a reference. Considering the availability of dielectric (PTFE) materials, the thickness of the dielectric layer: t_d should be a multiple of 5 mils (0.127mm). As t_d is thicker, the proposed models can achieve the above-mentioned desired operation. However, as t_d is thicker, the VSWR bandwidth becomes narrower. When t_d is 0.38 mm, the proposed model can achieve both the above-mentioned desired operation and the better performance of the VSWR bandwidth like the conventional model, allowing the conclusion that all the radiating slots in the 8×8-element subarray can be expected to excite uniformly. In the analysis, we confirmed that the effective wavelength in the region, as generated by the combination of the PTFE (ε_r = 2.17) and the air, should be closely similar to porous PTFE (ε_r = 1.28).

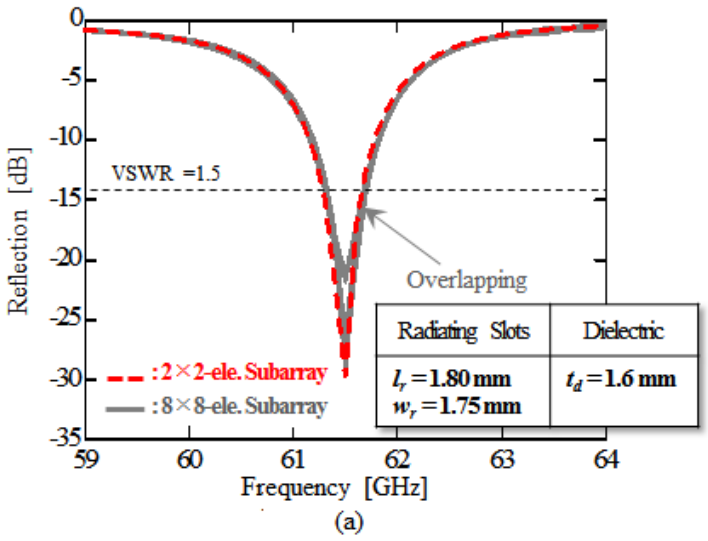

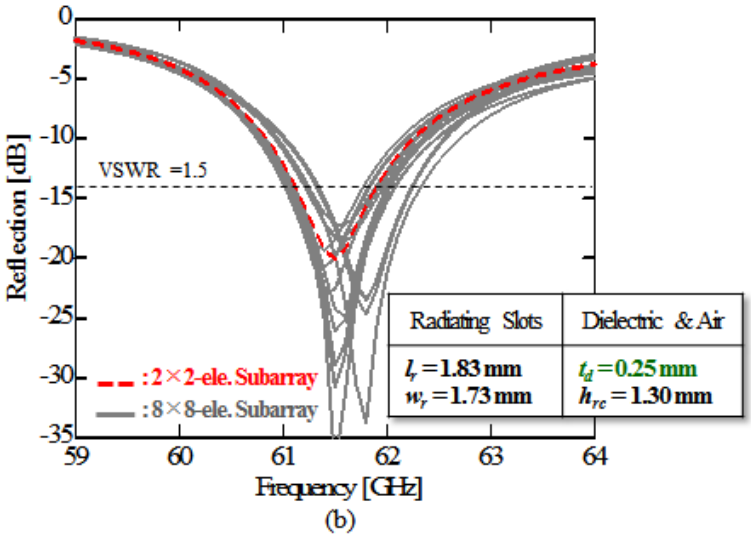

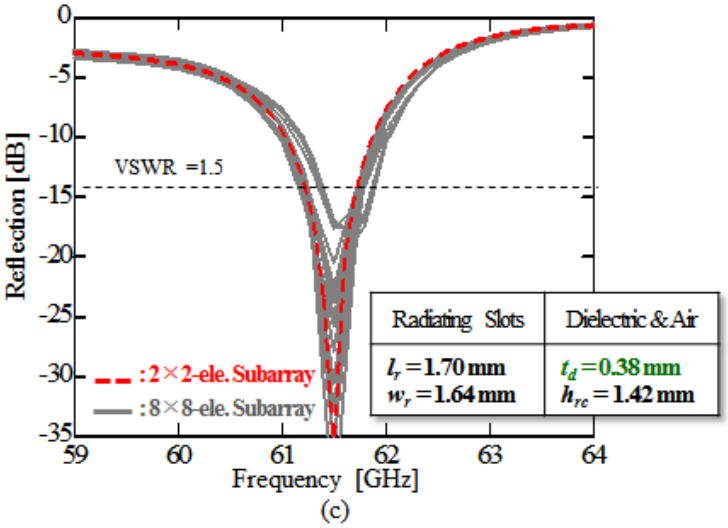

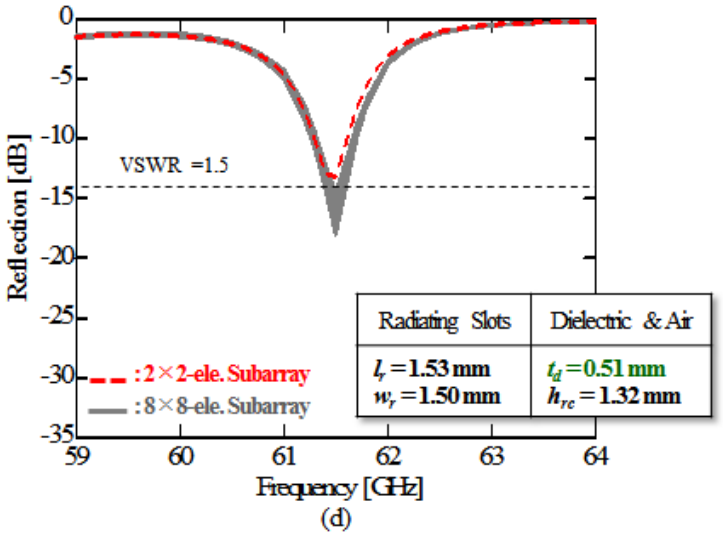

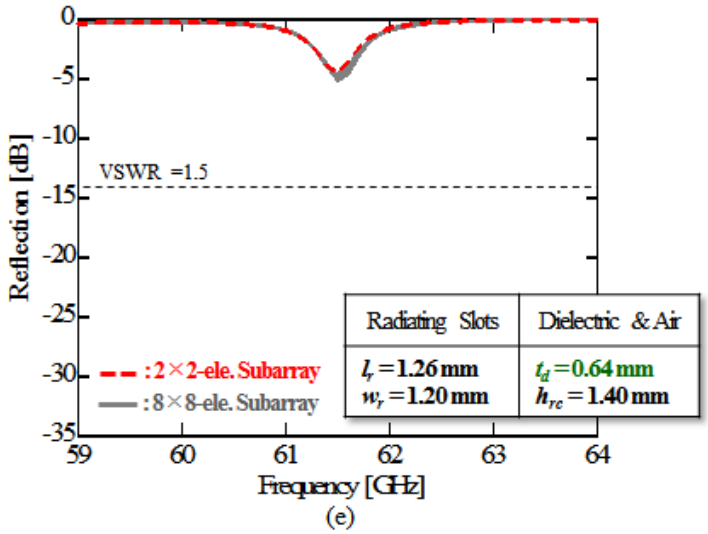

Fig. 3.4 Frequency characteristic of the reflection. (a) Conventional model (porous PTFE: ε_r = 1.28). (b) Proposed model (combination of PTFE: ε_r = 2.17 and air, t_d = 0.25 mm). (c) Proposed model combination of PTFE: ε_r = 2.17 and air, t_d = 0.38 mm). (b) Proposed model (combination of PTFE: ε_r = 2.17 and air, t_d = 0.51 mm). (b) Proposed model (combination of PTFE: ε_r = 2.17 and air, t_d = 0.64 mm).

To support the frequency characteristic of the reflections as shown in Fig. 3.4 (c), Fig. 3.5 show the E-field distribution (f = 61.5 GHz) on the cross section (*xz*-plane) of the 8×8-element subarray as a physical interpretation. As a reference, we also show the E-distribution of ε_r = 1.28 as shown in Fig. 2.6 (b). The combination of the PTFE and air almost has standing waves. However, compared to the E-distribution of ε_r = 1.28, that of the combination has slight distortion because of not using the best thickness (t_d = 0.51 mm or 0.64 mm) of dielectric. As a result, Fig. 3.5 (b) has slight discrepancy among reflections especially caused by the edge of the 8×8-element subarray. Considering the bandwidth of the VSWR as shown in Fig. 3.4 (d) and (e), indicating no impedance matching, t_d = 0.38 mm is better than others.

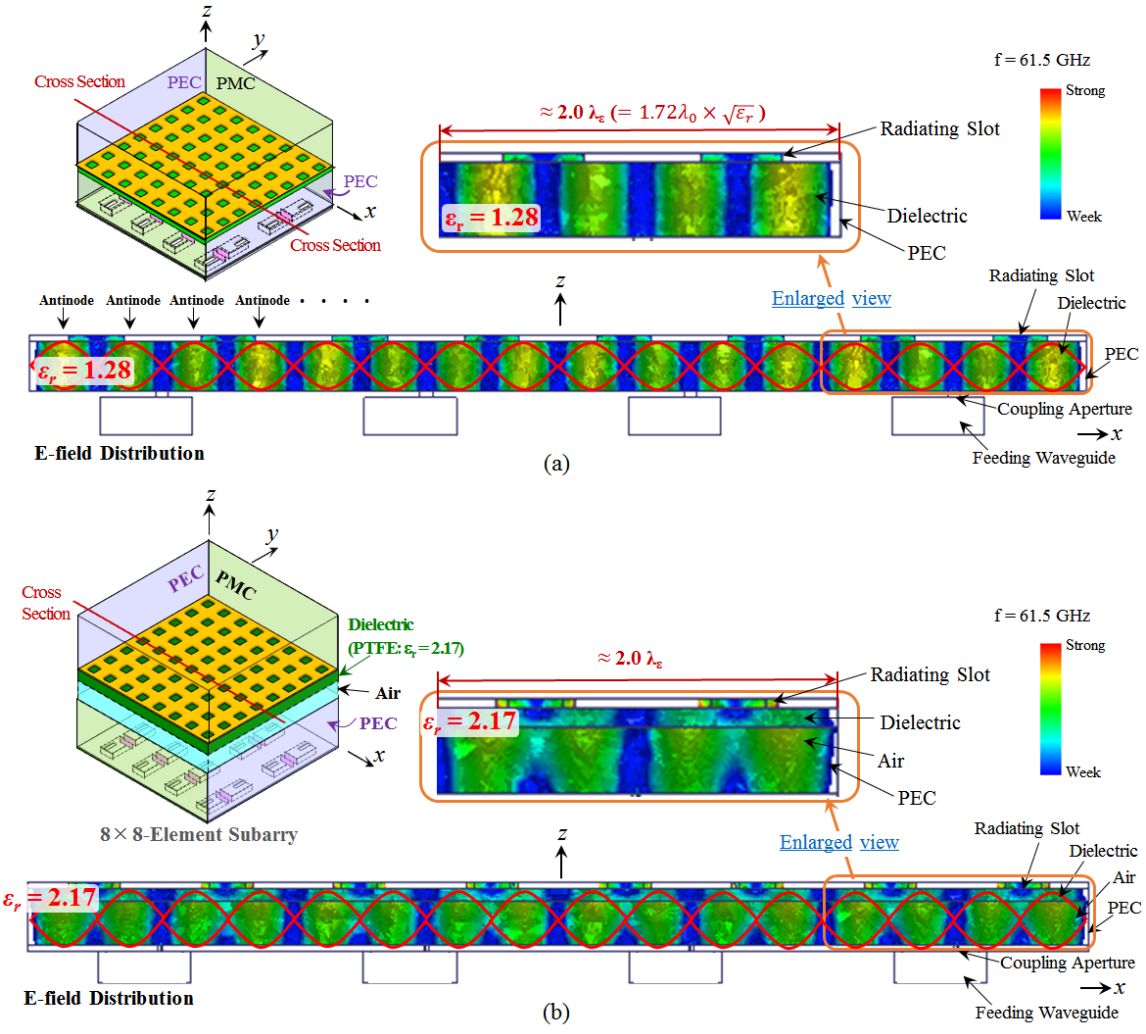

Fig. 3.5 E-field distribution at 61.5 GHz on the cross section (*xz*-plane) of the 8×8-element subarray. (a) ε_r = 1.28. (b) Air + PTFE (ε_r = 2.17).

3.3.2 Design of 2×2-Element Subarray

Fig. 3.6 shows the model for the analysis of the 2×2-element subarray. In the analysis, we use a dielectric layer of t_d = 0.38 mm and ε_r = 2.17 obtained from Fig. 3.4 (c). The conductivity 5.8×10^7 S/m of copper and a loss tangent 0.0006 of the dielectric are assumed. To improve the bandwidth of the VSWR and the axial ratio, the proposed model has the additional-slot layer. The parameters are as follows: the size of the additional slots, l_a, w_a, and c_a; the size of the parasitic slots, l_p, w_p, and c_p; the size of the radiating slots, l_r, w_r, and c_r; and the size of the coupling apertures, l_c and w_c. The c_a, c_p, and c_r are the trimming amounts at the two corners for the apertures. The air gap between the additional-slot and the parasitic-slot layers is h_{ap}, that between the parasitic-slot and the radiating-slot layers is h_{pr}, and that between the dielectric and coupling layers is h_{rc}. Considering the fabrication, we select a multiple of 0.20 mm as the thickness $h_{rc,}$ h_{pr} and h_{ap}. When h_{rc} is 0.60 mm and t_d is 0.38 mm, the effective electrical size of the 2×2-element subarray in the region between the radiating-slot layer and the coupling-aperture layer corresponds to 1.93 λ where λ is the wavelength in the parallel plates consisting of these dielectric and air layers derived based on [3.1]. It is close to 2.0 λ, and leads to exciting a standing wave in the region. Note that the discrepancy between 1.93 λ and 2.0 λ is arisen by the perturbation of the slots. The thicknesses of the additional-slot layer, the parasitic-slot layer, and radiating-slot layer is 0.40 mm, and that of the coupling-aperture layer is 0.20 mm. The size of the feeding waveguide is fixed: width a = 2.95 mm, thickness b = 1.00 mm and length g = 5.82 mm, and it has short end. The offset of the coupling aperture against the principal axis in the *x* direction is also fixed at 0.61 mm. The design procedure is the same as that in the previous subsection. The final values of the design parameters are listed in the figure.

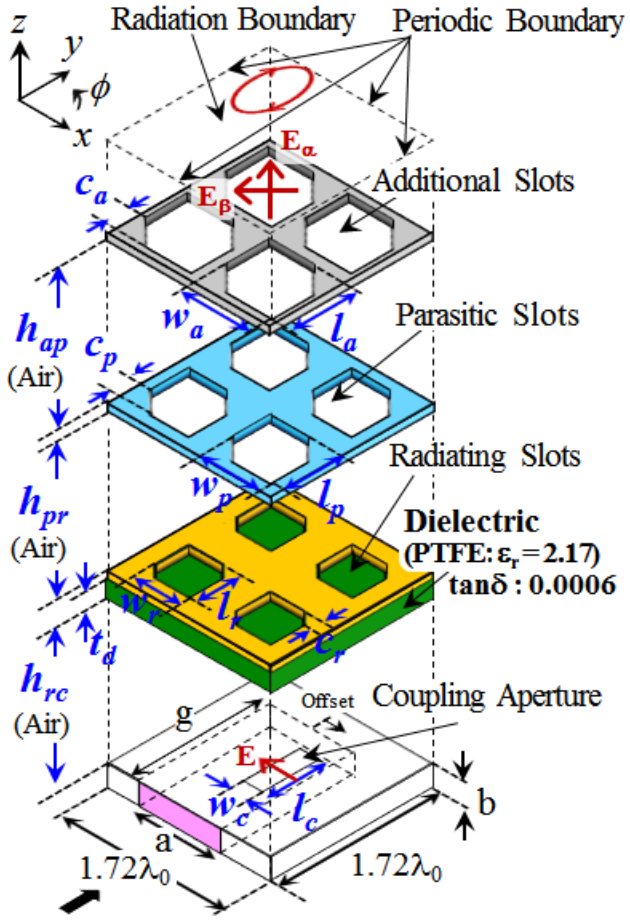

Unit : mm

Para.	W/	W/O
l_a	3.70	–
w_a	3.60	–
c_a	1.37	–
h_{ap}	0.80	–
l_p	3.48	3.48
w_p	3.24	3.36
c_p	1.09	1.46
h_{pr}	0.80	0.80
l_r	2.67	2.69
w_r	3.11	3.11
c_r	0.88	1.00
h_{rc}	0.60	0.60
t_d	0.38	0.38
l_c	2.85	3.15
w_c	1.07	0.40

a = 2.95 mm
b = 1.00 mm
g = 5.82 mm

Fig. 3.6 Model for the analysis of the 2×2-element subarray.

Fig. 3.7 shows the frequency characteristic of the reflection. As a reference, we also show the result without the additional-slot layer, and the parameters are listed in Fig. 3.6. The reflection of the 2×2-element subarray with the additional-slot layer is smaller than -14 dB over 11.4 % of the bandwidth ranging from 57.5 to 64.5 GHz. On the other hand, the reflection without the additional-slot layer is less than -14 dB over 1.8 % bandwidth.

Fig. 3.8 shows the frequency characteristic of the axial ratio. We also show the result without the additional-slot layer as a reference. The axial ratio with the additional-slot layer is below 3 dB over 15.3 % of the bandwidth from 55.7 to 65.1 GHz. The bandwidth is enhanced from 6.2 % due to the introduction of the additional-slot layer. In particular, the result indicates better axial ratios at 59.9 and 64.7 GHz. The effects of the additional-slot layer are demonstrated to improve the bandwidth of the VSWR and the axial ratio. The wideband characteristic is reviewed in the next subsection by eigenmode analysis.

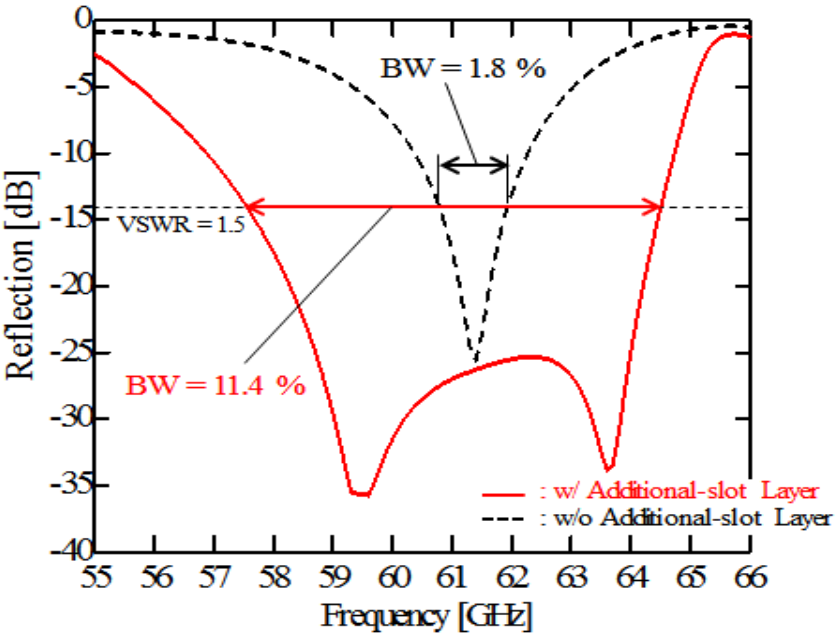

Fig. 3.7 Frequency characteristic of the reflection.

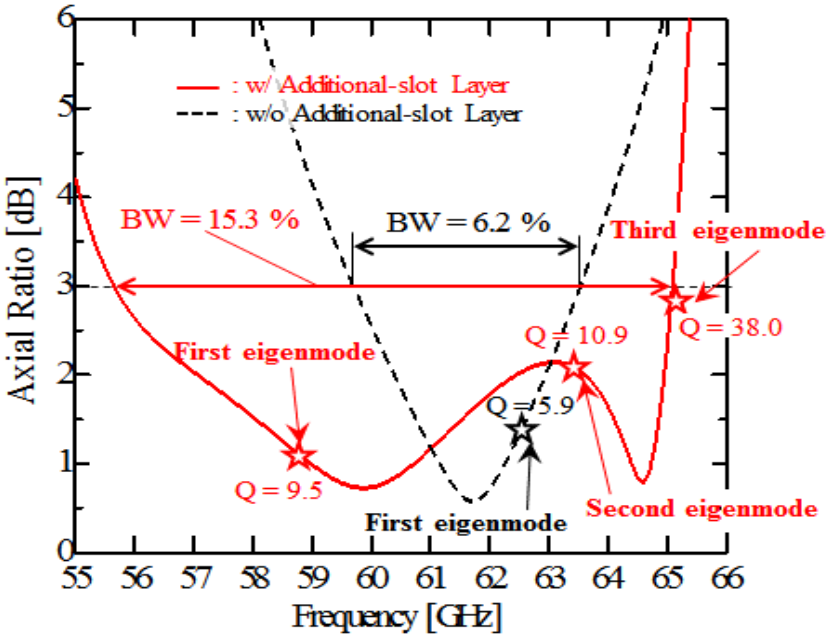

Fig. 3.8 Frequency characteristic of the axial ratio.

3.3.3 Review of Wideband Characteristic of Axial Ratio

To elucidate the wideband characteristic of the axial ratio, we introduce an eigenmode analysis. Fig. 3.9 shows the model for the analysis. The model consists of a 1×1-element because of its symmetric structure in the 2×2-element subarray. In the external regions, two sets of periodic boundaries are set in the *xz* and *yz* planes. The regions also include an impedance boundary with a distance of λ_0 from the additional slot at the top, and a PEC boundary is introduced for the effect of the metal plate at the position of the coupling aperture on the bottom. The parameters are the same as the analysis of the 2×2-element subarray shown in Fig. 3.6. Fig. 3.8 also shows the results of the eigenmode analysis marked with stars and includes the result without the additional-slot layer as a reference. Three eigenmodes are observed in the desired band. The first eigenmode has the lower Q factor, 9.5 at 58.8 GHz. Compared to the 1×1-element without the additional-slot layer, the number of Q factors is increased by the introduction of the additional-slot layer.

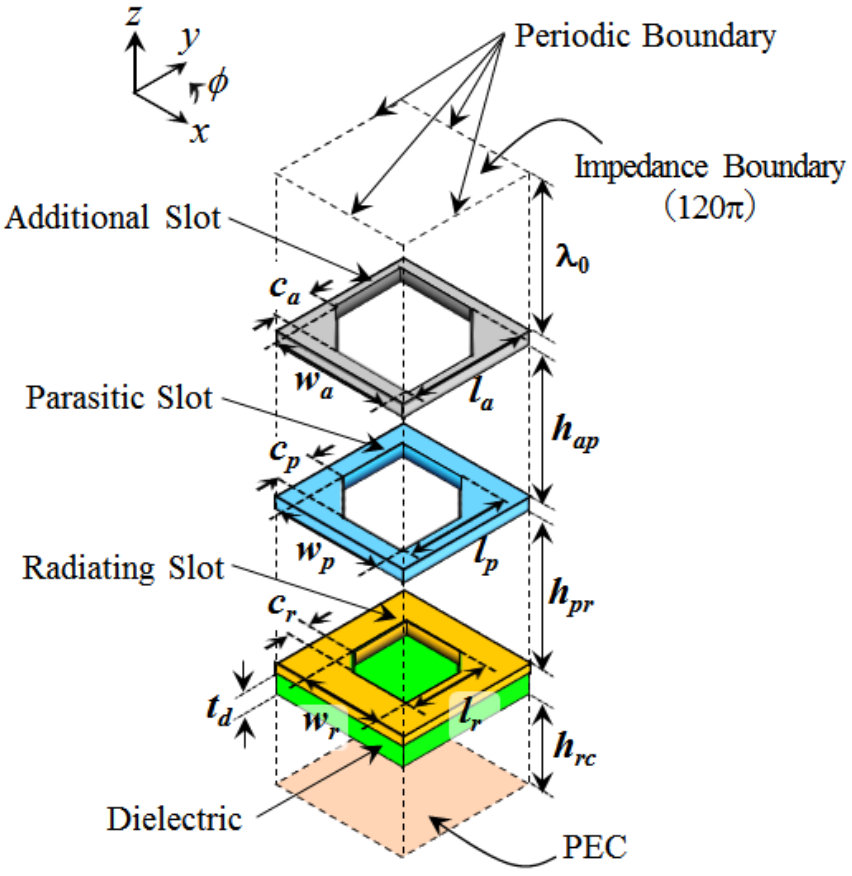

Fig. 3.9 Model for the analysis of the 1×1-element subarray.

Fig. 3.10 shows electric-field vectors of each eigenmode. For the pair of the second and the third eigenmodes, one of the resonant frequencies occurs almost at the frequency midway between the eigenmodes, with the lower axial ratio of 0.9 dB at 64.6 GHz. For the pair of the first and the second eigenmodes, there are no other resonant frequencies at the frequency midway between the eigenmodes, and the lowest axial ratio is 0.8 dB at 59.9 GHz. This difference would be caused by not fully considering the effect of the excitation involved in the coupling aperture and the feeding waveguide in the analysis.

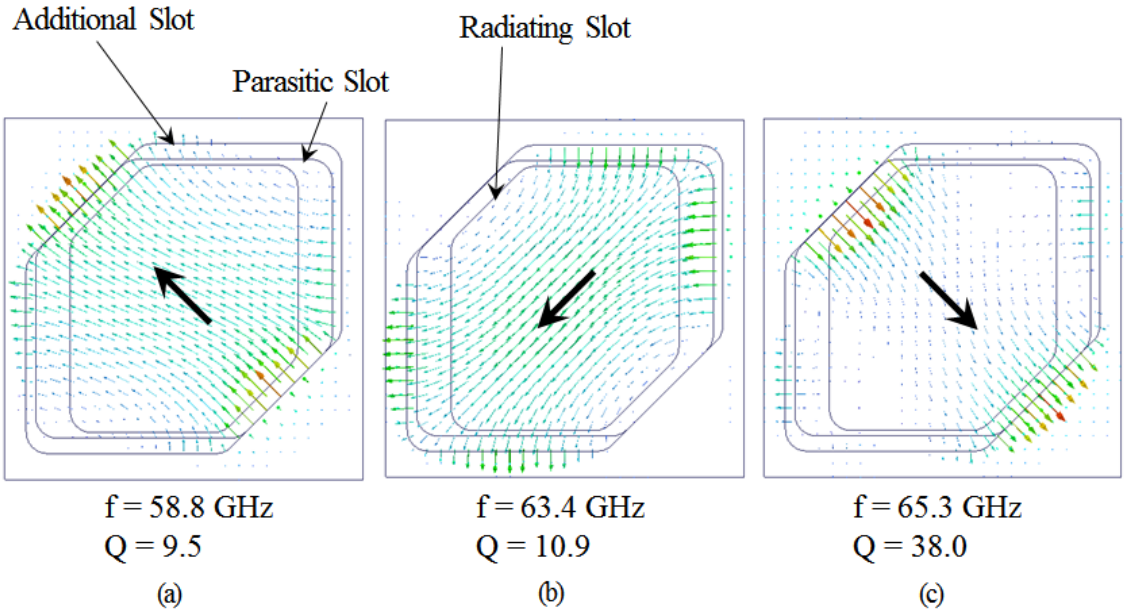

Fig. 3.10 Electric-field vectors on the surface of the additional slot. (a) First eigenmode, (b) Second eigenmode, and (c) Third eigenmode.

3.3.4 Full Structure Analysis

Fig. 3.11 shows the full structure of the four-layer circularly- polarized parallel-plate 16×16-element slot array antenna fed by the perpendicular corporate feed. In Fig.3.11, the plates are shown separately to expose the internal structure more fully, for the actual antenna, they are stacked closely. In the simulation, the conductivity of 5.8×10^7 S/m of copper and the loss tangent 0.0006 of the dielectric are assumed. Considering fabrication to maintain the flatness of the layers, the periphery of the four-layer parallel plates is terminated by (enclosed in) copper frames as shown in Fig. 3.12. Note that this copper termination does not result in a large cavity for the antenna operation. The

operation with a large cavity would degrade the antenna characteristic. All the metal plates and the dielectric layer are screwed together in the fabrication. The edge as PMC of the parallel plates is extended by 1.3 mm ($\approx 0.25\lambda_0$) only in the y direction and terminated by copper. The dimensions of the antenna in the xy-plane is 81.8 mm × 79.4 mm. The parameters are the same as the 2×2-element subarray shown in Fig. 3.6.

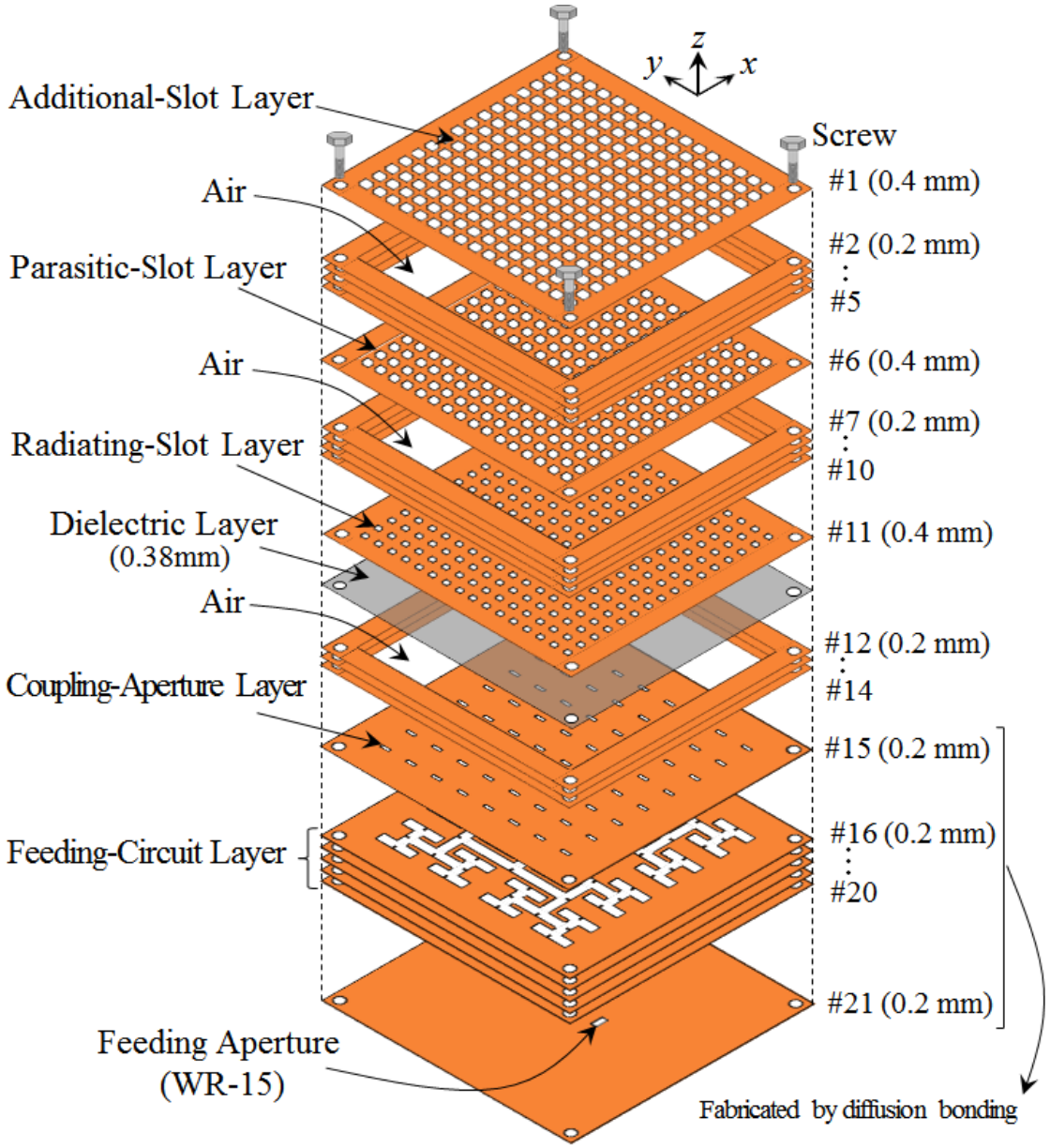

Fig. 3.11 Full structure of a perpendicular corporate feed in a four-layer circularly-polarized parallel-plate slot array antenna.

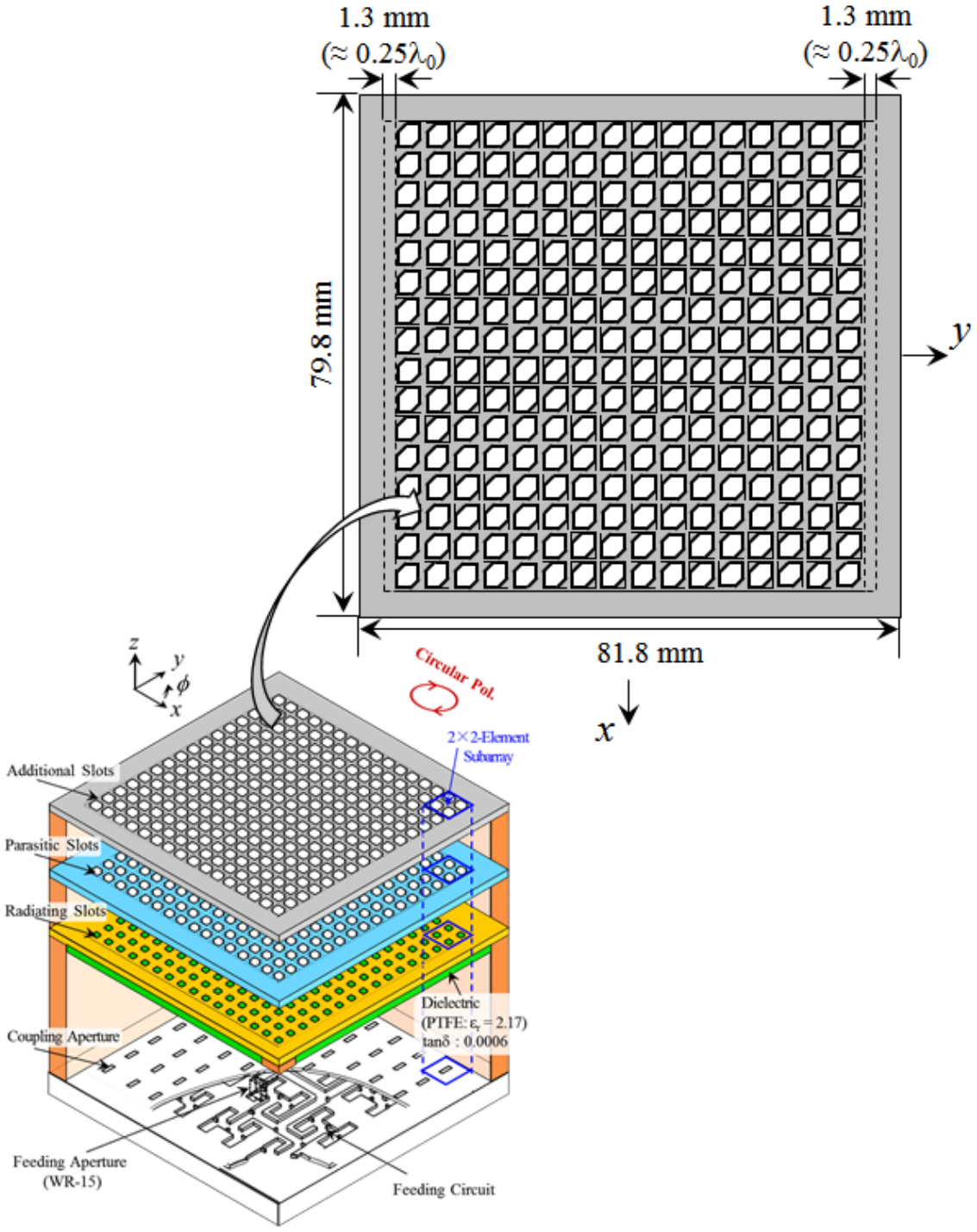

Fig. 3.12 Periphery of the structure.

Fig. 3.13 shows the frequency characteristic of the reflection. The reflection of the antenna is less than -14 dB over 11.2 % of the bandwidth from 57.6 to 64.5 GHz. The bandwidth is very similar to that of the 2×2-element subarray. The reflection shows a ripple caused by the reflection of the feeding circuit. Fig. 3.14 shows the frequency characteristic of the axial ratio. The axial ratio is less than 3 dB over 15.7 % of the bandwidth ranging from 55.5 to 65.2 GHz. The bandwidth is very similar to that of the 2×2-element subarray, and the wide bandwidth would be provided by the three eigenmodes shown in Fig. 3.10.

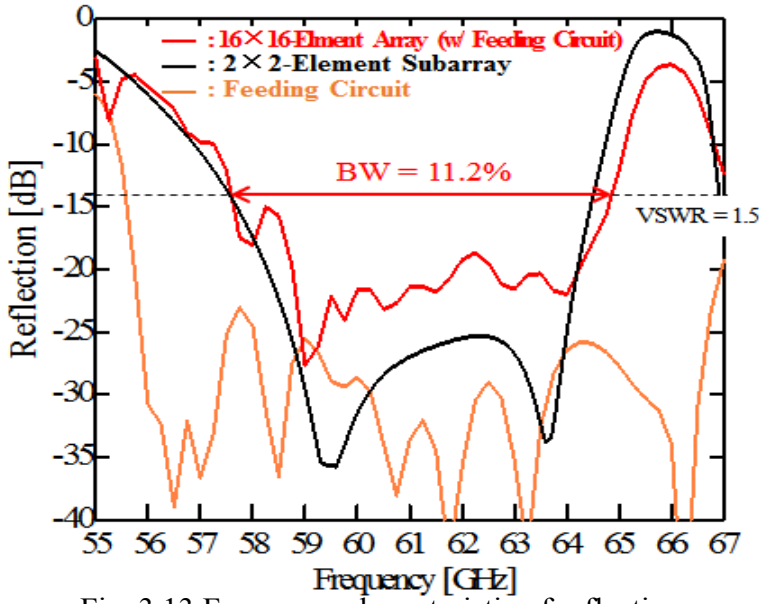

Fig. 3.13 Frequency characteristic of reflection.

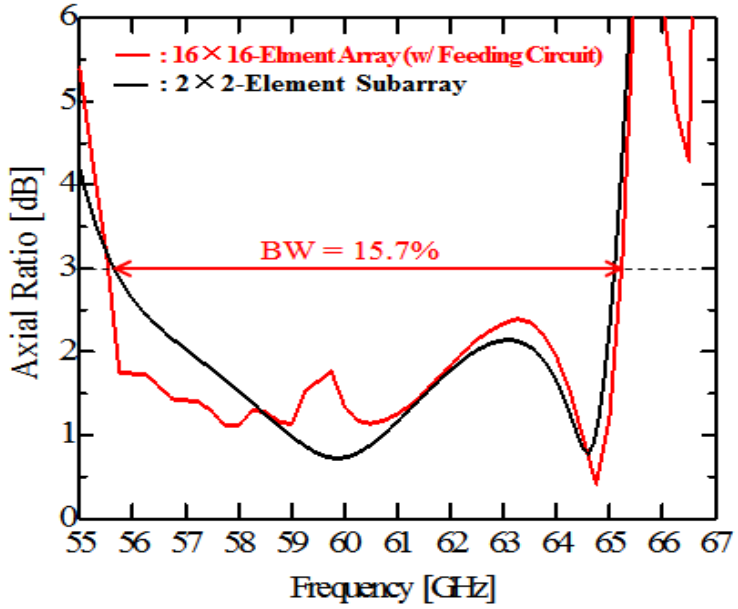

Fig. 3.14 Frequency characteristic of axial ratio.

3.4 Experimental Results

3.4.1 Fabricated Antenna

Fig. 3.15 shows photographs of the fabricated antenna. The total number of copper plates is 21. The feeding-circuit layer with the coupling-aperture layer composed of 7 plates is fabricated by the diffusion bonding of laminated thin copper plates. The rest of the plates with the feeding-circuit layer and including the coupling-aperture layer are set (screwed on) after placing the dielectric layer between the coupling-aperture and the radiating-slot layers. Air regions are mechanically supported by copper frames: plates #2-#5, #7-#10, and #12-#14 as shown in Fig. 3.11. The dimensions of each of the plates is 81.8 mm × 79.4 mm in the *xy*-plane. The total thickness of the fabricated antenna is 5.18 mm: 1.2 mm for the feeding-circuit layer; 0.2 mm for the coupling-aperture layer; 0.6 mm for the air gap between the coupling aperture layer and the dielectric layer; 0.38 mm for the dielectric layer; 0.4 mm for the radiating-slot layer; 0.8 mm for the air gap between the radiating-slot and parasitic-slot layers, 0.4 mm for the parasitic-slot layer; 0.8 mm for the air gap between the parasitic-slot and additional-slot layers; 0.4 mm for the additional-slot layer. We have attached a 6.0 mm thick choke flange to the antenna with screws to connect a standard WR-15 waveguide for the measurements. The 6.0 mm thickness is not required for the antenna operation, but for inserting the choke flange pins.

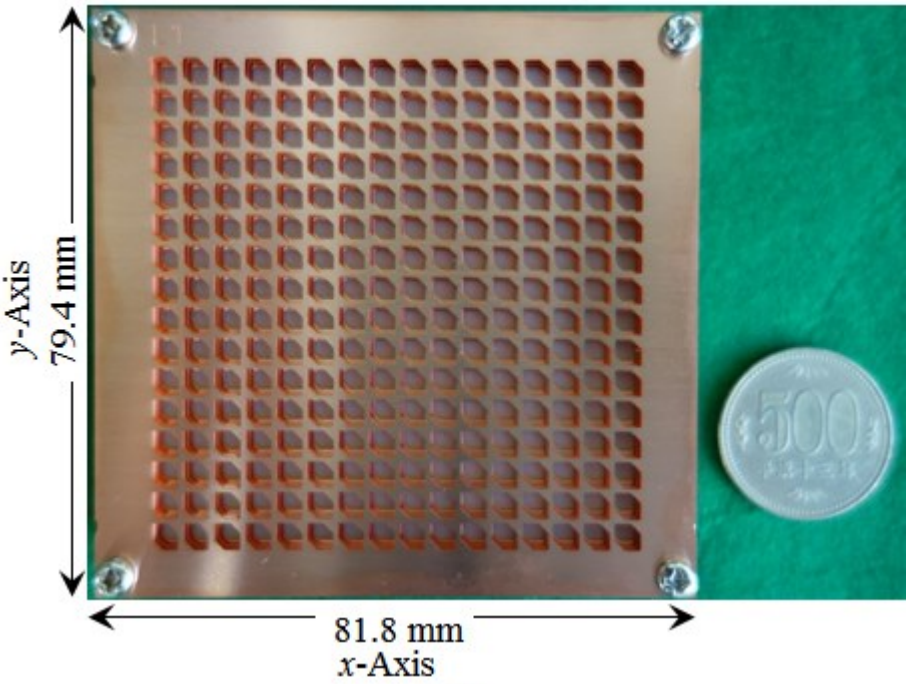

Fig. 3.15 Photos of the fabricated antenna. (a) Top view. (b) Side view.

3.4.2 Reflection and Axial Ratio

Fig. 3.16 shows the measured and the simulated reflection characteristic including the reflection characteristic of the choke flange. There is a large reflection in the measurement. To identify the reasons Fig. 3.17 (a) shows a time-gating analysis by a vector network analyzer (VNA). The frequency range used in the VNA is from 56 to 94 GHz. To review the spectrum, we separated the time domain response into three parts of reflection: the radiating part, the feeding circuit part, and the feeding aperture part as shown in Fig. 3.17. The reflection around the radiating part deteriorates the overall reflection from 58 to 62 GHz, and the reflection around the feeding circuit degrades the overall reflection from 62 to 64 GHz. The reflection from the feeding aperture is small in the desired frequency regardless of its large reflection in the time domain. It may be concluded that the main reason for the large reflection arises around the radiating part. The reflection of the feeding circuit shown in Fig. 3.17 (b) has more ripples in the frequency characteristic of the reflection than that of the radiating part and the feeding aperture. The feeding circuit has the cascade of H-planes and T-junctions. Fabrication errors would create the reflection of each H-plane and T-junction and the multiple reflection among them, and result in ripples in the frequency characteristic of the overall reflection.

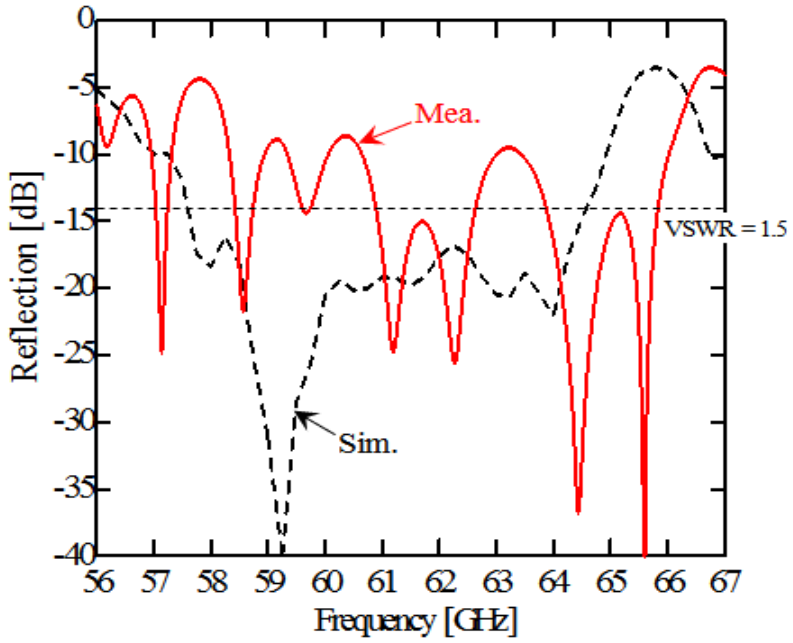

Fig. 3.16 Measured and simulated reflection characteristic.

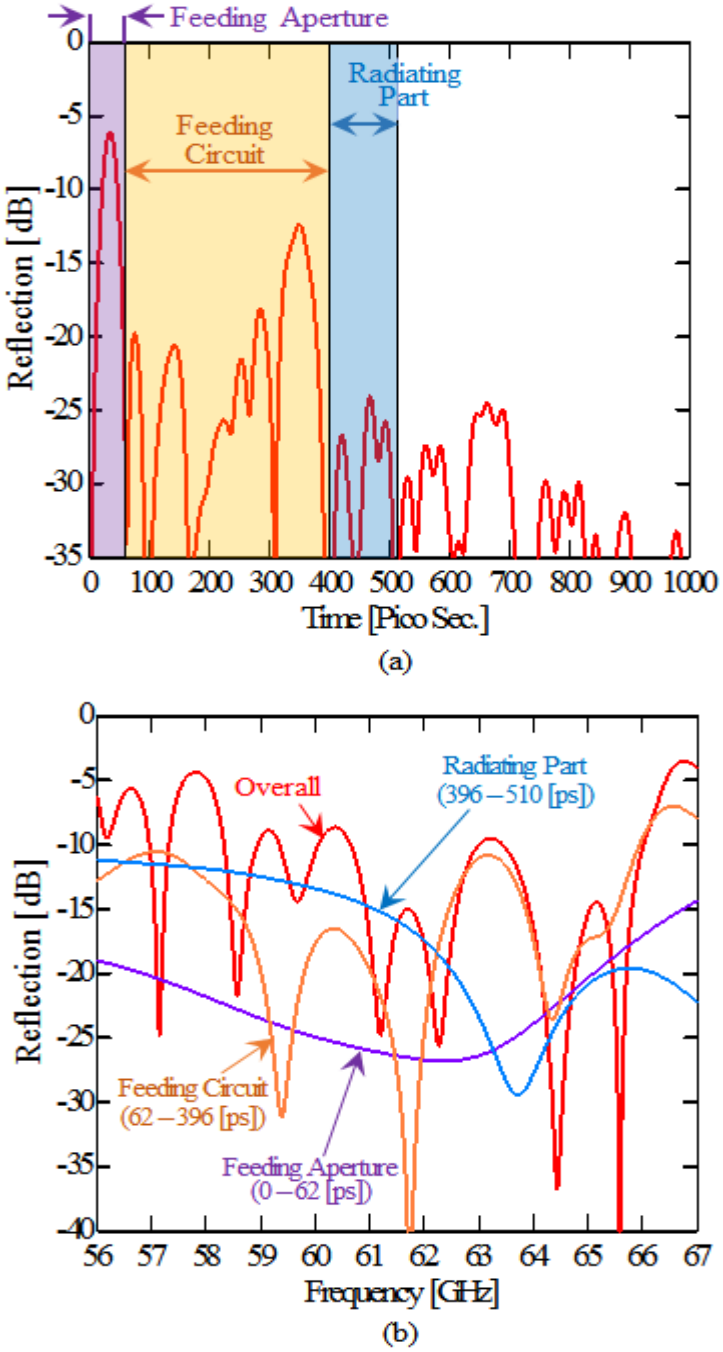

Fig. 3.17 Time-gating analysis. (a) Time domain. (b) Frequency domain.

It can be assumed that this degradation is caused by the placement of the dielectric layer. The dielectric layer is supported by the copper frame (#12) only at the four edges, and the center of the dielectric layer would be very slightly bent. To investigate this assumption, we simulated a 16×16-element array by adding a small air gap in the region between the radiating-slot and the dielectric layers as shown in Fig. 3.18.

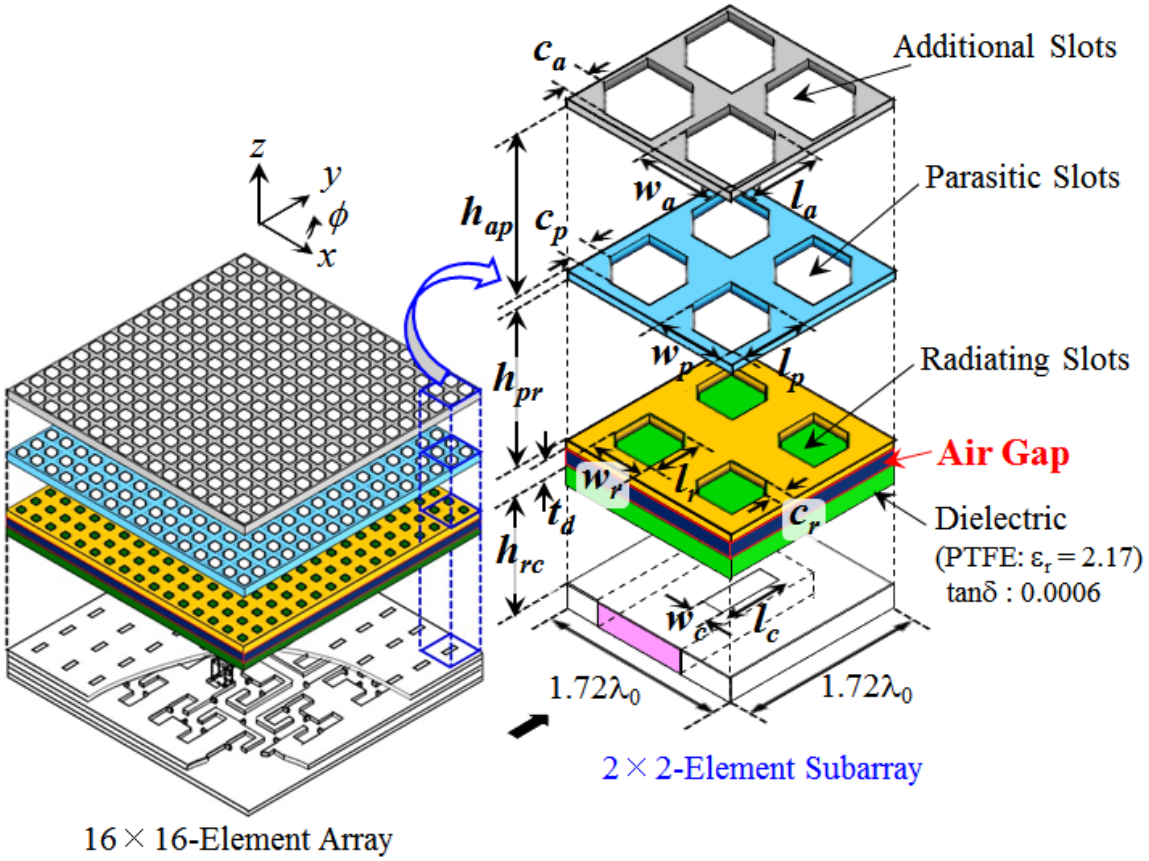

Fig. 3.18 Analysis model (16×16-element array by adding a small air gap into the region between the radiating-slot layer and dielectric layer).

Fig. 3.19 shows the frequency characteristic of the reflection and the axial ratio with this assumption. When the air gap is widened, the simulated reflection shifts to a higher frequency region and comes closer to the measured values. In the axial ratio values the simulated result is not degraded significantly by the change in the air gap. However, the measured axial ratio is below 3 dB over 11.9 % of the bandwidth from 55.5 to 62.8 GHz, which is degraded below that of the simulated ratio. It may be assumed that the degradation of the axial ratio is caused by over- and/or under- etching of slots. As an example, we analyzed the model with a 60 μm air gap by changing the length and width of the additional-, the parasitic-, and the radiating-slots, and Fig. 3.20 shows the resulting frequency characteristic of the axial ratios and reflections. When the length and width of the slots has 20 μm of over etching, the simulated result comes close to the measured

value, allowing the conclusion that the differences between the measured and the simulated results are mainly induced by the air gap and over-etching. The 20 μm over-etching offers fairly good agreement in the axial ratio, however there is still discrepancy in the reflection. Further investigation is required. It must be borne in mind that other reasons such as size errors in the coupling apertures and feeding circuit would also be involved.

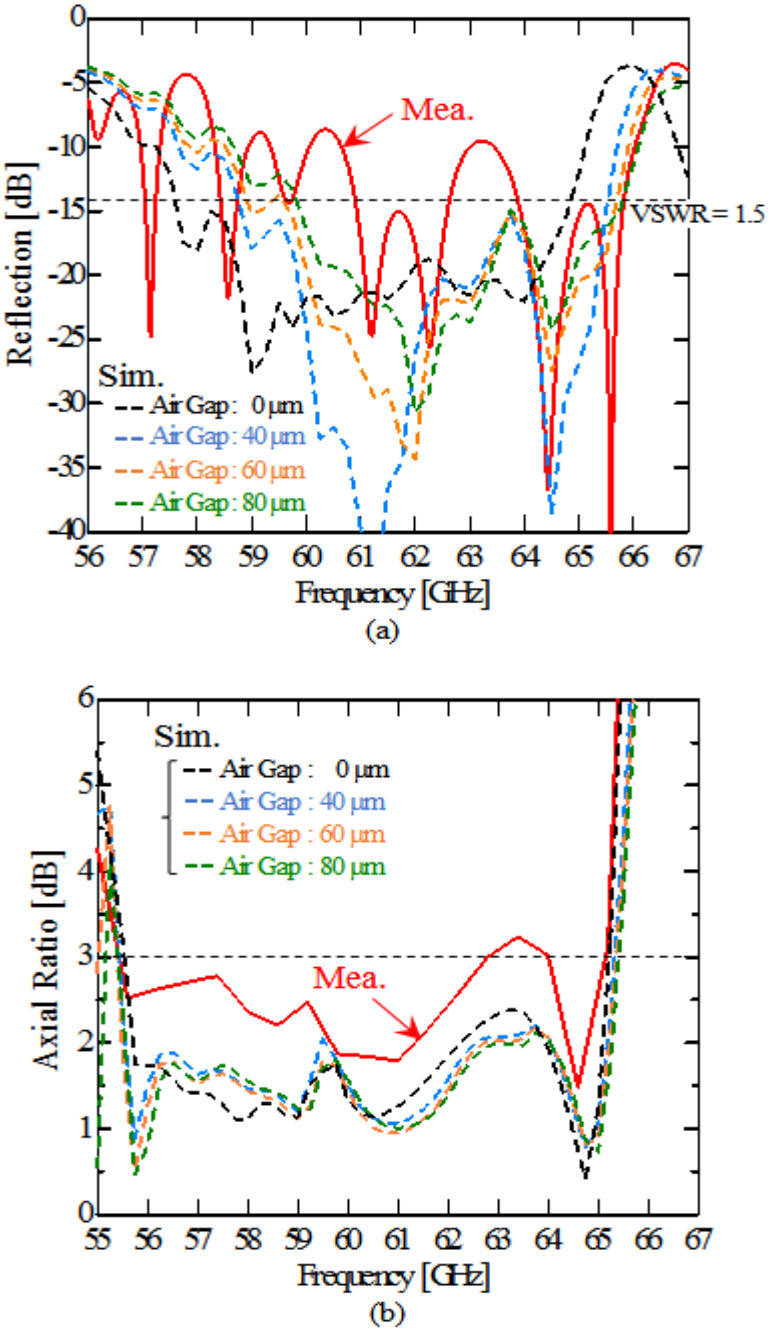

Fig. 3.19 Frequency characteristic of (a) reflection and (b) axial ratio.

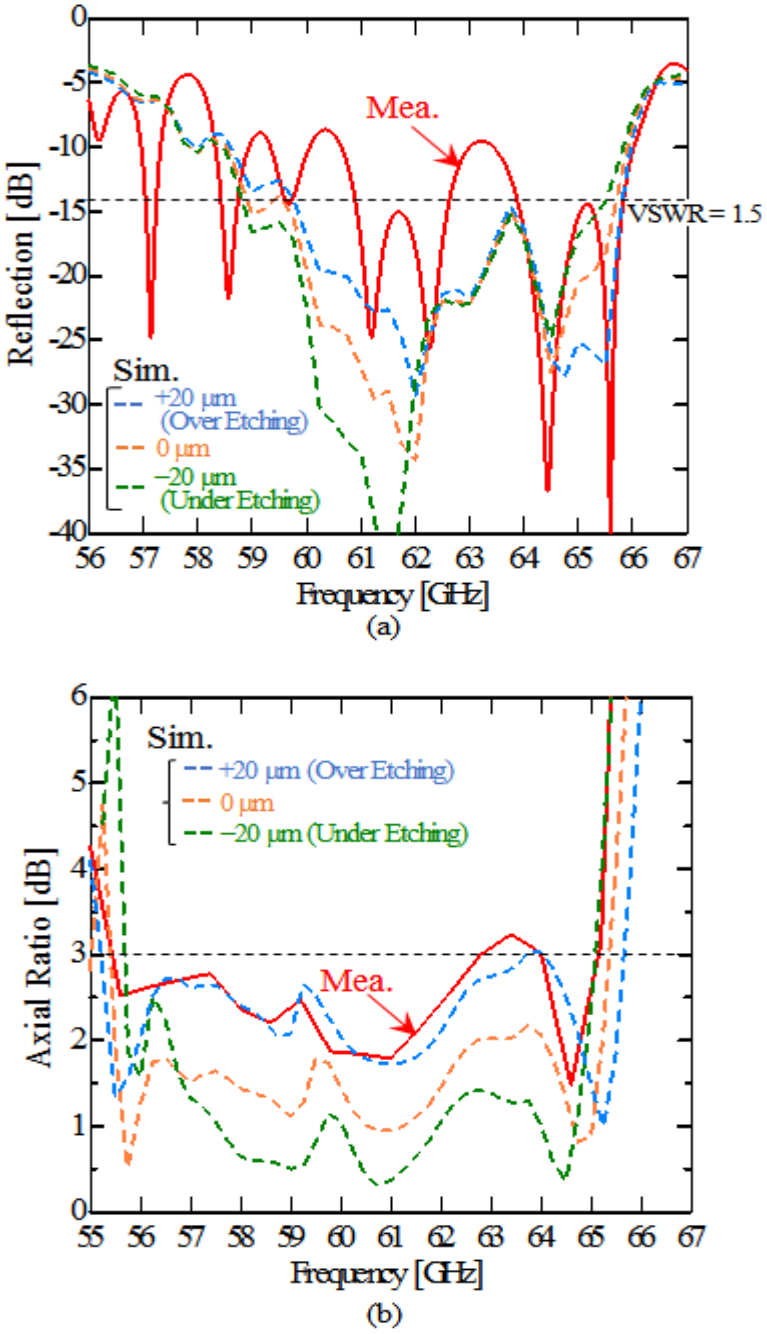

Fig. 3.20 Frequency characteristic of (a) reflection and (b) axial ratio w/ air Gap: 60μm between the radiating-slot and dielectric layers.

3.4.3 Radiation Patterns

Fig. 3.21 shows the measured and simulated radiation patterns at 61.5 GHz in the *xz*-plane, the *yz*-plane, and the 45 deg.-plane, measured by the spin linear method in an anechoic chamber. In the *xz*-plane, the measured pattern is in good agreement with the simulated pattern except for the ± 40-90 deg. regions. Reasons of the discrepancy around the ± 40-90 deg. region are not clear, but the sidelobe level is small (over -30 dB in the simulation and under -30 dB in the measurements), which would not be a cause of the problem. In the *yz*-plane, the measured pattern is in good agreement with the simulated one. In the 45 deg.-plane, the measured pattern coincides with the simulated one. The measured first-sidelobe levels are as follows: -15.7dB at -6.4 deg. and -15.2dB at +6.3 deg. in the *xz*-plane; -14.4 dB at -5.7 deg. and -13.4 dB at +6.7 deg. in the *yz*-plane; and -26.1 dB at -7.7 deg. and -29.2 dB at +9.1 deg. in the 45 deg.-plane. The structure is symmetrical in the *y*-direction, but not in the *x*-direction because all the coupling slots have an offset in the + *x*-direction. This offers slightly unsymmetrical patterns in the *xz*-plane also in the simulation. The measured patterns in each plane would not be completely symmetrical because of manufacturing errors in the etching and laminating processes; however, these differences are very small.

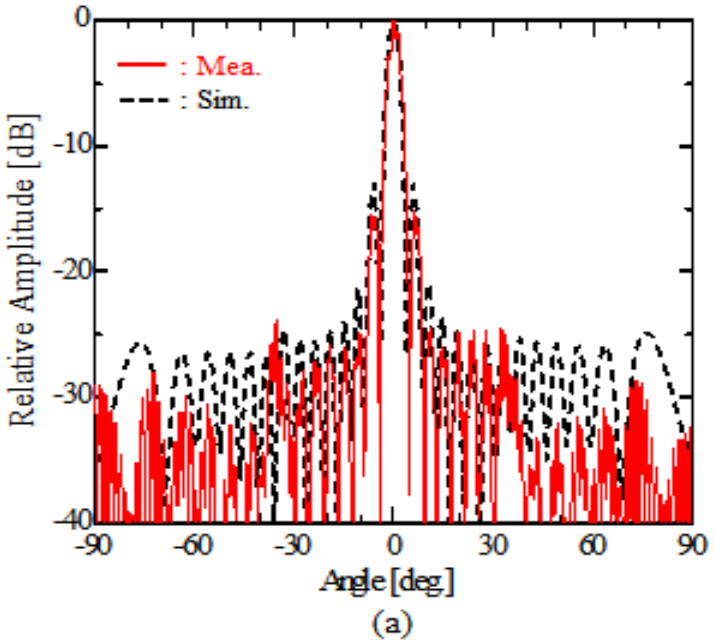

(a)

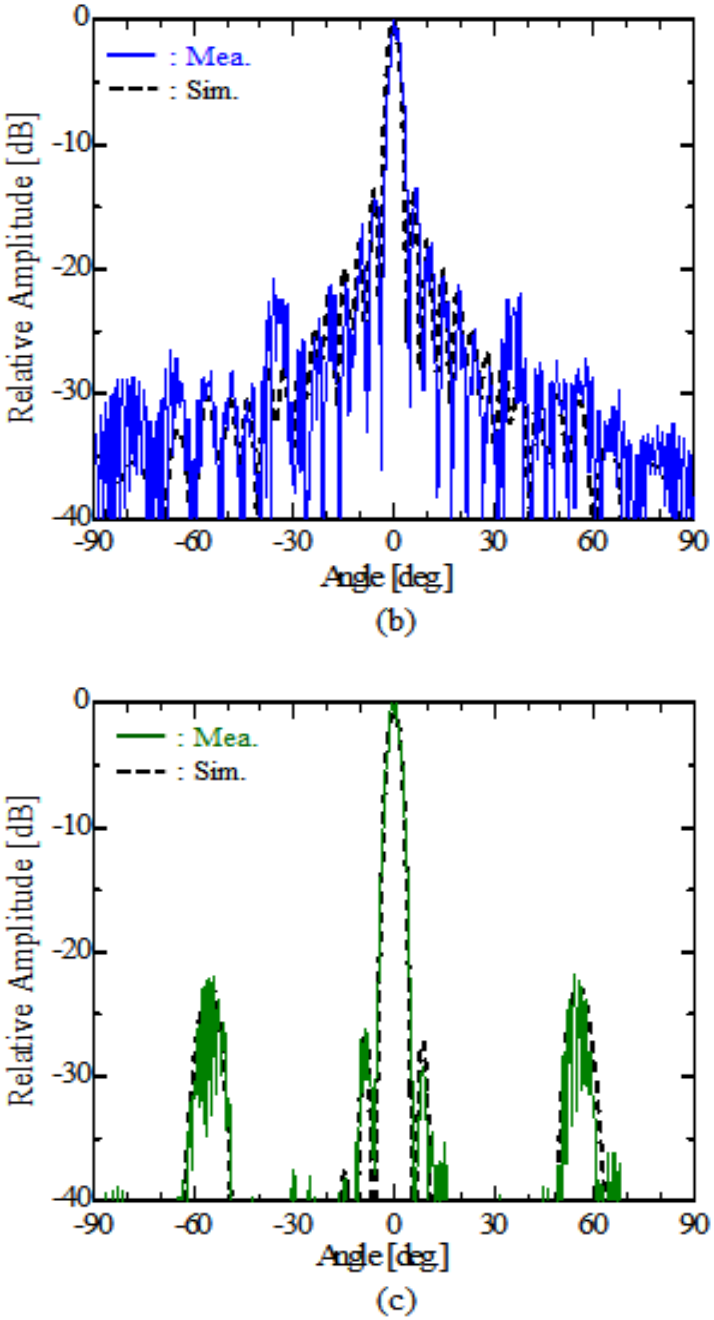

Fig. 3.21 Radiation patterns at 61.5 GHz. (a) *xz* -plane. (b) *yz* -plane. (c) 45 deg.- plane.

3.4.4 Realized Gain

Fig. 3.22 shows the measured and simulated realized-gains. The realized-gains, which include the reflection loss as well as conductor and dielectric losses and the aperture efficiency loss were measured against a standard gain horn antenna in an

anechoic chamber. The measured realized-gain is degraded more than the simulated value because of the reflection loss as shown in Fig. 3.20. At the design frequency, the measured realized gain is 32.7 dBi with the antenna efficiency of 75.5 %. As a reference, we also show a simulated result (black broken curve) based on fabrication errors of a 60 μm air gap in the region between the radiating-slot and dielectric layers and 20 μm over-etching of the slot layers. Here the realized gains tend to move toward the measured gains.

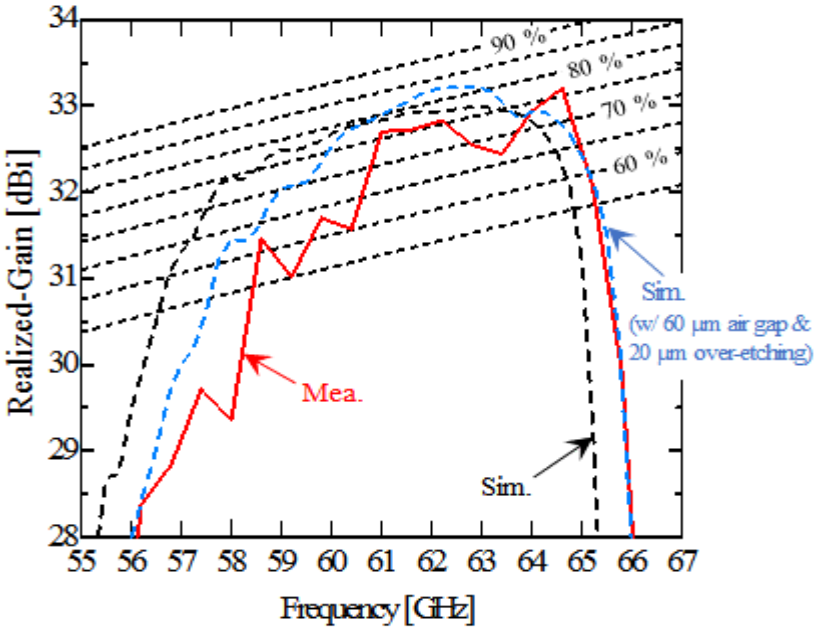

Fig. 3.22 Frequency characteristic of realized gain.

3.5 Tolerance of Manufacturing Errors

As a reference, we also present the tolerance of manufacturing errors by the analysis of a 2×2-element subarray. Fig. 3.23 shows the tolerance of slot sizes in the frequency characteristic of the reflection (a) and axial ratio (b). Parameters are the size of a coupling slot, radiating slots, parasitic slots and additional slots. Other parameters are fixed as shown in Fig. 3.6. Considering the bandwidth of the VSWR and the axial ratio, etching errors should be within ± 40 μm. In particular, the etching error of – 40 μm has a better performance than that of + 40 μm in both bandwidths of the VSWR and axial ratio. Fig. 3.24 also shows the tolerance of the relative permittivity of dielectric. Other parameters are fixed as shown in Fig. 3.6. Considering the bandwidth of the VSWR and the axial ratio, the error of the relative permittivity should be within 7 %. The bandwidth of the axial ratio is durable against the error of the relative permittivity relatively.

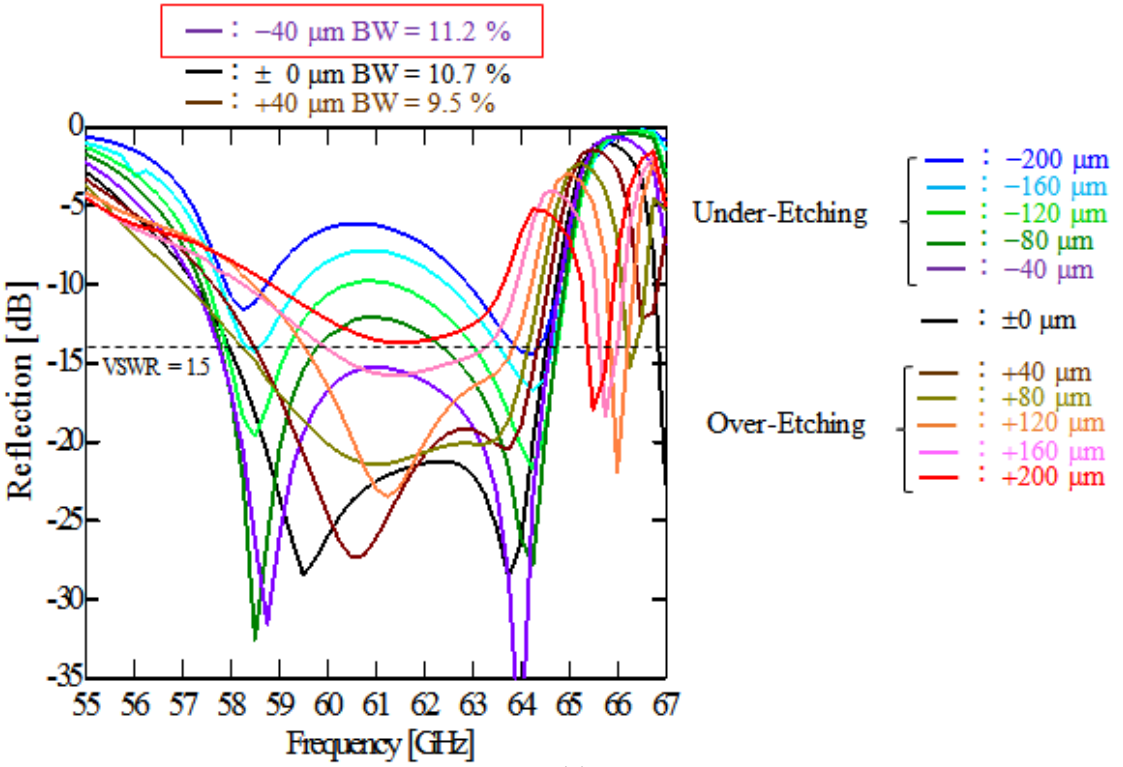

(a)

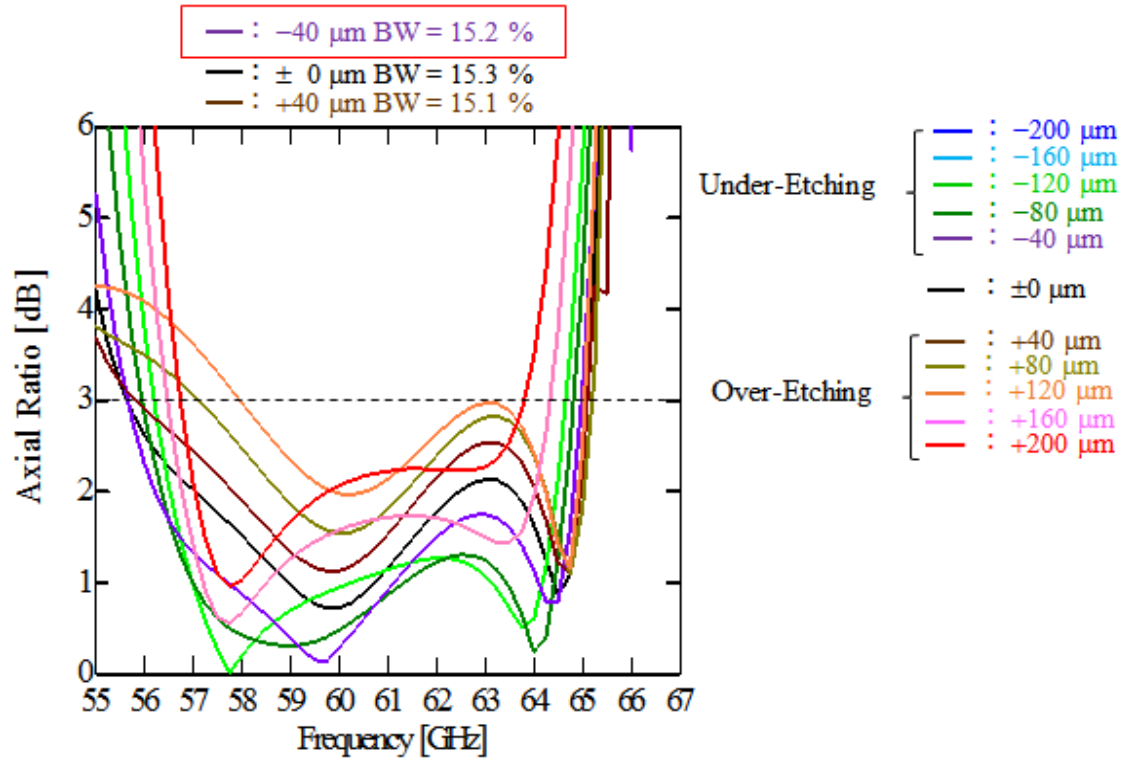

(b)

Fig. 3.23 Tolerance of slot sizes. Frequency characteristic of the reflection (a) and axial ratio (b).

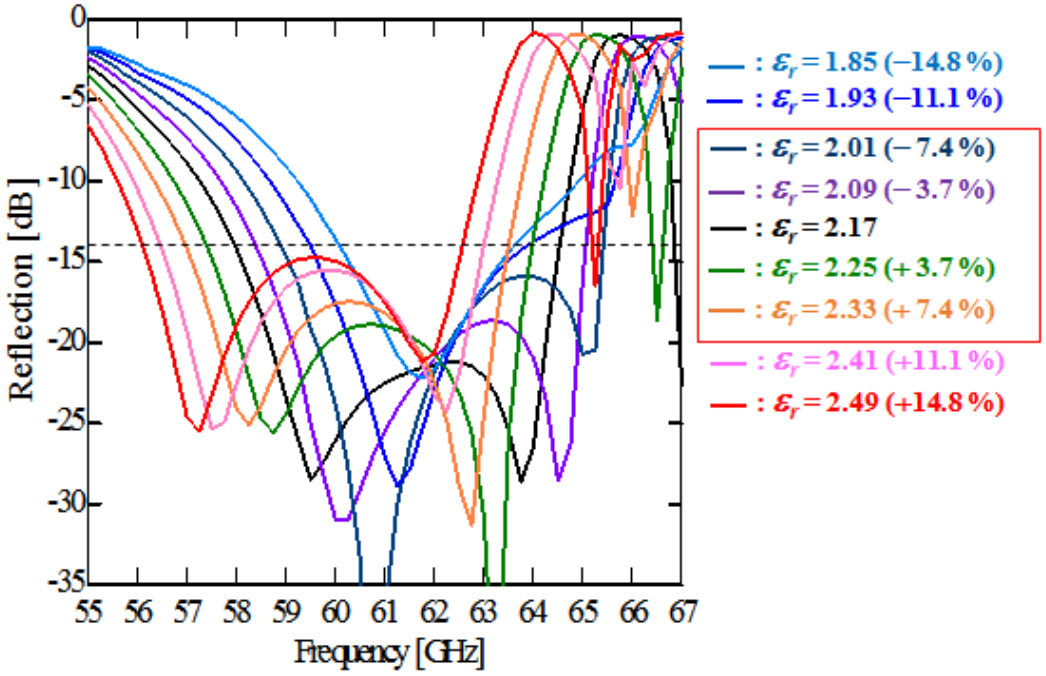

(a)

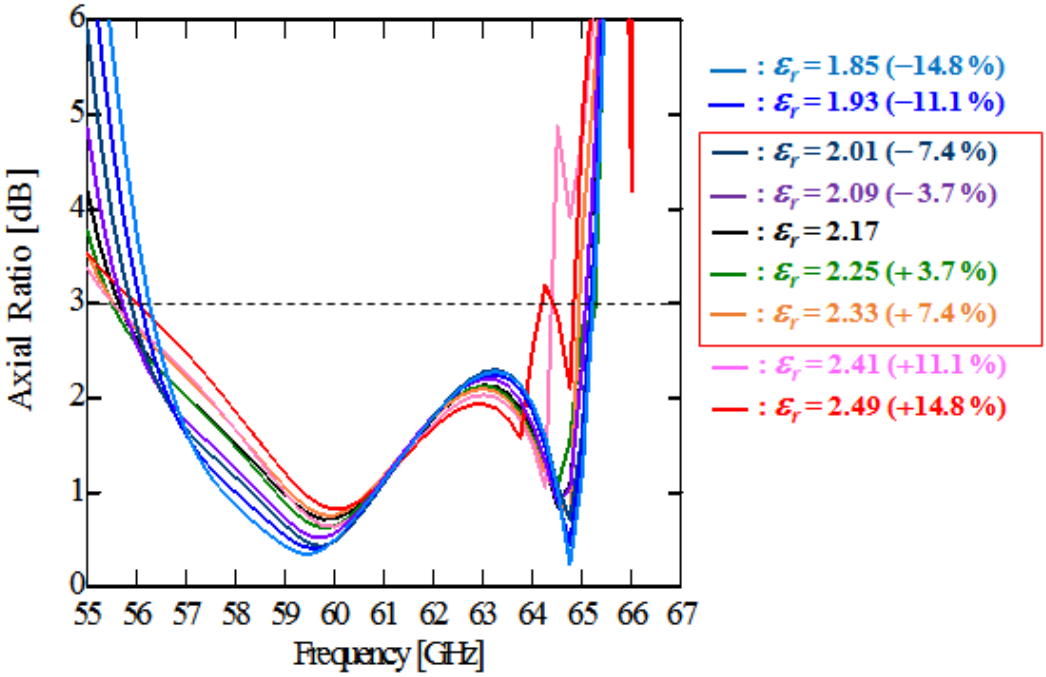

(b)

Fig. 3.24 Tolerance of the relative permittivity of dielectric. Frequency characteristic of the reflection (a) and axial ratio (b).

3.6 Concluding remarks

This Chapter proposed a perpendicular-corporate feed for a four-layer circularly-polarized parallel-plate slot array antenna. We have introduced a dielectric layer with adequate permittivity in the region between the coupling-aperture and the radiating-slot layers. This structure generates standing waves and thus uniform excitation. The dielectric layer combines PTFE and air considering fabrication limitations. The measured radiation patterns of a 16×16-element array antenna show uniform excitation. The four-layer structure with the apertures for circular polarization, which avoids electrical contact in the radiating part with the provision of air gaps, provides wideband characteristic for axial ratios arising from interaction between two of the three eigenmodes in the desired band range. We realize an 11.9 % bandwidth for axial ratios of less than 3 dB in the measurements. At the design frequency, the measured realized gain is 32.7 dBi with the antenna efficiency of 75.5 %.

References

[3.1] C. A. Balanis, “Advanced Engineering Electromagnetics”, John Wiley & Sons, pp.394-410, 1989.

Chapter 4

Design of Perpendicular-Corporate Feed in Four-Layer Parallel-Plate Linearly-Polarized Slot Array Antennas

4.1 Introductory Remarks

This chapter presents a perpendicular-corporate feed in a four-layer parallel-plate linearly-polarized (and 45-deg.-polarized) slot array antenna. This antenna is based on the structure of a perpendicular-corporate feed in a three-layer parallel-plate slot array antenna as described in the chapter 2, but several structural differences are involved as follows. To enhance the bandwidth of the VSWR, the proposed antenna has an additional-slot layer on the top of parasitic-slot layer with an air gap in the region between the two. Considering fabrication limitations, a dielectric layer is formed by the combination of polytetrafluoroethylene (PTFE, $\varepsilon_r = 2.17$) and air, resulting in the desired permittivity: porous PTFE, $\varepsilon_r = 1.28$ equivalently. First, we design a four-layer parallel-plate linearly-polarized slot array antenna as the previous step of creating 45-deg. polarization. Secondly, we analyze a model with pair slots in the additional slot layer to suppress grating lobes in the 45-deg. plane as a reference. Lastly, we analyze a four-layer parallel-plate 45-deg.-polarized slot array antenna. In this chapter, we focus on three types of the configuration of additional slots to achieve desired operations: linear polarization with wideband, linear polarization with low grating lobes and 45 deg. polarization.

This chapter is organized as follows. Section 4.2 describes the perpendicular-corporate feed in a four-layer linearly-polarized slot array. In this section, we explain the antenna configuration and the design process for a wideband operation by the analysis of a 2×2-element subarray and a 16×16-element array. Section 4.3 discusses the introduction of slot pairs in an additional-slot layer by the analysis of a 2×2-element array and a 16×16-element array to suppress grating lobes around ± 55 deg. in the 45-deg. plane. Section 4.4 presents the introduction of 45-deg.-inclined slots in the additional-slot layer by the analysis of a 2×2-element subarray and a 16×16-element array. In section 4.5, we conclude this chapter.

4.2 Antenna Configuration

Fig. 4.1 shows a perpendicular-corporate feed in a four-layer parallel-plate linearly-polarized slot array. The antenna consists of an additional-slot layer, a parasitic-slot layer, a radiating-slot layer, a dielectric layer, a coupling-aperture layer and a feeding-circuit layer. There are air gaps between the slot layers including the coupling-aperture layer, and so there is no metal to metal contact in the radiating part. The dielectric layer is formed by the combination of polytetrafluoroethylene (PTFE, ε_r = 2.17) and air, offering the desired permittivity equivalently. The configuration of all the slots is rectangular to create linear polarization, and the top slot layer has larger sized slots in this structure. In Fig. 4.1, the layers are drawn widely apart to show the internal structure. However, in the actual antenna, the layers are stacked much more closely together. The antenna is fed from the back (bottom in the figure) by a feed aperture. The feeding circuit feeds the coupling apertures in equal amplitude and phase. The coupling-aperture layer is placed between the feeding-circuit layer and the dielectric layer and with an air gap in between. The radiating-slot layer is mounted directly on the dielectric layer. The parasitic-slot layer is on top of the radiating-slot layer, also with an air gap in between. The additional-slot layer is over the parasitic-slot layer, similarly with an air gap to improve the VSWR bandwidth. The coupling apertures each excite 2×2 radiating slots and the electromagnetic field moves to the additional slots through the parasitic slots. The spacing of all the slot types is constant: $0.86\lambda_0$ (4.20 mm) in the *x* and *y* directions. Here, the λ_0 is the wavelength at the design frequency of 61.5 GHz.

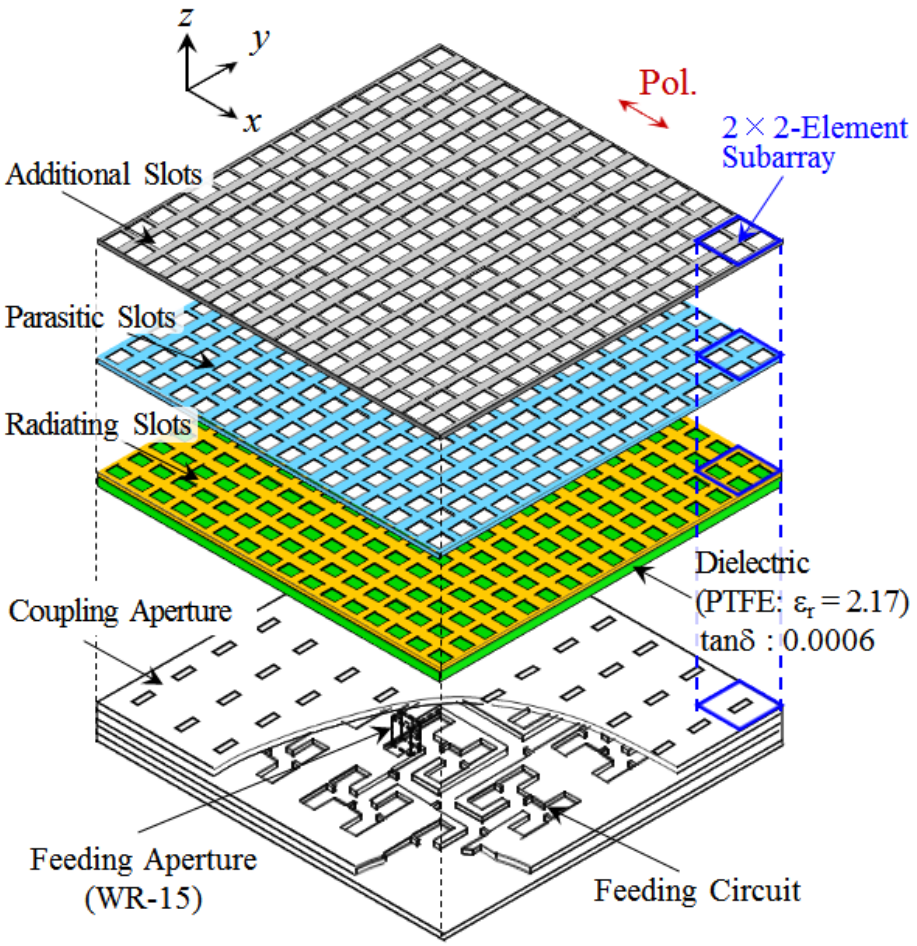

Fig. 4.1 Perpendicular-corporate feed in a four-layer parallel-plate linearly-polarized slot array.

4.3 Design

4.3.1 Design of 2×2-Element Subarray

To enhance the bandwidth of the VSWR, the proposed model has an additional-slot layer. Fig. 4.2 shows the model for the analysis of the 2×2-element subarray. In the analysis, we use a dielectric layer of t_d = 0.38 mm and ε_r = 2.17 obtained from the subsection 3.3.1. The conductivity 5.8×10^7 S/m of copper and a loss tangent 0.0006 of the dielectric are assumed. Considering the fabrication, we select a multiple of 0.20 mm as the thickness of layers and air gaps except for the dielectric layer. The parameters are as follows: the size of the additional slots, l_a, and w_a; the size of the parasitic slots, l_p and w_p; the size of the radiating slots, l_r and w_r; and the size of the coupling apertures, l_c and w_c. The air gap between the additional-slot and the parasitic-slot layers is h_{ap}, that between the parasitic-slot and the radiating-slot layers is h_{pr}, and that between the dielectric and

coupling layers is h_{rc}. Also, note that the thicknesses of the additional-slot layer, the parasitic-slot layer and radiating-slot layer is 0.20 mm, and that of the coupling-aperture layer is 0.20 mm. The size of feeding waveguide is fixed: width a = 2.95 mm, thickness b = 1.00 mm and length g = 5.64 mm, and it has short end. The offset of the coupling aperture against the principal axis in the x direction is also fixed at 0.61 mm. The final values of the design parameters are listed in the figure.

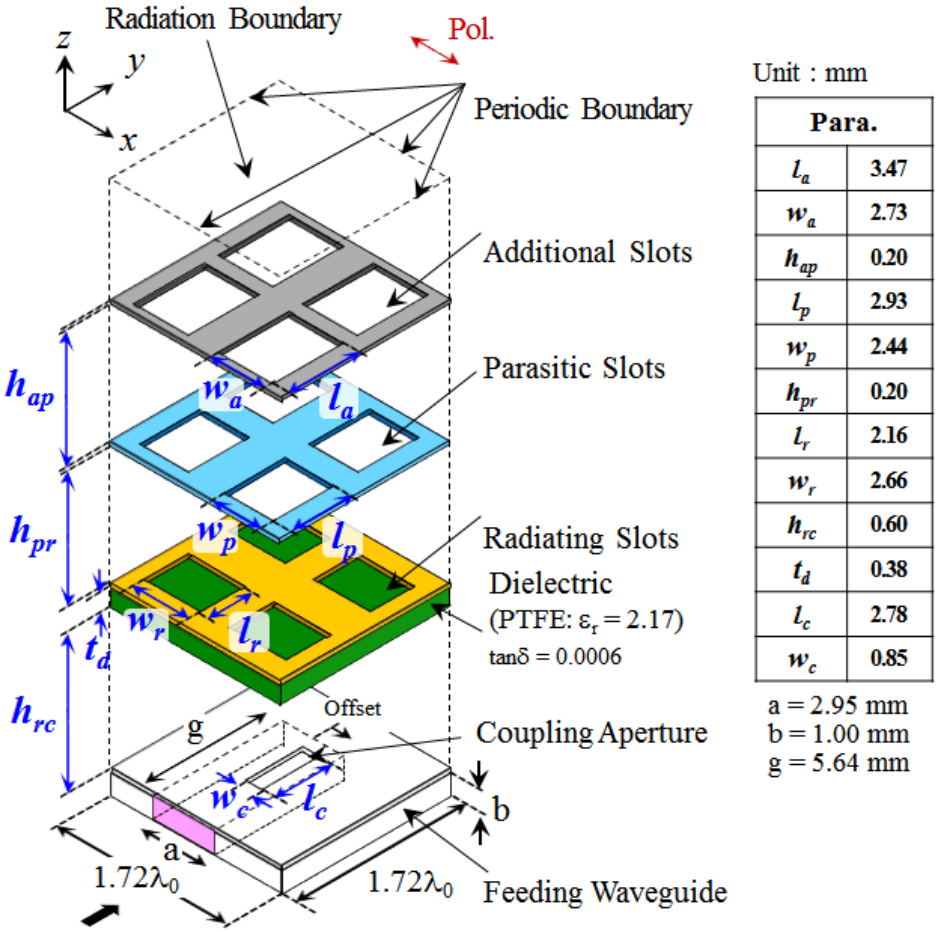

Unit : mm

Para.	
l_a	3.47
w_a	2.73
h_{ap}	0.20
l_p	2.93
w_p	2.44
h_{pr}	0.20
l_r	2.16
w_r	2.66
h_{rc}	0.60
t_d	0.38
l_c	2.78
w_c	0.85

a = 2.95 mm
b = 1.00 mm
g = 5.64 mm

Fig. 4.2 Model for the analysis of the 2×2-element subarray.

As a typical design process, we show the frequency characteristic of the reflection by changing the size of additional slots: l_a and w_a in the Fig. 4.3. In the analysis, we fixed other parameters as shown in Fig. 4.2. As l_a is larger, the antenna has the better performance of the reflection depending on w_a. Also, when w_a is 2.73 mm, the performance of the reflection is relatively good in all l_a. As a result, we set l_a = 3.47 mm and w_a = 2.73 mm to obtain the better performance of the reflection in the desired frequency domain.

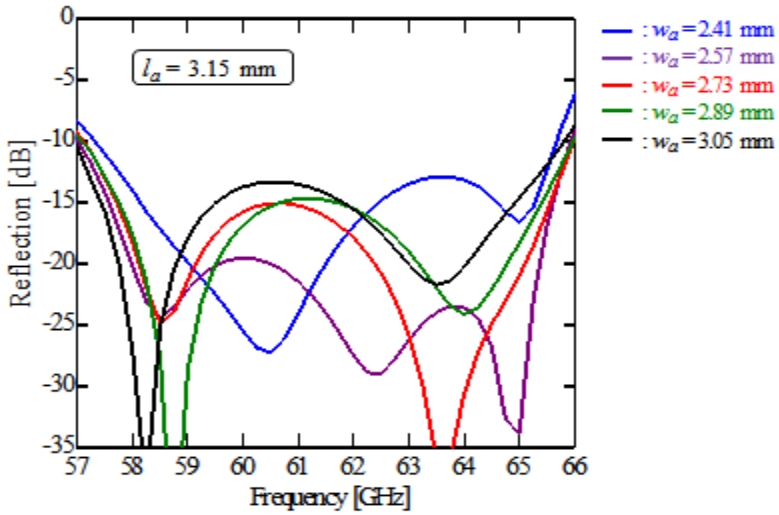
l_a = 3.15 mm
: w_a=2.41 mm
: w_a=2.57 mm
: w_a=2.73 mm
: w_a=2.89 mm
: w_a=3.05 mm
Reflection [dB]
Frequency [GHz]

(a)

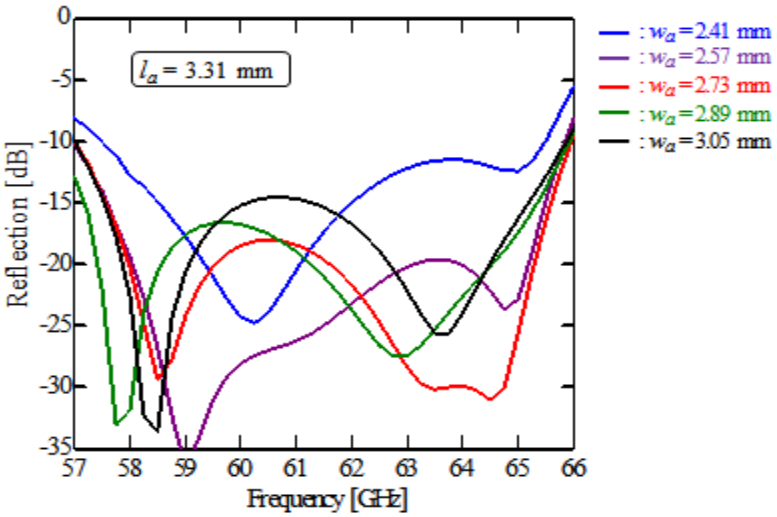
l_a = 3.31 mm
: w_a=2.41 mm
: w_a=2.57 mm
: w_a=2.73 mm
: w_a=2.89 mm
: w_a=3.05 mm
Reflection [dB]
Frequency [GHz]

(b)

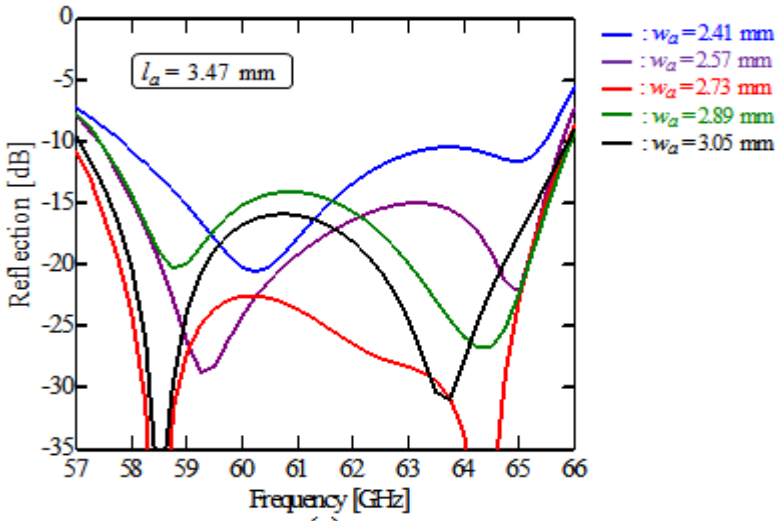
l_a = 3.47 mm
: w_a=2.41 mm
: w_a=2.57 mm
: w_a=2.73 mm
: w_a=2.89 mm
: w_a=3.05 mm
Reflection [dB]
Frequency [GHz]

(c)

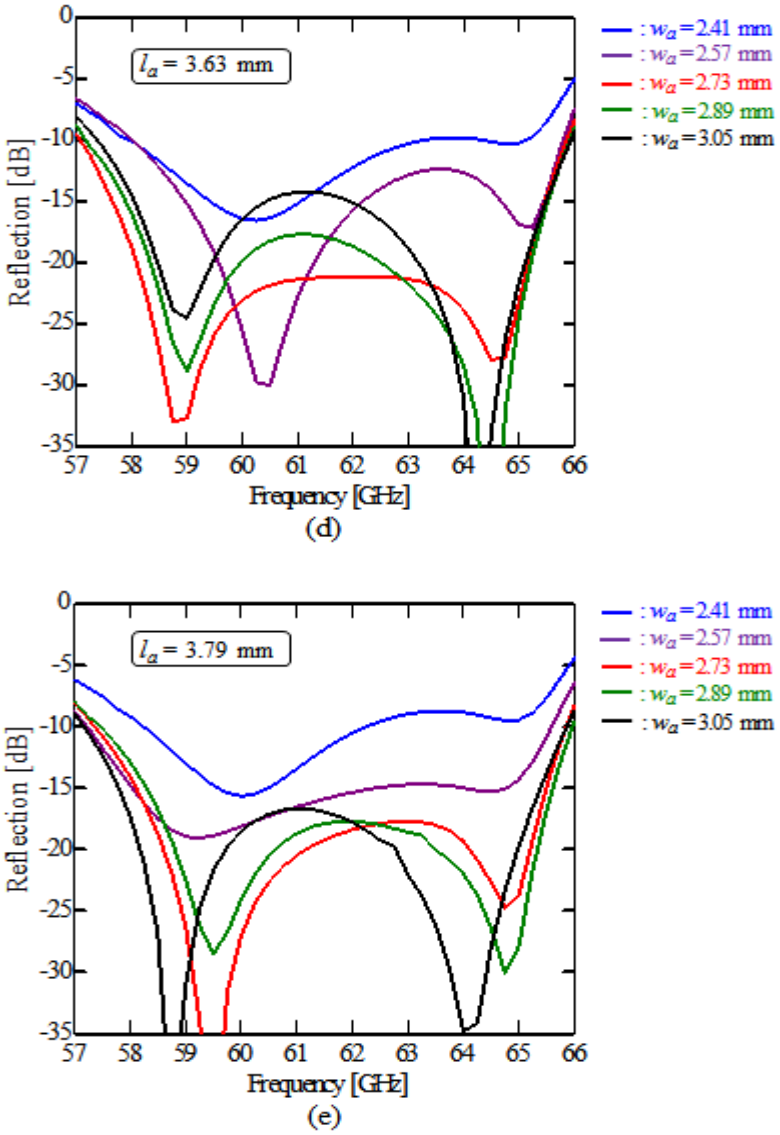

Fig. 4.3 Frequency characteristic of the reflection by changing the size of additional slots: l_a and w_a. (a) l_a = 3.15 mm. (b) l_a = 3.31 mm. (c) l_a = 3.47 mm. (d) l_a = 3.63 mm. (e) l_a = 3.79 mm.

Fig. 4.4 shows the frequency characteristic of the reflection when l_a and w_a are 3.47 mm and 2.73 mm respectively. As a reference, we also show the result of the three-layer linearly-polarized slot array antenna as shown in Fig. 2.10. The reflection of the 2×2-element subarray with the additional-slot layer is smaller than -14 dB over 13.4 % of the bandwidth ranging from 57.3 to 65.6 GHz. On the other hand, the reflection of the three-layer linearly-polarized slot array antenna is less than -14 dB over 7.7 % bandwidth

ranging from 59.2 to 63.9 GHz. The bandwidth is enhanced by almost 1.7 times due to the introduction of the additional-slot layer. To elucidate the enhanced bandwidth, we utilize an eigen mode analysis.

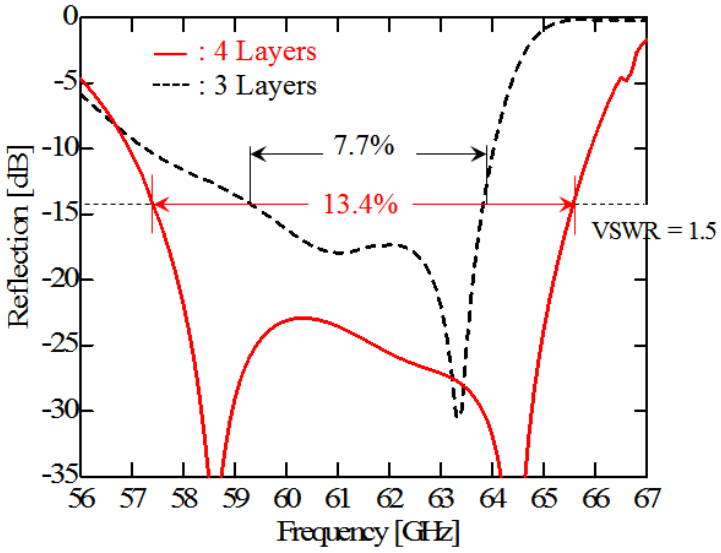

Fig. 4.4 Frequency characteristic of the reflection.

Fig. 4.5 show the model of the eigenmode analysis. To save calculation time, we use 1×1-element subarray because of the symmetric structure. Note that a coupling aperture is excluded in the model, instead a PEC boundary is used there. Around the periphery of the 1×1-element subarray, periodic, impedance and PEC boundaries are introduced. Parameters are the same as these of Fig. 4.2. As a reference, resonant frequencies of each slot are also shown in Fig. 4.5. The larger size of a slot has a higher resonant frequency: additional slot, 73.5 GHz; parasitic slot, 69.1 GHz and radiating slot, 60.1 GHz.

Fig. 4.6 shows Q factors and electric-field vectors of an additional slot in each eigenmode. For the better understanding, we plot the result in the frequency characteristic of the reflection as described in Fig. 4.4. As a reference, the result of the three-layer linearly-polarized slot array antenna is also shown in Fig. 4.6. The first eigenmode and second one are occurred at 58.5 GHz and 64.9 GHz, respectively. The values of Q factors are 9.9 and 10.2, respectively and lower than these of the three layers due to the introduction of the additional-slot layer. These lower Q factors contribute to enhancing the VSWR bandwidth.

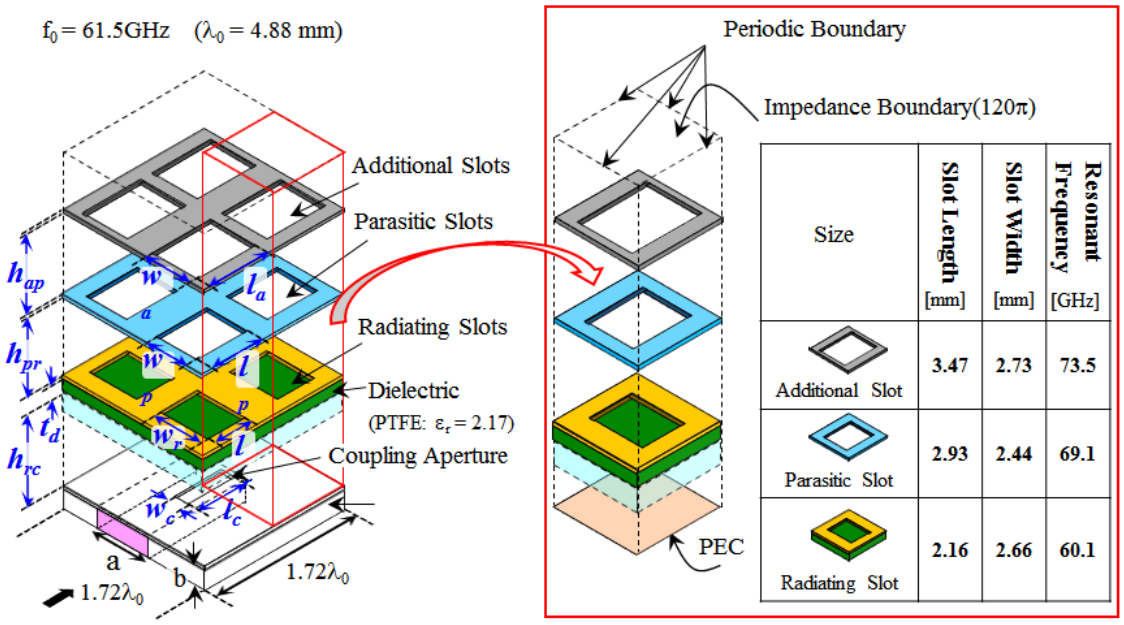

Fig. 4.5 Model for the eigenmode analysis of the 1×1-element subarray.

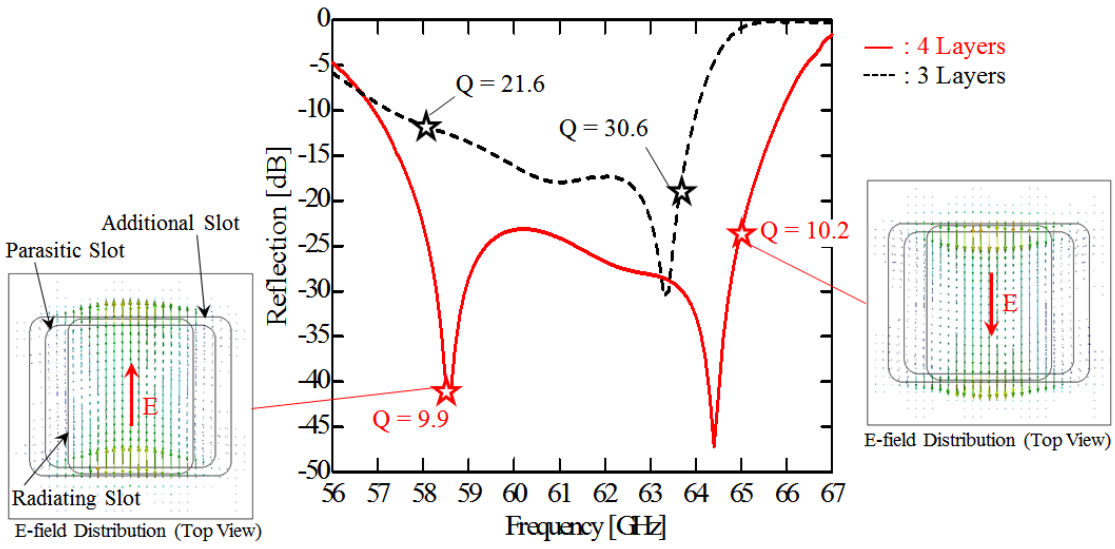

Fig. 4.6 Q factors and electric-field vectors of an additional slot in each eigenmode.

4.3.2 Full Structure Analysis

Fig. 4.7 shows the full structure of a 16×16-element four-layer linearly-polarized parallel-plate slot array antenna fed by a perpendicular corporate feed. In Fig. 4.7, the plates are shown separately to expose the internal structure more fully, for the actual antenna, they are stacked much more closely together. In the simulation, the conductivity of 5.8×10^7 S/m of copper and the loss tangent 0.0006 of the dielectric are assumed. Considering fabrication to maintain the flatness of the layers, the periphery of the four-layer parallel plates is terminated by (enclosed in) copper frames as shown in Fig. 4.7. The edge as PMC of the parallel plates is extended by 1.3 mm ($\approx 0.25\lambda_0$) only in the *y* direction and terminated by copper. The dimensions of the antenna in the *xy*-plane is 75.2 mm × 79.4 mm. The parameters are the same as these of the 2×2-element subarray shown in Fig. 4.2.

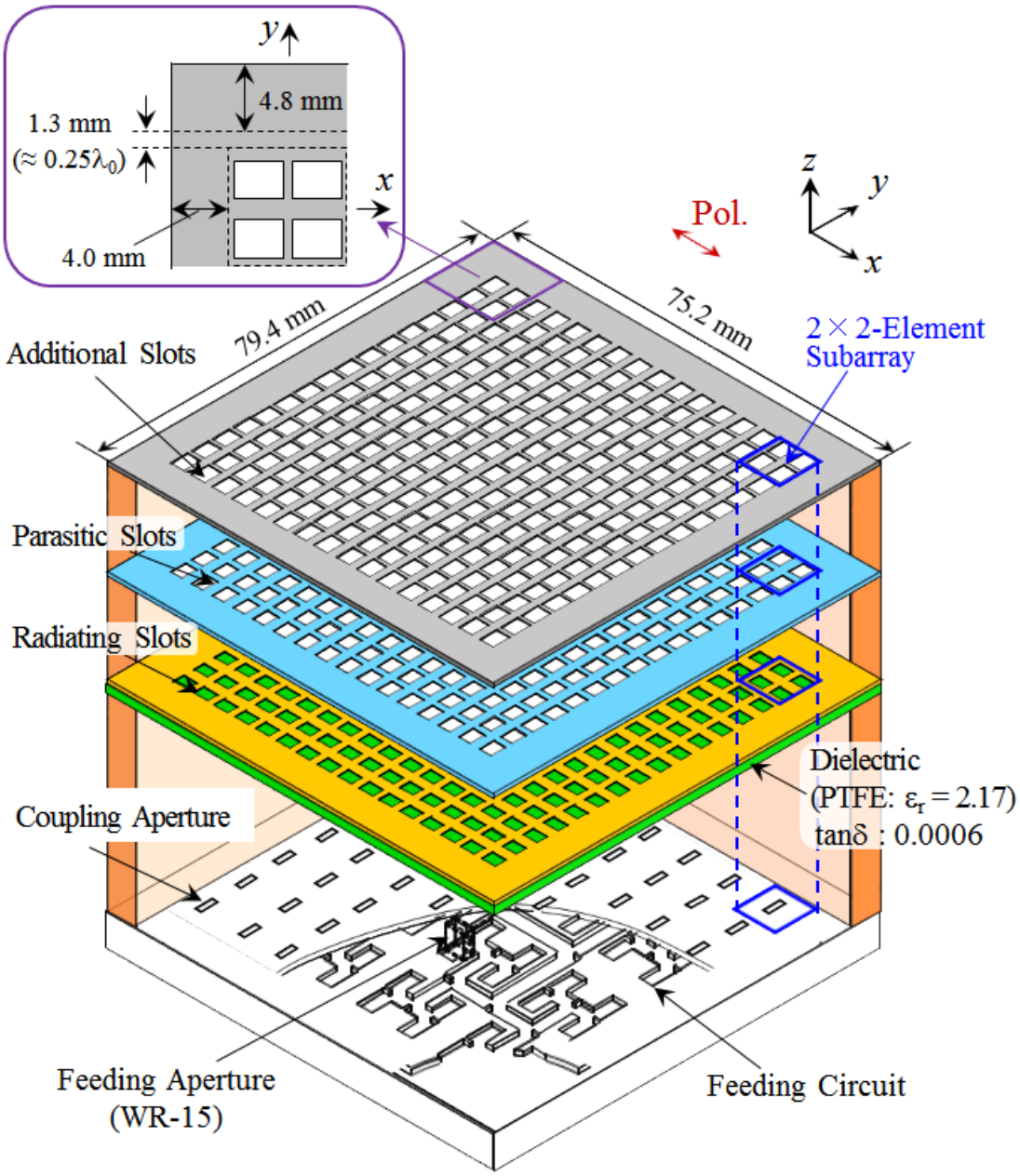

Fig. 4.7 Full structure of a perpendicular corporate feed in a four-layer linearly-polarized parallel-plate slot array antenna.

Fig. 4.8 shows the frequency characteristic of the reflection. As a reference, the reflections of 2×2-element subarray and the feeding circuit are also described. The reflection of the full structured antenna is less than -14 dB over 12.9 % of the bandwidth ranging from 57.8 to 65.7 GHz. The bandwidth is very similar to that of the 2×2-element subarray. Also, the reflection of the full structured antenna has slight ripples. This would be caused by the feeding circuit because the reflection of it has more clear ripples in Fig. 4.8.

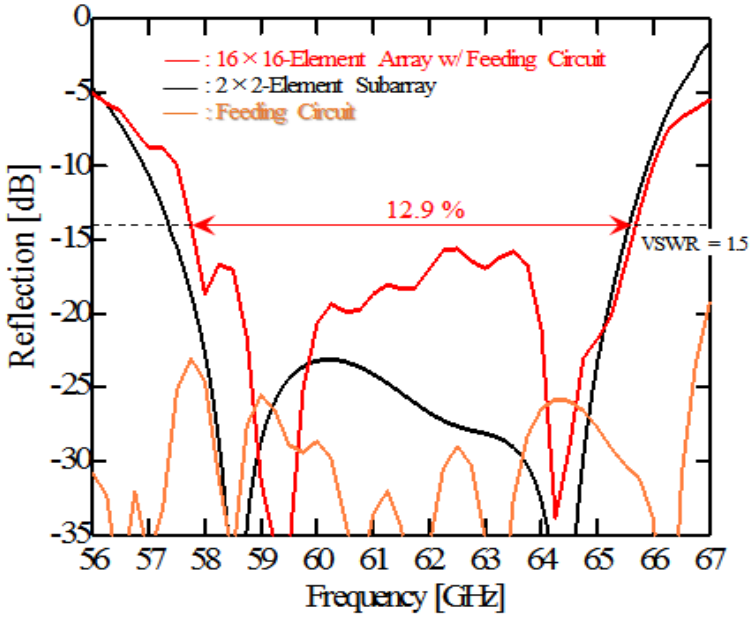

Fig. 4.8 Frequency characteristic of the reflection.

Fig. 4.9 shows radiation patterns at the design frequency (61.5 GHz) in the E-plane (*xz*), H-plane (*yz*) and 45 deg.-plane. In the E-plane, the radiation pattern has slightly high sidelobes in wide-angle regions ranging from ± 40 deg. to ± 90 deg. due to the effect of an omnidirectional element pattern. In the 45 deg.-plane, the radiation pattern has grating lobes around ± 50-60 deg. region due to the excitation difference in the plane. The relative amplitude of the grating lobes is -22 dB around ± 55 deg. This would be caused by wider configuration of slots.

Fig. 4.10 shows realized gain, gain and directivity. The realized gain includes the reflection loss as well as conductor and dielectric losses, and the aperture efficiency loss. We have achieved 12.6 % 1-dB-down bandwidth of realized gain in the 57.7 – 65.5 GHz range and 82% antenna efficiency at design frequency. The aperture efficiency greater than 80 % is achieved over 7-GHz bandwidth.

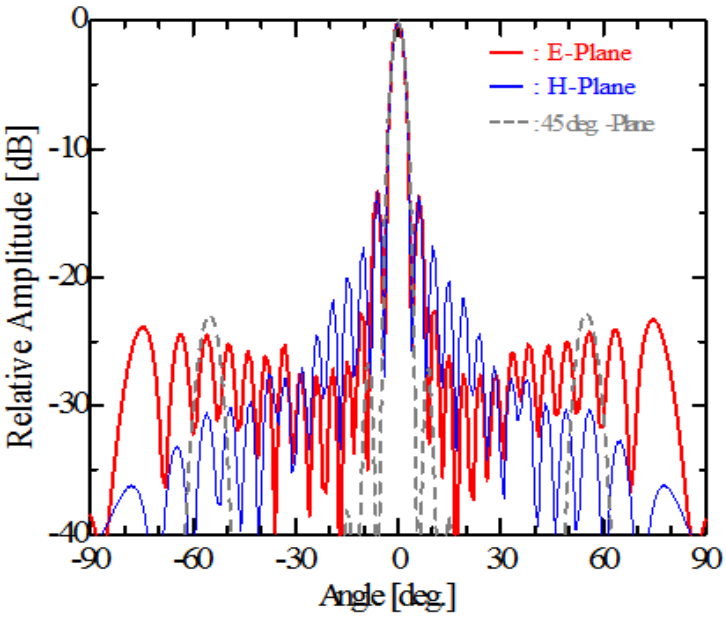

Fig. 4.9 Radiation patterns at 61.5 GHz

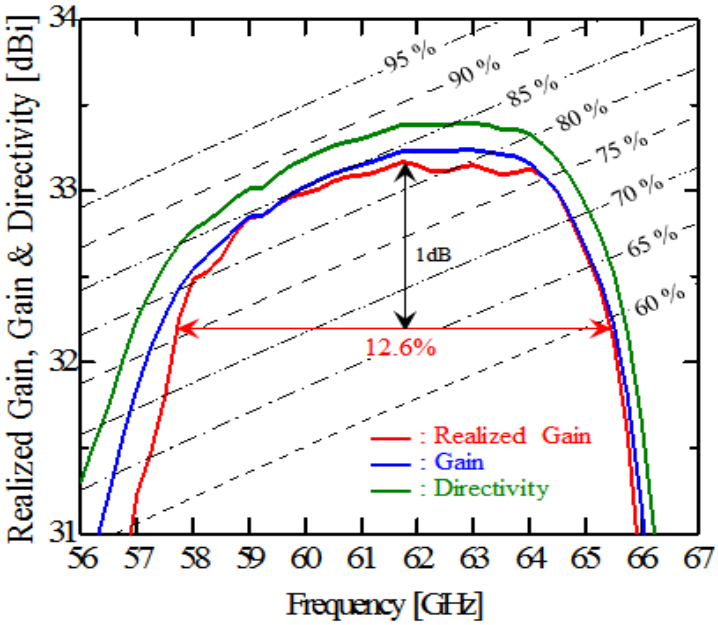

Fig. 4.10 Frequency characteristic of the realized gain, gain and directivity.

4.3.3 Concluding Remarks

This subsection presented a perpendicular-corporate feed for a four-layer linearly-polarized parallel-plate slot array antenna. The proposed antenna has additional-slot layer on the top of the parasitic-slot layer with an air gap between the two to enhance the bandwidth of the VSWR. The dielectric layer with adequate permittivity is placed in the region between the coupling-aperture layer and the radiating-slot layer to generates standing waves and thus uniform excitation. The dielectric layer combines PTFE and air considering fabrication limitations.

In the simulation, we have realized 12.9 % bandwidth for the VSWR of less than -14 dB due to the introduction of the additional-slot layer. Radiation patterns provide uniform-excitation patterns including an element pattern in both the E-plane and H-plane. This means the dielectric layer has adequate permittivity, resulting in generation of standing waves. However, in the 45 deg.-plane the radiation pattern has grating lobes around ± 50-60 deg. region because of the excitation difference in the plane. This would be caused by wider configuration of slots. The relative amplitude of the grating lobes is -22 dB around ± 55 deg. Also, we have achieved 12.6 % 1-dB-down bandwidth of realized gain and 82% antenna efficiency at design frequency. The aperture efficiency greater than 80 % is achieved over 7-GHz bandwidth.

4.4 Introduction of Slot Pairs in Additional-Slot Layer

4.4.1 Antenna Configuration

To suppress grating lobes around ± 55 deg. in the 45 deg. plane, we introduce slot-pair configuration in the additional-slot layer of the perpendicular-corporate feed in a four-layer parallel-plate linearly-polarized slot array. Fig. 4.11 shows a perpendicular-corporate feed in a four-layer parallel-plate linearly-polarized slot array with slot pairs. plane. The slot-pair configuration can suppress grating lobes by reducing higher modes while remaining the wideband design of the VSWR [4.1].

The antenna structure is based on Fig. 4.1 and consists of the additional-slot layer, the parasitic-slot layer, the radiating-slot layer, the dielectric layer, the coupling-aperture layer and the feeding-circuit layer. There are air gaps between the slot layers including the coupling-aperture layer, and so there is no metal to metal contact in the radiating part. For additional slots, the configuration of slot pairs is introduced to suppress grating lobes. The antenna is fed from the back (bottom in the figure) by a feed aperture. The feeding circuit feeds the coupling apertures in equal amplitude and phase. The coupling-aperture layer is placed between the feeding-circuit layer and the dielectric layer and with an air gap in between. The radiating-slot layer is mounted directly on the dielectric layer. The parasitic-slot layer is on top of the radiating-slot layer, also with an air gap in between. The additional-slot layer is over the parasitic-slot layer, similarly with an air gap to improve the VSWR bandwidth. The coupling apertures each excite 2×2 radiating slots and the electromagnetic field moves to the additional slots through the parasitic slots. The spacing of all the slot types is constant: $0.86\lambda_0$ (4.20 mm) in the x and y directions. Here, the λ_0 is the wavelength at the design frequency of 61.5 GHz. The top slot layer has larger sized slots in this structure.

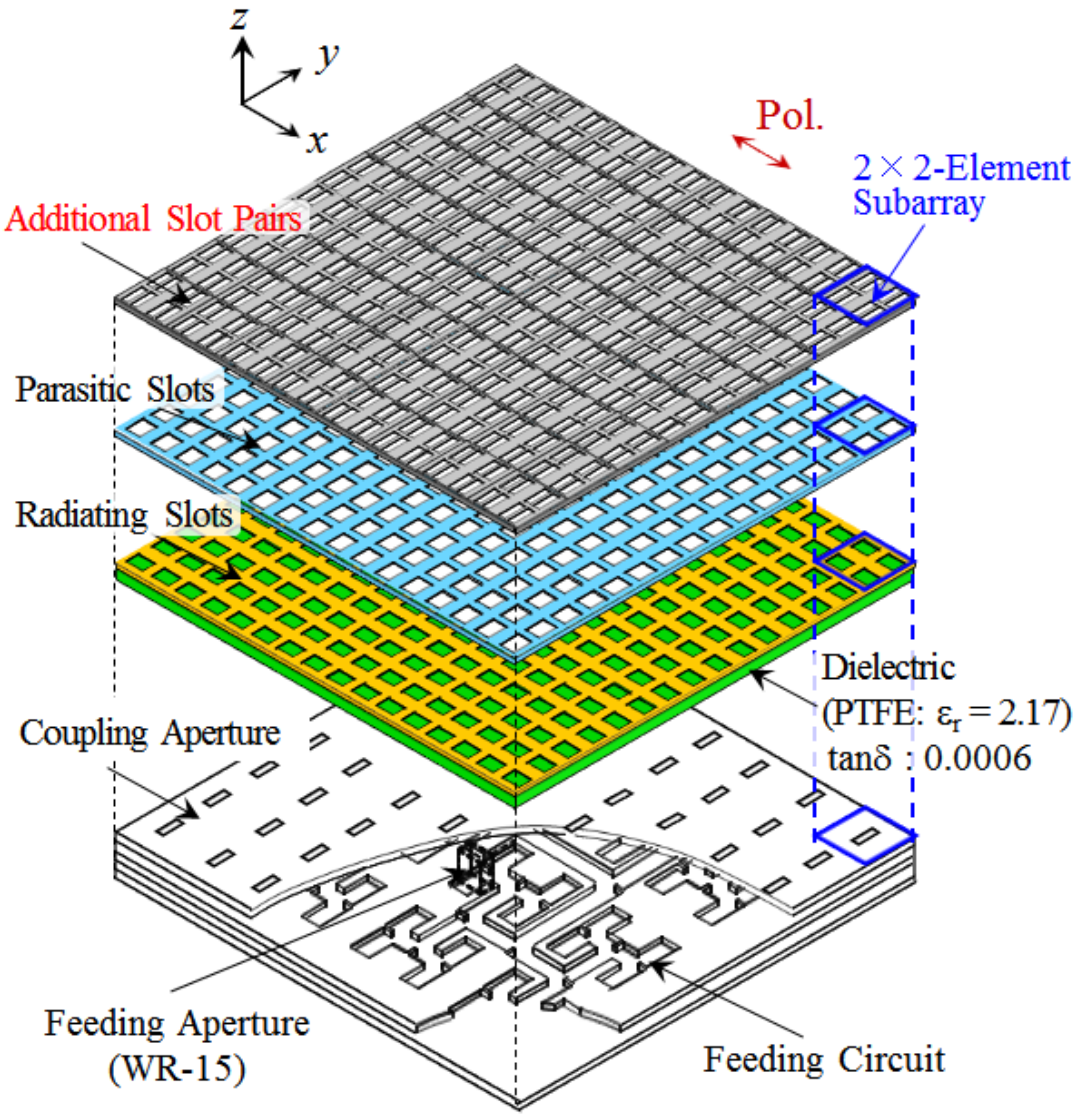

Fig. 4.11 Perpendicular-corporate feed in a four-layer parallel-plate linearly-polarized slot array with slot pairs.

4.4.2 Design of 2×2-Element Subarray

Fig. 4.12 shows the model for the analysis of the 2×2-element subarray. In the analysis, we use a dielectric layer of t_d = 0.38 mm and ε_r = 2.17 obtained from the subsection 3.3.1. The conductivity 5.8×10^7 S/m of copper and a loss tangent 0.0006 of the dielectric are assumed. To enhance the bandwidth of the VSWR, the proposed model has an additional-slot layer. The parameters are as follows: the size of the additional slot pairs, l_a and w_a; the space between additional slot pairs, s_a; the size of the parasitic slots, l_p and w_p; the size of the radiating slots, l_r and w_r; and the size of the coupling apertures,

l_c and w_c. The air gap between the additional-slot and the parasitic-slot layers is h_{ap}, that between the parasitic-slot and the radiating-slot layers is h_{pr}, and that between the dielectric and coupling layers is h_{rc}. Considering the fabrication, we select a multiple of 0.20 mm as the thickness h_{rc}. When h_{rc} is 0.60 mm and t_d is 0.38 mm. The thicknesses of the additional-slot layer, the parasitic-slot layer, and radiating-slot layer is 0.20 mm, and that of the coupling-aperture layer is 0.20 mm. The size of the feeding waveguide is fixed: width a = 2.95 mm, thickness b = 1.00 mm and length g = 5.65 mm, and it has short end. The offset of the coupling aperture against the principal axis in the x direction is also fixed at 0.60 mm. The final values of the design parameters are also listed in the figure.

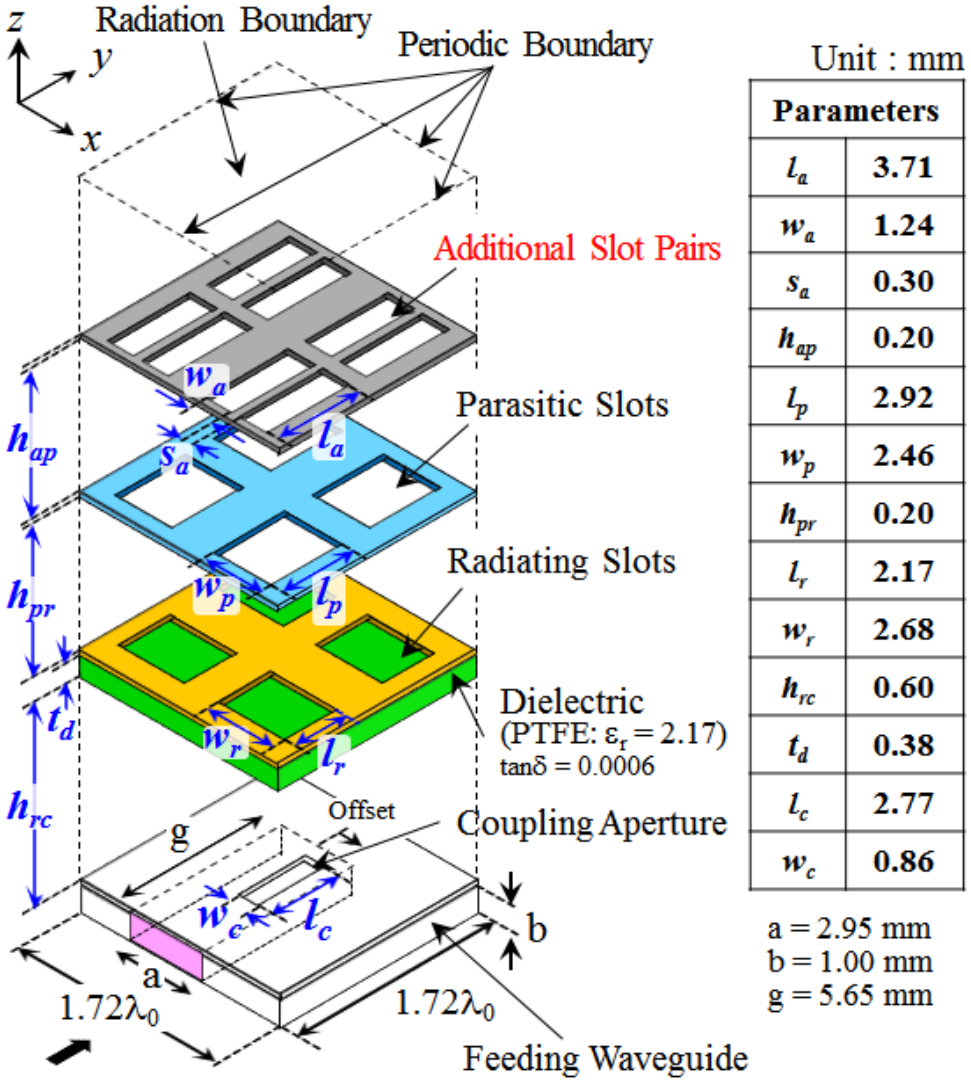

Fig. 4.12 Model for the analysis of the 2×2-element subarray.

As a typical design process, Fig.4.13 shows the frequency characteristic of the reflection by changing the size of additional slot pairs: l_a and w_a, and the space between additional slot pairs: s_a. Note that the minimum space between additional slot pairs should be 0.30 mm considering the fabrication limitation. We fixed other parameters as shown in Fig. 4.12. As w_a is larger, the antenna relatively has the better performance of the reflection in the desired frequency domain. We set w_a = 1.23 mm and s_a = 0.30 mm to achieve the performance of the reflection is relatively good in all l_a. As a result, when l_a, w_a and s_a are 3.71 mm, 1.23 mm and 0.30 mm respectively, the antenna has the better performance of the reflection in the desired frequency domain.

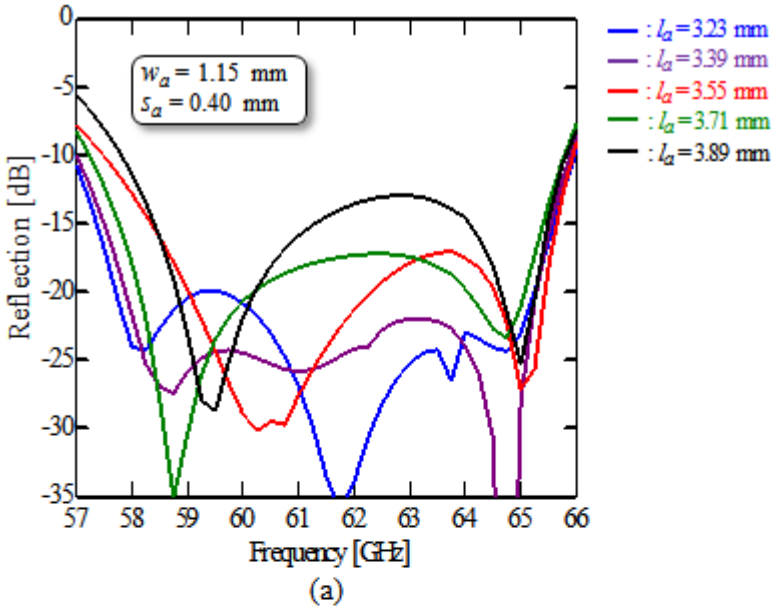

(a)

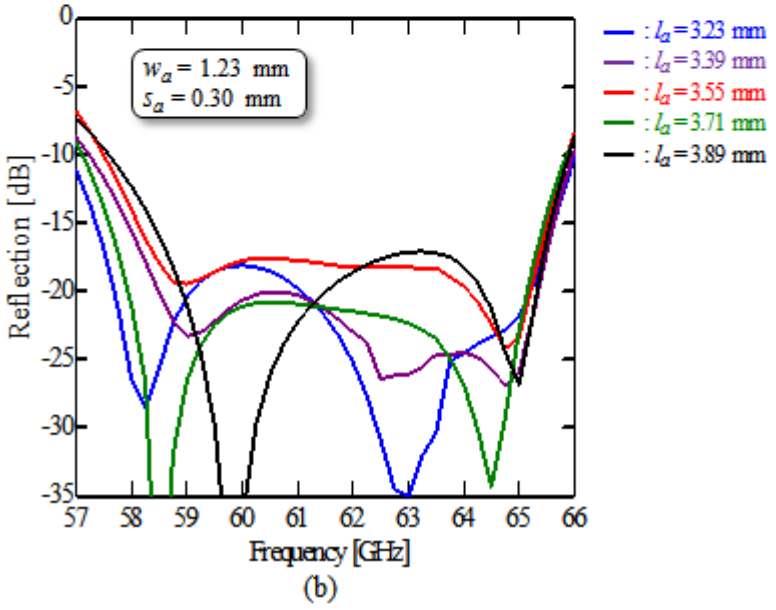

(b)

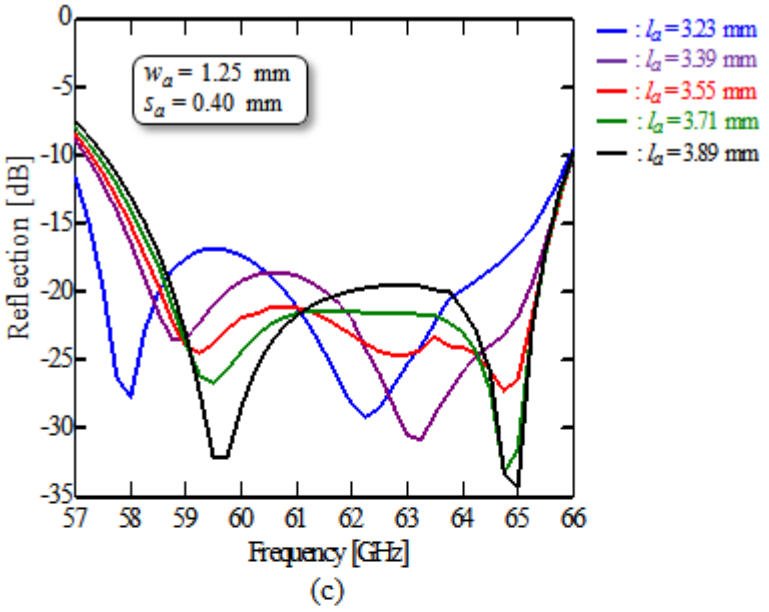

Fig. 4.13 Frequency characteristic of the reflection by changing the size of additional slots: l_a and w_a, and the space between additional slot pairs: s_a. (a) w_a = 1.15 mm, s_a = 0.40 mm. (b) w_a = 1.23 mm, s_a = 0.30 mm. (c) w_a = 1.25 mm, s_a = 0.40 mm. (d) w_a = 1.33 mm, s_a = 0.30 mm.

4.4.3 Full Structure Analysis

Fig. 4.14 shows the full structure of the 16×16-element four-layer linearly-polarized parallel-plate slot array antenna with slot pairs fed by the perpendicular corporate feed. In Fig.4.14, the plates are shown separated to expose the internal structure more fully, for the actual antenna, they are stacked closely. In the simulation, the conductivity of 5.8×10^7 S/m of copper and the loss tangent 0.0006 of the dielectric are assumed. Considering fabrication to maintain the flatness of the layers, the periphery of the four-layer parallel plates is terminated by (enclosed in) copper frames as shown in Fig. 4.7. The edge as PMC of the parallel plates is extended by 1.3 mm ($\approx 0.25\lambda_0$) only in the *y* direction and terminated by copper. The dimensions of the antenna in the *xy*-plane is 75.2 mm × 79.4 mm. The parameters are the same as the 2×2-element array shown in Fig. 4.12.

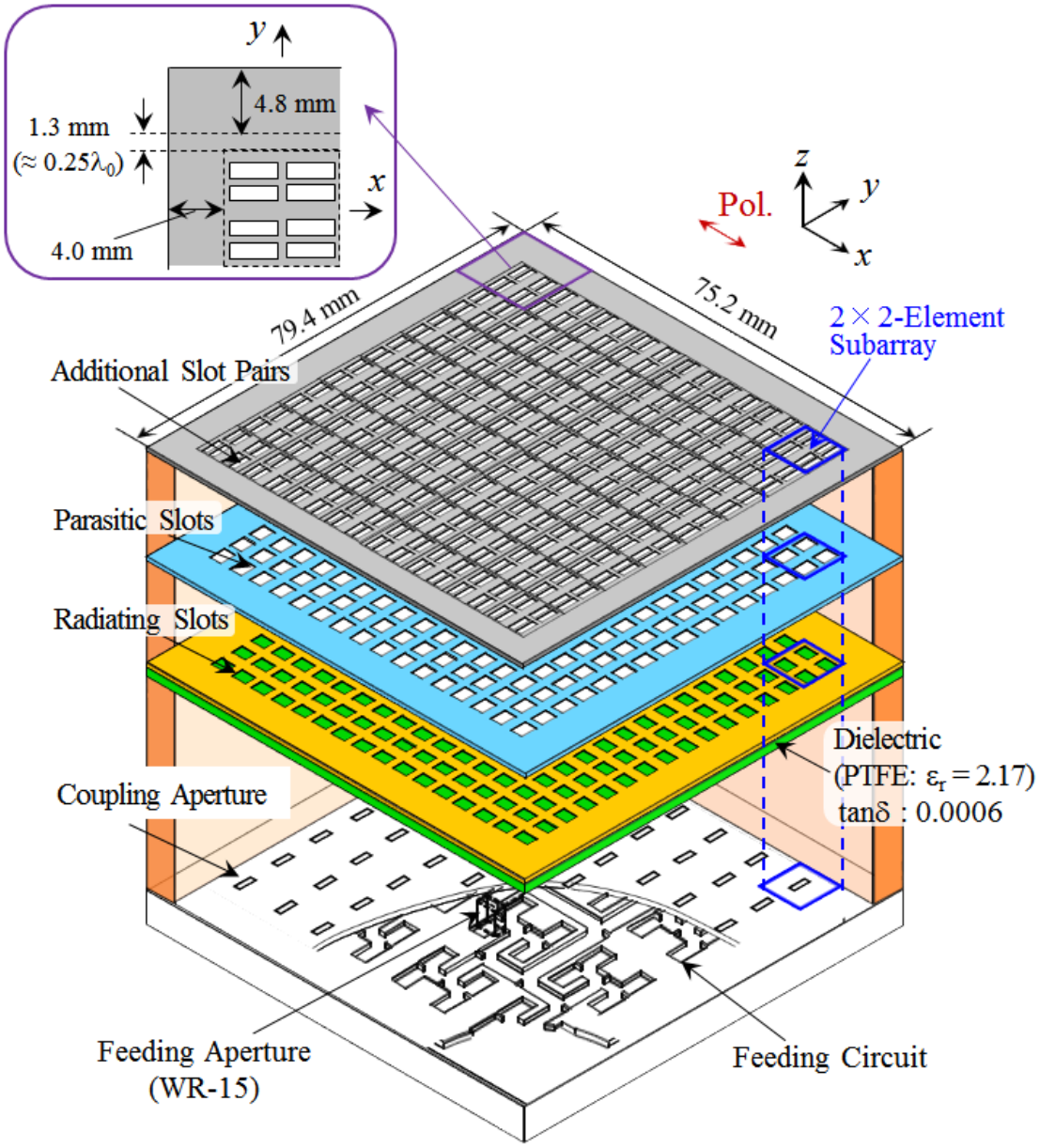

Fig. 4.14 Full structure of a perpendicular corporate feed in a four-layer linearly-polarized parallel-plate slot array antenna with slot pairs.

Fig. 4.15 shows the frequency characteristic of the reflection. As a reference, we also describe the reflections of no slot pairs as shown in Fig. 4.8 and the feeding circuit. The reflection of the full structured antenna is less than -14 dB over 12.8 % of the bandwidth ranging from 57.8 to 65.7 GHz. The bandwidth is very similar to that of the no slot pairs. Also, the reflection of the full structured antenna has slight ripples. This would be caused by the feeding circuit because the reflection of it has more clear ripples in the figure.

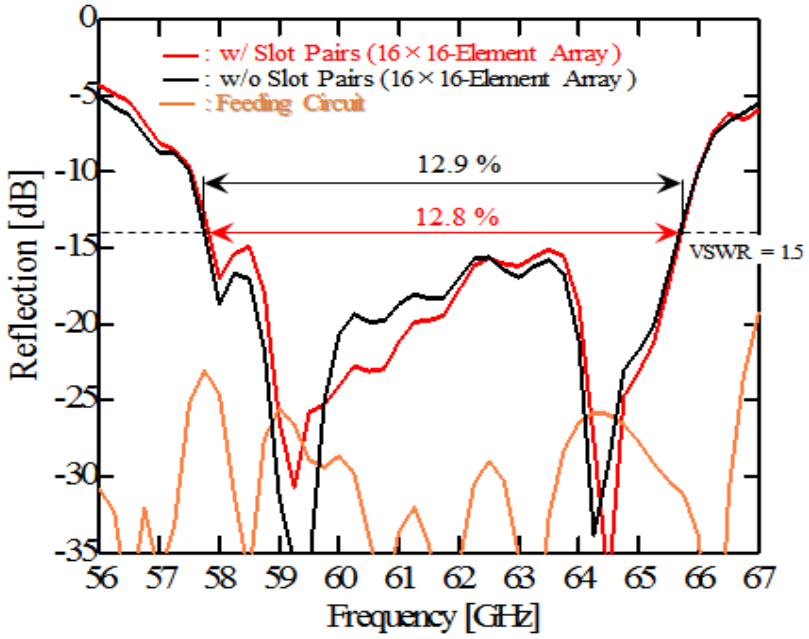

Fig. 4.15 Frequency characteristic of the reflection.

Fig. 4.16 shows radiation patterns at the design frequency (61.5 GHz) in the 45 deg.-plane, E-plane (*xz*) and H-plane (*yz*). In the 45 deg.-plane, grating lobes around ± 50-60 deg. region are suppressed to -35 dB from -22 dB (no slot pairs) by the introduction of slot pairs. However, in the E-plane, the radiation pattern slightly has grating lobes around ± 35 deg. comparing with these of no slot pairs due to excitation difference depending on the introduction of slot pairs. The relative amplitude of the grating lobes is -22 dB around ± 35 deg. In the H-plane, the radiation pattern presents a uniform-excitation pattern including an element pattern. Also, we review cross polarized patterns in both the E-plane and H-plane described in the figure (d) and (e). The introduction of slot pairs contributes to suppressing cross polarization in the both planes.

Fig. 4.17 shows realized gain, gain and directivity. As a reference, results of no slot pairs are shown in the figure. The realized gain includes the reflection loss as well as

conductor and dielectric losses and the aperture efficiency loss. We have achieved 12.7 % 1-dB-down bandwidth of realized gain in the 57.8 – 65.7 GHz range and 83% antenna efficiency at design frequency. The aperture efficiency greater than 85 % is achieved over 6-GHz bandwidth. The realized gain of the antenna with pair slots is larger than that of no slot pairs by 0.1 dB due to the effect of slot pairs.

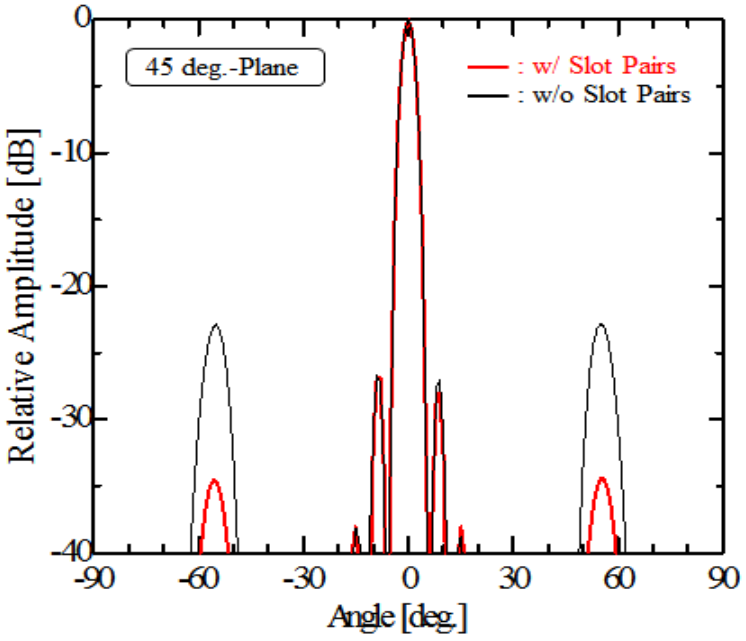

(a)

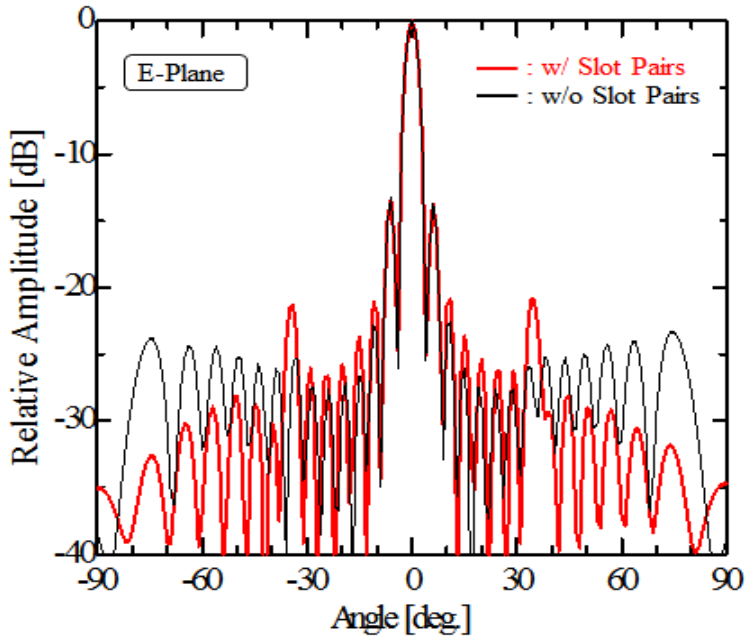

(b)

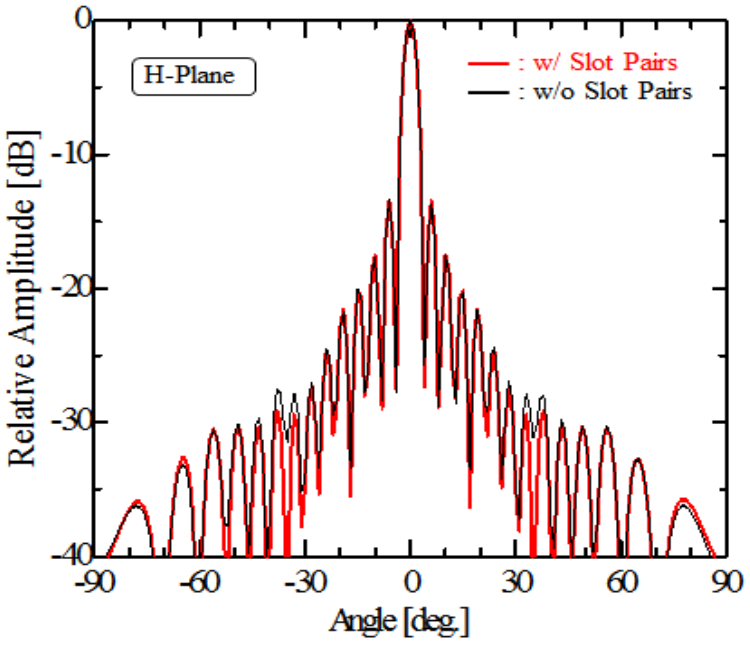
H-Plane
: w/ Slot Pairs
: w/o Slot Pairs
Relative Amplitude [dB]
0
-10
-20
-30
-40
-90
-60
-30
0
30
60
90
Angle [deg.]

(c)

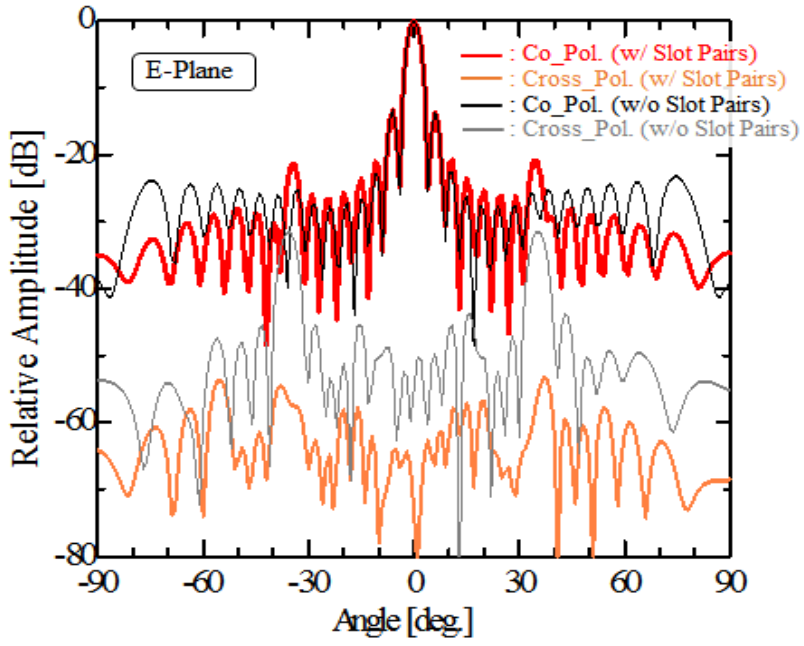
E-Plane
: Co_Pol. (w/ Slot Pairs)
: Cross_Pol. (w/ Slot Pairs)
: Co_Pol. (w/o Slot Pairs)
: Cross_Pol. (w/o Slot Pairs)
Relative Amplitude [dB]
0
-20
-40
-60
-80
-90
-60
-30
0
30
60
90
Angle [deg.]

(d)

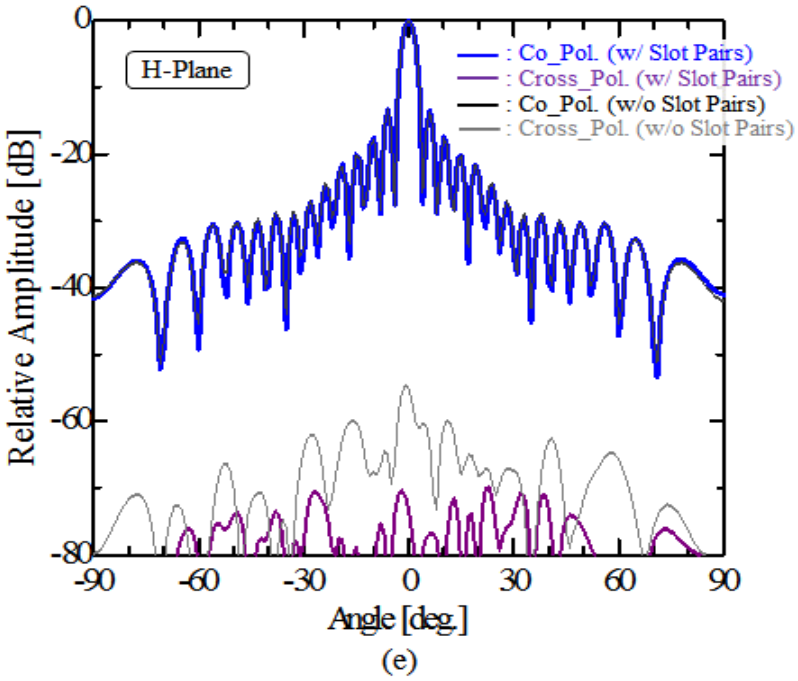

Fig. 4.16 Radiation patterns at 61.5 GHz. (a) 45 deg.-Plane. (b) E-Plane. (c) H-Plane. (d) E-Plane (w/ cross polarization). (e) H-Plane (w/ cross polarization).

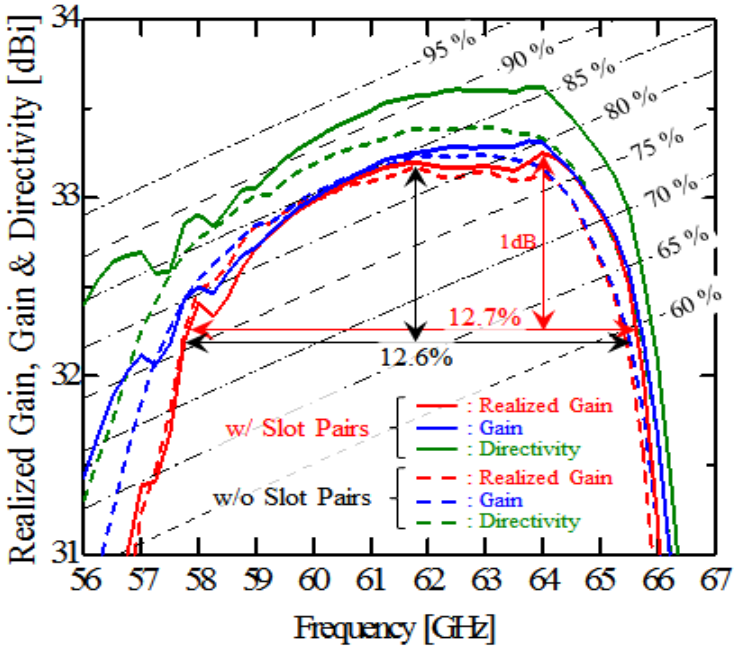

Fig. 4.17 Frequency characteristic of the realized gain, gain and directivity.

4.4.4 Concluding Remarks

This subsection presented a perpendicular-corporate feed for a four-layer linearly-polarized parallel-plate slot array antenna with slot pairs. The basic structure is similar to the perpendicular-corporate feed for a four-layer linearly-polarized parallel-plate slot array antenna as shown in the section 4.2 except for the configuration of additional slots. To suppress grating lobes around ± 55 deg., we introduce slot-pair configuration in the additional-slot layer.

In the simulation, the proposed antenna with slot pairs provides 12.8 % bandwidth for the VSWR of less than -14 dB. This bandwidth is very similar to that of no slot pairs. the radiation pattern, in the 45 deg.-plane, has lower grating lobes (-35 dB) around ± 50-60 deg. region than these of no slot pairs (-22 dB) due to the effect of slot pairs. Also, In the E-plane and H-plane, cross polarized patterns are also suppressed by the introduction of slot pairs. This concludes the structure of slot pairs offers the reduction of excitation difference. We have achieved 12.7 % 1-dB-down bandwidth of realized gain and 83% antenna efficiency at design frequency. The aperture efficiency greater than 85 % is achieved over 6-GHz bandwidth. The realized gain of the antenna with pair slots is larger than that of no slot pairs by 0.1 dB due to the effect of slot pairs.

4.5 Introduction of 45-deg.-inclined slots in Additional-Slot Layer

4.5.1 Antenna Configuration

To obtain 45 deg. polarization, we incline additional slots at a 45 deg. angle with respect to the principal axis. Fig. 4.18 shows a perpendicular-corporate feed in a four-layer parallel-plate 45 deg.-polarized slot array. The antenna structure is based on Fig. 4.1 and consists of an additional-slot layer, a parasitic-slot layer, a radiating-slot layer, a dielectric layer, a coupling-aperture layer and a feeding-circuit layer. There are air gaps between the slot layers including the coupling-aperture layer, and so there are no metal to metal contact in the radiating part. To create 45-deg. polarization, only additional slots, are inclined at an angle of 45 deg. with respect to the principal angle. The antenna is fed from the back (bottom in the figure) by a feed aperture. The feeding circuit feeds the coupling apertures in equal amplitude and phase. The coupling-aperture layer is placed between the feeding-circuit layer and the dielectric layer and with an air gap in between. The radiating-slot layer is mounted directly on the dielectric layer. The parasitic-slot layer is on top of the radiating-slot layer, also with an air gap in between. The additional-slot layer is over the parasitic-slot layer, similarly with an air gap to improve the VSWR bandwidth. The coupling apertures each excite 2×2 radiating slots and the electromagnetic field moves to the additional slots through the parasitic slots. The spacing of all the slot types is constant: $0.86\lambda_0$ (4.20 mm) in the *x* and *y* directions. Here, the λ_0 is the wavelength at the design frequency of 61.5 GHz. The top slot layer has larger sized slots in this structure.

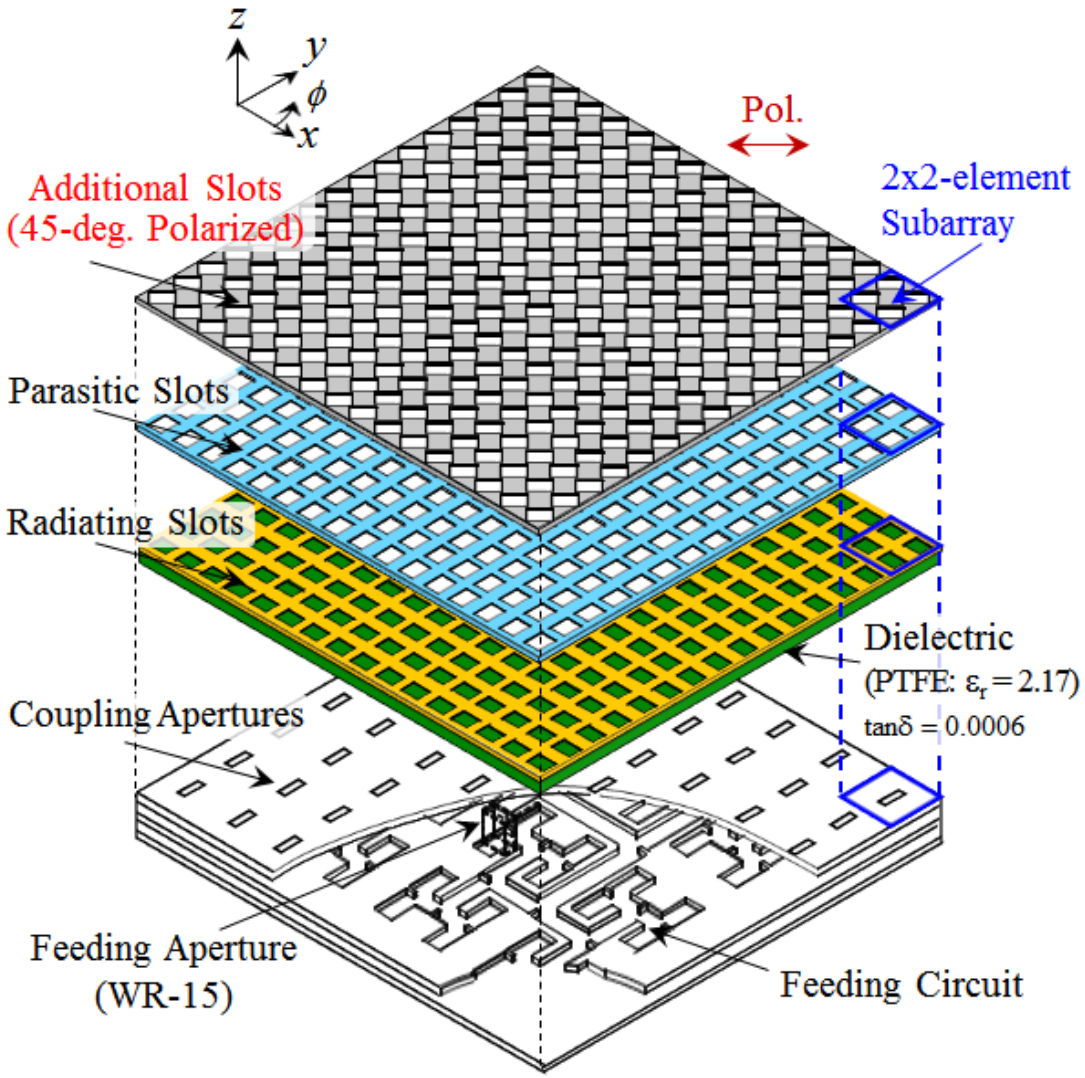

Fig. 4.18 Perpendicular-corporate feed in a four-layer parallel-plate 45-deg.-polarized slot array.

4.5.2 Design of 2×2-Element Subarray

Fig. 4.19 shows the model for the analysis of the 2×2-element subarray. In the analysis, we use a dielectric layer of t_d = 0.38 mm and ε_r = 2.17 obtained from the subsection 3.3.1. The conductivity 5.8×10^7 S/m of copper and a loss tangent 0.0006 of the dielectric are assumed. To enhance the bandwidth of the VSWR, the proposed model has the additional-slot layer. The configuration of additional slots is inclined at an angle of 45 deg. with respect to the principal angle to create 45-deg. polarization. The parameters are as follows: the size of the additional slots, l_a and w_a; the size of the parasitic

slots, l_p and w_p; the size of the radiating slots, l_r and w_r; and the size of the coupling apertures, l_c and w_c. The air gap between the additional-slot and the parasitic-slot layer is h_{ap}, that between the parasitic-slot and the radiating-slot layers is h_{pr}, and that between the dielectric and coupling layers is h_{rc}. Considering the fabrication limitation, we select a multiple of 0.20 mm as the thickness h_{rc}. When h_{rc} is 0.60 mm and t_d is 0.38 mm. The thicknesses of the additional-slot layer, the parasitic-slot layer, and radiating-slot layer is 0.20 mm, and that of the coupling-aperture layer is 0.20 mm. The size of feeding waveguide is fixed: width a = 2.95 mm, thickness b = 1.00 mm and length g = 5.65 mm, and it has short end. The offset of the coupling aperture against the principal axis in the x direction is also fixed at 0.60 mm. The final values of the design parameters are listed in the figure.

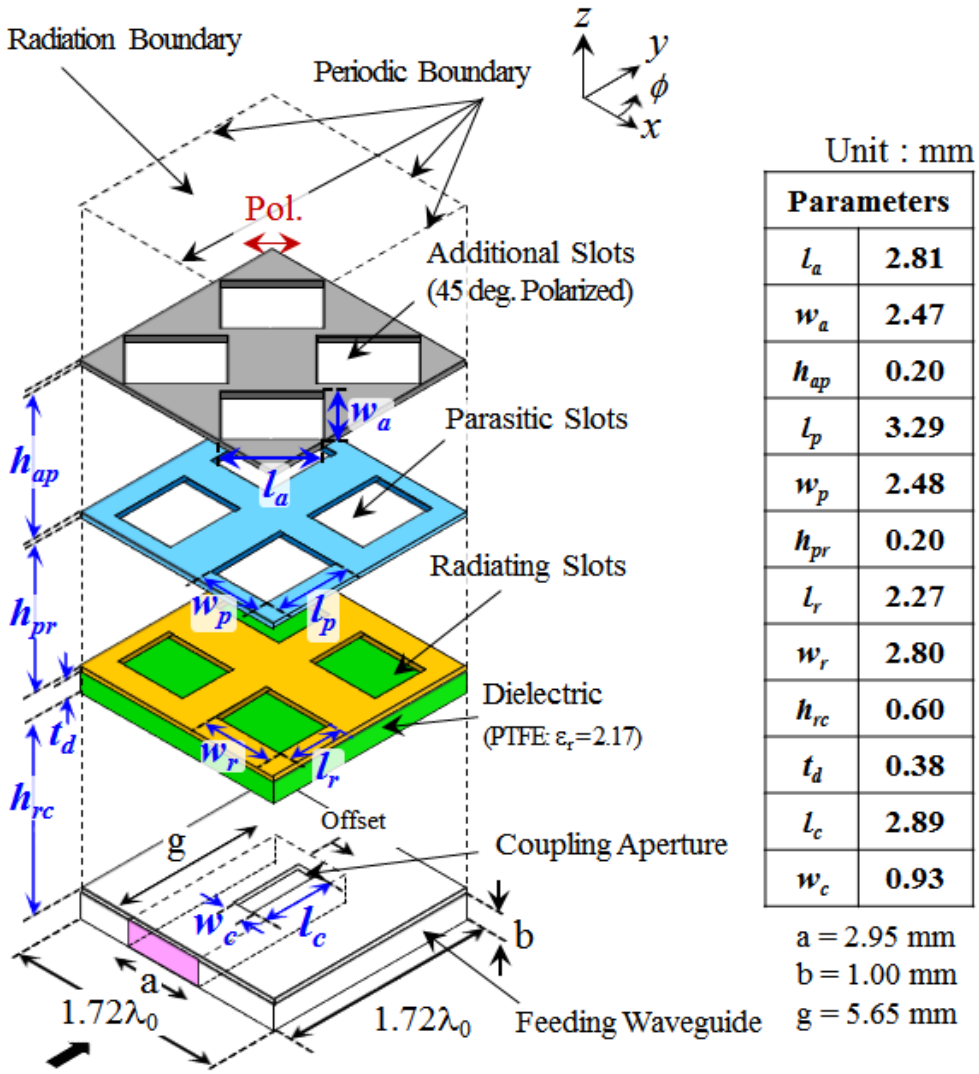

Fig. 4.19 Model for the analysis of the 2×2-element subarray.

As a typical design process, Fig. 4.20 shows the frequency characteristic of the reflection by changing the size of additional slots: l_a and w_a in the Fig. 4.20. As l_a is larger, the better performance of the reflection is shifted to a lower frequency domain from higher one. Also, as l_a is more than 2.97 mm, the performance of the reflection is relatively worse. When l_a and w_a are 2.81 mm and 2.47 mm respectively, the antenna has the better performance of the reflection in the desired frequency domain. We use these values for the analysis of the full structure.

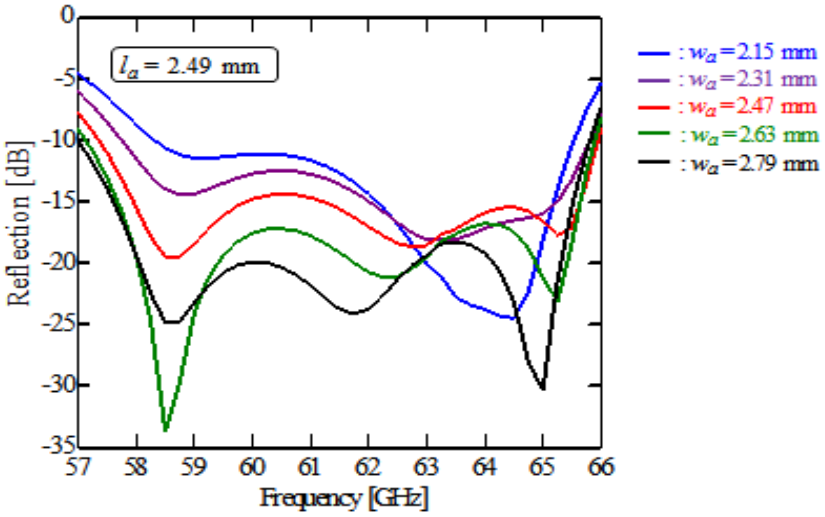

(a)

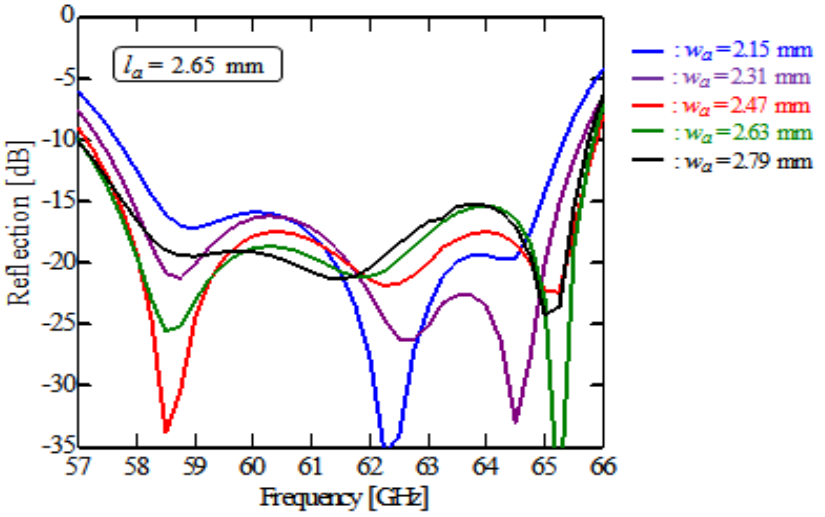

(b)

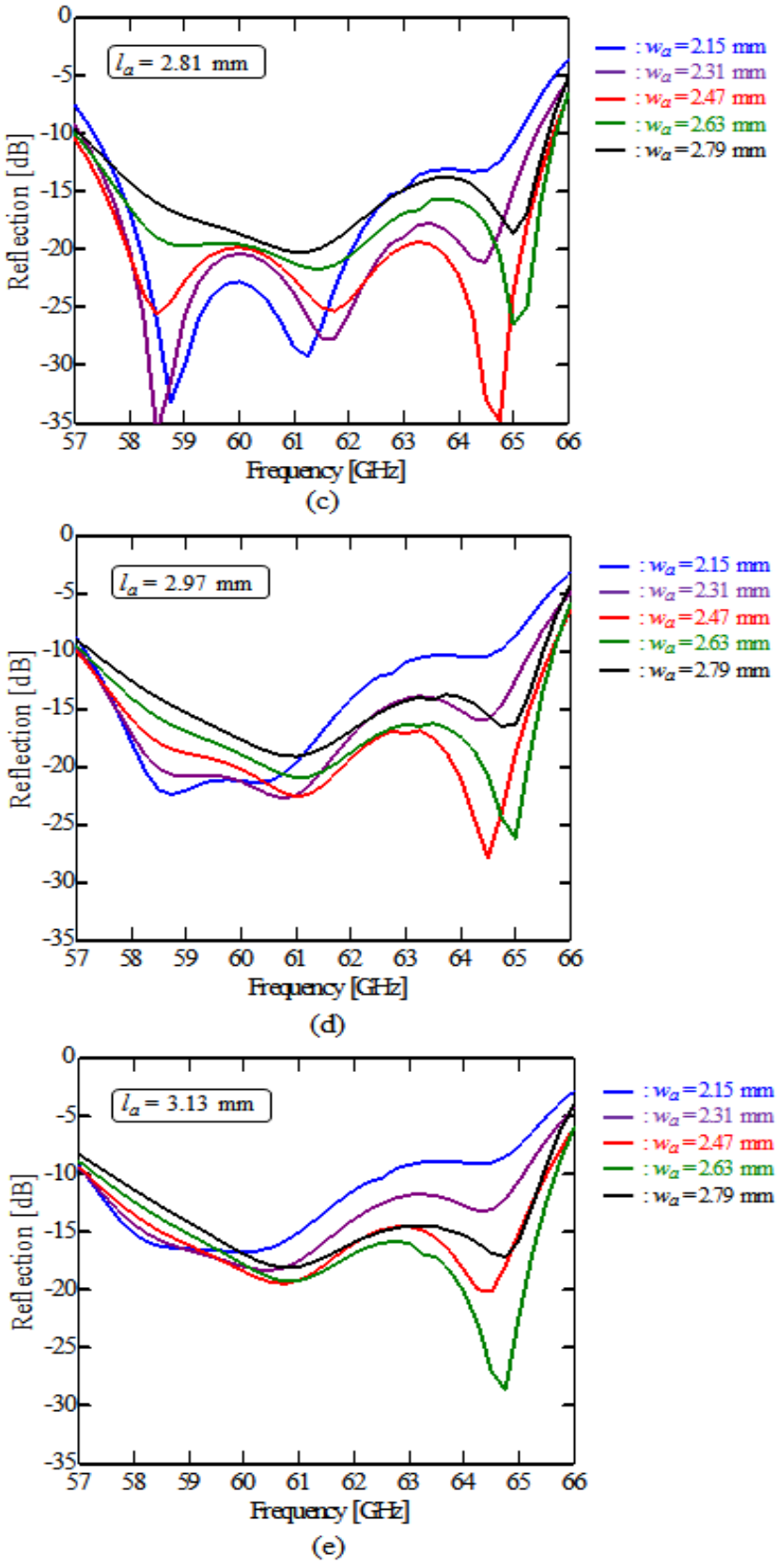

Fig 4.20 Frequency characteristic of the reflection by changing the size of additional slots: l_a and w_a. (a) l_a = 2.49 mm. (b) l_a = 2.65 mm. (c) l_a = 2.81 mm. (d) l_a = 2.97 mm. (e) l_a = 3.13 mm.

4.5.3 Eigenmode Analysis

Fig. 4.21 show the model of the eigenmode analysis. To save calculation time, we used 1×1-element subarray because of the symmetric structure. Note that a coupling aperture is excluded in the model, instead a PEC boundary is used. Around the periphery of the 1×1-element subarray, periodic, impedance and PEC boundaries are introduced. Parameters are the same as these of Fig. 4.19. As a reference, resonant frequencies of each slot are also shown in Fig. 4.21.

Fig. 4.22 shows Q factors and electric-field distribution of an additional slot in each eigenmode. For the better understanding, we plot results in the frequency characteristic of the reflection described in Fig. 4.20 (c). The first eigenmode and second one are occurred at 57.9 GHz and 63.7 GHz, respectively. The values of Q factors are 13.5 and 18.1, respectively. For Q = 13.5, the resonance is caused by a parasitic slot and a radiating slot in the *yz*-cross section. For Q = 18.1, the resonance is caused by an air gap between additional slot and parasitic slot in the *yz*-cross section. These Q factors contribute to enhancing the VSWR bandwidth.

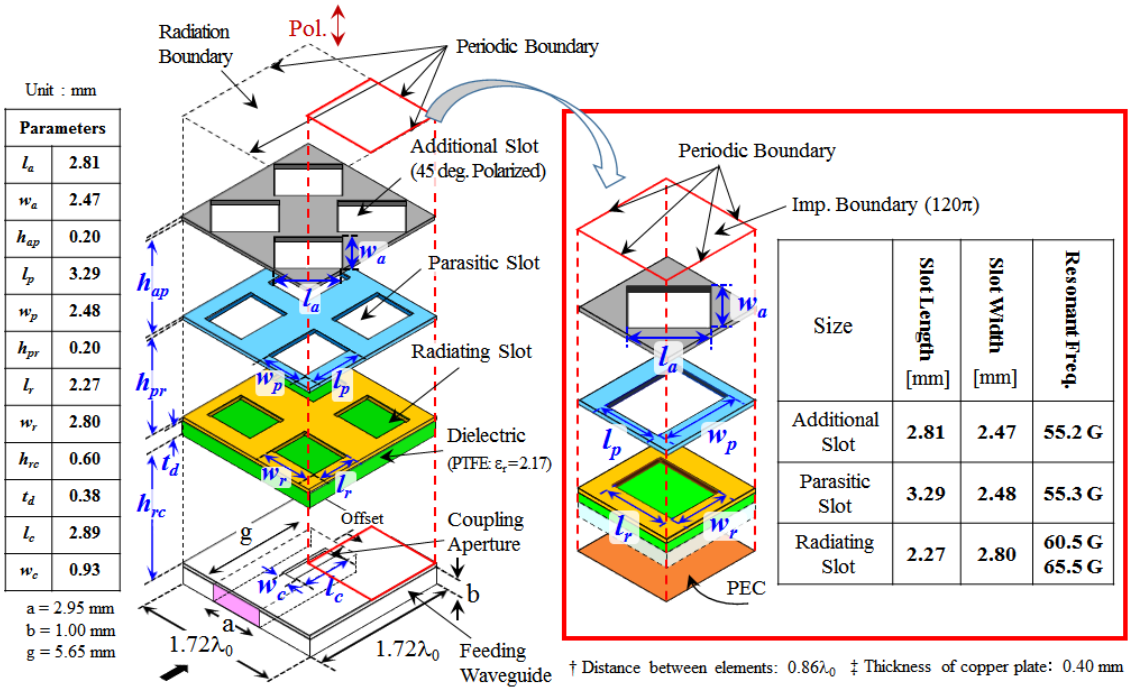

Fig. 4.21 Model of the eigenmode analysis.

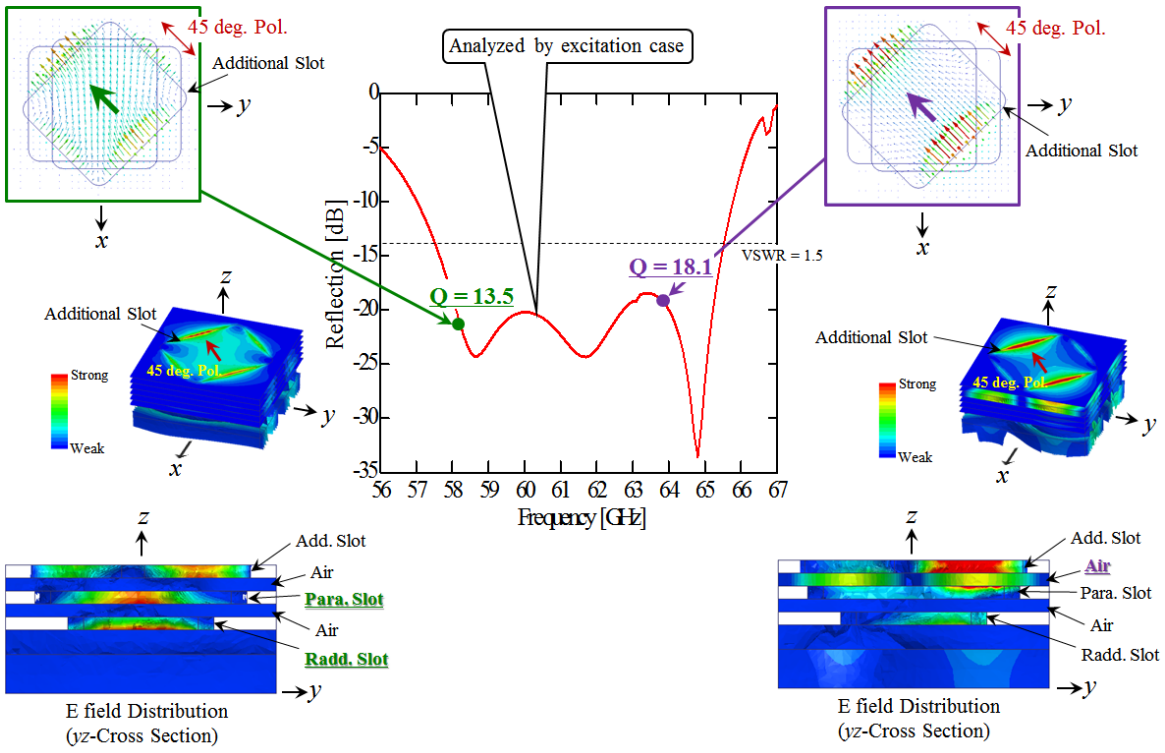

Fig. 4.22 Q factors and electric-field vectors of an additional slot in each eigenmode.

4.5.4 Full Structure Analysis

Fig. 4.23 shows the full structure of a 16×16-element four-layer 45-deg.-polarized parallel-plate slot array antenna fed by the perpendicular corporate feed. In Fig. 4.23, the plates are shown separated to expose the internal structure more fully, for the actual antenna they are stacked much more closely together. In the simulation, the conductivity of 5.8×10^7 S/m of copper and the loss tangent 0.0006 of the dielectric are assumed. Considering fabrication to maintain the flatness of the layers, the periphery of the four-layer parallel plates is terminated by (enclosed in) copper frames as shown in Fig. 4.14. The edge as PMC of the parallel plates is extended by 1.3 mm ($\approx 0.25\lambda_0$) only in the *y* direction and terminated by copper. The dimensions of the antenna in the *xy*-plane is 75.2 mm × 79.4 mm. The parameters are the same as these of the 2×2-element array shown in Fig. 4.19.

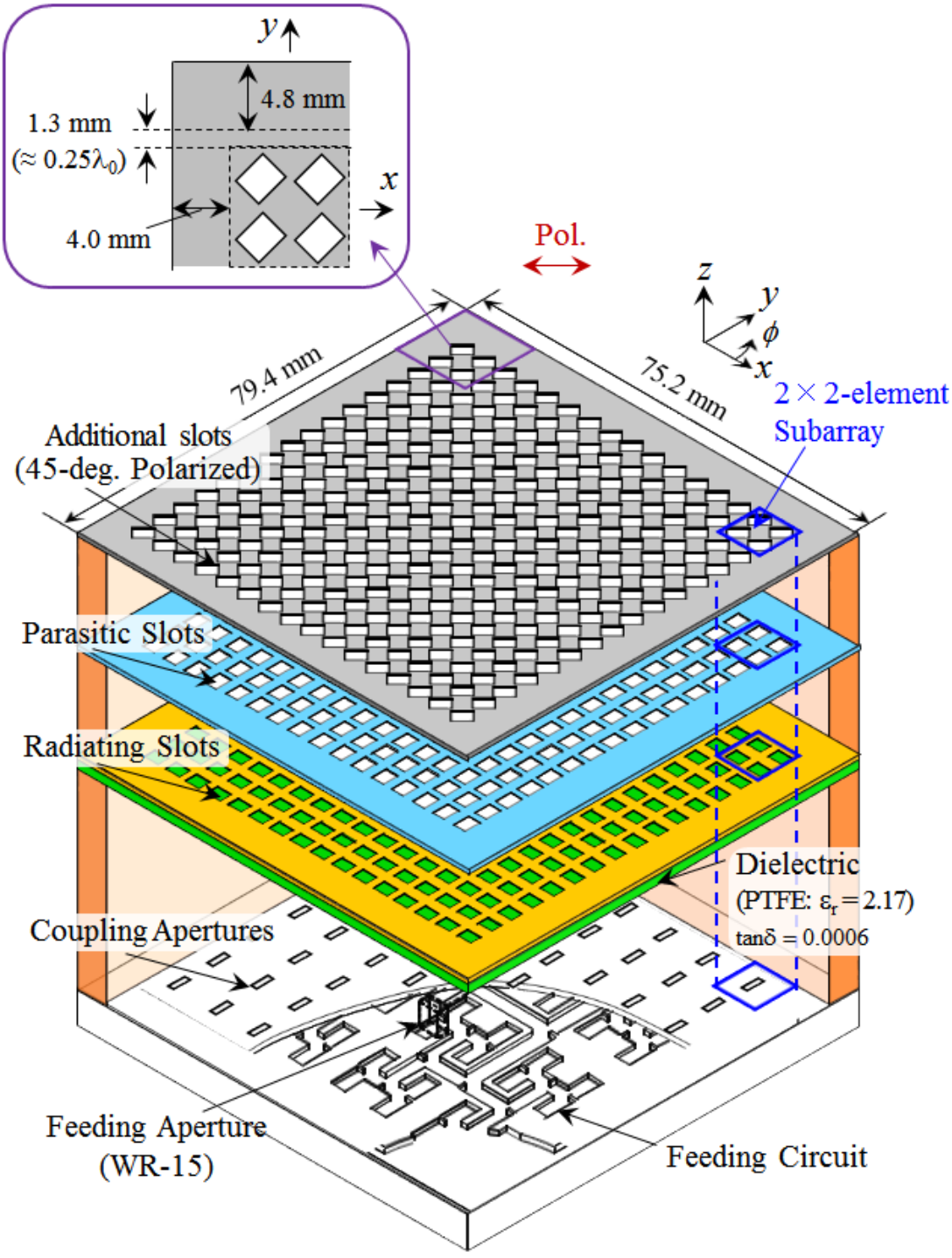

Fig. 4.23 Full structure of a perpendicular corporate feed in a four-layer 45-deg.-polarized parallel-plate slot array antenna with slot pairs.

Fig. 4.24 shows the frequency characteristic of the reflection. As a reference, the reflections of the 2×2-element subarray and the feeding circuit are also described. The reflection of the full structured antenna is less than -14 dB over 12.9 % of the bandwidth ranging from 57.5 to 65.4 GHz. The bandwidth is very similar to that of the 2×2-element subarray. Also, the reflection of the full structured antenna has slight ripples. This would be caused by the feeding circuit because the reflection of it has much clearer ripples in Fig. 4.24.

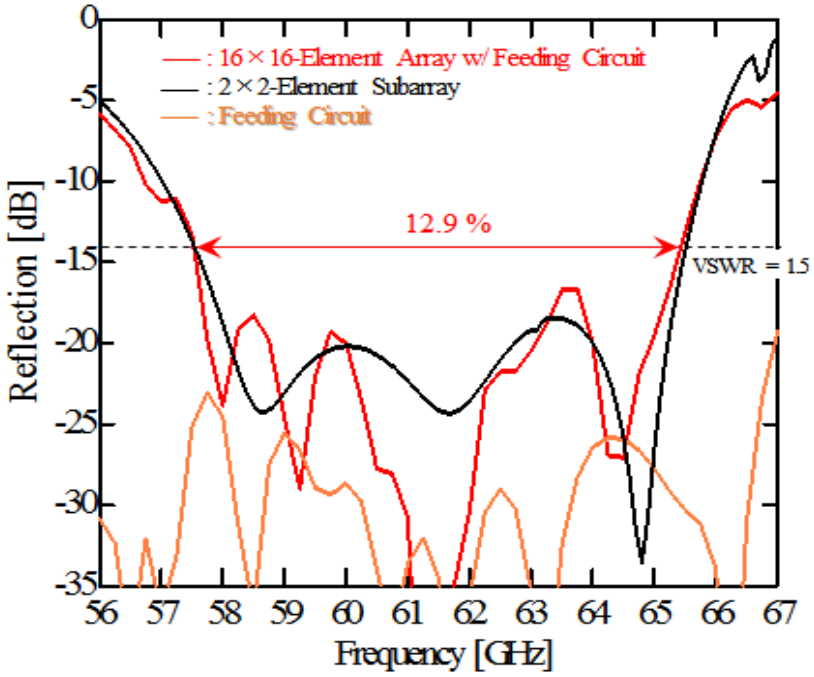

Fig. 4.24 Frequency characteristic of the reflection.

Fig. 4.25 shows radiation patterns at the design frequency (61.5 GHz) in the 0 deg.-plane, 45 deg.-plane, 90 deg.-plane and 135 deg.-plane. In the 45 deg.-plane and 135 deg.-plane, the radiation patterns have grating lobes around ± 50-60 deg. region due to the excitation difference in both the planes. This would be caused by wide configuration of slots. In the 0 deg.-plane, the radiation pattern slightly has high sidelobes in wide-angle regions ranging from ± 40 deg. to ± 90 deg. because of an omnidirectional-element pattern. The relative amplitude of the grating lobes is about -22 dB around ± 55 deg. In the 90 deg.-plane, the radiation pattern presents a uniform-excitation pattern including an element pattern.

Fig. 4.26 shows realized gain, gain and directivity. The realized gain includes the reflection loss as well as conductor and dielectric losses, and the aperture efficiency loss.

We have achieved 12.7 % 1-dB-down bandwidth of realized gain in the 57.5 – 65.3 GHz range and 78 % antenna efficiency at design frequency. The aperture efficiency greater than 75 % is achieved over 7-GHz bandwidth.

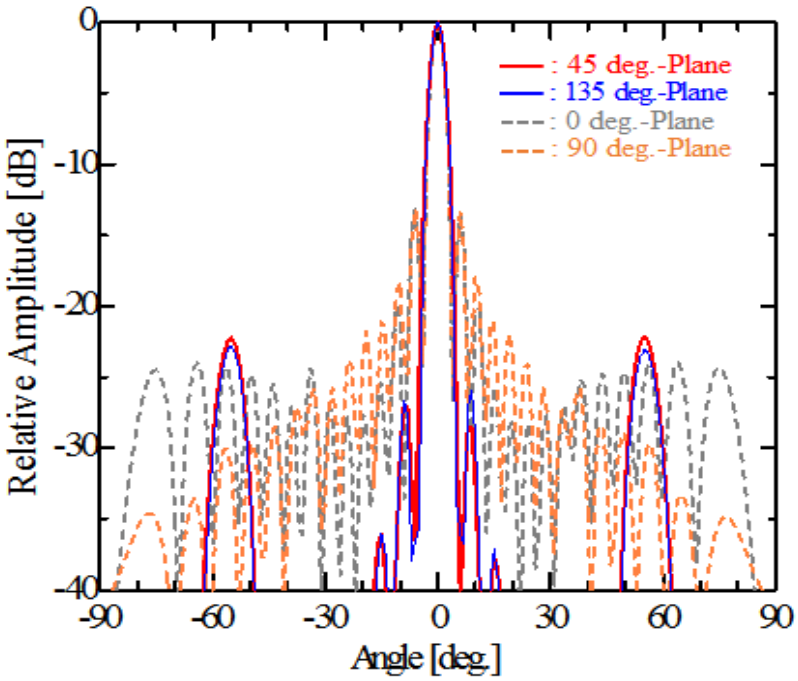

Fig. 4.25 Radiation patterns at the design frequency (61.5 GHz)

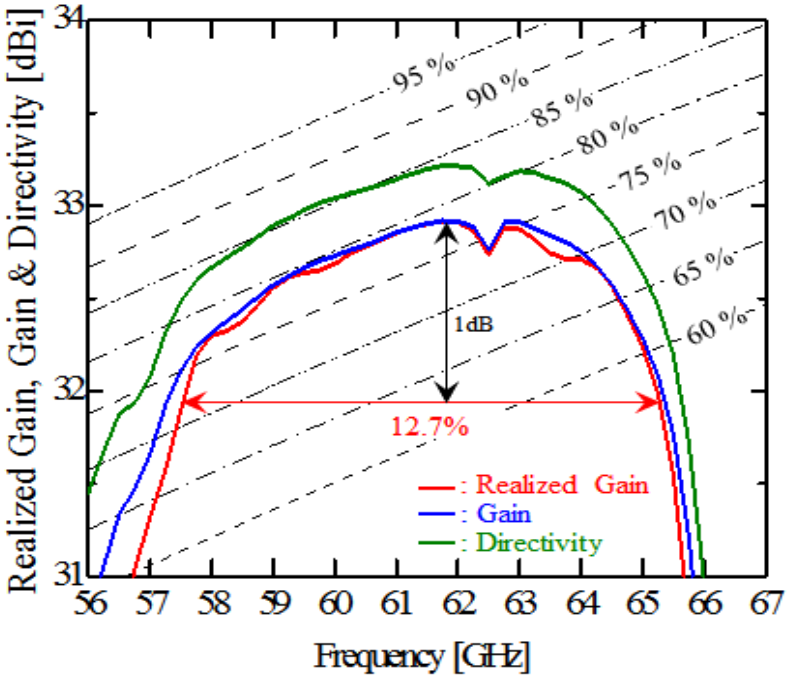

Fig. 4.26 Frequency characteristic of the realized gain, gain and directivity.

4.5.5 Concluding Remarks

This subsection presented a perpendicular-corporate feed for a four-layer 45-deg.-polarized parallel-plate slot array antenna. The basic structure is similar to the perpendicular-corporate feed for a four-layer linearly-polarized parallel-plate slot array antenna as shown in the section 4.2 except for the configuration of additional slots. To create 45 deg. polarization, additional slots are inclined at an angle of 45 deg. with respect to the principal angle.

In the simulation, we have realized 12.9 % bandwidth for the VSWR of less than -14 dB even in the structure with 45-deg. polarization. Radiation patterns provide uniform -excitation patterns including an element pattern in the 0 deg. and 90 deg. planes. However, In the 45 deg.-plane and 135 deg.-plane, the radiation patterns have grating lobes around ± 50-60 deg. region due to the excitation difference in both the planes. This would be caused by wide configuration of slots. The relative amplitude of the grating lobes is -22 dB around ± 55 deg. Also, we have achieved 12.7 % 1-dB-down bandwidth of realized gain and 78% antenna efficiency at design frequency. The aperture efficiency greater than 75 % is achieved over 7-GHz bandwidth.

For a proposed application, this antenna would be used for synthetic aperture radars (SAR) mounted on drones. 45-deg.-polarized antennas have lower side lobes without tapered aperture distribution because the diagonal plane (45◦) has tapered excitation equivalently. Lower side lobes can provide radar systems with reduced clutter and multipath reflection, resulting in better detection of targets. Also, considering millimeter bands, which have the plenty of frequency resources, SAR systems can provide the ultra-high resolution of images. When we have disaster-relief operations, SAR systems can offer informative images in affected areas and these images contribute to operators' quick decision.

4.6 Concluding Remarks

This chapter presented three types of a perpendicular-corporate feed for a four-layer linearly-polarized parallel-plate slot array antenna. By changing the configuration of additional slots, proposed antennas provide linear polarization with wideband, linear polarization with lower grating lobes and 45-deg. polarization. Fig 4.27 shows the summary of the antenna characteristic in proposed antennas. The bandwidth of the VSWR and 1 dB-down realized gain is very similar among proposed models. Realized gain and antenna efficiency is also similar to each other at design frequency. These results indicate only the change of configuration in the additional slots offers operational functions with maintaining basic antenna characteristic.

Polarization		**Linearly Polarized**	**Linearly Polarized (Slot Pairs)**	**45 deg. Polarized**
16 × 16-Element Array		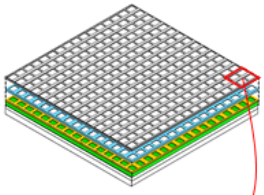	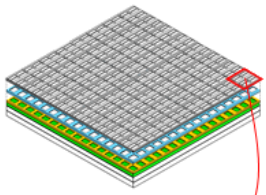	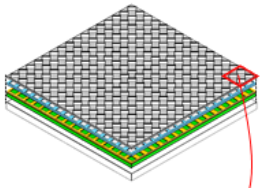
Configuration of Additional Slots in 2 × 2-Element Subarray		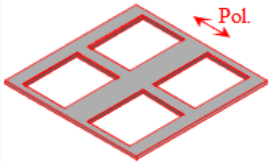	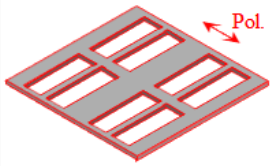	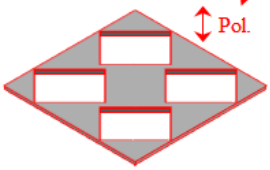
VSWR < 1.5 Bandwidth		12.9 %	12.8 %	12.9 %
1-dB down Realized Gain		12.6 %	12.7 %	12.7 %
Realized Gain @ 61.5 GHz		33.1 dBi	33.2 dBi	32.9 dBi
Antenna Efficiency @ 61.5 GHz		82 %	83 %	78 %
Aperture Efficiency		> 80 %, over 7 GHz BW	> 85 %, over 7 GHz BW	> 75 %, over 7 GHz BW
Sidelobe Level (± θ = 55 deg.)	0 deg. Plane	-25 dB	-22 dB	-25 dB
	45 deg. Plane	-23 dB	-35 dB	-22 dB
	90 deg. Plane	-31 dB	-30 dB	-30 dB

Fig. 4.27 Summary of the antenna characteristic in proposed antennas.

References

[4.1] T. Tomura, J. Hirokawa, T. Hirano, and M. Ando, “A 45◦ linearly polarized hollow-waveguide 16×16-slot array antenna covering 71-86 GHz band,” IEEE Trans. Antennas Propag., vol. 62, no. 10, pp. 5061 – 5067, Oct. 2014.

Chapter 5

Design of Perpendicular-Corporate Feed in Three-Layer Parallel-Plate Dual-Polarized Slot Array Antenna

5.1 Introductory Remarks

This chapter presents a perpendicular-corporate feed in a three-layer parallel-plate dual-polarized slot array antenna. This antenna is based on the structure of a perpendicular-corporate feed in a three-layer linearly-polarized parallel-plate slot array antenna as shown in the chapter 2, but a few structural differences are involved as follows. The proposed antenna has cross-slot configurations in a parasitic-slot layer, radiating-slot layer and cross-coupling-aperture layer to create a dual-polarized operation. For the same reason, two-layered feeding circuits are introduced in the structure. Also, the proposed antenna has two dielectric layers: one of them is between the cross-coupling layer and the radiating-slot layer with an air gap in between, and the other is between the radiating-slot layer and the parasitic-slot layer with an air gap in between to improve the VSWR bandwidth.

This chapter is organized as follows. Section 5.2 describes the perpendicular-corporate feed in a two-layer dual-polarized slot array as a basic model. To study a basic operation, this model does not have a parasitic-slot layer. In this section, we discuss the antenna configuration and the design process by the analysis of a 2×2-element subarray. To enhance the VSWR bandwidth, section 5.3 describes the introduction of a parasitic-slot layer on the top of the radiating-slot layer with an air gap in between by the analysis of a 2×2-element subarray and a 16×16-element array. Note that this introduction is involved with the placement of a new dielectric layer between the parasitic-slot layer and the air gap. In section 5.4, we conclude this chapter.

5.2 Antenna Configuration

Fig. 5.1 shows a perpendicular-corporate feed in a two-layer parallel-plate dual-polarized slot array. We analyze this model to confirm a basic antenna operation. The antenna consists of a radiating-slot layer, a dielectric layer, a cross-coupling-aperture layer, a coupling-aperture layer, a feeding-circuit-1 layer and a feeding-circuit-2 layer. There is an air gap between the radiating-slot layer and cross-coupling-aperture layer, and so there is no metal to metal contact in the radiating part. In Fig. 5.1, the layers are drawn widely apart to show the internal structure. However, in the actual antenna, the layers are stacked much more closely together. The antenna is fed from the back (bottom in the figure) by a feed aperture. The feeding circuit 1 feeds the coupling apertures in equal amplitude and phase. The feeding circuit 2 feeds the cross-coupling apertures in equal amplitude and phase. The coupling-aperture layer is placed between the feeding-circuit layer 1 and the feeding circuit 2. The cross-coupling-aperture layer is placed between the feeding circuit 2 and the dielectric layer and with an air gap in between. The radiating-slot layer is mounted directly on the dielectric layer. For the *x*-polarized operation, the coupling apertures excites 2×2 radiating slots through the cross-coupling-apertures. For the *y*-polarized operation, the cross-coupling-apertures excites the radiating slots directly. The spacing of all the slot types is constant: $0.86\lambda_0$ (4.12 mm) in the *x* and *y* directions. Here, the λ_0 is the wavelength at the design frequency of 62.6 GHz.

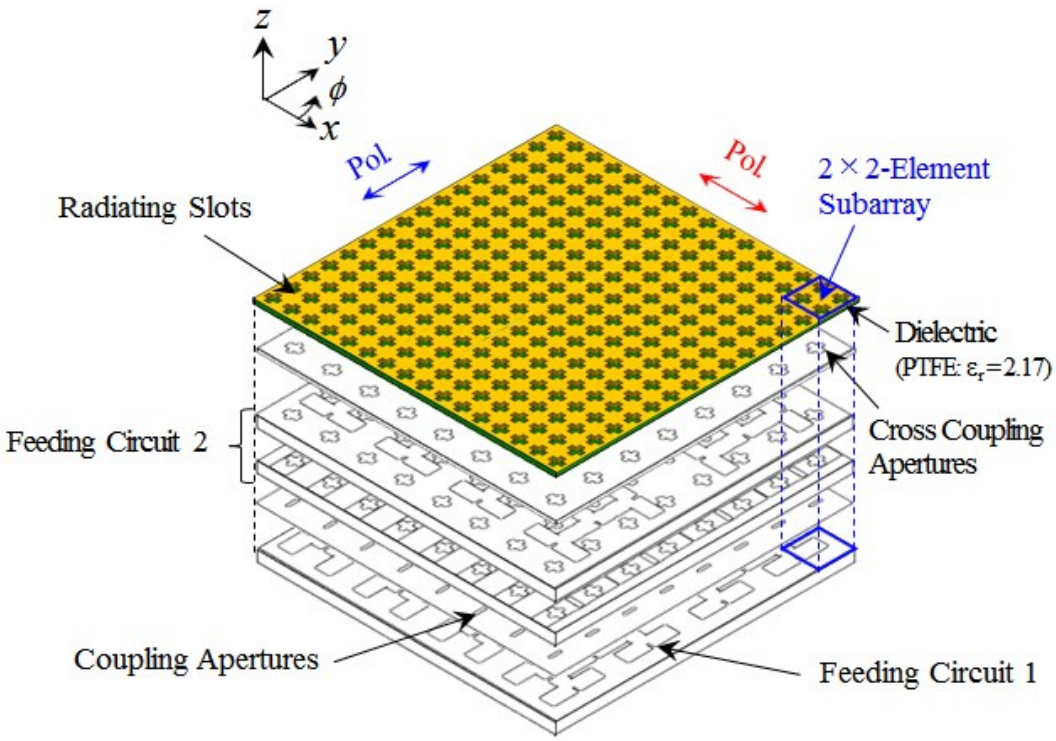

Fig. 5.1 Perpendicular-corporate feed in a two-layer parallel-plate dual-polarized slot array.

Fig. 5.2 shows the configuration of the feeding circuit 1 and the feeding circuit 2. Both circuits are a planar corporate feed composed of H-planes and T-junctions. Depending on the structural constraint, the feeding circuit 2 also has additional feeding waveguides colored with orange to excite cross-coupling apertures as shown in the figure (b). These feeding waveguides have short end.

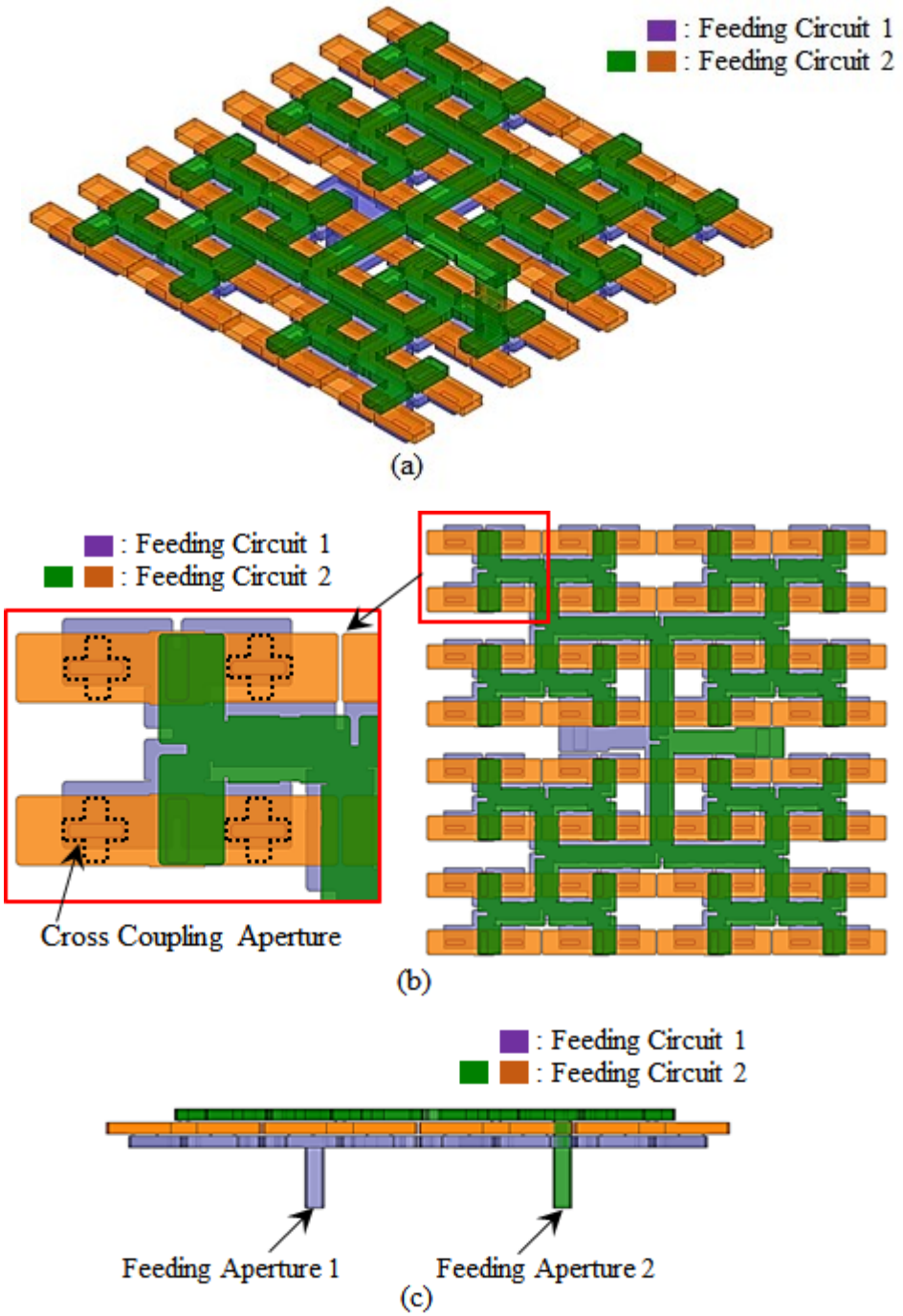

Fig 5.2 Configuration of the feeding circuit 1 and feeding circuit 2. (a) Perspective view. (b) Top view. (c) Side view.

Fig 5.3 shows the reflections of the feeding circuit 1 and the feeding circuit 2. Both circuits have lower reflection, less than -25 dB ranging from 60.5 GHz to 64.5 GHz. There are ripples in both the reflections because of multiple reflections in their structures.

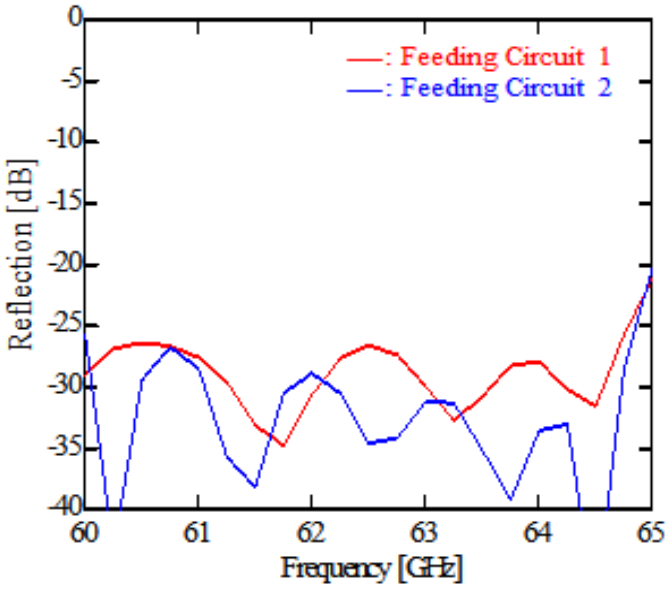

Fig 5.3 Reflections of the feeding circuit 1 and the feeding circuit 2.

5.3 Design

5.3.1 Design of 2×2-Element Subarray

Fig. 5.4 shows the model for the analysis of the 2×2-element subarray. In the analysis, the conductivity 5.8×10^7 S/m of copper and a loss tangent 0.0006 of the dielectric are assumed. The parameters are as follows: the size of the radiating slots, l_{rs_X}, l_{rs_Y}, w_{rs_X} and w_{rs_Y}; the size of the cross-coupling apertures, l_{cca_X}, l_{cca_Y}, w_{cca_X}, and w_{cca_Y}; and the size of the coupling apertures, l_{ca} and w_{ca}. The thickness of the air gap between the cross-coupling-aperture layer and the radiating-slot layer is h_{rc} Considering the fabrication, we select a multiple of 0.20 mm for layers as the thickness. The thickness of the coupling-aperture layer is 0.20 mm, that of the cross coupling aperture layer is 2.40 mm, that of the radiating-slot layer is 0.40 mm, that of the cross-coupling-aperture layer is 0.20 mm and that of the coupling-aperture layer is 0.20 mm. Note that the thickness of the cross-coupling-aperture layer is much thicker than that of others due to creating the space (colored with orange in Fig5.2 (b)) for a part of the feeding circuit 2 in the region. Given the availability of dielectric (PTFE) materials, the thickness of the dielectric layer: t_d should be a multiple of 5 mils (0.127mm). The size of feeding waveguide 1 is fixed:

width a1 = 3.3 mm, thickness b1 = 1.20 mm and length g1 = 5.35 mm, and it has short end. The offset of the coupling aperture against the principal axis in the *x* direction is fixed at 0.80 mm. The size of feeding waveguide 2 is fixed: width a2 = 3.40 mm, thickness b2 = 1.20 mm and length g2 = 7.86 mm, and it has short end. The cross coupling aperture is placed in the center without any offsets. The final values of the design parameters are listed in the figure.

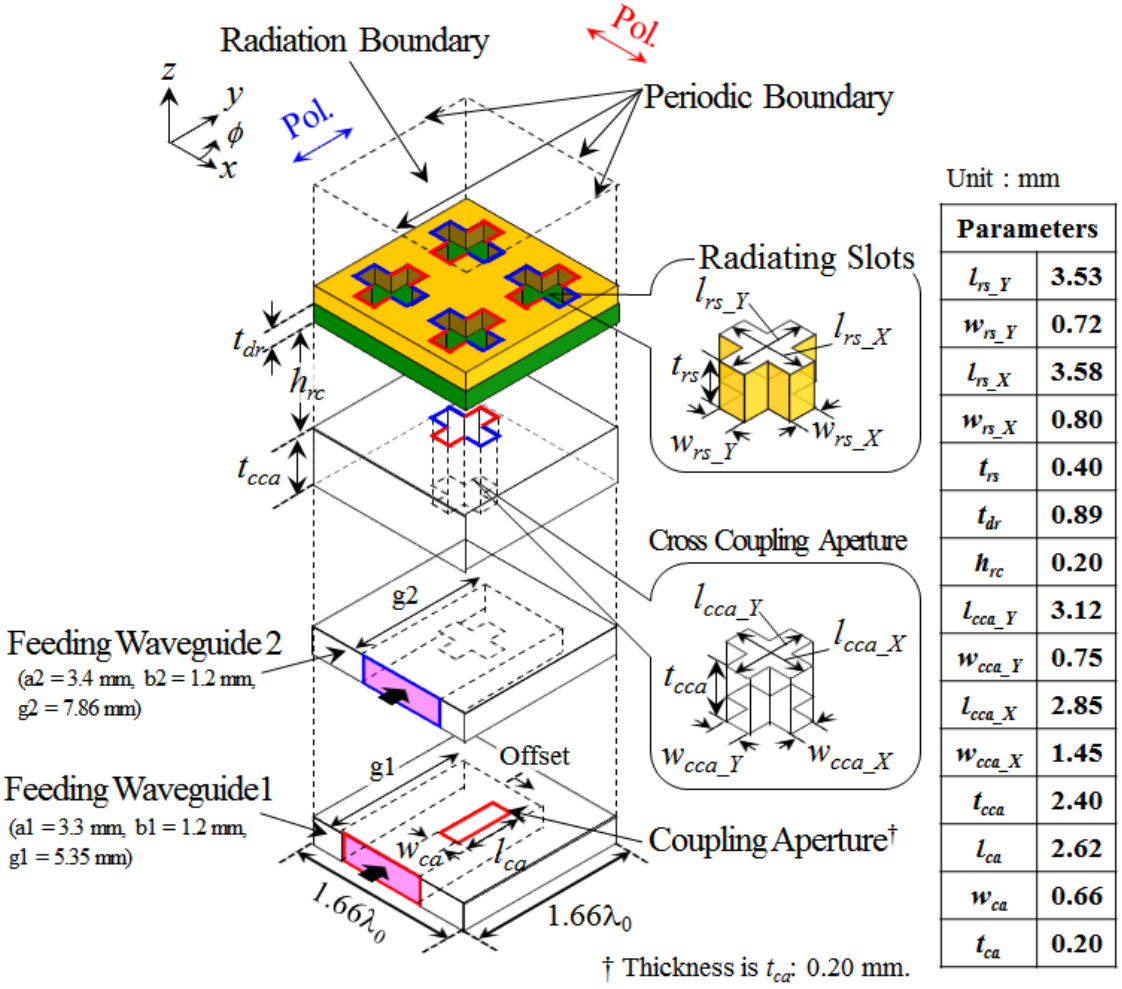

Parameters	
l_{rs_Y}	3.53
w_{rs_Y}	0.72
l_{rs_X}	3.58
w_{rs_X}	0.80
t_{rs}	0.40
t_{dr}	0.89
h_{rc}	0.20
l_{cca_Y}	3.12
w_{cca_Y}	0.75
l_{cca_X}	2.85
w_{cca_X}	1.45
t_{cca}	2.40
l_{ca}	2.62
w_{ca}	0.66
t_{ca}	0.20

Fig. 5.4 Model for the analysis of the 2×2-element subarray.

Fig. 5.5 shows the frequency characteristic of the S-parameters by changing the thickness of the dielectric layer t_{dr}. Other parameters are fixed and shown in Fig. 5.4. As t_{dr} is thicker, the frequency characteristic of the S-parameters shifts to a lower frequency domain. S_{11} is in good agreement with S_{22} in all t_{dr}. When t_{dr} is 0.89 mm, the antenna has

the better performance of the S-parameter characteristic around the design frequency. However, this model does not meet the VSWR bandwidth less than 1.5.

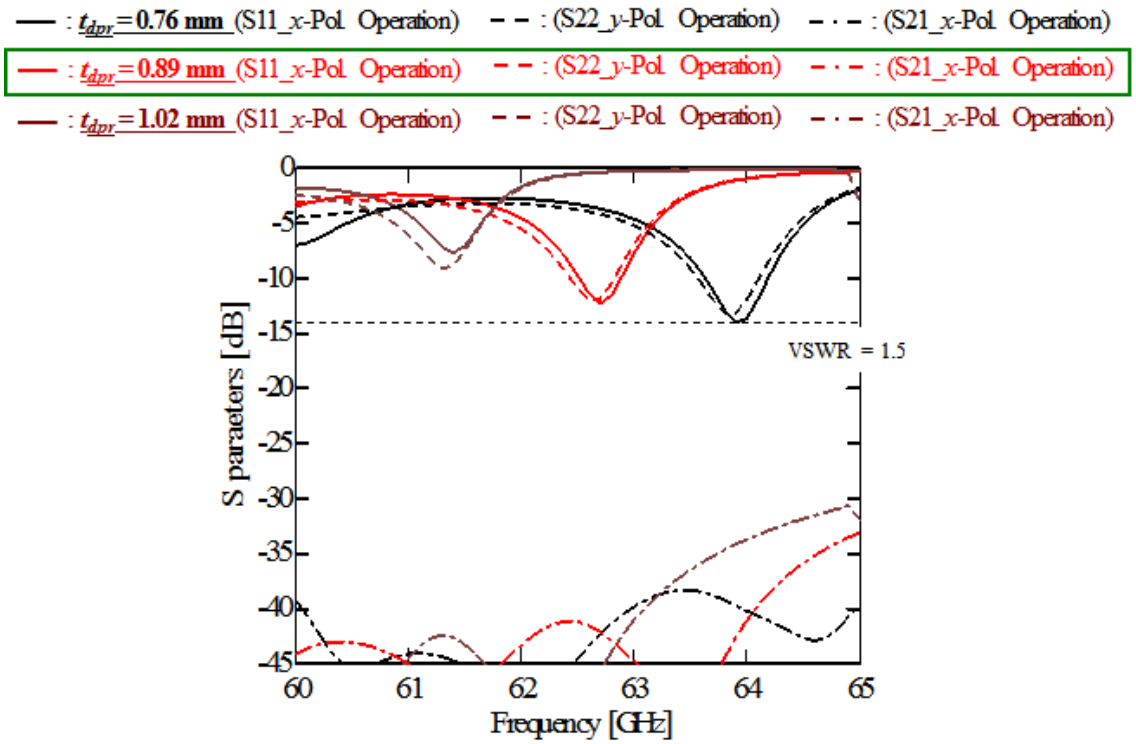

Fig. 5.5 Frequency characteristic of the S-parameters by changing the thickness of the dielectric layer t_{dr}.

5.3.2 Introduction of Parasitic-Slot Layer with Dielectric

To improve the VSWR bandwidth, we introduce a parasitic-slot layer on the top of the radiating-slot layer, an air gap and a dielectric layer in between the two. The size of the parasitic slots should be larger than that of the radiating slots. Fig. 5.6 shows the model for the analysis of the 2×2-element subarray. In this analysis, we review all values of parameters shown in Fig. 5.4. As a result of the parameter resetting, the thickness of the dielectric layer t_{dr} is 0.38 mm. Air gaps h_{rc} and h_{pr} are 0.20 mm. The size of feeding waveguide 1 is fixed: width a1 = 3.3 mm, thickness b1 = 1.20 mm and length g1 = 5.35 mm, and it has short end. The offset of the coupling aperture against the principal axis in the x direction is fixed at 0.80 mm. The size of feeding waveguide 2 is fixed: width a2 = 3.40 mm, thickness b2 = 1.20 mm and length g2 = 7.86 mm, and it has short end. The cross coupling aperture is placed in the center without any offsets. The final values of the design parameters are listed in the figure.

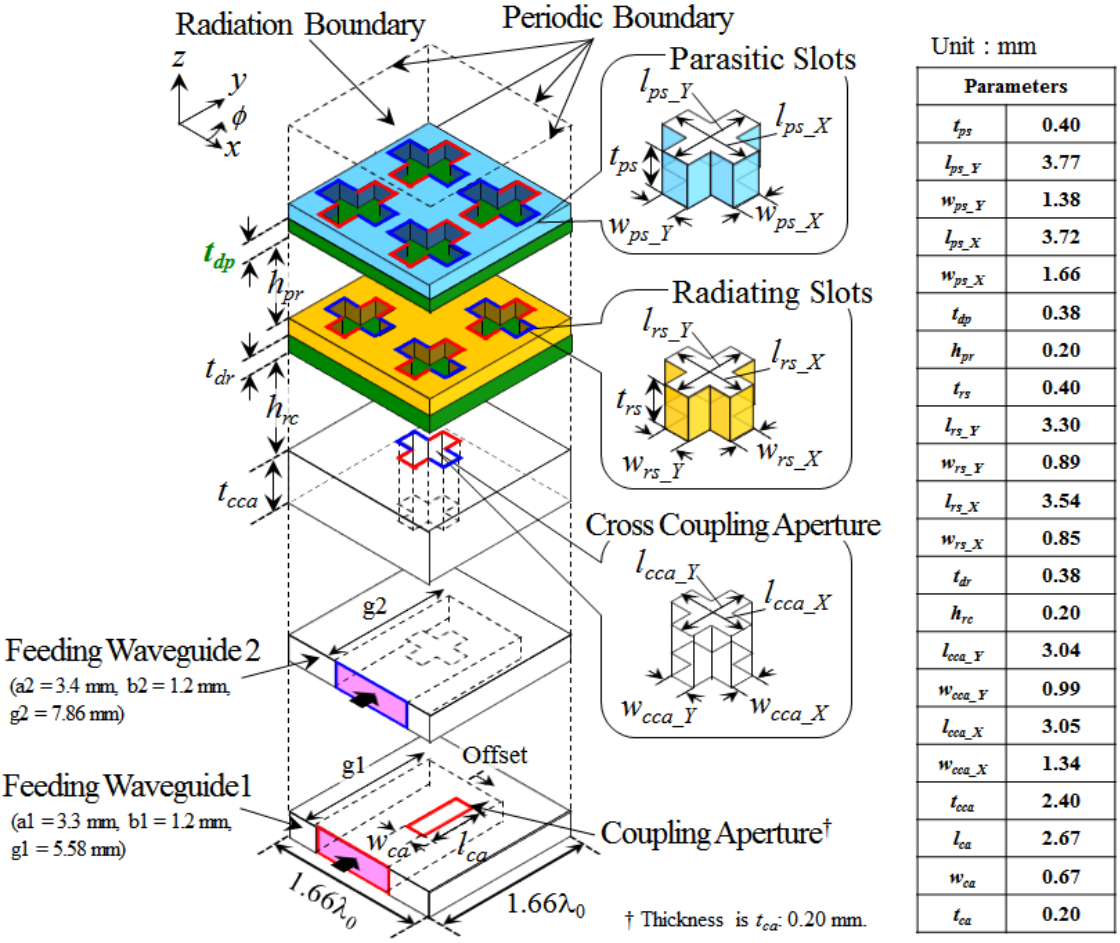

Unit : mm

Parameters	
t_{ps}	0.40
l_{ps_Y}	3.77
w_{ps_Y}	1.38
l_{ps_X}	3.72
w_{ps_X}	1.66
t_{dp}	0.38
h_{pr}	0.20
t_{rs}	0.40
l_{rs_Y}	3.30
w_{rs_Y}	0.89
l_{rs_X}	3.54
w_{rs_X}	0.85
t_{dr}	0.38
h_{rc}	0.20
l_{cca_Y}	3.04
w_{cca_Y}	0.99
l_{cca_X}	3.05
w_{cca_X}	1.34
t_{cca}	2.40
l_{ca}	2.67
w_{ca}	0.67
t_{ca}	0.20

Fig. 5.6 Model for the analysis of the 2×2-element subarray.

Fig. 5.7 shows the frequency characteristic of the S-parameters, changing the thickness of the dielectric layer t_{dp}. Other parameters are fixed and shown in Fig. 5.6. As t_{dp} is thicker, the frequency characteristic of the S-parameters shifts to a lower frequency domain. S_{11} is in good agreement with S_{22} in all t_{dr}. When t_{dr} is 0.38 mm, the antenna has the better performance of the S-parameter characteristic around the design frequency. The bandwidth of the VSWR less than 1.5 is 4.5 % for *x*-pol. operation and 4.3 % for *y*-pol. operation. In the above-mentioned frequency band, S_{21} is less than -37 dB.

Fig. 5.8 shows the comparison of the total thickness of models between two-layer and three- layer of parallel-plate dual-polarized slot array antenna. The thickness of two layers is 6.69 mm and that of three layers is 7.16 mm. Introducing the parasitic-slot layer does not result in a much thicker structure.

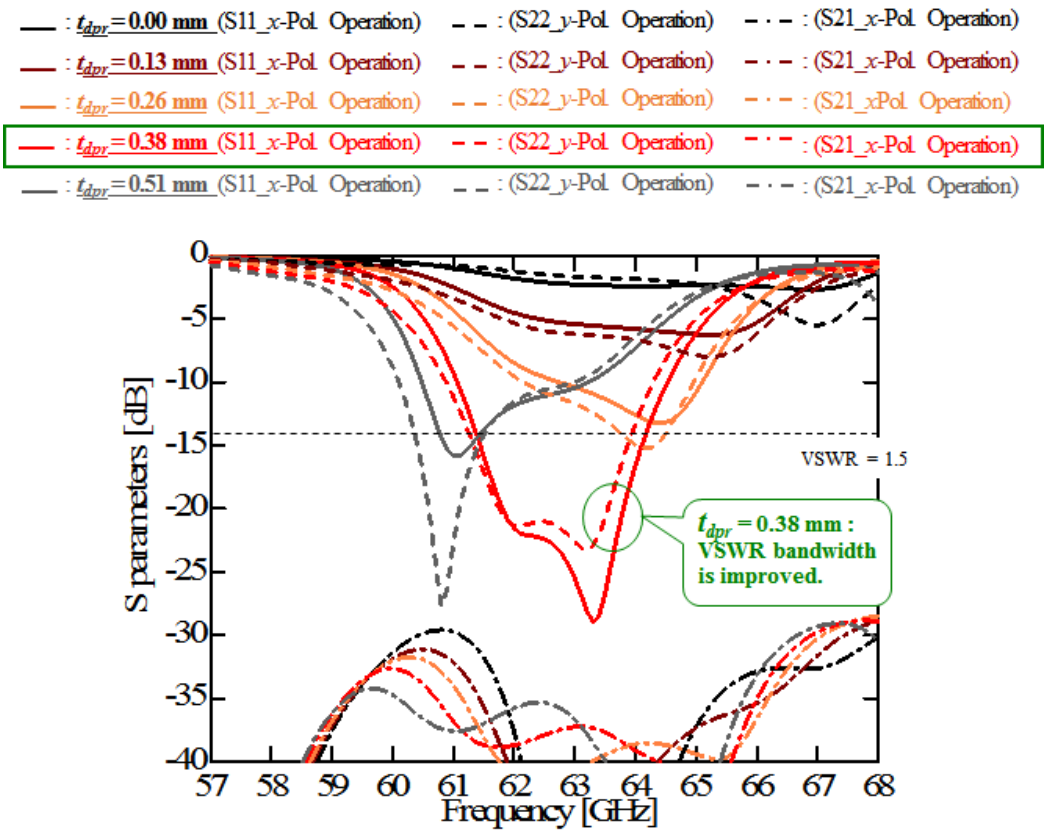

Fig. 5.7 Frequency characteristic of the S-parameters, changing the thickness of the dielectric layer t_{dp}.

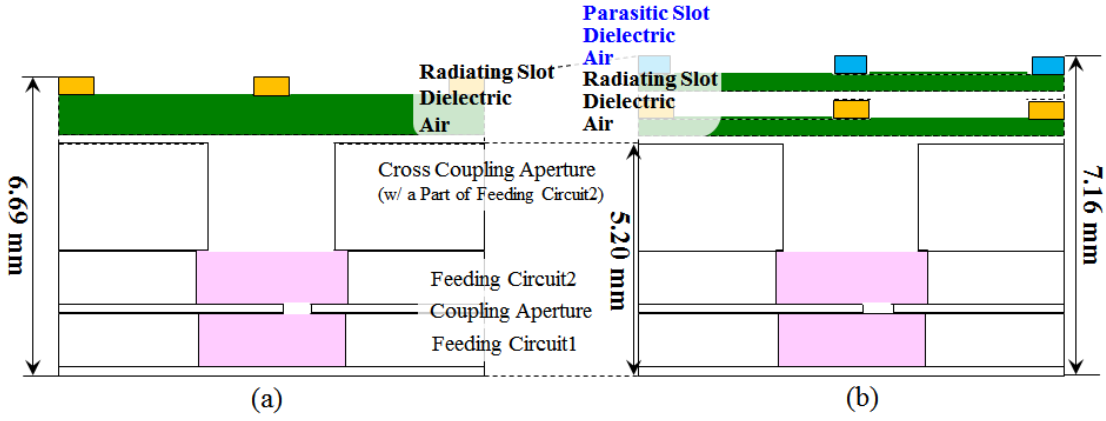

Fig. 5.8 Comparison of the height between two-layer and three-layer of parallel-plate dual-polarized slot array antennas. (a) Two layers. (b) Three layers.

5.3.3 Full Structure analysis

Fig. 5.9 shows the full structure of a 16×16-element three-layer dual-polarized parallel-plate slot array antenna fed by the perpendicular corporate feed. In Fig. 5.8, the plates are shown separated to expose the internal structure more fully, for the actual antenna, they are stacked much more closely. In the simulation, the conductivity of 5.8×10^7 S/m of copper and the loss tangent 0.0006 of the dielectric are assumed. Considering fabrication to maintain the flatness of the layers, the periphery of the four-layer parallel plates is terminated by (enclosed in) copper frames as shown in Fig. 5.9. The edge of the parallel plates is extended by 0.20 mm both in the *x* and *y* direction and terminated by copper. The dimensions of the antenna in the *xy*-plane is 72.0 mm × 72.0 mm. The parameters are the same as these of the 2×2-element subarray shown in Fig. 5.6.

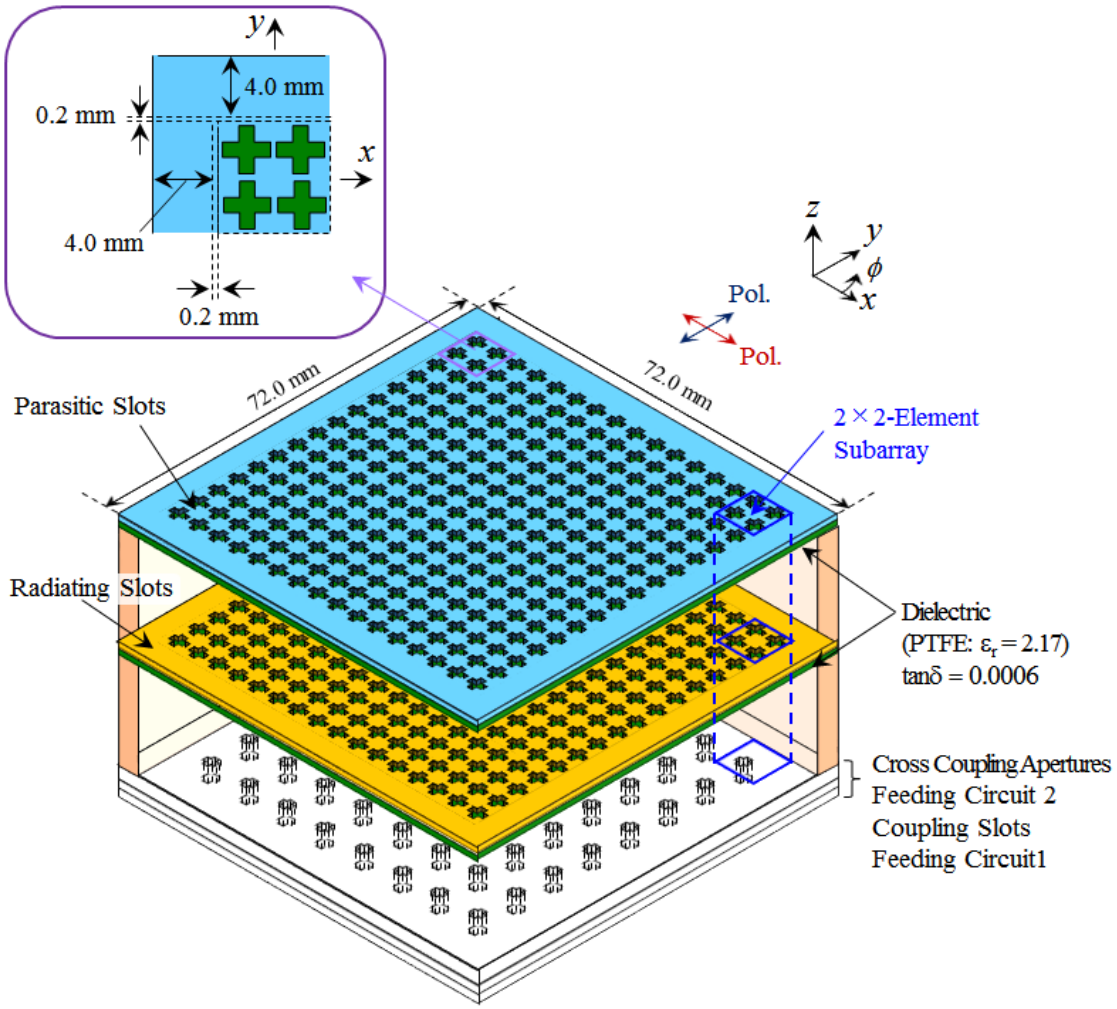

Fig. 5.9 Full structure of a perpendicular corporate feed in a three-layer dual-polarized parallel-plate slot array antenna.

Fig. 5.10 shows the frequency characteristic of S parameters. As a reference, the reflections of 2×2-element subarray is also described. For the *x*-polarized operation (excited by the feeding circuit 1), the reflection of the full structured antenna is less than -14 dB over 4.1 % of the bandwidth ranging from 61.1 to 63.7 GHz. For the *y*-polarized operation (excited by the feeding circuit 2), the reflection of the full structured antenna is less than -14 dB over 4.3 % of the bandwidth ranging from 61.0 to 63.7 GHz. Both the bandwidths are similar to these of the 2×2-element subarray. The isolation (S21) is lower than -55 dB in the VSWR less than 1.5, but this is not low enough considering a system. For example, some systems require the isolation less than -80 dB. To reduce isolation, the cross configuration of a copper would be effective. This configuration is introduced into the center of parasitic slots, and so behaves as slot pairs as shown in subsection 4.4.2. It could contribute to lowering the isolation.

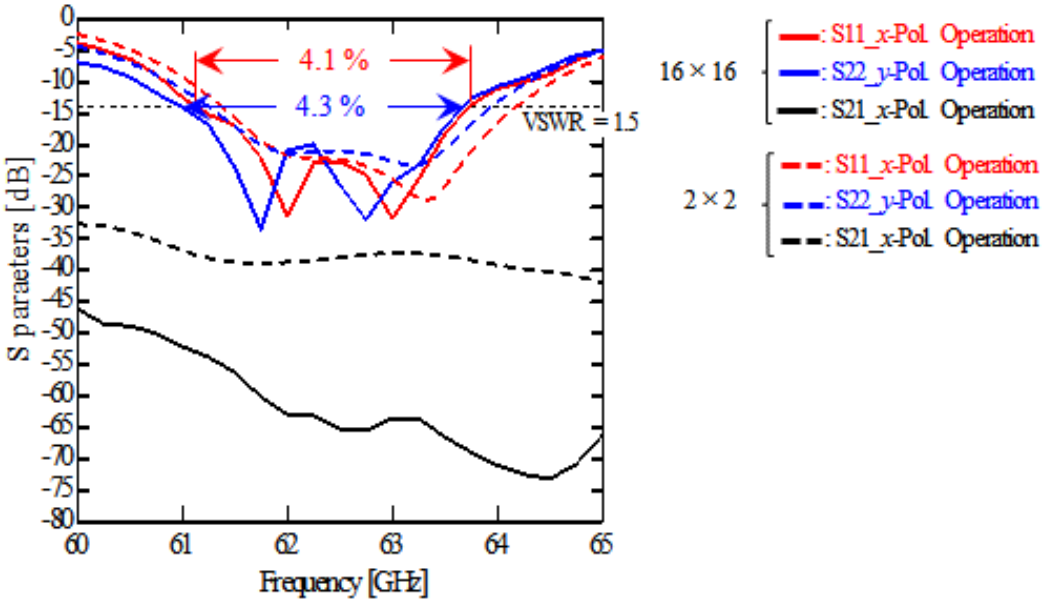

Fig. 5.10 Frequency characteristic of S parameters.

Fig. 5.11 shows radiation patterns at 62.5 GHz in the 0 deg.-plane (*xz*), 45 deg.-plane and 90 deg.-plane (*yz*), and cross polarization discriminations (XPD). For *x*-polarized operation, the radiation pattern in the 0 deg.-plane presents a uniform-excitation pattern including an element pattern. The radiation pattern in the 90 deg.-plane also provides a uniform-excitation pattern including an element pattern. Note that an element pattern has an omnidirectional pattern only in 0 deg.-plane, resulting in relatively higher sidelobes in wide-angle regions. The radiation pattern in the 45 deg.-plane has relatively

lower grating lobes around ± 55 deg. comparing to these of the linearly-polarized slot array antenna as shown in the chapter 4. Cross polarization is suppressed enough as shown in (c). The level is less than -52 dB. For *y*-polarized operation, the radiation pattern in the 0 deg.-plane presents a uniform-excitation pattern including an element pattern. The radiation pattern in the 90 deg.-plane also provides a uniform-excitation pattern including an element pattern. Note that an element pattern has an omnidirectional pattern only in 90 deg.-plane, resulting in relatively higher sidelobes in wide-angle regions. The radiation pattern in the 45 deg.-plane has relatively lower grating lobes around ± 55 deg. comparing to these of the linearly-polarized slot array antenna as shown in the chapter 4. Cross polarization is suppressed enough as shown in (d). The level is less than -51 dB. Cross polarization discriminations are shown in (e). For both operations, results are less than -55 dB in the desired frequency band.

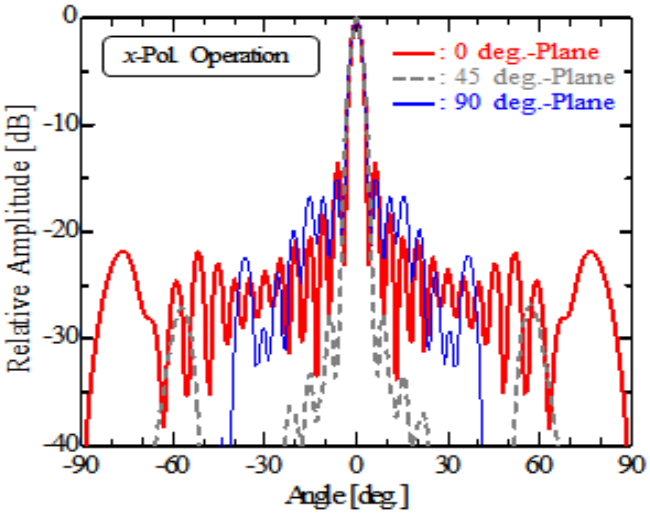

(a)

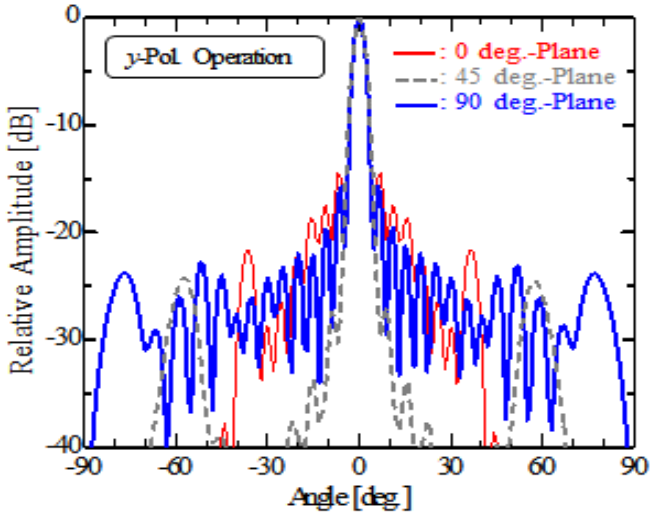

(b)

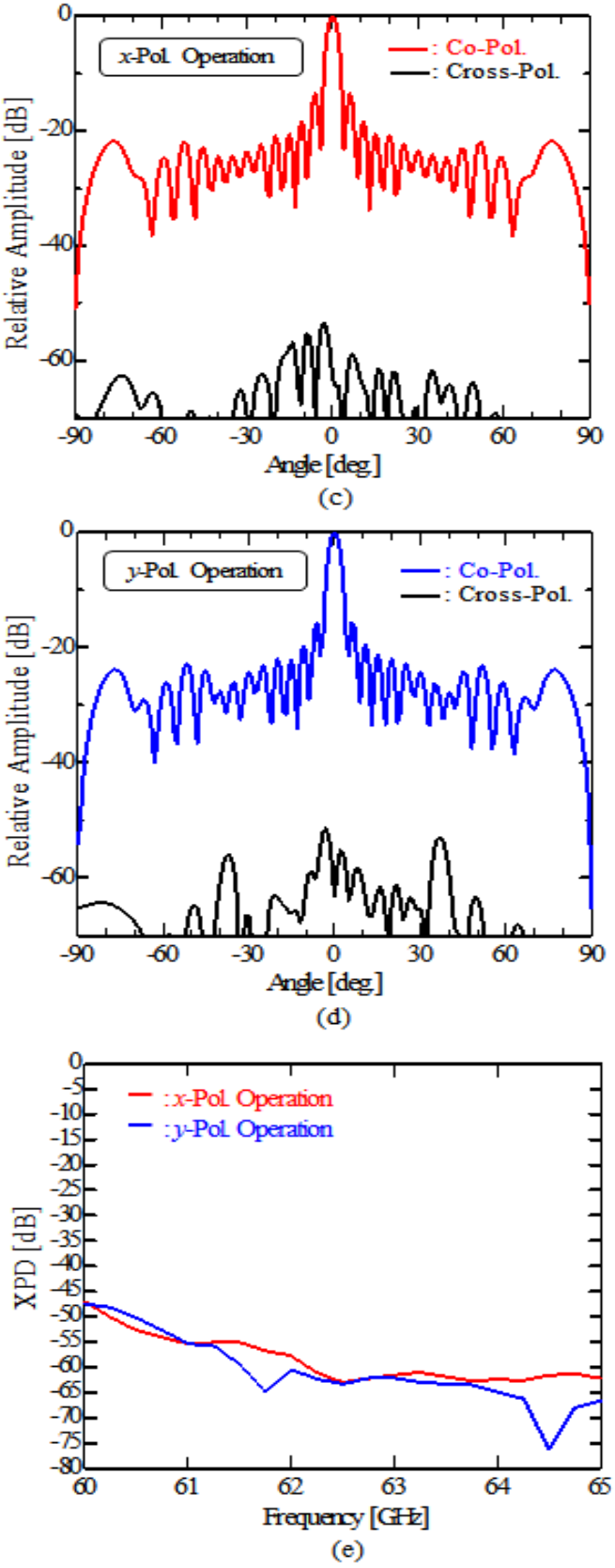

Fig. 5.11 Radiation patterns at 62.5 GHz. (a) *x*-polarized operation. (b) *y*-polarized operation. (c) *x*-polarized operation (w/ cross polarization). (d) *y*-polarized operation (w/ cross polarization) (e) XPD

Fig. 5.12 shows realized gain, gain and directivity. The realized gain includes the reflection loss as well as conductor and dielectric losses, and the aperture efficiency loss. For the *x*-polarized operation, we have achieved 5.4 % 1-dB-down bandwidth of realized gain in the 60.9 – 64.2 GHz range and 78 % antenna efficiency at design frequency. The aperture efficiency greater than 65 % is achieved over 3-GHz bandwidth. For the *y*-polarized operation, we have also achieved 5.6 % 1-dB-down bandwidth of realized gain in the 60.7 – 64.2 GHz range and 77 % antenna efficiency at design frequency. The aperture efficiency greater than 65 % is achieved over 3-GHz bandwidth.

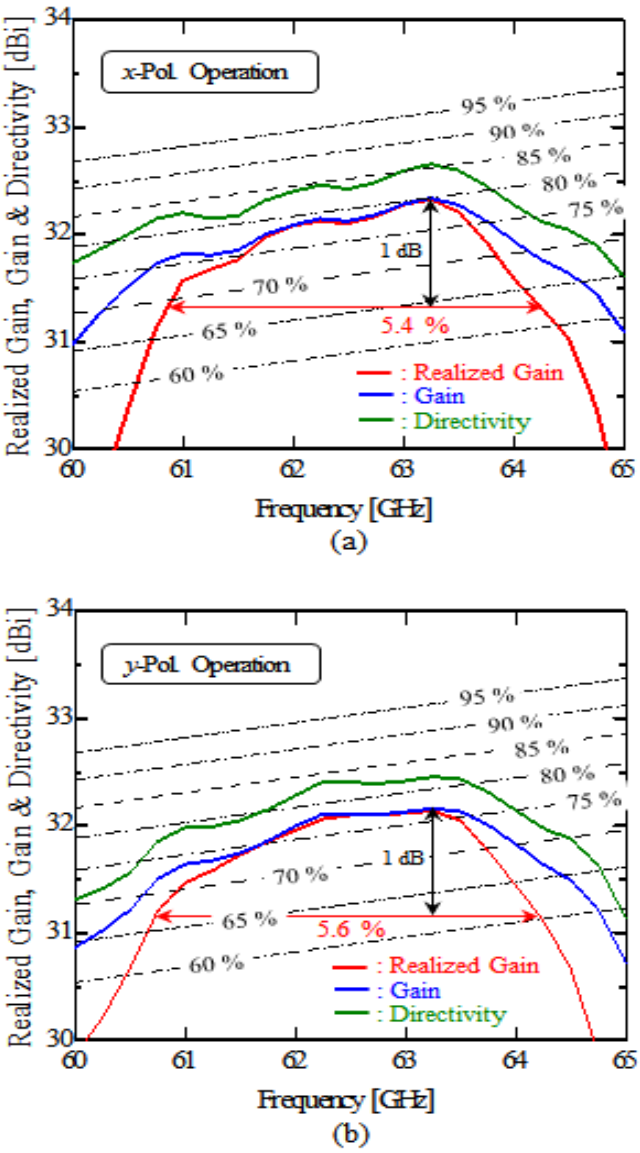

Fig. 5.12 Frequency characteristic of the realized gain, gain and directivity. (a) *x*-polarized operation. (b) *y*-polarized operation.

5.4 Concluding Remarks

This chapter presented a perpendicular-corporate feed for a three-layer dual-polarized parallel-plate slot array antenna. To create dual polarization, cross-slot configuration is introduced in cross-coupling apertures, radiating slots and parasitic slots. Dielectric layers are placed not only between the cross-coupling-aperture later and the radiating-slot layer but also between the radiating-slot layer and the parasitic-slot layer to achieve desired operation. Layers do not have metal contact because of air gaps placed under both dielectric layers.

In the simulation, we have realized 4.1 % bandwidth for the VSWR of less than -14 dB for *x*-polarized operation and 4.3 % for *y*-polarized operation. Radiation patterns provide uniform-excitation patterns including an element pattern in the 0 deg. and 90-deg, in both the *x*-polarized and *y*-polarized operations. However, in the 45 deg.-plane and 135 deg.-plane, the radiation patterns have grating lobes around ± 50-60 deg. region due to the excitation difference in both the planes. The relative amplitude of the grating lobes is -24 dB around ± 55 deg. Also, we have achieved 5.4 % 1-dB-down bandwidth of realized gain for the *x*-polarized operation and 5.6 % for the *y*-polarized operation. For both the operations, the aperture efficiency greater than 65 % is achieved over 3-GHz bandwidth.

Obtained results do not have much wider bandwidth than these of linear, circular and 45-deg. polarized antennas. However, if we introduce an additional-slot layer into the structure, the bandwidth of the VSWR would be advanced. At that time, we need to improve the reflection of feeding circuit 1 and 2 because their reflection level has not been low enough to achieve a wideband design yet.

Chapter 6

Conclusions

6.1 Summary of Preceding Chapters

This thesis proposed a perpendicular corporate feed in multi-layer parallel-plate slot array antennas. We place dielectric with adequate permittivity in the region between coupling-aperture and radiating-slot layers to remove x-shaped cavity walls completely in the radiating part of conventional antennas. This excites standing waves in the region and so provides 2×2-element subarrays with uniform excitation. Considering the availability of dielectric, we combine polytetrafluoroethylene (PTFE, $\varepsilon_r = 2.17$) and air to create desired permittivity ($\varepsilon_r = 1.28$) of dielectric equivalently, instead of using porous PTFE. Proposed antennas consists of slotted parallel plates, air gaps and a feeding circuit fabricated by the diffusion bonding of laminated thin copper plates. Air gaps are placed between the slotted plates in the radiating part. None of the slot layers are in electrical contact due to air gaps between the slot layers, resulting in low losses. To achieve the wideband design, we introduce a parasitic-slot layer and an additional-slot layer on the top of the radiating-slot layer with air gaps. To realize multi-functionalized operations, we apply this structure to circularly-polarized, 45-deg.-polarized and dual-polarized antennas by changing the configuration of slots, depending on polarizations.

In the chapter 1, the background of this study is presented by descriptions of millimeter-wave wireless communications, high gain antennas, array antennas with the corporate feed and parallel-plate slot array antennas with the corporate feed in millimeter-wave bands.

In chapter 2, we present the design process and characterization of a perpendicular-corporate feed in a three-layer linearly-polarized parallel-plate slot array antenna as the feasibility study of the perpendicular-corporate feed. In the design process, we discuss the effect of dielectric by the analysis of a 2×2-element subarray and an 8×8-element subarray, and describe the wideband design of the VSWR by introducing a parasitic-slot layer. The measured amplitude distribution of the near-field demonstrates a symmetric distribution on both the *x*-axis and *y*-axis, indicating that uniform excitation is created in the 16×16-element array antenna. The aperture efficiency greater than 90 % is achieved over 5-GHz bandwidth in the measured directivity. At the design frequency, the

measured directivity is 33.5 dBi with the antenna efficiency of 90.6 %. Radiation patterns provide uniform-excitation patterns including element patterns in both the E-plane and H-plane.

Chapter 3 presents the design process and characterization of a perpendicular-corporate feed in a four-layer parallel-plate circularly-polarized slot array antenna. In the design process, we discuss the configuration of slots to generate the circular polarization and the introduction of an additional-slot layer on top of a parasitic-slot layer with an air gap to enhance the bandwidth of the VSWR and the axial ratio. Considering fabrication constrains, the dielectric layer is composed of PTFE, ($\varepsilon_r = 2.17$) and air instead of using porous PTFE ($\varepsilon_r = 1.28$), and this combination achieves the desired permittivity ($\varepsilon_r = 1.28$) equivalently. We realize an 11.9 % bandwidth for the axial ratio of less than 3 dB in the measurements. At the design frequency, the measured realized gain is 32.7 dBi with the antenna efficiency of 75.5 %. Radiation patterns provide uniform-excitation patterns including element patterns in both the *xz*-plane and *yz*-plane.

Chapter 4 presents the design process and characterization of a perpendicular-corporate feed in a four-layer parallel-plate 45-deg.-polarized slot array antenna. We especially focus on three types of the configuration of additional slots to achieve desired operations: linear polarization with wideband, linear polarization with low grating lobes and 45 deg. polarization. For linear polarization with wideband, in the simulation we have realized 12.9 % bandwidth for the VSWR of less than -14 dB due to the introduction of the additional-slot layer, which has wider slots. Radiation patterns provide uniform-excitation patterns including element patterns in both the E-plane and H-plane. However, in the 45 deg.-plane the radiation pattern has grating lobes around ± 50-60 deg. region because of the excitation difference in the plane. The relative amplitude of the grating lobes is -22 dB around ± 55 deg. Also, we have achieved 12.6 % 1-dB-down bandwidth of realized gain and 82% antenna efficiency at design frequency. The aperture efficiency greater than 80 % is achieved over 7-GHz bandwidth. For linear polarization with low grating lobes, in the simulation the proposed antenna with slot pairs provides 12.8 % bandwidth for the VSWR of less than -14 dB. This bandwidth is very similar to that of no slot pairs. the radiation pattern, in the 45 deg.-plane, has lower grating lobes (-35 dB) around ± 50-60 deg. region than these of no slot pairs (-22 dB) due to the effect of slot pairs. Also, In the E-plane and H-plane, cross polarized patterns are also suppressed by the introduction. This means the configuration of slot pairs offers the reduction of excitation difference. We have achieved 12.7 % 1-dB-down bandwidth of realized gain and 83% antenna efficiency at design frequency. The aperture efficiency greater than 85 % is achieved over 6-GHz bandwidth. The realized gain of the antenna with pair slots

is larger than that of no slot pairs by 0.1 dB due to the effect of slot pairs. For 45-deg. polarization, in the simulation we have realized 12.9 % bandwidth for the VSWR of less than -14 dB even in the structure with 45 deg.-polarization. Radiation patterns provide uniform-excitation patterns including element patterns in the 0 deg. and 90 deg. planes. However, In the 45 deg.-plane and 135 deg.-plane, the radiation patterns have grating lobes around ± 50-60 deg. region due to the excitation difference in both the planes. The relative amplitude of the grating lobes is -22 dB around ± 55 deg. Also, we have achieved 12.7 % 1-dB-down bandwidth of realized gain and 78% antenna efficiency at design frequency. The aperture efficiency greater than 75 % is achieved over 7-GHz bandwidth. Among proposed models in this chapter, the bandwidth of the VSWR and 1 dB-down realized gain is very similar. Realized gain and antenna efficiency at design frequency is also very similar. These results indicate only the change of configuration in the additional slots offers operational functions with maintaining basic antenna characteristic.

Chapter 5 presents the design process and characterization of a perpendicular-corporate feed in a three-layer parallel-plate dual-polarized slot array antenna. To create dual polarization, we introduce the configuration of cross slots in layers and multi-layered feeding circuits. A new dielectric layer with an air gap is also introduced between the parasitic-slot layer and radiating-slot layer to improve the bandwidth of the VSWR. In the simulation, we have realized 4.1 % bandwidth for the VSWR of less than -14 dB for *x*-polarized operation and 4.3 % for *y*-polarized operation. Radiation patterns provide uniform-excitation patterns including an element pattern in the 0 deg. and 90-deg, in both *x*-polarized and *y*-polarized operations. However, in the 45 deg.-plane and 135 deg.-plane, the radiation patterns have grating lobes around ± 50-60 deg. region due to the excitation difference in both the planes. The relative amplitude of the grating lobes is -24 dB around ± 55 deg. Also, we have achieved 5.4 % 1-dB-down bandwidth of realized gain for the *x*-polarized operation and 5.6 % for the *y*-polarized operation. For both the operations, the aperture efficiency greater than 65 % is achieved over 3-GHz bandwidth.

Finally, Fig.6.1 shows the list of functions and performance in proposed antennas. The results are obtained by the analysis of 16×16-emenet arrays in the simulations. The perpendicular corporate feed can provide various functionalities by changing the configuration of slots depending on polarization and wideband characteristic by having a multi-layered structure.

Polarization		Linear	Circular	Linear	Linear	45-deg. Linear	Dual
16 × 16-Element Array		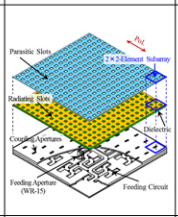	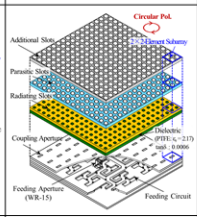	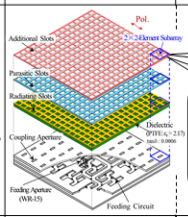	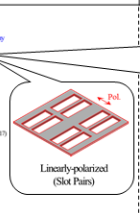	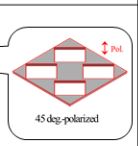	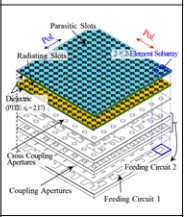
VSWR < 1.5 BW		7.3 %	**11.2 % (AR<3dB: 15.7 %)**	**12.9 %**	**12.8 %**	**12.9 %**	**4.1 %(*x*-pol.) 4.3 %(*y*-pol.)**
1 dB-down Realized Gain		7.5 %	**10.8 %**	**12.6 %**	**12.7 %**	**12.7 %**	**5.4 %(*x*-pol.) 5.6 %(*y*-pol.)**
Realized Gain @ 61.5 GHz		33.0 dBi	32.7 dBi	33.1 dBi	33.2 dBi	32.9 dBi	32.1 dBi @62.6GHz
Antenna Efficiency @ 61.5 GHz		84 %	79 %	82 %	83 %	78 %	77 % @62.6GHz
Aperture Efficiency		90 % Over 5 GHz BW	75 % Over 6.5 GHz BW	80 % over 7 GHz BW	**85 % over 7 GHz BW**	75 % over 7 GHz BW	75 % over 3 GHz BW
SLL (±θ=55°)	0-deg. plane	-26 dB	-26 dB	-25 dB	-22 dB	-25 dB	-22 dB
	45-deg. plane	-27 dB	-22 dB	-23 dB	**-35 dB**	-22 dB	-24 dB
	90-deg. plane	-27 dB	-30 dB	-31 dB	-30 dB	-30 dB	-23 dB

Fig. 6.1 List of functions and performance in proposed antennas.

6.2 Remarks for Future Studies

For the future studies, in the measurement we realized dielectric sheets are slightly bent, causing the deterioration of the antenna performance as described in chapter 2 and 3. In particular, bent dielectric sheets degrade the reflection characteristic of antennas because of changing the relative permittivity of dielectric equivalently. Considering the fabrication of large-sized arrays such as 32×32-element array and 64×64-element array, this deterioration would be much more significant. We should achieve the robust design of the multi-layer structure with the perpendicular corporate feed by having more simulations and measurements. For example, we could feed back the measured results to the design process with a simulator by estimating the change of the relative permittivity of bent dielectric. This enables to design a model by including slightly different relative permittivity of dielectric in advance. Also, we could use PTFE with copper foil. This PTFE is hard to be bent relatively so that the change of relative permittivity would not be caused significantly in the fabrication process.

In this thesis, we have analyzed models by using the Finite Element Method (FEM). This solver is time consuming due to large number of mesh in models and

analytical spaces, so it is difficult to obtain optimized results of models quickly. To enhance antenna performance such as the bandwidth of the VSWR, the axial ratio and realized gain, we should analyze models by the Method of Moments (MoM) in the next step. This is very advantageous over saving analysis time because of a small number of unknown parameters. Unknown is only the current on the surface of antennas and this leads to the optimized design quickly. As another problem, analyzed models have grating lobes around ± 55 deg. in the 45 deg.-plane because of excitation difference. The difference would be caused by wider slots creating higher modes. On the other hands, wider slots contribute to enhancing the bandwidth of the VSWR. To solve excitation difference while maintaining the characteristic of the wide bandwidth, the introduction of the MoM would also be beneficial because optimized results can provide lower grating lobes while having the wide bandwidth of the VSWR.

This thesis describes multi-layered structure provides the wider bandwidth of the VSWR, but how many layers can offer the best performance of the VSWR. More layered structure should be analyzed to find the best number of layers with the perpendicular corporate feed in various operations.

Although chapter 4 presents the effect of the configuration of slot pairs in additional-slot layer, the best location of slot pairs is not revealed in models of the perpendicular-corporate feed. This future work includes the number of introduced grids (slot pairs has one grid) in slots. Since the structure of slot pairs enhances the performance of antennas with perpendicular-corporate feed, the optimized location of slot pairs or grids should be found in various layers.

To decide antenna structure uniquely, we could apply the filter-design theory to the design of a 2×2-element subarray [6.1] - [6.3]. When a designed antenna is described as an equivalent circuit, parameters of the equivalent circuit are derived by the circuit synthesis of the filter-design theory. Then, the relation between the parameters and the physical structure of components is calculated, and so can decide the physical structure of the designed antenna. As an example, Fig 6.2 shows the equivalent circuit of the 2×2-element subarray of the perpendicular-corporate feed in a four-layer linearly-polarized slot array antenna. Dielectric with an air gap and air gaps are described as series-resonant circuits; parasitic slots, radiating slots and a coupling aperture are described as ideal transformers; and additional slots are described as a radiating resistance. This structure is expressed by the equivalent circuit of a triple-resonator direct-coupled type filter equivalently composed of resonant frequency: f_0, exterior Q-value: Q_{ext}, coupling coefficient: k_{ij} and radiating Q-value: Q_{rad}. Parameters of it are decided by a desired transmission characteristic.

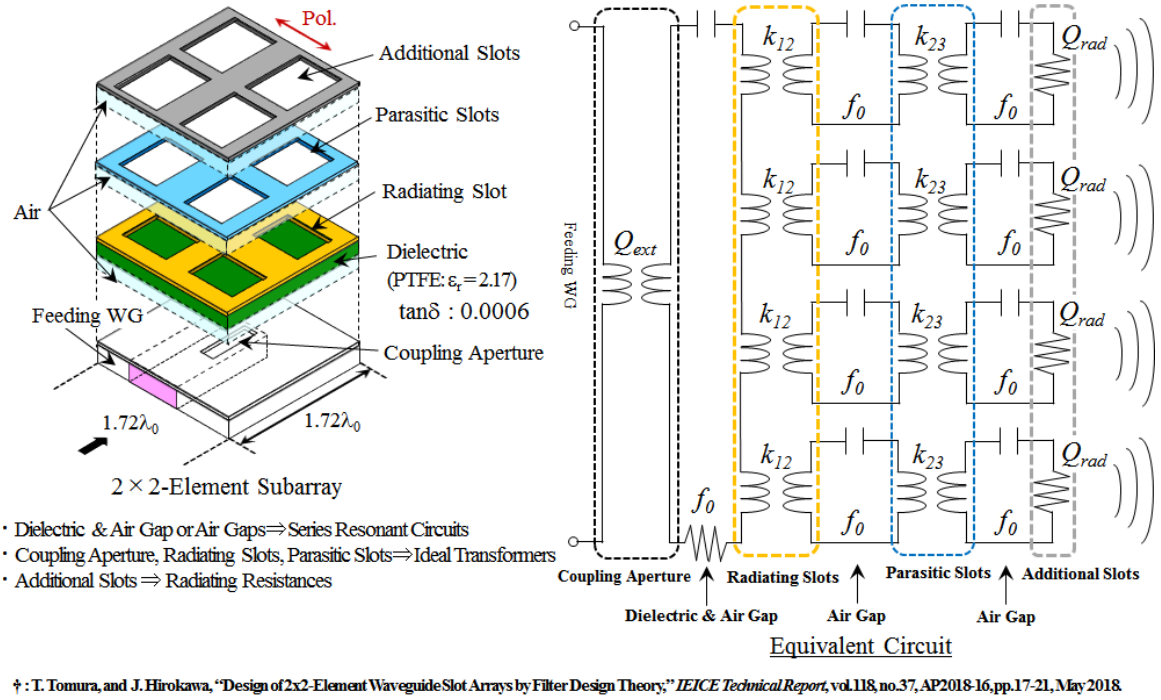

† : T. Tomura, and J. Hirokawa, "Design of 2x2-Element Waveguide Slot Arrays by Filter Design Theory," *IEICE Technical Report*, vol.118, no.37, AP2018-16, pp.17-21, May 2018.

Fig. 6.2 Equivalent circuit of 2×2-element subarray.

We have not found feature parameters in operations. Which parameters mostly influence the bandwidth of the VSWR depending on operations. There are parameters: size of slots in additional-slot, parasitic-slot and radiating-slot layers, the thickness of air gaps between slot layers, the thickness of slot layers and the relative permittivity of dielectric in the structure of multi layers with a perpendicular-corporate feed. To find feature parameters leads to having quick design process. As an example, subsection 6.2.1 shows the influence of air gaps among linear, circular and 45-deg. polarizations. This analysis is not enough to conclude feature parameters depending on operations, but we can obtain informative results.

Finally, these efforts will contribute to establishing the structure of a perpendicular corporate feed in multi-layer parallel-plate slot array antennas in the future.

6.2.1 Feature Parameters

To obtain feature parameters in the structure of a perpendicular corporate feed in multi-layer parallel-plate slot array antennas, we analyze 2×2-element subarrays of linear, circular and 45-deg. polarizations by changing only air gaps: h_{ap} and h_{pr} as an example. We evaluate how the change of air gaps influences the bandwidth of the VSWR, depending on polarizations. Fig. 6.3 shows the characteristic of the VSWR bandwidth by changing air gaps. For the better understanding, histograms are also shown in the figure. We change air gaps by 0.20 mm and ranging from 0.00 mm to 1.20 mm due to the availability of copper plates. For a linear polarization, lower values of air gaps provide the better bandwidth of the VSWR. Especially when h_{ap} is 0.20 mm and h_{pr} is 0.20 mm, the bandwidth of the VSWR less than 1.5 is wider 13.3 %. This means we should set h_{ap} and h_{pr} at specific values to obtain the best performance of the VSWR bandwidth and these values are in low for the design of a linear polarization. On the other hand, a circular polarization has various values of air gaps for the better bandwidth of the VSWR. Especially when h_{ap} is 1.00 mm and h_{pr} is 0.80 mm, the bandwidth of the VSWR less than 1.5 is wider 11.2 %. Also, averaged bandwidth of the VSWR is 7.3 % in Fig. 6.3 (d), wider than others. This means we should set h_{ap} and h_{pr} at some values to obtain the best performance of the VSWR bandwidth and these values are in middle when designing a circular polarization. For a 45-deg. polarization, lower values of air gaps provide the better bandwidth of the VSWR. Especially when h_{ap} is 0.20 mm and h_{pr} is 0.20 mm, the bandwidth of the VSWR less than 1.5 is wider 13.1 %. This characteristic is similar to that of a linear polarization, but the averaged bandwidth of the VSWR is 3.0 % in Fig. 6.3 (e), higher than (b). This means we should set h_{ap} and h_{pr} at specific values to obtain the best performance of the VSWR bandwidth and these values are in low when designing a 45-deg. polarization. Note that we need to analyze more cases such as changing the size of slots to achieve specific feature parameters, but this subsection would be useful for future analysis.

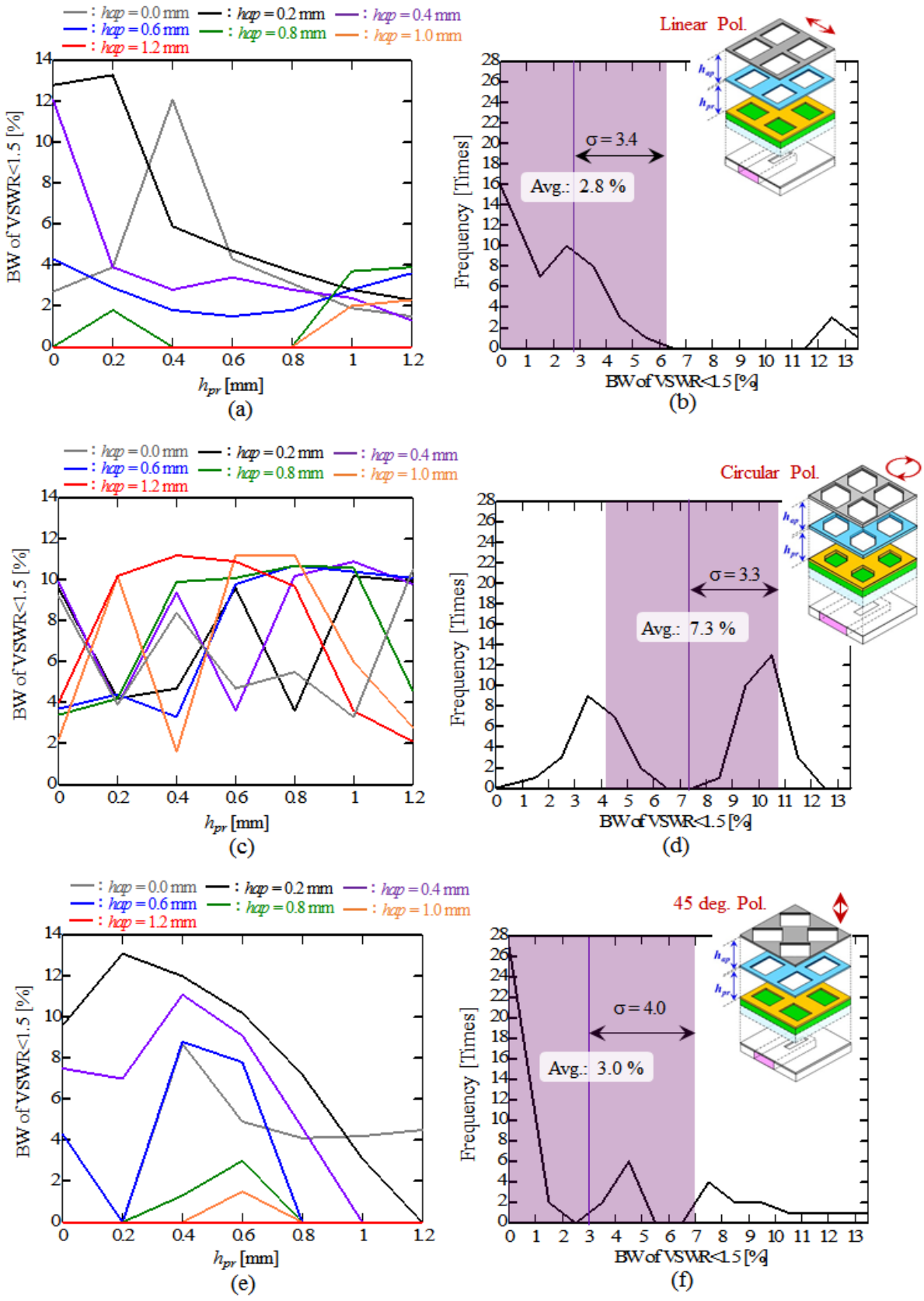

Fig. 6.3 Characteristic of VSWR bandwidth by changing air gaps. (a) B.W. of Linear pol. (b) Histogram of linear pol. (c) B.W. of circular pol. (d) Histogram of circular pol. (a) B.W. of 45-deg. pol. (b) Histogram of 45-deg. pol.

Reference

[6.1] Y. Yusuf, H. Cheng, and X. Gong, IEEE Trans. Antennas Propag., vol. 59, no. 11, pp. 4016-4022, Nov. 2011.

[6.2] M. Ohira, K. Yamanaka, Z. Ma, IEICE Trans. Electron., vol. E99-C, no. 7, July 2016.

[6.3] T. Tomura, and J. Hirokawa, “Design of 2x2-Element Waveguide Slot Arrays by Filter Design Theory,” IEICE Technical Report, vol.118, no.37, AP2018-16, pp.17-21, May 2018.

Acknowledgements

I would like to express my sincere gratitude to my supervisor, Professor Jiro Hirokawa for his continuous support, guidance and encouragement. His energetic instructions advanced my knowledge of antenna and propagation, and inspired me to study harder all my life.

I am also grateful to Professor Makoto Ando for his helpful advice.

I also thank my dissertation committee, Professor Kei Sakaguchi, Associate Professor Atsuhiro Nishikata, Associate Professor Takahiro Aoyagi, Associate Professor Nobuhiko Nishiyama. Many thanks for their instructive proposals and comments, which have greatly improved the quality of this dissertation.

I also wish to express my gratitude to Associate Professor Takashi Tomura for his fruitful advice.

I am also grateful to Professor Kiyomichi Araki for his valuable comments.

I am also grateful to Specially Appointed Professor Fumio Watanabe for his valuable comments.

I also wish to all of the member and the alumni of Hirokawa Laboratory for their support and help.

I would like to express my gratitude to all of my friends for their help and support.

Finally, I would like to express my respects to my family for their supports.

List of Publications

Journals

- H. Irie, and J. Hirokawa, “Perpendicular-Corporate Feed in Three-Layered Parallel-Plate Radiating-slot Array,” *IEEE Trans. Antennas Propag.*, vol. 65, no. 11, pp. 5829 - 5836, Nov. 2017.
- H. Irie, and J. Hirokawa, “Perpendicular-Corporate Feed in a Four-Layer Circularly-Polarized Parallel-Plate Slot Array,” *IEICE Trans. Commun.*, vol. E102-B, no.1, pp. 137-146, Jan. 2019.

International conferences

- H. Irie, and J. Hirokawa, “Feasibility of Perpendicular-Corporate Feed for a Multi-Layered Parallel-Plate Slot Array Antenna,” *Proc. of Euro. Conf. Antenna Propag. (EuCAP)*, Poster_06.21, pp. 3109-3110, Paris, France, Mar. 19-24, 2017
- H. Irie, T. Tomura, and J. Hirokawa, “Measurement of a Perpendicular-Corporate Feed in a Three-Layered Parallel-Plate Slot Array,” *Proc. of IEEE International Symposium on Antennas and Propag. and USNC-URSI Radio Science Meeting (APS/URSI)*, TU-UB.3P, Boston, Massachusetts, Jun. 8-13, 2018.
- H. Irie, T. Tomura, and J. Hirokawa, “Design of a 2×2-Element for a Perpendicular-Corporate Feed Four-layer Parallel-Plate Pair-Slot Array Antenna,” *Proc. of International Symposium on Antennas and Propag. (ISAP)*, A10_1001, Busan, Korea, Oct. 23-26, 2018.

Domestic conferences

- H. Irie, and J. Hirokawa, “Feasibility of Perpendicular-Corporate Feed for a Multi-Layered Parallel-Plate Slot Array Antenna,” *IEICE Technical Report*, vol.116, no.317, AP2016-108, pp.7-11, Nov. 2016.
- H. Irie, T. Tomura, and J. Hirokawa, “Design of a Circularly-Polarized 2×2-Element for Perpendicular-Corporate Feed Four-Layered Parallel-Plate Slot Array Antenna," *Proc. of IEICE Society Conf.*, B-1-84, Tokyo, Japan, Sep. 2017.

- H. Irie, T. Tomura, and J. Hirokawa, “Design of a Perpendicular-Corporate Feed in a Four-Layered Parallel-Plate Circularly-Polarized Slot Array Antenna,” *IEICE Technical Report*, vol.117, no.242, AP2017-97, pp.15-18, Oct. 2017.
- H. Irie, T. Tomura, and J. Hirokawa, “Design of a 2×2-Element for Perpendicular-Corporate Feed Four-Layered Parallel-Plate Slot Array Antenna,” *Proc. of the IEICE General Conf.*, B-1-99, Tokyo, Japan, Mar. 2018.
- H. Irie, T. Tomura, and J. Hirokawa, “Design of a 2×2-Element for a Perpendicular-Corporate Feed Three-Layer Parallel-Plate Dual-Polarized Slot Array Antenna,” *Proc. of IEICE Society Conf.*, B-1-84, Kanazawa, Japan, Sep. 2018.
- H. Irie, T. Tomura, and J. Hirokawa, “Design of a Perpendicular-Corporate Feed in a Four-Layer Parallel-Plate 45 deg.-Polarized Slot Array Antenna,” *IEICE Technical Report*, vol.118, no.358, AP2018-145, pp.1-4, Dec. 2018.

Appendix A

Design of Perpendicular-Corporate Feed in Five-Layer Parallel-Plate Linearly-Polarized Slot Array Antenna

A.1 Introductory Remarks

This appendix presents a perpendicular-corporate feed in a five-layer parallel-plate linearly-polarized slot array antenna. The proposed antenna is based on the structure of a perpendicular-corporate feed in a four-layer linearly-polarized parallel-plate slot array antenna as shown in the chapter 4, but has a new-slot layer (defined as extra-slot layer) on the top of the additional slot layer with an air gap in between the two. The aim of this analysis is to evaluate how many layers contribute to improving antenna performance.

This appendix is organized as follows. Section A.2 describes the characteristic of a perpendicular-corporate feed in a five-layer linearly-polarized slot array antenna by the analysis of a 2×2-element subarray. section A.3 elucidates the effective of introducing the extra-slot layer compared with three-layer and four-layer models by the analysis of a 16×16-element array. In section A.4, we conclude this appendix.

A.2 Design of 2×2-Element Subarray

To evaluate how many slot layers contribute to advancing antenna performance, the proposed model has an extra-slot layer on the top of the additional-slot layer with an air gap in between the two. Fig. A.1 shows the model for the analysis of a 2×2-element subarray. In the analysis, we use a dielectric layer of t_d = 0.38 mm and ε_r = 2.17 obtained from the subsection 3.3.1. The conductivity 5.8×10^7 S/m of copper and a loss tangent 0.0006 of the dielectric are assumed. Considering the fabrication, we select a multiple of 0.20 mm as the thickness of layers and air gaps except for the dielectric layer. The parameters are as follows: the size of the extra slots, l_e, and w_e; the size of the additional slots, l_a, and w_a; the size of the parasitic slots, l_p and w_p; the size of the radiating slots, l_r

and w_r; and the size of the coupling apertures, l_c and w_c. The air gap between the extra-slot and the additional-slot layers is h_{ea}, that between the additional-slot and the parasitic-slot layers is h_{ap}, that between the parasitic-slot and the radiating-slot layers is h_{pr}, and that between the dielectric and coupling layers is h_{rc}. Also, note that the thicknesses of the extra-slot layer, the additional-slot layer, the parasitic-slot layer, and radiating-slot layer is 0.20 mm, and that of the coupling-aperture layer is also 0.20 mm. The size of the feeding waveguide is fixed: width a = 2.95 mm, thickness b = 1.00 mm and length g = 5.65 mm, and it has short end. The offset of the coupling aperture against the principal axis in the x direction is also fixed at 0.60 mm. The final values of the design parameters are listed in the figure.

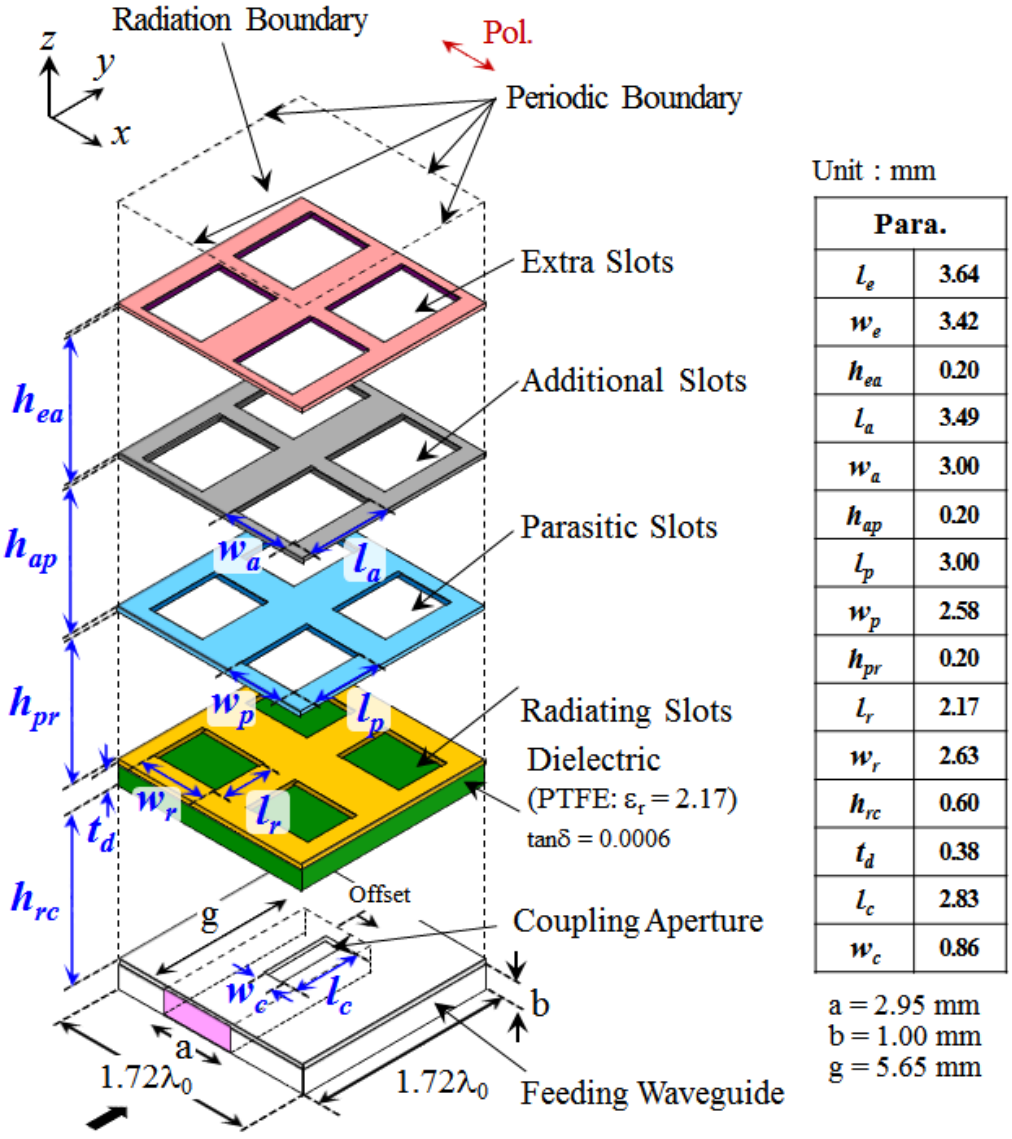

Unit : mm

Para.	
l_e	3.64
w_e	3.42
h_{ea}	0.20
l_a	3.49
w_a	3.00
h_{ap}	0.20
l_p	3.00
w_p	2.58
h_{pr}	0.20
l_r	2.17
w_r	2.63
h_{rc}	0.60
t_d	0.38
l_c	2.83
w_c	0.86

a = 2.95 mm
b = 1.00 mm
g = 5.65 mm

Fig. A.1 Model for the analysis of the 2×2-element subarray.

Fig. A.2 shows the frequency characteristic of the reflection. As a reference, we also show the result of the four-layer linearly-polarized slot array antenna as shown in Fig. 4.4. The reflection of the 2×2-element subarray with the extra-slot layer is smaller than -14 dB over 12.7 % of the bandwidth ranging from 57.5 to 65.3 GHz. On the other hand, the reflection of the four-layer linearly-polarized slot array antenna is less than -14 dB over 13.4 % bandwidth ranging from 57.3 to 65.6 GHz. The bandwidth is not enhanced by the introduction of the extra-slot layer. To elucidate the reason, we utilize an eigen mode analysis and the results are also shown in Fig. A.2. We used 1×1-element subarray for the eigen mode analysis because of the symmetric structure as shown in Fig. A.1. In the analysis, both the models have two Q-factors in the desired band and they are almost the same. This does not have significant difference of the VSWR bandwidth.

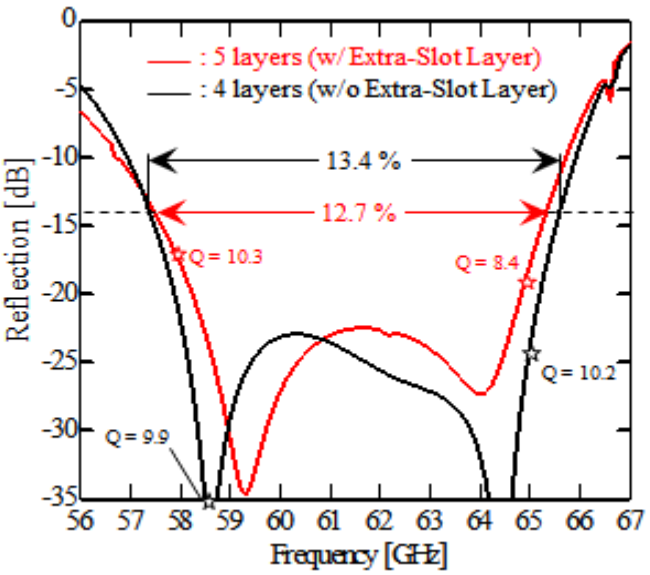

Fig. A.2 Frequency characteristic of the reflection.

A.3 Full Structure Analysis

Fig. A.3 shows the full structure of the 16×16-element five-layer linearly-polarized parallel-plate slot array antenna fed by the perpendicular corporate feed. In Fig.A.3, the plates are shown separated to expose the internal structure more fully, for the actual antenna, they are stacked much more closely together. In the simulation, the conductivity of 5.8×10^7 S/m of copper and the loss tangent 0.0006 of the dielectric are assumed. Considering fabrication to maintain the flatness of the layers, the periphery of the five-layer parallel plates is terminated by (enclosed in) copper frames as shown in Fig.

A.3. The edge as PMC of the parallel plates is extended by 1.3 mm (≈ 0.25λ_0) only in the *y* direction and terminated by copper. The dimensions of the antenna in the *xy*-plane is 75.2 mm × 79.4 mm. The parameters are the same as these of the 2×2-element array shown in Fig. A.1.

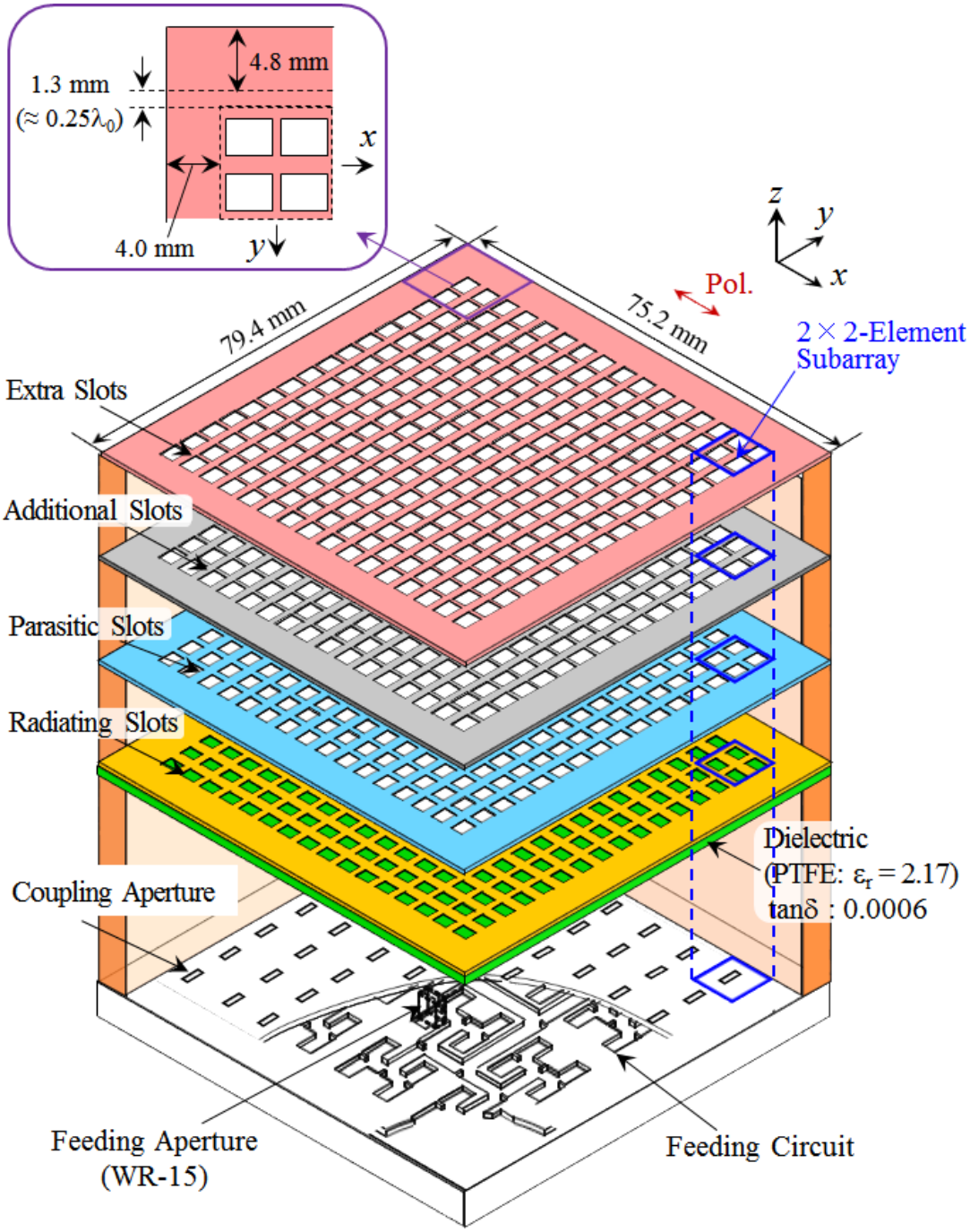

Fig. A.3 Full structure of a perpendicular corporate feed in a five-layer linearly-polarized parallel-plate slot array antenna.

Fig. A.4 shows the frequency characteristic of the reflection. As a reference, the reflections of four layers, the 2×2-element subarray and the feeding circuit are also described. The reflection of the full structured antenna is less than -14 dB over 12.8 % of the bandwidth ranging from 57.5 to 65.3 GHz. The bandwidth is very similar to that of the four layers and the 2×2-element subarray. Also, the reflection of the full structured antenna has slight ripples. This would be caused by the feeding circuit because the reflection of it has more clear ripples in Fig. A.4.

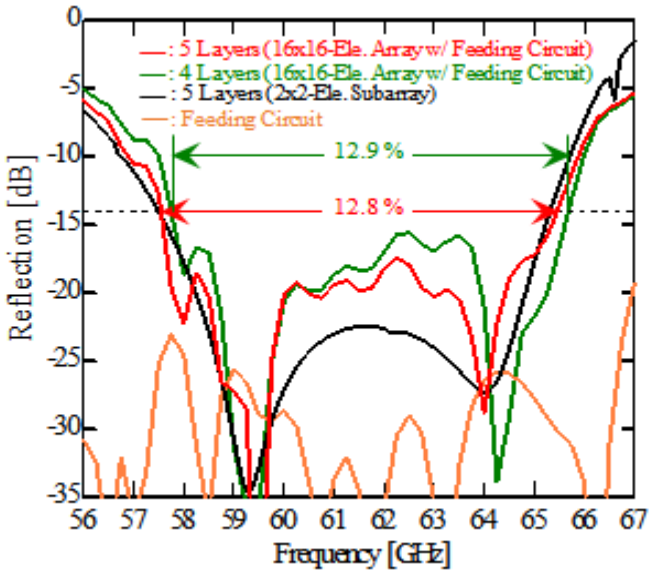

Fig. A.4 Frequency characteristic of the reflection.

Fig. A.5 shows radiation patterns at the design frequency (61.5 GHz) in the E-plane (*xz*), H-plane (*yz*) and 45 deg.-plane. In the E-plane and H-plane, the radiation patterns present uniform-excitation patterns including element patterns. However, in the 45-deg. plane the radiation pattern has grating lobes around ± 55 deg. Also, we review radiation patterns in both the E-plane and H-plane including cross polarization. Both co-polarization and cross-polarizations do not have differences between five layers and four layers in E-plane and H-plane significantly. In addition, we evaluate radiation patterns between four layers and five layers in the 45-deg. plane and there are not any differences. The introduction of the extra–slot layer does not offer better performance of an antenna. We conclude the difference between four layers and five layers does not lead to improving radiation patterns.

Fig. A.6 shows realized gain, gain and directivity. As a reference, results of four layers are also described. The realized gain includes the reflection loss as well as conductor and dielectric losses and the aperture efficiency loss. We have achieved 13.0 % 1-dB-down bandwidth of realized gain in the 57.8 – 65.7 GHz range and 83% antenna efficiency at design frequency. The aperture efficiency greater than 80 % is achieved over 7-GHz bandwidth.

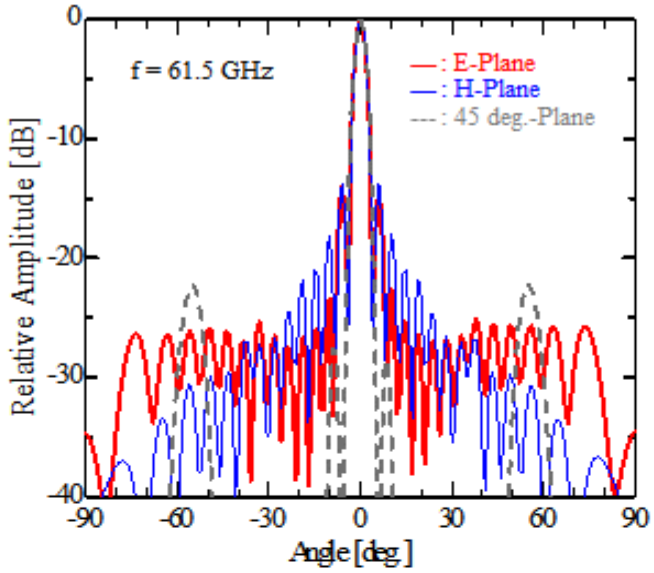

(a)

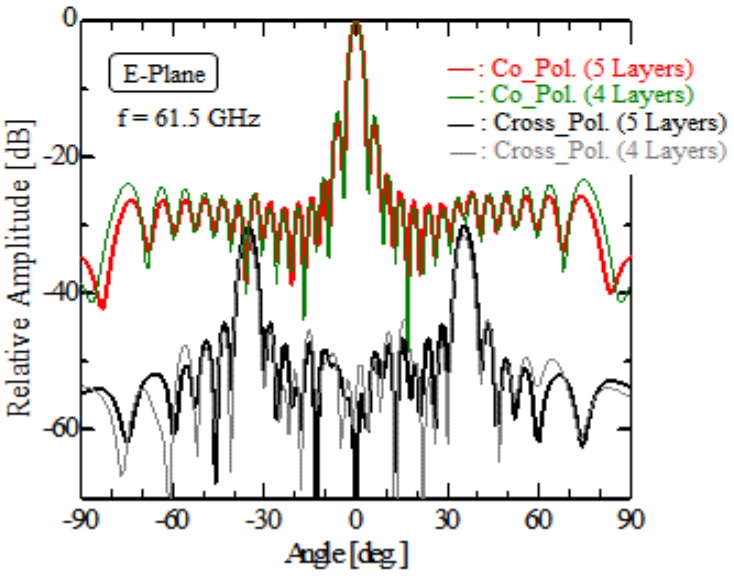

(b)

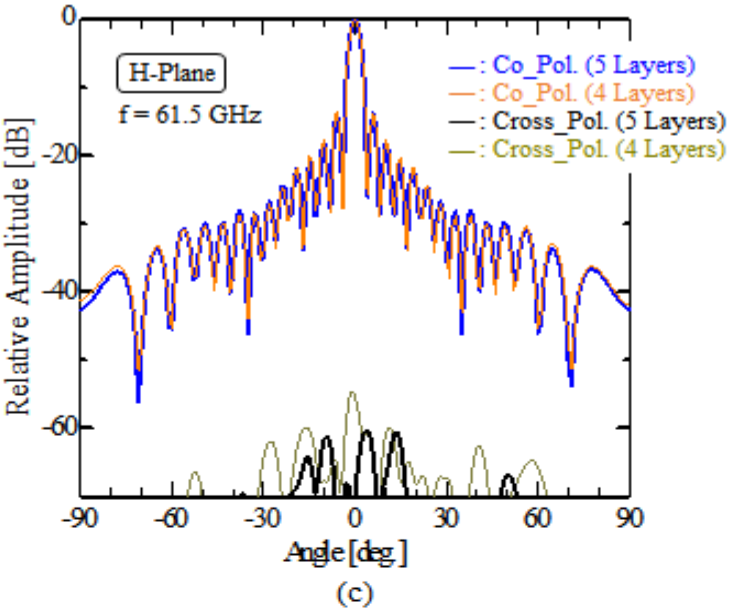

(c)

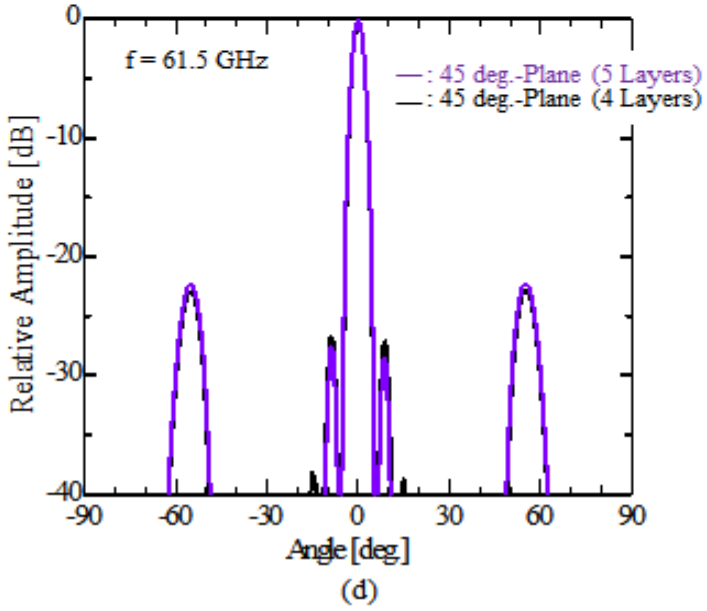

(d)

Fig. A.5 Radiation patterns at 61.5 GHz. (a) E-Plane, H-plane and 45 deg.-plane. (b) E-Plane (w/ cross polarization) in both four layers and five layers. (c) H-Plane (w/ cross polarization) in both four layers and five-layers. (d) 45 deg.-plane in both four layers and five layers

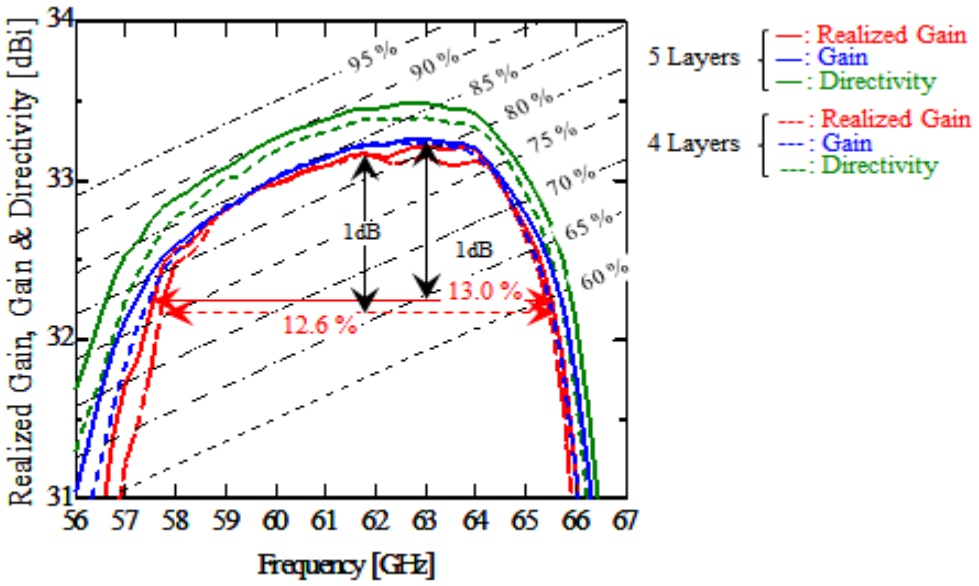

Fig. A.6 Frequency characteristic of the realized gain, gain and directivity.

A.4 Concluding Remarks

This appendix presented a perpendicular-corporate feed for a five-layer linearly-polarized parallel-plate slot array antenna. The proposed antenna is based on the structure of a perpendicular-corporate feed in a four-layer linearly-polarized parallel-plate slot array antenna as shown in the chapter 4, but has an extra-slot layer on the top of the additional slot layer with an air gap in between the two.

In the simulation, the proposed antenna provides 12.8 % bandwidth for the VSWR of less than -14 dB. This bandwidth is very similar to that of four layers. Radiation patterns offer uniform-excitation patterns including element patterns in both the E-plane and H-plane. However, grating lobes are occurred in the 45-deg. plane. All radiation patterns are very similar to these of four layers. We have achieved 13.0 % 1-dB-down bandwidth of realized gain in the 57.8 – 65.7 GHz range and 83% antenna efficiency at design frequency. The aperture efficiency greater than 80 % is achieved over 7-GHz bandwidth. The results of realized gain, gain and directivity are better than these of 4 layers, but we evaluate the results of five layers are similar to these of four layers and the effect of introducing more slot layers (six layers or more) with air gaps would not be advanced significantly. We assume the performance of more layers with air gaps would be degraded because larger size of slots in more layers causes mutual coupling, resulting in deterioration.

Appendix B

Design of Perpendicular-Corporate Feed in 4×4-Element-Unit Three-Layer Parallel-Plate Linearly-Polarized Slot Array Antenna

B.1 Introductory Remarks

This appendix presents a perpendicular-corporate feed in a 4×4-element-unit three-layer parallel-plate linearly-polarized slot array antenna. The proposed antenna is based on the structure of a perpendicular-corporate feed in a three-layer linearly-polarized parallel-plate slot array antenna as shown in the chapter 2, but the minimum unit of a subarray consists of 4×4 elements. This subarray has a potential to facilitate the design of a feeding circuit. We evaluate the effect of introducing a 4×4-element-unit subarray as a minimum unit in a perpendicular-corporate feed.

This chapter is organized as follows. Section B.2 describes the results of a perpendicular-corporate feed in a 4×4-element-unit three-layer parallel-plate linearly-polarized slot array antenna by the analysis of a 4×4-element subarray. section B.3 elucidates the introduction of grids under a radiating-slot layer to advance the antenna performance. In section B.4, we conclude this appendix.

B.2 Design of 4×4-Element-Unit Subarray

Fig. B.1 shows the model for the analysis of the 4×4-element-unit subarray. The proposed structure consists of a parasitic-slot layer, radiating-slot layer with dielectric, a coupling-aperture layer and a feeding waveguide. The distance between slots of the parasitic-slot layer is constant $0.86\lambda_0$ in both the x and y directions and that between slots of the radiating-slot layer is constant $1.72\lambda_0$ in both the x and y directions. In the analysis, we use a dielectric layer of t_d = 0.38 mm and ε_r = 2.17 obtained from the subsection 3.3.1. The conductivity 5.8×10^7 S/m of copper and a loss tangent 0.0006 of the dielectric are assumed. Considering the fabrication, we select a multiple of 0.20 mm as the thickness of slot layers including the coupling aperture and air gaps. The parameters are as follows: the

size of the parasitic slots, l_p and w_p; the size of the radiating slots, l_r and w_r; and the size of the coupling apertures, l_c and w_c. The air gap between the parasitic-slot and the radiating-slot layers is h_{pr} and that between the dielectric and coupling layers is h_{rc}. The thickness of the parasitic-slot layer, radiating-slot layer and the coupling-aperture layer should be 0.20 mm. The size of the feeding waveguide is fixed: width a = 2.95 mm, thickness b = 1.00 mm and length g = 11.55 mm, and it has short end. The offset of the coupling aperture against the principal axis in the x direction is also fixed at 0.40 mm. The design frequency is 61.5 GHz. The final values of the design parameters are listed in the figure.

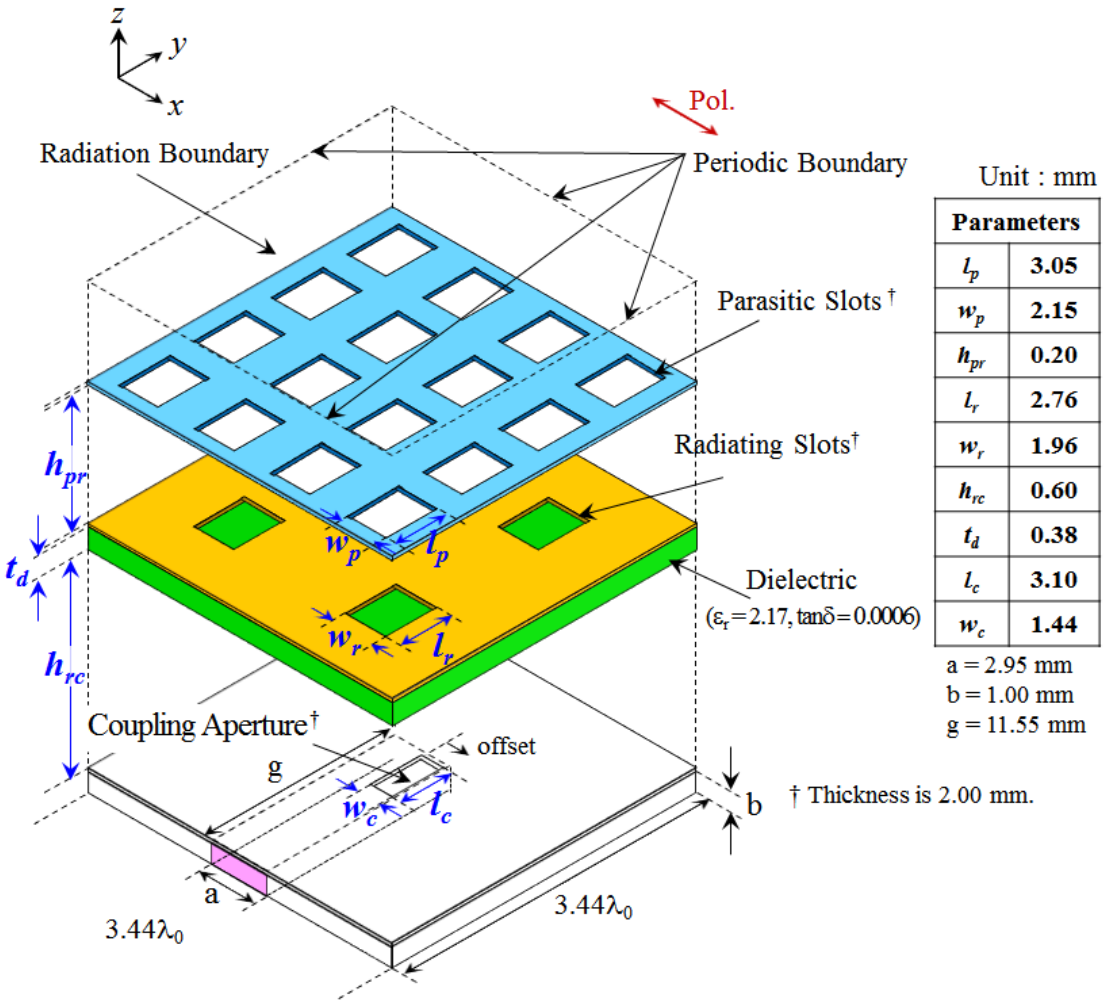

Fig. B.1. Model for the analysis of the 4×4-element-unit subarray.

Fig. B.2 shows the frequency characteristic of the reflection. The reflection of the 4×4-element-unit subarray is smaller than -14 dB over 3.5 % of the bandwidth ranging from 61.0 to 63.1 GHz. The bandwidth of the proposed model is not wider than that of the 2×2-emenet subarray as shown in Fig. 2.10.

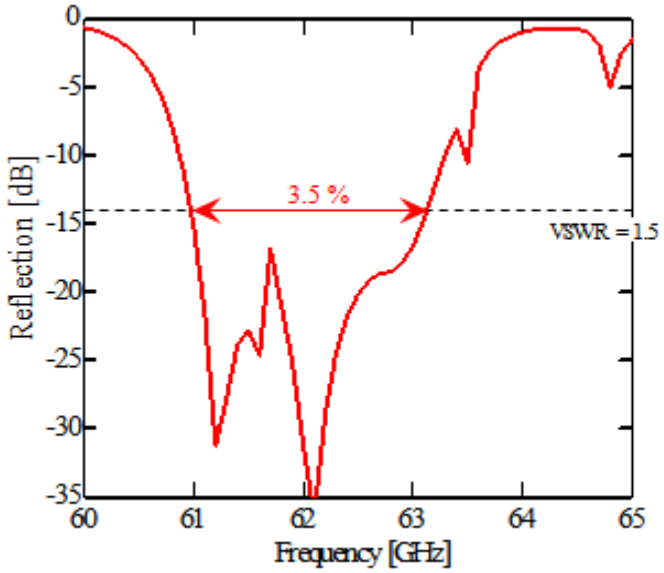

Fig. B.2 Frequency characteristic of the reflection.

Fig. B.3 shows radiation patterns at the design frequency in the E-plane (*xz*), H-plane (*yz*) and 45 deg.-plane. In the E-plane and H-plane, the radiation patterns present uniform-excitation patterns including element patterns. However, H-plane has grating lobes around ± 35 deg. and in the 45-deg. plane the radiation pattern has grating lobes around ± 55 deg. This would be caused by excitation difference in the H-plane.

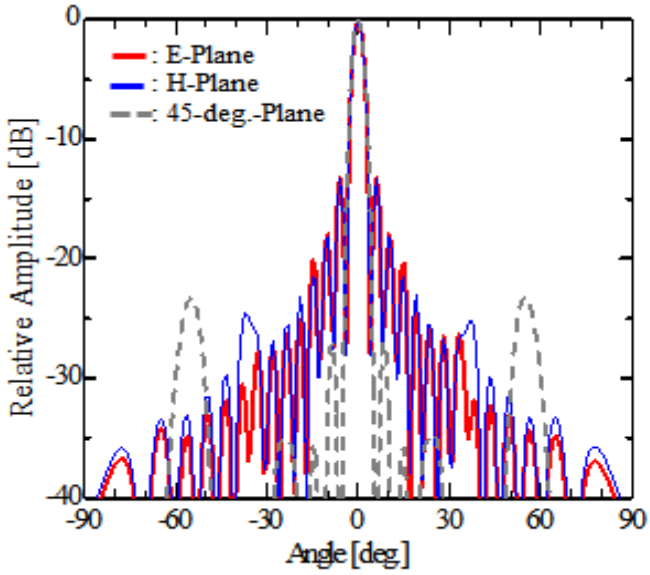

Fig. B.3 Radiation patterns (61.5 GHz).

B.3 Introduction of grids

To reduce the effect of excitation difference, we introduce grids under the radiating-slot layer. Fig. B.4 shows the model for the analysis of the 4×4-element-unit subarray with grids. Most of parameters are the same as Fig B.1, but new parameters are the size of grids: w_g and t_g. As a typical analysis, we use three grids.

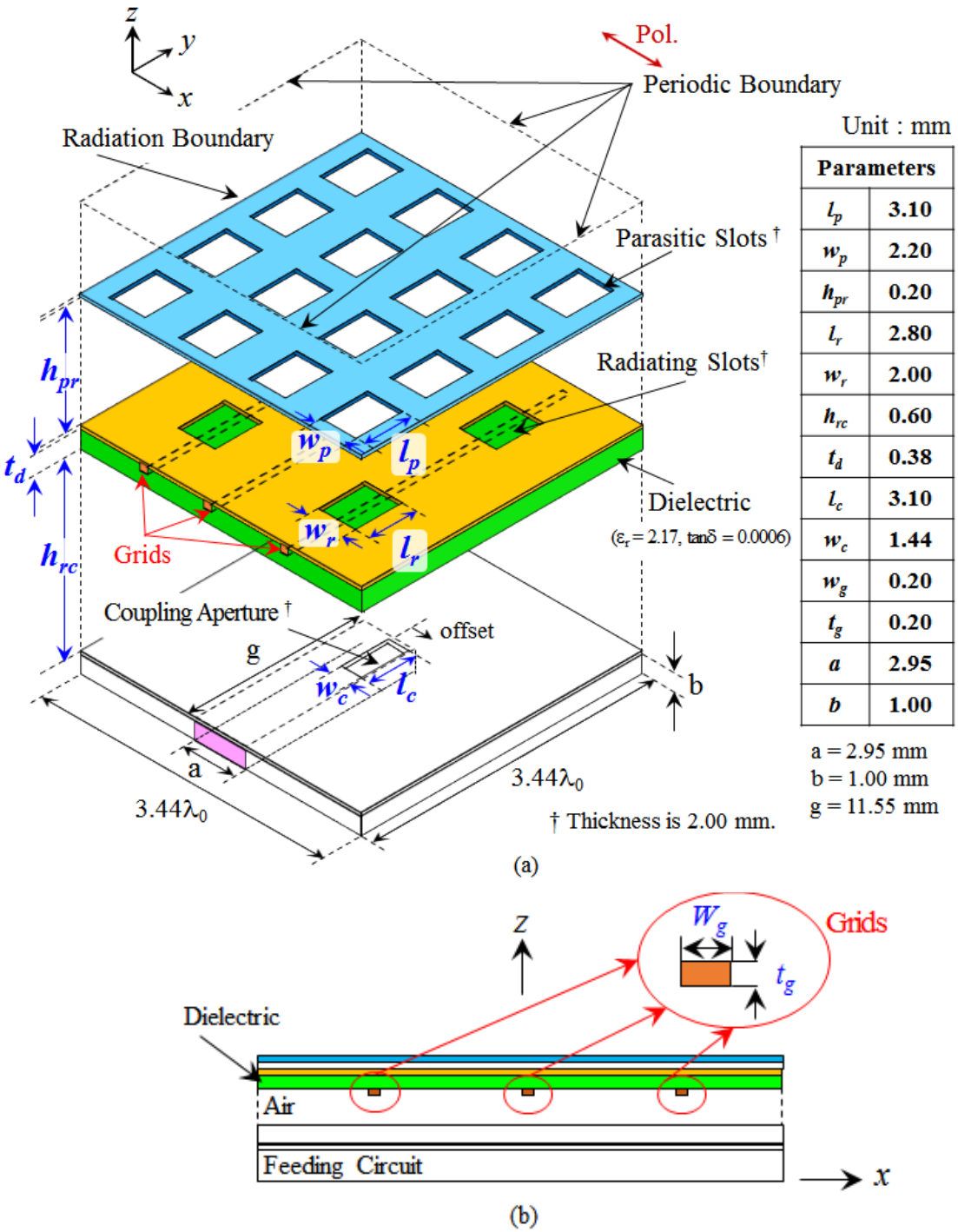

Fig. B.4. Model for the analysis of the 4×4-element-unit subarray w/ grids. (a) Perspective view. (b) Side view.

Fig. B.5 shows the frequency characteristic of the reflection. The reflection of the 4×4-element-unit subarray is not improved by the introduction of grids. We have not had clear reasons yet, but we assume a 4×4-element-unit subarray is not excited uniformly enough because of the wider distance between radiating slots in both the *x* and *y* directions.

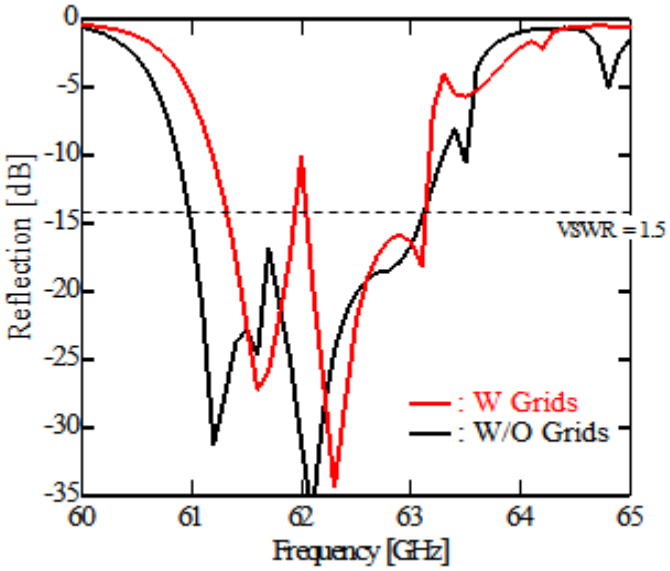

Fig. B.5 Frequency characteristic of the reflection.

Fig. B.6 shows radiation patterns at the design frequency in the E-plane (*xz*), H-plane (*yz*) and 45 deg.-plane. In the E-plane and H-plane, the radiation patterns present uniform-excitation patterns including element patterns. However, H-plane has grating lobes around ± 35 deg. and in the 45-deg. plane the radiation pattern has grating lobes around ± 55 deg. because excitation difference would remain in the subarray. We also compare radiation patterns of the 4×4-element-unit subarray with these of w/o grids. In all planes, radiation patterns of the proposed model are similar to these of w/o grids.

Fig B.7 shows the frequency characteristic of realized gain, gain and directivity. As a reference, the results of w/o grids are also described. These results have strong deterioration around 62 GHz and 63.2 GHz. This would be caused by excitation difference based on higher modes. Even though the subarray has the introduction of grids, excitation difference still remains in the structure.

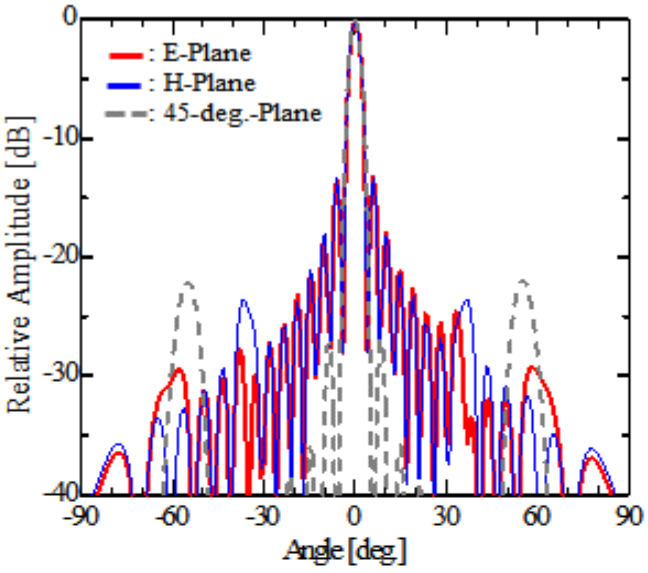
: E-Plane
: H-Plane
: 45-deg.-Plane
Relative Amplitude [dB]
0
-10
-20
-30
-40
-90
-60
-30
0
30
60
90
Angle [deg.]

(a)

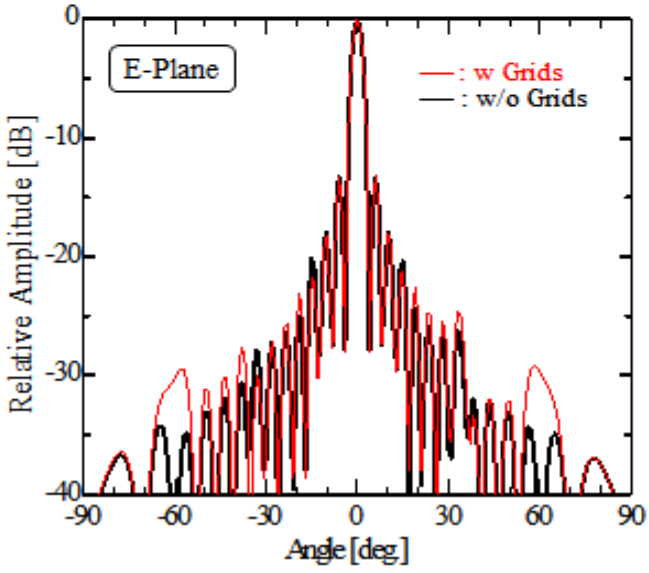
E-Plane
: w Grids
: w/o Grids
Relative Amplitude [dB]
0
-10
-20
-30
-40
-90
-60
-30
0
30
60
90
Angle [deg.]

(b)

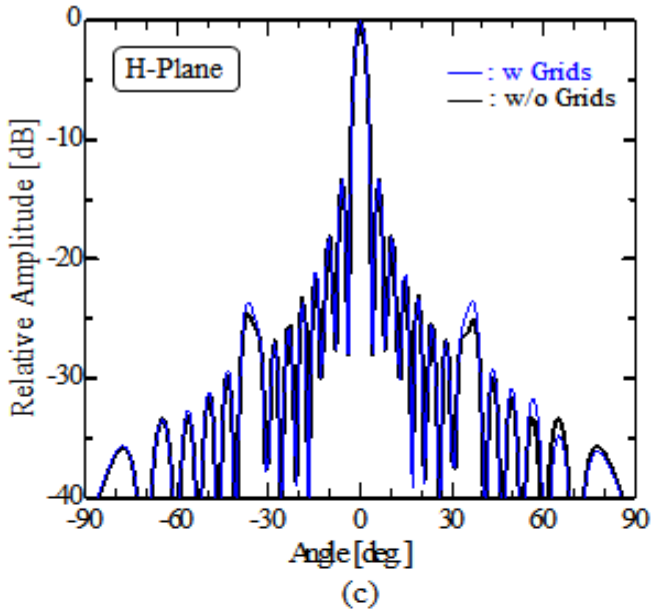

(c)

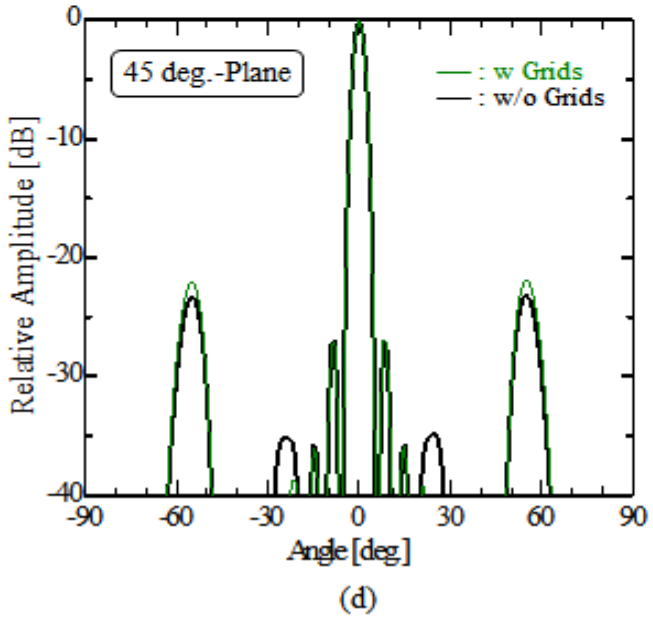

(d)

Fig. B.6 (a) Radiation patterns (61.5 GHz). (b) Comparison between w grids and w/o grids in the E-plane. (c) Comparison between w grids and w/o grids in the H-plane. (d) Comparison between w grids and w/o grids in the 45-deg. plane.

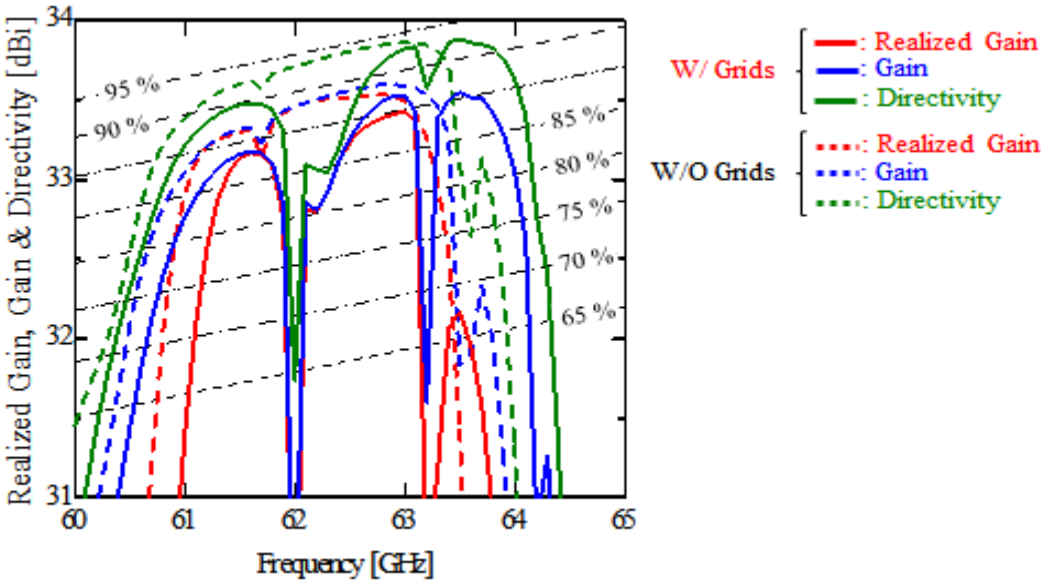

Fig. B.7 Frequency characteristic of realized gain, gain and directivity.

B.4 Concluding Remarks

This appendix presented a perpendicular-corporate feed in a 4×4-element-unit three-layer parallel-plate linearly-polarized slot array antenna. The proposed antenna is based on the structure of a perpendicular-corporate feed in a three-layer linearly-polarized parallel-plate slot array antenna as shown in the chapter 2, but the minimum unit of a subarray consists of 4×4 elements.

In the simulation, the reflection of the 4×4-element-unit subarray is smaller than -14 dB over 3.5 % of the bandwidth ranging from 61.0 to 63.1 GHz. The bandwidth is not wider than a 2×2-emenet subarray as shown in the chapter 2. Radiation patterns present uniform-excitation patterns including element patterns. However, H-plane has grating lobes around ± 35 deg. and in the 45-deg. plane the radiation pattern also has grating lobes around ± 55 deg. These would be caused by excitation difference in both the planes.

To reduce the effect of excitation difference, we introduce grids under the radiating-slot layer. The reflection of the 4×4-element-unit subarray is not improved by the introduction of grids. This is similar to the reflection of no grids. We have not had clear reasons yet, but we assume a 4×4-element-unit subarray is not excited uniformly enough because of the wider distance between radiating slots in both the *x* and *y* directions.

Appendix C

Design of Perpendicular-Corporate Feed in 32×32-Element Four-Layer Parallel-Plate Circularly-Polarized Slot Array Antenna

C.1 Introductory Remarks

This appendix presents a perpendicular-corporate feed in a 32×32-element four-layer parallel-plate circularly-polarized slot array antenna. The proposed antenna is based on the structure of a perpendicular-corporate feed in a four-layer circularly-polarized parallel-plate slot array antenna as shown in the chapter 3. We apply the parameters obtained from the chapter 3 to the analysis of a 32×32-element array.

This appendix is organized as follows. Section C.2 describes the results of a perpendicular-corporate feed in a 32×32-element four-layer parallel-plate circularly-polarized slot array antenna. section C.3 concludes this appendix.

C.2 Full Structure Analysis

Fig. C.1 shows the configuration of a perpendicular-corporate feed in a 32×32-element four-layer parallel-plate circularly-polarized slot array antenna. The figure also includes the configuration of the feeding circuit. Basic structure is the same as Fig. 3.11 in the chapter 3, but the number of an element is 1024 (32×32 elements). Parameters of this model is shown in Fig. 3.5. The edge as PMC of the parallel plates is extended by 1.3 mm ($\approx 0.25\lambda_0$) only in the y direction and terminated by copper. In the xy-plane, the dimensions of the antenna are 142.4 mm × 146.6 mm. Total thickness of the model is 5.18 mm.

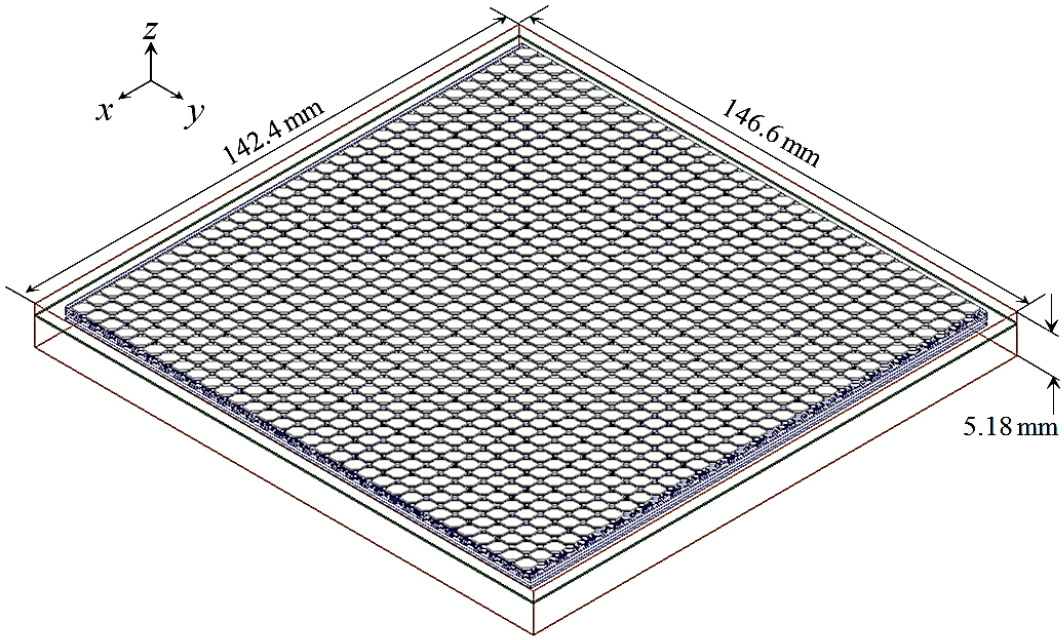

(a)

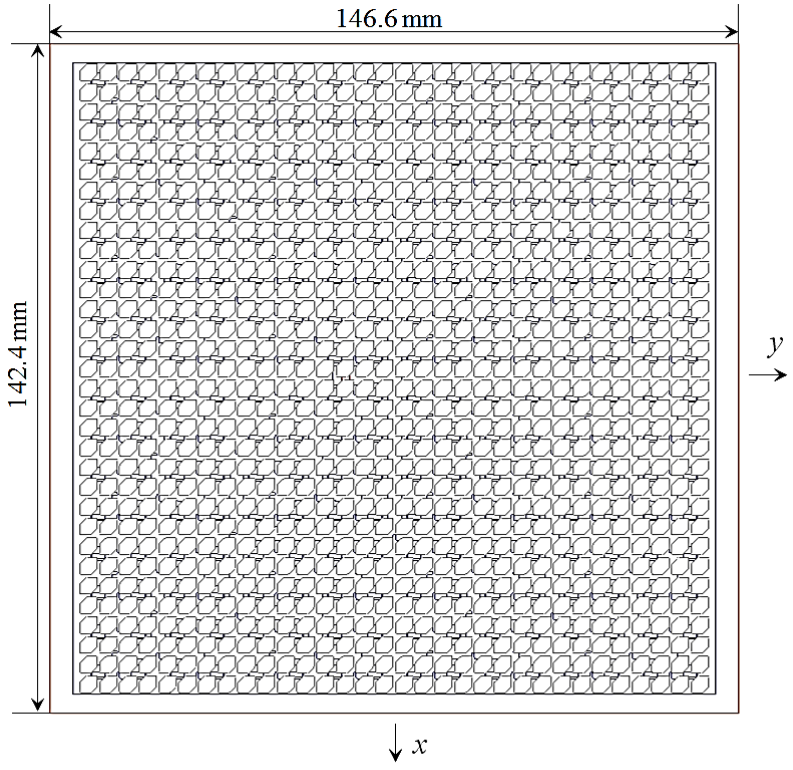

(b)

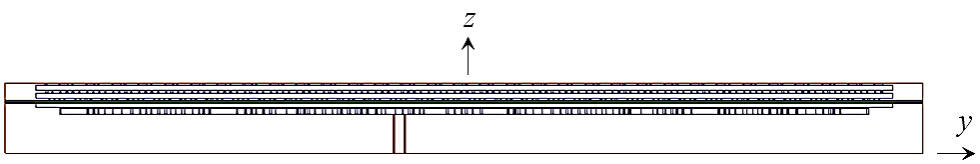

(c)

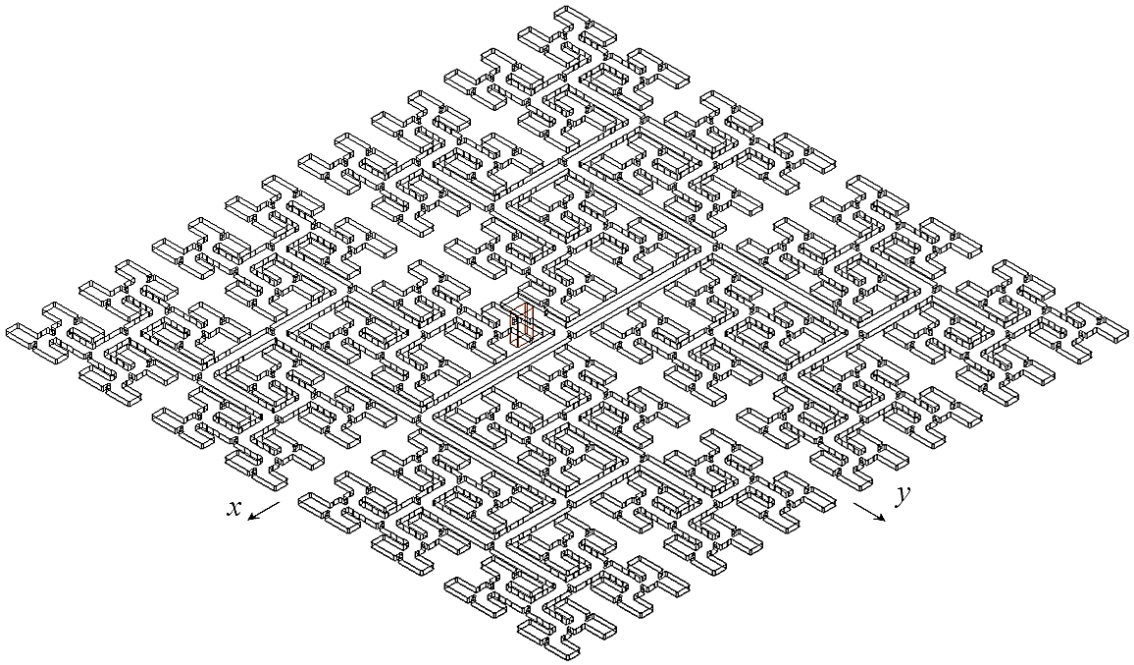

(d)

Fig. C.1 Perpendicular-corporate feed in a 32×32-element four-layer parallel-plate circularly-polarized slot array antenna. (a) Perspective view. (b) Top view. (C) Side view. (d) Perspective view (Feeding circuit).

Fig. C.2 shows the frequency characteristic of the reflection. As a reference, we also show the result of the 2×2-element subarray as shown in Fig. 3.6. The reflection of the 32×32-element array is smaller than -14 dB over 12.0 % of the bandwidth ranging from 57.3 to 64.7 GHz, but note that reflection around 63.0 GHz is more than -14dB. This would be caused by the reflection of the feeding circuit.

Fig. C.3 shows the frequency characteristic of the axial ratio. We also show the result of the 2×2-element subarray as a reference. The axial ratio is below 3 dB over 15.7 % of the bandwidth from 55.5 to 65.2 GHz. The bandwidth is similar to that of the 2×2-element subarray. We can see the feeding circuit does not strongly influence the axial ration.

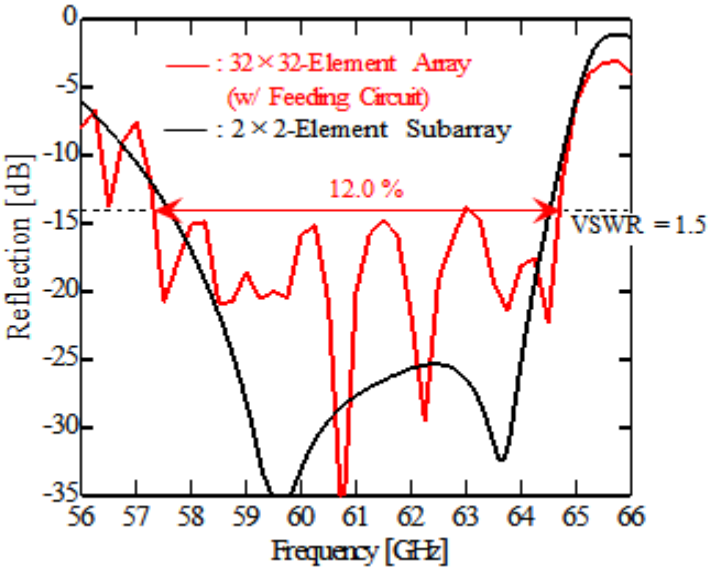

Fig. C.2 Frequency characteristic of reflection.

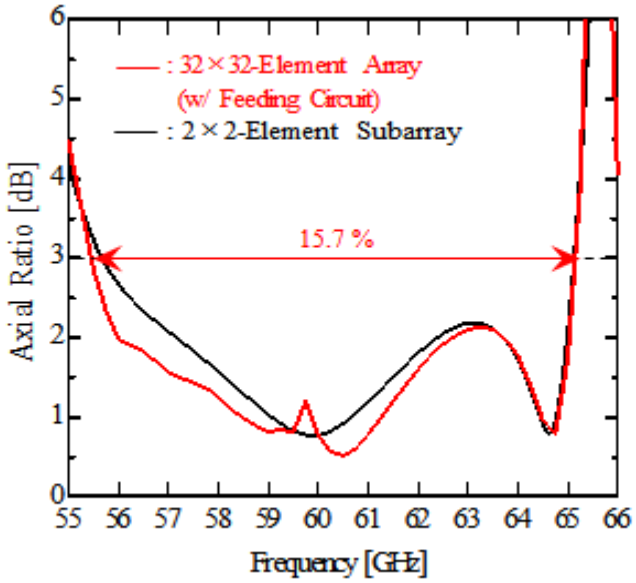

Fig. C.3 Frequency characteristic of axial ratio.

Fig. C.4 shows radiation patterns at the design frequency in the *xz*-plane, *yz*-plane and 45 deg.-plane. In the *xz* -plane and *yz*-plane, the radiation patterns present uniform-excitation patterns including element patterns. Both planes slightly have grating lobes around ± 35 deg., but the level of them is small, -30 dB. For 45 deg.-plane there are grating lobes around ± 55 deg. because excitation difference would be caused.

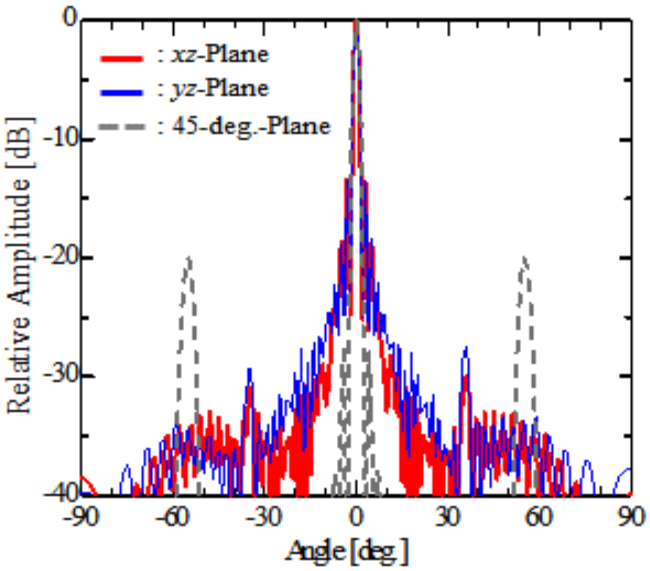

Fig. C.4 Radiation patterns (61.5 GHz).

Fig C.5 shows the frequency characteristic of realized gain, gain and directivity. The realized gain includes the reflection loss as well as conductor and dielectric losses and the aperture efficiency loss. The maximum of the realized gain is 38.9 dBi at 62.3 GHz. We have achieved 11.3 % 1-dB-down bandwidth of realized gain in the 57.8 – 64.7 GHz range and 76 % antenna efficiency at design frequency. The aperture efficiency greater than 75 % is achieved over 6-GHz bandwidth.

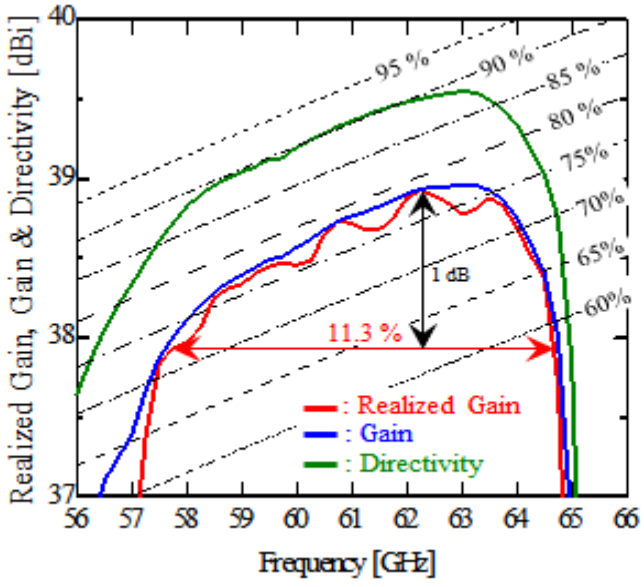

Fig. C.5 Frequency characteristic of realized gain, gain and directivity.

C.3 Concluding Remarks

This appendix presents a perpendicular-corporate feed in a 32×32-element four-layer parallel-plate circularly-polarized slot array antenna. The proposed antenna is based on the structure of a perpendicular-corporate feed in a four-layer circularly-polarized parallel-plate slot array antenna as shown in the chapter 3. We apply the parameters obtained from the chapter 3 to the analysis of a 32×32-element array.

In the simulation, the reflection of the 32×32-element array is smaller than -14 dB over 12.0 % of the bandwidth ranging from 57.3 to 64.7 GHz, but note that reflection around 63.0 GHz is more than -14dB. This would be caused by the reflection of the feeding circuit. The axial ratio is below 3 dB over 15.7 % of the bandwidth from 55.5 to 65.2 GHz. The bandwidth is similar to that of the 2×2-element subarray. This bandwidth is very similar to that of four layers. Radiation patterns present uniform-excitation patterns including element patterns in the *xz*-plane and *yz*-plane. However, in the 45deg.-plane there are grating lobes around ± 55 deg. because excitation difference would be caused. The maximum of the realized gain is 38.9 dBi at 62.3 GHz. We have achieved 11.3 % 1-dB-down bandwidth of realized gain in the 57.8 – 64.7 GHz range and 76 % antenna efficiency at design frequency. The aperture efficiency greater than 75 % is achieved over 6-GHz bandwidth.

Appendix D

Design of Perpendicular-Corporate Feed in 2×2-Element Four-Layer Parallel-Plate Linearly-Polarized Slot Array Antenna in 80-GHz Band

D.1 Introductory Remarks

This appendix presents a perpendicular-corporate feed in a 2×2-element four-layer parallel-plate linearly-polarized slot array antenna in the 80-GHz band. The proposed antenna is based on the structure of a perpendicular-corporate feed in a four-layer linearly-polarized parallel-plate slot array antenna as shown in the chapter 4. We apply the parameters obtained from the chapter 4 to the analysis of a 2×2-element subarray after modifying them based on the wavelength of the 80-GHz band.

The aim of this analysis is to obtain the feasibility of higher frequency model without changing the thickness of copper plates and the relative permittivity of dielectric considering the availability of them.

This appendix is organized as follows. Section D.2 describes the results of a perpendicular-corporate feed in a 2×2-element four-layer parallel-plate linearly-polarized slot array antenna in the 80-GHz band. section D.3 concludes this appendix.

D.2 Design of 2×2-Element Subarray

Fig. D.1 shows the configuration of a perpendicular-corporate feed in a 2×2-element four-layer parallel-plate linearly-polarized slot array antenna. Basic structure is the same as Fig. 4.2, but the center frequency is different from 61.5 GHz to 78.5 GHz. 78.5 GHz is the middle frequency ranging from 74.0 GHz to 83.0 GHz. We do not change the thickness of copper plates and dielectric, and the relative permittivity of the dielectric as described in Fig 4.2. the thicknesses of the additional-slot layer, the parasitic-slot layer

and radiating-slot layer is 0.20 mm, and that of the coupling-aperture layer is 0.20 mm. The thickness of the dielectric is 0.38 mm and the relative permittivity of it is 2.17. The offset of the coupling aperture against the principal axis in the *x* direction is also fixed at 0.48 mm. The feeding waveguide has short end and the length is 4.42 mm. The final values of the designed parameters are listed in the figure. We also describe the change ratio of parameters for the better understanding there. 78 % is a basic change ratio in this case.

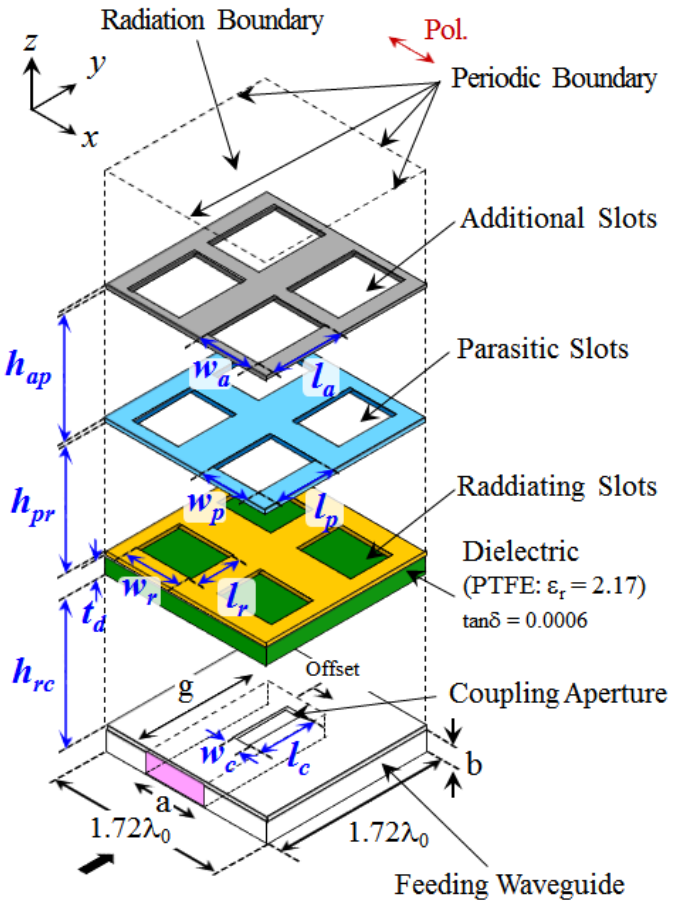

Parameters (mm)			Change Ratio
λ_0 (f_0)	4.88 (61.5G)	3.82 (78.5G)	78%
l_a	3.47	2.73	79%
w_a	2.73	2.23	82%
t_a	0.20	0.20	0%
h_{ap}	0.20	0.20	0%
l_p	2.93	2.32	79%
w_p	2.44	2.00	82%
t_p	0.20	0.20	0%
h_{pr}	0.20	0.20	0%
l_r	2.16	1.66	77%
w_r	2.66	2.15	81%
t_r	0.20	0.20	0%
h_{rc}	0.60	0.60	0%
t_d	0.38	0.38	0%
t_c	0.20	0.20	0%
l_c	2.78	2.18	78%
w_c	0.85	0.67	79%
a	2.95	2.31	78%
b	1.00	0.78	78%
g	5.64	4.42	78%

Fig. D.1 Model for the analysis of the 2×2-element subarray.

Fig. D.2 shows the frequency characteristic of the reflection. As a reference, we also show the result of the 60-GHz band as shown in Fig. 4.4. The reflection of the 2×2-element subarray in the 80-GHz band is smaller than -14 dB over 15.3 % of the bandwidth

ranging from 73.1 to 82.5 GHz. On the other hand, the reflection of the 60-GHz band is less than -14 dB over 13.4 % bandwidth ranging from 57.3 to 65.6 GHz. The bandwidth is enhanced by almost 1.14 times probably because 80-GHz band has wider slots than these of the 60-GHz band. Another reason would be the thickness of copper plates and air gaps become large against the electric wavelength of the 80-GHz band equivalently, contributing to the wide bandwidth.

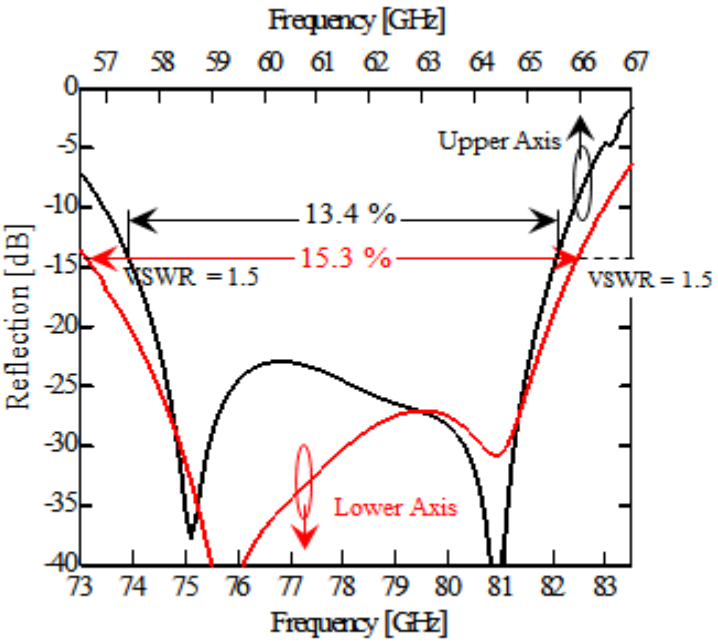

Fig. D.2 Frequency characteristic of the reflection

Fig. D.3 shows radiation patterns at 78.5 GHz (a) in the E-plane, H-plane and 45-deg. plane. As a reference, we also show the results of radiation patterns at 61.5 GHz (b). These results are calculated by the array-setup function (16×16-element array) of the HFSS. In the E-plane and H-plane, the radiation patterns present uniform-excitation patterns including element patterns in both the frequency bands. For 45 deg.-plane there are grating lobes around ± 55 deg. at the both frequency bands because excitation difference would be caused. The level of them at 78.5 GHz is higher than that of 61.5 GHz probably because 78.5 GHz has wider slots than these of 61.5 GHz. The level difference is not small around 5 dB.

Fig D.4 shows the frequency characteristic of the realized gain. The realized gain includes the reflection loss as well as conductor and dielectric losses and the aperture efficiency loss. As a reference, we also show the result of the 60-GHz band. The maximum of the realized gain is 33.6 dBi at 81.5 GHz. We have achieved 16.6 % 1-dB-

down bandwidth of realized gain in the 73.2 – 83.4 GHz range and 85 % antenna efficiency at the design frequency. 1-dB-down bandwidth of the realized gain in the 80-GHz band is wider than that in the 60-GHz band probably because of wider slots. Another reason would be the thickness of copper plates and air gaps become large against the electric wavelength of the 80-GHz band equivalently, contributing to the wide bandwidth.

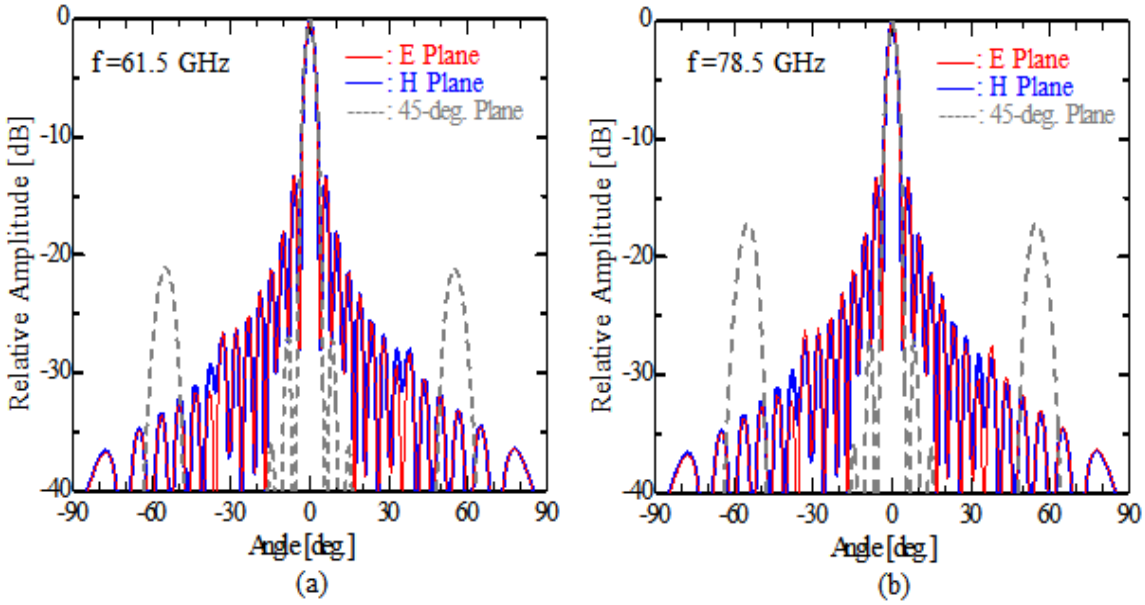

Fig. D.3 Radiation patterns. (a) 61.5 GHz. (b) 78.5 GHz.

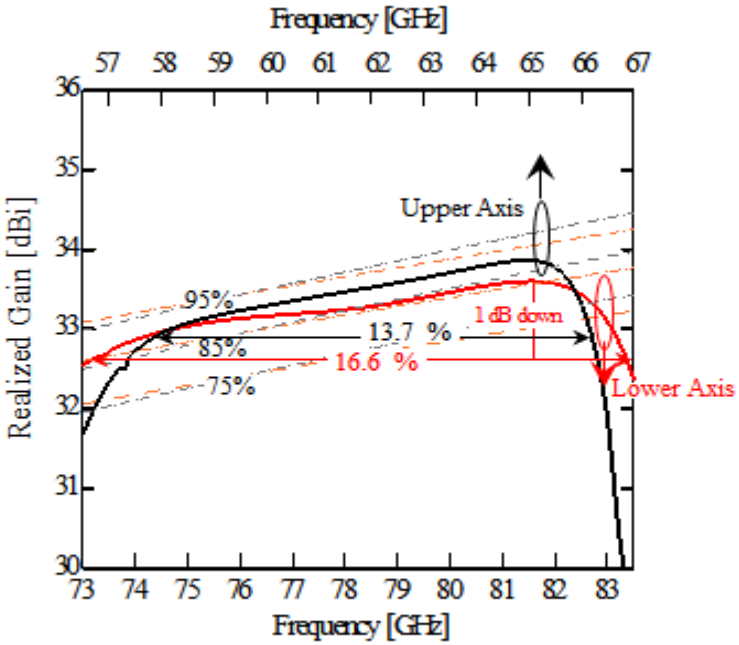

Fig. D.4 Frequency characteristic of realized gain.

D.3 Concluding Remarks

To obtain the feasibility of a higher frequency model, this appendix presented a perpendicular-corporate feed for a four-layer linearly-polarized parallel-plate slot array antenna in the 80-GHz band. This model is based on that in the chapter 4. We apply parameters obtained from the chapter 4 to the analysis of a 2×2-element array after modifying them, depending on the wavelength of the 80-GHz band. Also, we do not change the thickness of copper plates 0.20 mm and dielectric 0.38 mm, and the relative permittivity 2.17 of the dielectric considering the availability of them.

In the simulation, the proposed antenna provides 15.3 % bandwidth for the VSWR of less than -14 dB. This bandwidth is wider than that of 60-GHz band probably due to wider slots of 80-GHz-band model. Radiation patterns offer uniform-excitation patterns including element patterns in both the E-plane and H-plane. However, grating lobes are occurred in the 45-deg. plane. The level is relatively high -17 dB. This would be caused by wide slots. We have achieved 16.6 % 1-dB-down bandwidth of the realized gain in the 73.2 – 83.4 GHz range and 85% antenna efficiency at the design frequency. This bandwidth is also wider than that of 60-GHz band. We conclude the higher frequency model will be achieved without changing the thickness of copper plates and dielectric, and relative permittivity of the dielectric. However, we need to consider the influence of the manufacturing errors by measurements to have accurate evaluation.